Università degli Studi di Trento
Dipartimento di Fisica

Ph.D. Thesis

STRONGLY CORRELATED QUANTUM
FLUIDS AND EFFECTIVE
THERMALIZATION IN NON-MARKOVIAN
DRIVEN-DISSIPATIVE PHOTONIC SYSTEMS

José Lebreuilly

Advisor
Dr. Iacopo Carusotto

December 2017

Strongly correlated quantum fluids and effective thermalization in non-Markovian driven-dissipative photonic systems

José Lebreuilly

A dissertation submitted to the

Dipartimento di Fisica
Università degli Studi di Trento

In fulfilment of the requirements for the Degree of
Philosophiæ Doctor in Physics

Under the Supervision of
Dr. Iacopo Carusotto

Dottorato di Ricerca XXX Ciclo
December 7th, 2017

Supervisor:

Dr. Iacopo Carusotto

Members of the committee:

Prof. Sebastian Diehl - University of Cologne

Dr. Francesco Piazza - MPI-PKS, Dresden

Prof. Pietro Faccioli - University of Trento

Abstract

Collective quantum phenomena are fascinating, as they repeatedly challenge our comprehension of nature and its underlying mechanisms. The qualification *"quantum"* can be attributed to a generic many-body system whenever the interference effects related to the underlying wave nature of its elementary constituents can not be neglected anymore, and a naive classical description in terms of interacting billiard balls fails to catch its most essential features.

This interference phenomenon called *"quantum degeneracy"* which occurs at weak temperatures, leads to spectacular collective behaviours such as the celebrated Bose-Einstein Condensation (BEC) phase transition, where a macroscopic fraction of a bosonic system of particles collapses below a critical temperature T_c on a single-particle state. Quantum coherence, when combined with inter-particle interactions, gives rise to highly non-classical frictionless hydrodynamic behaviours such as superfluidity (SF) and superconductivity (SC).

Even more exotic quantum phases emerge in presence of important interactions as matter reaches a *"strongly correlated regime"* dominated by quantum fluctuations, where each particle is able to affect significantly the surrounding fluid: characteristic examples are the so-called Mott-Insulator (MI) quantum phase where particles are localized on a lattice due to a strong interaction-induced blockade, along with the Tonks-Girardeau (TG) gas where impenetrable bosons in one-dimension acquire effective fermionic statistics up to a unitary transformation, and the Fractional Quantum Hall (FQH) effect which occurs in presence of a gauge field, and features a special type of elementary excitation possessing a fractional charge and obeying to fractional statistics called 'anyon'.

These quantum many-body effects were explored in a first place in systems well isolated from the external environment such as ultra-cold atomic gases or electrons in solid-state systems, within a physical context well described by *"equilibrium statistical mechanics"*. Yet, over the last two decades a broad community has started investigating the possibility of stabilizing interacting quantum phases in novel nonlinear quantum optics architectures, where interacting photons have replaced their atomic and electronic counterpart. Thanks to their high level of controllability and flexibility, and the possibility of reaching the quantum degeneracy regime at exceptionally high temperatures, these platforms appear as extremely promising candidates for the *"quantum simulation"* of the most exotic many-body quantum problems: while the precursors experiments in semiconductor exciton-polariton already allow to reach the Bose-Einstein Condensation and superfluid regimes, novel platforms such as superconducting circuits, coupled cavity arrays or photons coupled to Rydberg EIT (Electromagnetically induced Transparency) atoms have entered the so-called 'photon blockade' where photons behave as impenetrable particles, and open a encouraging pathway toward the future generation of strongly correlated phases with light.

A specificity of quantum optics devices is their intrinsic *"non-equilibrium"* nature: the interplay between the practically unavoidable radiative and non-radiative losses and the external drive needed to replenish the photon gas leads the many-body system toward a steady-state presenting important non-thermal features. One one hand, an overwhelmingly large quantity of novel quantum phenomena is expected in the non-equilibrium framework, as breaking the thermal equilibrium condition releases severe constraints on the state of a quantum system and on the nature of its surrounding environment. On the other hand, we

do not benefit yet of an understanding of non-equilibrium statistical mechanics comparable with its well-established equilibrium counterpart, which relies on strong historical foundations. Understanding how to tame (and possibly exploit) non-equilibrium effects in order to stabilize interesting quantum phases in a controlled manner often reveals a hard challenge.

In that prospect, an important conceptual issue in the non-equilibrium physics of strongly interacting photons regards the possibility of stabilizing *"incompressible quantum phases"* such as the Mott-Insulator or Fractional Quantum Hall states, and more generally to stabilize the ground-state of a given particle-number conserving Hamiltonian, in a physical context where dissipative losses can not be neglected. While being able to quantum simulate those emblematic strongly correlated quantum phases in this novel experimental context would strongly benefit to the quantum optics community, gaining such a kind of flexibility would also contribute to fill an important bridge between the equilibrium and the non-equilibrium statistical physics of open quantum systems, allowing to access in a controlled manner a whole new phenomenology at the interface between the two theories.

In this thesis I address those questions, which I reformulate in the following manner:

- *What are the conditions for the emergence of analogue equilibrium properties in open quantum systems in contact with a non-thermal environment ?*

- *In particular, is it possible to stabilize strongly correlated quantum phases with a perfectly defined particle number in driven-dissipative photonic platforms, in spite of environment-induced losses and heating effects ?*

The structure of the thesis is the following.

Chapter 1. We give an overview of the physics of many-body photonic systems. As a first step we address the weakly interacting regime in the physical context of exciton-polaritons: after describing the microscopic aspects of typical experiments, we move to the discussion of non-equilibrium Bose-Einstein Condensation and the various mechanisms related to the emergence of thermal signatures at steady-state. The second part of this Chapter is dedicated to strongly interacting fluids. After drawing a quick overview of several experimental platforms presenting a good potential for the study of such physics in a near future, we discuss the relative performance of several schemes proposed in order to replenish the photonic population

Chapter 2. We investigate the potential of a non-Markovian pump scheme with a narrow bandpass (Lorentzian shaped) emission spectrum for the generation of strongly correlated states of light in a Bose-Hubbard lattice. Our proposal can be implemented by mean of embedded inverted two-level emitters with a strong incoherent pumping toward the excited state. Our study confirms in a single cavity the possibility of stabilizing photonic Fock states in a single configuration, and strongly localized $n = 1$ Mott-Insulator states in a lattice with $n = 1$ density. We show that a relatively moderate hopping is responsible for a depletion of the Mott-state, which then moves toward a delocalized state reminiscent of the superfluid regime. Finally, we proceed to a mean-field analysis of the phase diagram, and unveil a Mott-to-Superfluid transition characterized by a spontaneous breaking of the $U(1)$ symmetry and incommensurate density.

The results of this Chapter are based on the following publications:

1. J. Lebreuilly, M. Wouters and I. Carusotto, *"Towards strongly correlated photons in arrays of dissipative nonlinear cavities under a frequency-dependent incoherent pumping"*, C. R. Phys., **17** (8), 836, 2016.

2. A. Biella, F. Storme, J. Lebreuilly, D. Rossini, R. Fazio, I. Carusotto and C. Ciuti, *"Phase diagram of incoherently driven strongly correlated photonic lattice"*, Phys. Rev. A, **96**, 023839, 2017.

Chapter 3. In view of improving the performance of the scheme introduced in last chapter, and reproducing in particular the equilibrium zero temperature phenomenology in driven-dissipative photonic lattices, we develop a fully novel scheme based on the use of non-Markovian reservoirs with tailored broadband spectra which allows to mimick

the effect of tunable chemical potential. Our proposal can be implemented by mean of a small number of emitters and absorbers and is accessible to current technologies.

We first analyse the case of a frequency-dependent emission with a square spectrum and confirm the possibility of stabilizing Mott insulator states with arbitrary integer density. Unlike the previous proposal the Mott state is robust against both losses and tunneling. A sharp transition toward a delocalized superfluid-like state can be induced by strong values of the tunneling or a change in the effective chemical potential. While an overall good agreement is found with the $T = 0$ predictions, our analysis highlights small deviations from the equilibrium case in some parts of the parameters space, which are characterized by a non-vanishing entropy and the kinetic generation of doublon excitations. We finally consider an improved scheme involving additional frequency-dependent losses, and show in that case that the Hamiltonian ground-state is fully recovered for any choice of parameters. Our proposal, whose functionality relies on generic energy relaxation mechanisms and is not restricted to the Bose-Hubbard model, appears as a promising quantum simulator of zero temperature physics in photonic devices.

The results of this Chapter are based on the following publication:

1. J. Lebreuilly, A. Biella, F. Storme, D. Rossini, R. Fazio, C. Ciuti and I. Carusotto, *"Stabilizing strongly correlated photon fluids with non-Markovian reservoirs"*, Phys. Rev. A **96** , 033828 (2017).

Chapter 4. We adopt a broader perspective, and analyse the conditions for the emergence of analogous thermal properties in driven-dissipative quantum systems. We show that the impact of an equilibrated environment can be mimicked by several non-Markovian and non-equilibrated reservoirs. Chapter 2 already features a preliminary result in that direction, showing that in presence of a broad reservoir spectral density a given quantum system will evolve toward a Gibbs ensemble with an artificial chemical potential and temperature. In this chapter we develop a broader analysis focusing as a counterpart part on the exactly solvable model of a weakly interacting Bose Gas in the BEC regime. Our formalism based on a quantum Langevin model, allows in particular to access both static and dynamical properties: remarkably, we demonstrate not only the presence of an equilibrium static signature, but also the validity of the fluctuation-dissipation theorem. While our results apply only for low-energy excitations for an arbitrary choice of reservoir spectral densities, we predict that a fine tuned choices of reservoirs mimicking the so-called Kennard Stepanov condition will lead to a full apparent equilibration. Such effect that we call *"pseudo-thermalization"* implies that under very specific conditions, an open quantum system can present all the properties of an equilibrated one in spite of the presence of an highly non equilibrated environment. The results of this Chapter are based on the following paper:

1. J. Lebreuilly, A. Chiocchetta and I. Carusotto, *"Pseudo-thermalization in driven-dissipative non-Markovian open quantum systems"*, arXiv:1710.09602 (submitted for publication).

Contents

Contents

List of Acronyms

BEC Bose-Einstein Condensation/Bose-Enstein Condensate

BH Bose-Hubbard

BKT Berezinskii-Kosterlitz-Thouless

DBR Distributed Bragg Reflector

DMRG Density Matrix Renormalization Group

DOS Density of States

EIT Electromagnetically Induced Transparency

FDT Fluctuation Dissipation Theorem

FQH Fractional Quantum Hall

GP Gross-Pitaevskii

JC Jaynes-Cummings

JCH Jaynes-Cummings-Hubbard

KPZ Kardar-Parisi-Zhang

KMS Kubo-Martin-Schwinger

KS Kennard-Stepanov

LO Longitudinal Optical

MF Mean-Field

MI Mott Insulator

MPO Matrix Product Operators

MPS Matrix Product States

OPO Optical Parametric Oscillator

QED Quantum Electrodynamics

QW Quantum Well

RG Renormalization Group

RWA Rotating Wave Approximation

SF Superfluidity

SSB Spontaneous Symmetry Breaking

VCSEL Vertical Cavity Surface Emitting Laser

TG Tonks-Girdardeau

SSB Spontaneous Symmetry Breaking

TG Tonks-Girdardeau

Chapter 1

Non-equilibrium many-body quantum physics with light

Since the discovery of superconductivity in a pure metal by Kamerlingh Onnes in 1911, quantum fluids have been the object of a constantly renewed interest and investigated in a very wide variety of physical contexts. Although historically, most of the research activity was concentrated on physical systems made of material particles ranging from ultra-cold atoms [151], electrons [189], helium [150], quark-gluon plasmas [164] and neutrons [160] in neutron stars, a growing attention has been devoted within the last decades to the possibility of stabilizing quantum phases with light [76, 84, 29]. Yet, at the early stages of these theoretical/experimental developments the possibility was still missing that photons could present strong enough inter-particle interactions so to observe interesting quantum collective phenomena: quantum electrodynamics (QED) theory indeed was predicting in the vacuum the existence of a photon-photon scattering cross section related to the creation of virtual hole-positron pairs (Delbrück scattering [23]), but the resulting physical effect was so weak that it could not have led to any significant phenomenology in standard optics and microwave platforms.

One important breakthrough in that direction was to make light propagate in novel non-linear optical materials possessing an important $\chi^{(3)}$ susceptibility [19], where photon-photon interactions can be mediated (quasi-)resonantly by matter degrees of freedom (the most simplest case being hole-electron pairs in a semiconductor) rather than virtual high-energy excitations. A powerful strategy to engineer strong enough photon-photon interaction has been to reach the so-called 'strong coupling' regime between light and the matter degrees of freedom. In this configuration, the dynamics coherently mixes photonic and matter degrees of freedom, leading to the emergence of a dressed quasi-particle named 'polariton' [83]. This allowed for the development of a wide range of experimental platforms suited for the investigation of many-body quantum effects in a photonic context, ranging from exciton-polaritons [29], cavity electrodynamics platforms [76], superconducting quantum circuits [84], photons interacting with Rydberg atoms [147]. Thanks to these advancements, many celebrated many-body quantum phenomena such as Bose-Einstein Condensation [99] and superfluidity [3] have been reproduced in the regime of weak interactions. The opposite photon blockade regime [86] in which photons start behaving as impenetrable particles, has been reached in a single cavity configuration in many optical platforms [13, 116, 55, 157, 147, 91], opening a possible pathway toward the stabilization in lattices of strongly correlated photonic phases, such as the Tonks-Girardeau gas [67], Mott Insulators [59] or FQH states [117]. The fundamental difference distinguishing many-body optical systems with respect to the case of material particles such as electronic/atomic gases is the intrinsic non-equilibrium nature of the underlying dynamics: photons typically have a finite lifetime, and thus a pumping scheme has to be implemented in the apparatus in order to obtain a stable quantum fluid. As a result, the photonic open quantum system generally reaches a non-thermal steady-state, whose properties depend in a strongly non-universal manner

on the way it interacts with its surrounding environment. While this important aspect does not represent a fundamental obstacle for the stabilization of non-equilibrium BECs, as spontaneous symmetry breaking (SSB) phenomena are not directly related to the particle number conservation, the situation is much less clear regarding the possibility of generating incompressible quantum phases with a fluctuationless density.

This Chapter reviews some of the various experimental platforms and major progresses in the field of photonic many-body physics, with a particular stress on the environment-induced features of a non-equilibrium type.

In Sec. 1, we focus on the weakly interacting regime of a quantum fluid of photons: after a brief review of the physics of quantum well exciton-polaritons in semiconductors, we move to the discussion of non-equilibrium Bose-Einstein Condensation of light: we first introduce a simplified model for the dynamics of a dissipative condensate under the form of a driven-dissipative Gross-Pitaevskii (GP) equation. Secondly, we describe the underlying mechanisms for Bose-Einstein Condensation in exciton-polariton experiments, highlighting the role played by the temperature of the apparatus and the detuning between excitons and photons in determining whether steady-state properties will present thermal or non-equilibrium features. In Sec. 2, we move to the strongly interacting regime, and describe the current experimental and theoretical state-of-the-art. After a brief review of several experimental platforms such as Superconducting circuits and Coupled cavity arrays allowing to explore the regime of strong correlations, and a description of the single-site Jaynes-Cummings (JC) model, we discuss the extended lattice configuration where the interesting many-body physics is expected to occur: we first study the isolated case, showing that these platforms allow to engineer emblematic Hamiltonians of the physics of strong correlation such as the Bose-Hubbard model. Secondly, we discuss the more realistic non-equilibrium configuration where Hamiltonian effects are associated to losses and pumping: after reviewing the phenomenology associated to the commonly used coherent drive scheme, which has attracted until now most of the research activity, we explain why it is not suited for the stabilization of strongly correlated states such as the Mott-Insulator and FQH states. Finally, we present the more recent promising proposals based on incoherent non-Markovian pump schemes or the engineering of an artificial chemical potential for light, in view of stabilizing incompressible quantum phases.

1.1 Exciton-polaritons and non-equilibrium Bose-Einstein condensation of light

1.1.1 Exciton-Polaritons

1.1.1.1 Quantum well excitons and photons

A quantum well (QW) [47] consists in a thin layer of a semiconductor of some chemical composition with an high $\chi^{(3)}$ susceptibility (such as GaAs or CdTe), sandwiched between two external semiconductor layers of a different composition (e.g., GaAlAs or CdMgTe). If the bottom (as well as the top) of the conduction (resp. valence) band of the intermediate layer is located at a lower (resp. higher) energy than the bottom (resp. the top) of the the conduction (resp. valence) bands of the external layer, then this configuration acts as an external potential limiting the motion of hole and electron excitations to the quasi two-dimensional region defined by the QW layer. This spatial confinement has for major consequence to enhance the effect of Coulombian interactions, enabling for the formation of an exciton-hole bound state called 'exciton'.

QW excitons are neutral bosonic excitations with a mass m_X of same order of magnitude as the electronic mass. They can interact by mean of short range interactions related to the Coulomb interaction between their underlying charged constituents, which can be well represented by a contact potential of significative strength g_X. In typical experimental setups [99, 7] (see Fig. 1.1, panel a)), the confinement of the surrounding quantum electromagnetic field by mean of distributed Bragg reflector (DBR) mirrors allows for the reversible coherent conversion of an exciton into a optical photon. In addition, due to confinement the photon acquires a modified dispersion law along the two remaining QW dimensions characterized by an effective finite mass $m_{\rm ph}$ (typically 4-5 orders of magnitude smaller than the excitonic
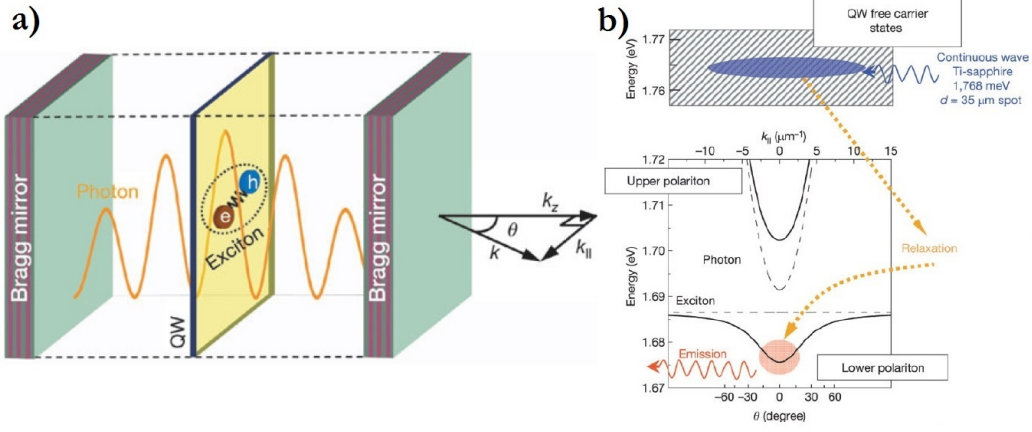
Figure 1.1: Panel a): semiconductor microcavity made of a quantum well and two DBR mirrors: light is injected inside the device by an external drive, and the confined cavity mode can interact with quantum-well excitons by mean of Rabi oscillation processes. Panel b): one can see the two polariton dispersion laws (measured by angle-resolved spectroscopy) arising from the coupling between the photonic and excitonic branches, for a positive detuning $\delta = \omega_{\mathrm{ph}} - \omega_{\mathrm{X}}$. The in-plane momentum k is proportional to the output angle θ of the emitted photon. At high momenta, the lower (resp. upper) polariton branch is almost purely excitonic (resp. photonic) due to the strong detuning between the photon and exciton branches. At lower momenta, the two branches strongly mix the excitonic and photonic degrees of freedom. This panel features also a typical incoherent pumping scheme for exciton-polaritons: the drive generates high energy hole-electron pairs which relax into bounded excitons in the lower polariton branch. Scattering between excitons and acoustic phonons progressively allows the generated exciton reservoir to partially relax toward the bottom of the lower polariton branch. Figure adapted from [99].

one). A toy model Hamiltonian $H = H_0 + H_{\mathrm{int}}$ implementing all these features can be written (in units of $\hbar = 1$) under the form [29]

$$H_0 = \sum_{\mathbf{k}} \left\{ \left[\omega_{\mathrm{X}}(\mathbf{k}) a_{\mathrm{X}}^{\dagger}(\mathbf{k}) a_{\mathrm{X}}(\mathbf{k}) + \omega_{\mathrm{ph}}(\mathbf{k}) a_{\mathrm{ph}}^{\dagger}(\mathbf{k}) a_{\mathrm{ph}}(\mathbf{k}) \right] + \Omega_{\mathrm{R}} \left[a_{\mathrm{X}}^{\dagger}(\mathbf{k}) a_{\mathrm{ph}}(\mathbf{k}) + \mathrm{hc} \right] \right\},$$

$$H_{\mathrm{int}} = \frac{g_{\mathrm{X}}}{S} \sum_{\mathbf{k}, \mathbf{k}', \mathbf{q}} a_{\mathrm{X}}^{\dagger}(\mathbf{k} + \mathbf{q}) a_{\mathrm{X}}^{\dagger}(\mathbf{k}' - \mathbf{q}) a_{\mathrm{X}}(\mathbf{k}') a_{\mathrm{X}}(\mathbf{k}) \tag{1.1}$$

where S is the QW surface, $a_{\mathrm{X}}(\mathbf{k})$ and $a_{\mathrm{X}}^{\dagger}(\mathbf{k})$ (resp. $a_{\mathrm{ph}}(\mathbf{k})$ and $a_{\mathrm{ph}}^{\dagger}(\mathbf{k})$) are the annihilation and creation operators of a single exciton (resp. photon) of momentum $\mathbf{k}$, and $\omega_{\mathrm{X}}(\mathbf{k}) = \omega_{\mathrm{X}} + \frac{\mathbf{k}^2}{2m_{\mathrm{X}}}$ and $\omega_{\mathrm{ph}}(\mathbf{k}) = \omega_{\mathrm{ph}} + \frac{\mathbf{k}^2}{2m_{\mathrm{ph}}}$ are the corresponding excitonic and photonic kinetic energies. Due to confinement the two components of $\mathbf{k}$ are contained within the QW 2D plane. Finally, one has to add the dissipation loss term under the form of a superoperator acting on the density matrix for the photonic and excitonic degrees of freedom:

$$\mathcal{L}_{\mathrm{l}}(\rho) = \frac{\Gamma_{\mathrm{l}}}{2} \sum_{\mathbf{k}} \left[2 a_{\mathrm{ph}}(\mathbf{k}) \rho a_{\mathrm{ph}}(\mathbf{k})^{\dagger} - a_{\mathrm{ph}}(\mathbf{k})^{\dagger} a_{\mathrm{ph}}(\mathbf{k}) \rho - \rho a_{\mathrm{ph}}(\mathbf{k})^{\dagger} a_{\mathrm{ph}}(\mathbf{k}) \right] \tag{1.2}$$

The density matrix dynamics obey then the master equation

$$\frac{d\rho}{dt} = -i\left[\rho, H\right] + \mathcal{L}_{\mathrm{l}}(\rho) + \mathrm{pump\ term} \tag{1.3}$$

where the pump term has not been specified here since it depends on the pump scheme implemented in the experiment.

This simplified model could be subject to further refinements, as it neglects in particular the excitonic losses (usually much slower than the radiative loss [153]), as well as the excitonic fermionic composite nature (which the system does not feel at weak densities) and spin degrees of freedom [41, 161], it already encapsulates most essential features for the understanding of the phenomenology in typical experiments. More details on these topics can be found in [47, 29]

1.1.1.2 Exciton-polaritons in the strong coupling regime

In its more formal form, the strong light-matter coupling regime is defined as $\Omega_R \geq \Gamma_l$: the coupling term dominates losses, and light and matter degrees or freedom are free to perform Rabi oscillations before undergoing decoherence effects. In this regime one needs to re-express the Hamiltonian H_0 in its diagonal form in order to correctly interpret the dynamics

$$H_0 = \sum_{\mathbf{k}} \left[\omega_{LP}(\mathbf{k}) a^\dagger_{LP}(\mathbf{k}) a_{LP}(\mathbf{k}) + \omega_{UP}(\mathbf{k}) a^\dagger_{UP}(\mathbf{k}) a_{UP}(\mathbf{k}) \right]. \tag{1.4}$$

Strong coupling leads to the emergences of two independent quasi-particles mixing photonic and excitonic degrees of freedom called upper and lower polaritons of respective dispersion laws $\omega_{(UP/LP)}(\mathbf{k}) = \frac{\omega_X(\mathbf{k}) + \omega_{ph}(\mathbf{k})}{2} \pm \sqrt{\Omega_R^2 + [\omega_X(\mathbf{k}) - \omega_{ph}(\mathbf{k})]^2}$ (shown in Fig. 1.1, panel b)), splitted by a minimal energy $2\Omega_R$.

Of course loss processes happen in the photonic basis and are not diagonal in the new polaritonic one. However, by definition of the strong coupling, they are not fast enough to couple the two-polaritonic branches which are well separated in energy. Eliminating the coupling to fastly rotating terms in Eq. (1.2), the polaritonic Lindblad loss term can thus be expressed as

$$\mathcal{L}_l^{(P)}(\rho) = \frac{\Gamma_l}{2} \sum_{\mathbf{k}} \left\{ |u_{LP}(\mathbf{k})|^2 \left[2a_{LP}(\mathbf{k}) \rho a_{LP}(\mathbf{k})^\dagger - a_{LP}(\mathbf{k})^\dagger a_{LP}(\mathbf{k}) \rho - \rho a_{LP}(\mathbf{k})^\dagger a_{LP}(\mathbf{k}) \right] \right.$$
$$\left. + |u_{UP}(\mathbf{k})|^2 \left[2a_{UP}(\mathbf{k}) \rho a_{UP}(\mathbf{k})^\dagger - a_{UP}(\mathbf{k})^\dagger a_{UP}(\mathbf{k}) \rho - \rho a_{UP}(\mathbf{k})^\dagger a_{UP}(\mathbf{k}) \right] \right\} \tag{1.5}$$

where $|u_{(UP/LP)}(\mathbf{k})|^2$ is the momentum-dependent photonic fraction of the upper/lower polariton.

Regarding the interaction term such projective operation is less legitimate

If the interaction strength is weak enough in such a way that $g_X n_{(UP/LP)} \ll \Omega_R$, where $n_{(UP/LP)}$ is the upper/lower polaritonic density, a similar argument applies for the Hamiltonian contribution H_{int} with the following subtlety: while the weak interaction condition only precludes non-resonant collisions, still some resonant branch conversion processes (LP+LP→LP+UP) might be energetically allowed by the dynamics. However, the photonic density of state (DOS) is extremely small with respect to the excitonic one (by a factor $\sim 10^{-5}$), and thus scattering processes (LP+LP→LP+UP) between excitons (belonging to the lower polaritonic branch) leading to the formation of upper polaritons have been predicted [186] and verified experimentally [45] to be extremely rare with respect to collisions (LP+LP→LP+LP) : since most experiments [99] are configured for the initial generation of a reservoir of excitons, one can safely project the interaction term on the lower polaritonic branch. By restricting ouserlves for the sake of simplicity to a low-momentum description one obtains for the inter-polariton interactions:

$$H_{int}^{(LP)} = \frac{g_X |v_{LP}^0|^2}{S} \sum_{\mathbf{k},\mathbf{k}',\mathbf{q}} a^\dagger_{LP}(\mathbf{k}+\mathbf{q}) a^\dagger_{LP}(\mathbf{k}'-\mathbf{q}) a_{LP}(\mathbf{k}') a_{LP}(\mathbf{k}), \tag{1.6}$$

where $|v_{LP}(\mathbf{k})|^2 = 1 - |u_{LP}(\mathbf{k})|^2$ is the excitonic fraction of the lower polariton, and $v_{LP}^0 = v_{LP}(\mathbf{k}=0)$.

In addition to this reduced representation of a quantum fluid composed of a single type of interacting particles, subject to dissipative loss processes and refilled by an external pump (not included yet at this point), the effect of longitudinal optical phonons and acoustic phonons might be included in the formalism as they respectively play an important role in the pumping of new excitons and the thermalization of the excitonic cloud. Their impact will be partially discussed in 1.1.2.2. The interested reader can see [46] for more details on this topics.

1.1.2 Non-equilibrium dynamics and thermalization kinetics of exciton-polaritons BECs

There is a well-known connection between Bose-Einstein Condensation, where a macroscopic fraction of a quantum fluid collapses on a single quantum state, and the phenomenon of lasing

where a dynamical instability leads an optical device to break its $U(1)$ symmetry [170]. While a mono-mode optical cavity could be seen as a zero-dimensional object and thus does not really fall into our representation of the thermodynamic limit, the interpretation of lasing in terms of a Bose-Einstein Condensation second order phase transition becomes the most clearest in spatially extended configurations such as vertical surface cavity emitting lasers (VCSEL) [85], where the spontaneous symmetry breaking (SSB) is characterized by the emergence of long range order and temporal coherence:

$$\lim_{|t-t'|,|\mathbf{r}-\mathbf{r}'|\to\infty} \left[g^{(1)}(\mathbf{r}-\mathbf{r}',t-t') \equiv \left\langle \hat{\psi}^\dagger(\mathbf{r},t)\hat{\psi}(\mathbf{r}',t') \right\rangle \right] \neq 0 \tag{1.7}$$

In spite of the close resemblance between the two phenomena, the theory of equilibrium Bose-Einstein Condensation and lasing usually do not fully overlap: unlike atomic gases, a photonic system typically reaches at long times a steady-state presenting non-thermal thermal signatures, as it is determined by the interplay between Hamiltonian dynamics and dissipative effects such as losses, pump and dephasing. While photon-photon interactions are rather negligible in VCSEL devices which in consequence operate in a strongly non-equilibrium regime, this is a priori less clear for exciton-polariton experiments where frequent interparticle collisions might allow the system to thermalize in spite of the effect of its environment. The lattice temperature T_{lat} of the external apparatus is also an important parameter: on one hand, the presence of a finite T_{lat} should favour equilibration by kinetically activating energy exchange processes with the thermalized phononic environment and increasing the collision rates between polaritons and excitons. On the other hand the time scales related as loss processes are rather independent from thermal effects, and thus non-equilibrium are expected to be dominant at lower T_{lat}.

1.1.2.1 Non-equilibrium dynamics of a driven-dissipative Bose-Einstein Condensate

Although the model restricted to a single polariton branch introduced in Sec. 1.1.1 provides a refined quantum description of the dynamics of a driven-dissipative interacting fluid, it is in most cases impossible to treat exactly by mean of modern theoretical and numerical tools. A standard approach providing an accessible framework while keeping simultaneously many important features of non-equilibrium BEC of interacting photons consists in a mean-field description, which takes the form of a driven-dissipative Gross-Pitaevskii [29] for the photonic/polaritonic field $\psi(\mathbf{r},t)$:

$$i\partial_t\psi(\mathbf{r},t) = \left[\omega_0 - \frac{\nabla_\mathbf{r}^2}{2m} + g|\psi(\mathbf{r},t)|^2 \right]\psi(\mathbf{r},t) + i\left[\mathcal{F}_{\text{pump}}[\psi] - \frac{\tilde{\Gamma}_l}{2} \right]. \tag{1.8}$$

Basing ourselves on the polaritonic model of Sec. 1.1.1, the bare frequency ω_0 and the effective mass m can be extracted from the LP dispersion law $\omega_{\text{LP}}(\mathbf{k}) \underset{\mathbf{k}\to0}{\simeq} \omega_0 + \frac{\mathbf{k}^2}{2m}$, $g = |v_{\text{LP}}(\mathbf{k} = 0)|^2 g_{\text{X}}$ is the effective strength of polaritons contact interaction, and $\tilde{\Gamma}_l = |u_{\text{LP}}(\mathbf{k} = 0)|^2\Gamma_l$ is the lower-polariton loss rate. The pump contribution in Eq. (1.8) highly depends on the specific experimental scheme used to inject new polaritons within the system. A frequently used model for the description of the condensate dynamics, which was introduced in [208] and inspired from the semi-classical theory of lasing [94], consists in adding a *"incoherent pumping term"* combined to a saturation effect to the driven-dissipative GP Eq. (1.8)

$$\mathcal{F}_{\text{pump}}^{\text{(incoh)}}[\psi] = \frac{\Gamma_{\text{pump}}/2}{1 + R_{\text{sat}}|\psi(\mathbf{r},t)|^2}\psi(\mathbf{r},t): \tag{1.9}$$

polaritons are injected by an incoherent reservoir of excitons, which is himself refilled in time by mean of an external source. Eq. (1.8) then results from the adiabatic elimination of those additional degrees of freedom. At low polaritonic density $|\psi(\mathbf{r},t)|^2$, the polariton pump rate is given by Γ_{pump}. At higher $|\psi(\mathbf{r},t)|^2$, stimulated emission is reinforced by the presence of already existing polaritons and the reservoir is not refilled fast enough by the external drive so to maintain its pump efficiency: this leads to a saturation effect taking the form of a nonlinear contribution in Eq. (1.9). This pump scheme is called incoherent in the sense that it does not explicitly break the $U(1)$ gauge symmetry. In addition, it is

completely Markovian, in the sense that the photon emission does not depend on frequency. A non-Markovian quantum extension of Eq. (1.8) will be the subject of Chapter 4.

The driven-dissipative GP equation corresponds to the rough classical approximation of a photonic quantum fluid, whose dynamics is reduced to the one of a pure Bose-Einstein Condensate. Such a simplified level of description is expected to be valid in a regime in which the condensate depletion is rather negligible: this implies in particular a low-enough temperature, which is characterized by the absence of noise in Eq. (1.8), and weak enough inter-particle interactions, in such a way that quantum fluctuations can be treated perturbatively. Approaches beyond mean-field such as the truncated-Wigner representation [63] for the quantum field or the quantum Boltzmann equation [178], which are designed for the investigation of small quantum corrections and noise activated depletion of the condensate, allow in particular for the description of the normal phase or the region close the lasing/condensation threshold. Methods based on a truncated hierarchy of equations for the correlators [31] allow for the investigation of higher order quantum deviations, such as the non-Gaussian corrections related to the non-equilibrium counterpart of the atomic Beliaev decay and Landau scattering [156].

Under the assumption of an homogeneous pump Eq. (1.8) presents a uniform steady-state

$$\psi = \psi_{\mathrm{BEC}} e^{i\mathbf{k}_{\mathrm{BEC}} \cdot \mathbf{r}} e^{-i\omega_{\mathrm{BEC}} t}, \tag{1.10}$$

where $n_{\mathrm{BEC}} = |\psi_{\mathrm{BEC}}|^2$ is the condensate density and is reached when pump perfectly compensates with losses, and the condensate frequency ω_{BEC} is blue-shifted with respect to the bare frequency ω_0 due to repulsive interactions:

$$\begin{cases} \tilde{\Gamma}_l = \frac{\Gamma_{\mathrm{pump}}}{1 + R_{\mathrm{sat}} n_{\mathrm{BEC}}} \\ \omega_{\mathrm{BEC}} = \omega_0 + g n_{\mathrm{BEC}}. \end{cases} \tag{1.11}$$

Paradoxically, Eq. (1.8) predicts that Bose-Einstein Condensation is equally likely to occur at any momentum $\mathbf{k}_{\mathrm{BEC}}$, which somehow contrasts with our intuition providing from thermodynamic in the equilibrium case [151], but also with observations in non-equilibrium BEC experiments [99], since also there the system is tempted to minimize its energy due to relaxation effects related to phonon emission. A simple extension of Eq. (1.8) implementing the effect of a non-trivial frequency dependence of the pump was introduced in [209], and confirmed that condensation in the zero-momentum mode $\mathbf{k}_{\mathrm{BEC}} = 0$ indeed led to the highest dynamical stability.

One of the biggest successes of the driven-dissipative GP introduced in [208] (along with [209]) has been to predict the photoluminiscence spectrum

$$\omega_{\mathrm{BOG}}^{\Gamma}(k) = -i\frac{\Gamma}{2} \pm \sqrt{\frac{k^2}{2m}\left(\frac{k^2}{2m} + 2g n_{\mathrm{BEC}}\right) - (\Gamma/2)^2} \tag{1.12}$$

of the elementary excitations on top of the condensate (show in Fig. 1.2). Hints toward an experimental confirmation can be found in [196]. The non-standard spectral profile (1.12), which can be obtained from Eq. (1.8) by mean of Bogoliubov linearization procedure, possesses significantly different features with respect to the isolated case of equilibrium BECs [151] in cold atomic gases

$$\omega_{\mathrm{BOG}}^{\mathrm{iso}}(k) = \lim_{\Gamma \to 0} \omega_{\mathrm{BOG}}^{\Gamma}(k) = \pm\sqrt{\frac{k^2}{2m}\left(\frac{k^2}{2m} + 2g n_{\mathrm{BEC}}\right)}. \tag{1.13}$$

The non-trivial parameter $\Gamma \equiv \frac{\Gamma_{\mathrm{pump}} R_{\mathrm{sat}} n_{\mathrm{BEC}}}{(1 + R_{\mathrm{sat}} n_{\mathrm{BEC}})^2}$ arises from a subtle interplay between dissipation and the pump saturation. At high momenta $k \gg k_0$, the real part $\mathrm{Re}[\omega_{\mathrm{BOG}}^{\Gamma}(k)]$ of the excitation spectrum converges toward the prediction for the isolated case.

The most spectacular change in behaviour occurs below a critical momentum k_0 verifying $\omega_{\mathrm{BOG}}^{\mathrm{iso}}(k_0) = \Gamma/2$, where the excitation spectrum becomes purely imaginary ($\mathrm{Re}[\omega_{\mathrm{BOG}}^{\Gamma}(k)] = 0$) and the corresponding imaginary parts split. The first mode is a massive one ($\omega_{\mathrm{BOG}}^{\Gamma}(k) \underset{k \to 0}{\to} \Gamma$) and is related to amplitude fluctuations: this mode characterizes the time scale needed for relaxation of intensity fluctuations in analogy with a laser [131], and does not have any
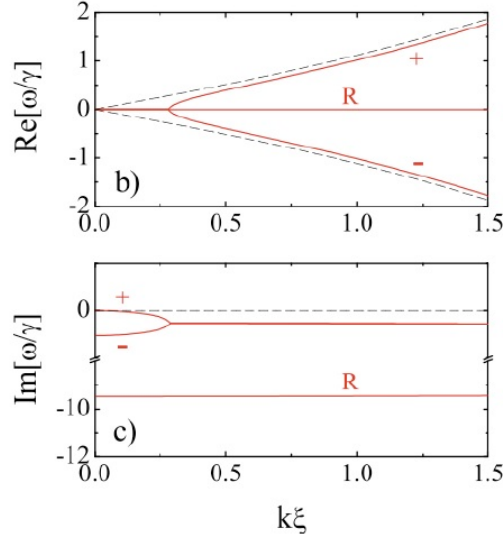
Figure 1.2: Excitation spectrum of an incoherently pumped driven-dissipative Bose-Einstein Condensate. The branches labelled (+/-) represent the BEC modes, and the branches labelled (R) correspond to additional relaxation modes of the reservoir degrees of freedom. Adpated from [208].

equivalent in the equilibrium isolated case for which density is fixed. The second mode is a Goldstone soft mode tending to zero at low momenta (in analogy with the phononic excitations in isolated BECs [151]), and is related to the underlying $U(1)$ symmetry of our model: as a global change in phase can not lead to any relaxation, likewise long range phase modulation take a very long time to damp. The Goldstone mode can also be related in quantum optics to the phase relaxation dynamics in a single-mode laser induced by the zero-point quantum fluctuations, and the corresponding damping time τ_{coh} is determined by the so-called Schawlow-Townes [167] linewidth (above the lasing threshold, τ_{coh} is usually much longer than the decay related to intensity fluctuations): while in a monomode laser τ_{coh} is typically finite, here long time phase coherence is made possible by the extended spatial geometry and one has $\tau_{coh} \to \infty$.

In addition to the exotic structure for excitation spectrum of Eq. (1.12), many other effects contrasting with the equilibrium case of isolated quantum gases have been predicted to derive from the model (1.8), such as the possibility for a moving impurity to feel a non-zero drag force at arbitrary speed even in the superfluid regime [209, 3], which is very counter-intuitive in the usual equilibrium representation of superfluidity based on Landau criterion [151]. Other studies [176, 177, 2, 199, 80] applied renormalization group (RG) methods to the study of a stochastic version of Eq. (1.8) including additional (experimentally unavoidable) classical noise, and the long range phase dynamics was connected the Kardar-Parisi-Zhang (KPZ) equation [71] (which was historically employed to describe the non-equilibrium classical dynamics of growing surfaces): in three dimension $d = 3$, the critical dynamics were shown to be altered with respect to the equilibrium case and a novel critical exponent accounting for these features was introduced in [176], although the underlying driven-dissipative nature of the dynamics appears not to lead to major changes in the long range properties of the condensed and normal phase at a static level. However, the most striking behaviour occurs in $d = 1$ [80] and $d = 2$ [2], where the KPZ equation is predict to build strong correlations, and even nearly vanishing deviations from equilibrium are amplified at long distances. When in $d = 2$ the KPZ description is completed by the inclusion of (unavoidable) topological defects, the physics is modified in an even more dramatic manner [199]: the Berezinsky-Kosterlitz-Thouless (BKT) transition [130] was then shown to be severely compromised by a long-range phenomenon of vortex unbinding occurring at an even smaller length scale with respect to the KPZ deviations.

While, the simplified GP description introduced here allows to catch important properties of a driven-dissipative Bose-Einstein Condensate, and would represent quite accurately the

dynamics of simple microscopic models [35, 88], in exciton-polariton experiments it should be completed by a refined description of the polaritonic environment: indeed the complex non-Markovian nature of the polaritonic pump, related to the frequency-dependent scattering processes by excitons and thermal phonons, is known to play a major role regarding the possibility of formation of a polariton BEC and the emergence of a thermal signature [185, 100]. Kinetic methods based on semi-classical Boltzmann equations have been developed in order to describe the environment-induced transfer of exciton and polariton populations [186, 129, 153], although they somehow lose information on the wave effects related to the underlying quantum nature of the problem, and fail in particular to describe the emergent Bogoliubov spectrum in the condensed regime. More advanced quantum kinetic methods [79, 78] mixing the advantages of both approaches have been developed recently in order to account for both quantum effects and exchange processes with the reservoir. This rather novel approach, which obviously leads to more complexity, has been used up to now to re-derive known results (such as the classical driven-dissipative GP equation) and has not brought yet new contributions, although it could prove helpful in the future. In Chapter. 4 we will present a simpler non-Markovian quantum Langevin formalism, similar to the one used in [35], which encapsulate both the effect of noise and quantum dynamics. Our approach, which is developed in the Bogoliubov regime and thus strongly relies on the hypothesis of a rather weak depletion of the non-equilibrium BEC, allows to compute the resulting non-equilibrium Bogoliubov spectrum while keeping information on the environment/interaction-induced quantum and classical fluctuations.

1.1.2.2 Exciton-polariton BEC experiments: thermal versus non-equilibrium signatures

Thanks to their extremely low mass (10^9 times smaller than atomic ones) and their resulting very weak density of states, photons and polaritons in confined geometries are able to enter the quantum degeneracy regime at uniquely high temperatures, ranging from cryogenic temperatures with an apparatus cooled at a few Kelvin in the precursors works [99, 9, 7], until the more recent observations of room temperature Bose-Einstein Condensation in exciton-polaritons [101, 152] in different kind of materials and purely photonic experiments [108, 109]. The criterion determining whether a defined material allows to maintain the strong light-matter coupling at high temperature is related to the excitonic binding energy E_X: while QWs based on organic materials, polymers and some semiconductors such as GaN have been shown to present very high E_X allowing for the presence of strongly bounded excitons resisting to an high level of thermal fluctuations, in semiconductors like GaAs or CdTe presenting a weaker E_X, excitons get quickly converted into free hole electron pairs at temperatures of the order of $50K$.

The first BEC experiments [6, 66, 172] with exciton-polaritons were based on a 'coherent drive' scheme and were not suited for the study of spontaneous symmetry breaking (SSB) and the observation of a true phase transition toward a Bose-Condensed state: light was injected within the apparatus by mean of an external laser drive with a perfectly defined phase and frequency at the bottom of the lower polariton branch, inducing automatically the presence of a $\mathbf{k} = 0$ condensate. The first observation of SSB was reported in [181, 11] in the different 'optical parametric oscillator' (OPO) scheme: in this configuration photons are coherently injected close to the inflexion point of the lower polariton branch and resonant scattering processes lead to the formation of a $k = 0$ signal and an additional idler signal at higher momentum [165, 39, 133, 166]. Above a certain threshold for pump intensity stimulated scattering ultimately leads to a dynamical instability where the $k = 0$ and idler signals enter a coherent state with a randomly chosen relative phase. The wave superposition between the various momenta leads to the presence of moving fringes in the parametric instability regime [28]. OPO schemes can also lead to more complex non-linear hydrodynamic behaviours such as vortex-anti vortex pairs or more complex density patterns [18, 204].

Due to the direct resonant injection of polaritons inside the lower polaritonic branch, the OPO experiments usually present strong non-equilibrium signatures. Here we will set the focus on the next generation of experiments [99, 9, 7] based on a gauge invariant incoherent pump scheme analogous to the one presented in Eq. (1.9), which usually present a closer connection with equilibrium physics. The first BEC observation in this configuration was reported in [99]: as shown in Fig. 1.1 (panel b)), in the scheme used in [99], which has
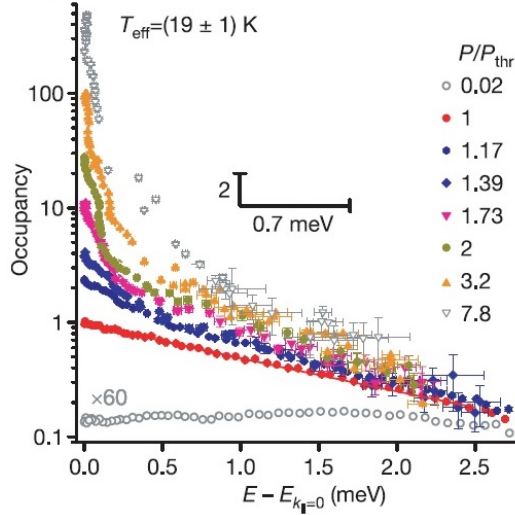
Figure 1.3: Polariton occupancy in function of the energy for various pump intensities P measured at fixed detuning δ and lattice temperature $T_{\text{lat}} = 5K$: at low pump intensities, one can see that the distribution is not thermal, while at pump intensities above the pump threshold P_{th} the distribution fits well with a Bose-Einstein distribution at temperature $T_{\text{eff}} = 19K$. Figure adapted from [99].

been then reproduced in many other experiments, an external drive is responsible for the generation of high energy electron-hole excitations which fastly relax into excitons by mean of the emission of longitudinal optical (LO) phonons. Interactions between excitons and low-energy acoustical phonons are responsible for the thermalization of the excitonic reservoir (namely the high momentum part of the lower polariton branch which is mostly excitonic) and for populating the bottom of the LP branch close to $\mathbf{k} = 0$ (which contains an higher photonic fraction, and thus is subject to faster losses) where the condensate will be formed.

At weak pump intensities, due to their fast decay, polaritons in the bottom of the branch are almost not populated. Above a certain pump intensity, polaritons start to accumulate around the $\mathbf{k} = 0$ momentum mode and the level of quantum degeneracy increases, leading to stimulated scattering. Ultimately above a pump threshold P_{th} (typically one order of magnitude smaller than the threshold for conventional photonic lasing, as the lasing/BEC instability in those these experiments does not rely on an inversion of population, due to a similar mechanism to [134]), a sharpening in the emission spectrum linewidth and in the momentum distribution are observed and the emergence of long-range correlations is confirmed by an interferometry procedure, indicating the formation of a Bose-Einstein Condensate, i.e., the onset of polaritonic lasing. Of course, due to the underlying bi-dimensional nature of the quantum fluid a true long-range order is never observed [137], but quasi-long range decaying behaviours of correlations such as algebraic order were not observable in the first experiments due to the finite size of the polaritonic cloud.

In Kasprzak work [99] and other low-T experiments [9, 7], equilibrium signatures were observed in the condensed phase, where the polariton occupancy takes the form of a Bose-Einstein distribution at a temperature T_{eff} differing from the lattice apparatus temperature T_{lat} (see Fig. 1.3). At lower pump intensities, the reduced scattering rate induced by the weak polaritonic/excitonic density has been shown to lead to poor thermalization and non-equilibrium signatures. Our goal will not be to provide a complete discussion of the microscopic origins of thermalization in exciton-polariton BEC experiments with incoherent pump schemes, as this question is still matter to an active debate in the community: indeed, although most early theoretical studies and experimental interpretation only involved the scattering by acoustic phonons and excitons in order to describe the equilibration dynamics, subsequent experimental evidence was found in [132] that the scattering processes assisted by LO phonons of excitons into the lower polariton branch might be a dominant relaxation channel. Due to the lack of theoretical material on this topic and for simplicity purposes we will not involve LO phonons in our description (although we will analyse in Sec. 4.4.1.3
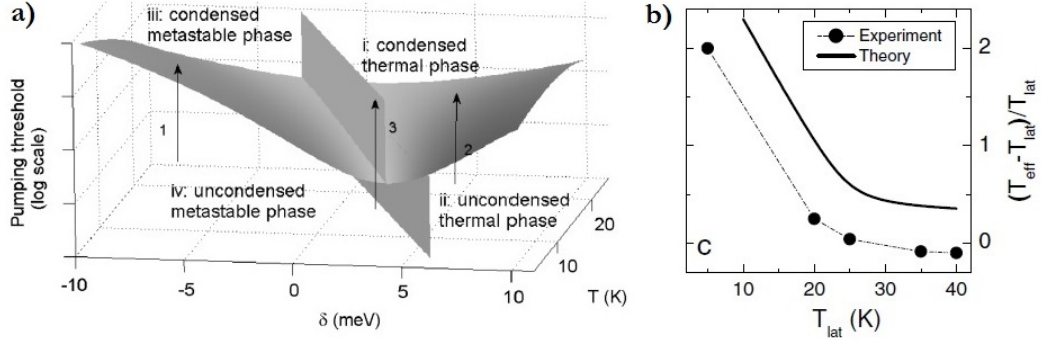
Figure 1.4: Characterization of the efficiency of equilibration in exciton-polariton BEC experiments. Panel a): phase diagram of incoherently pumped exciton-polaritons in function of the temperature T_{lat}, the detuning δ and the pump intensity P. The authors chose to call *metastable* a state which can not be described at all by a thermal state. Panel b): discrepancy $\frac{T_{\text{eff}} - T_{\text{lat}}}{T_{\text{lat}}}$ between the effectively measured polaritonic temperature and the lattice temperature, at a fixed positive detuning $\delta = +0.26\Omega_R$. For this positive detuning, the polariton distribution presents a thermal signature at any T_{lat}. Adapted from [100].

what could be the impact of a LO phonon-assisted polariton relaxation model, and show how this might lead to the emergence of artificial thermal properties). Instead we will try to build a synthesis of the first generation of theoretical studies and experimental observations. We will base our discussion especially on a work [100] by Kasprzak. et al., which investigated experimentally the efficiency of thermalization and its dependence on T_{lat} and on the detuning $\delta = \omega_{\text{ph}} - \omega_{\text{X}}$ between the uncoupled photonic and excitonic branches. For more developments the interested reader might look at [46, 29].

The phase diagram of incoherently pumped exciton-polaritons is shown in Fig. 1.4 (panel a)) in function of δ, T_{lat} and the pump intensity P. The authors chose to call *'metastable'* a phase which does not present any thermal signature. First, for positive δ and low temperatures ($T_{\text{lat}} = 5 - 30\,K$), the photonic fraction is relatively weak and loss processes are expected thus to occur on a rather long time scale, comparable with the scattering processes of excitons by acoustic phonons (occurring on a time scale $\simeq 1\,ns$) which, along with exciton (X-X$\rightarrow$ X-LP) scattering processes [153], play a part in the emergence of a BEC. While below the BEC/lasing pump threshold the equilibration kinetics is not yet fast enough in this range of temperatures to allow for thermalization of the polaritonic cloud, at the onset of lasing stimulated scattering induced by quantum degeneracy allows to complete the equilibration process and a Bose distribution is generally observed within the BEC phase, as shown in the panel. However, the effective temperature T_{eff} is generally found to be higher than T_{lat} (Fig. 1.4, panel b)), possibly due to several heating effects on the excitonic reservoir such as excitonic injection processes ($h - e^- \rightarrow X - $LO phonon) by the incoherent pump [153].

Secondly, for negative δ and the same temperature range, the photonic fraction becomes significant and losses in the bottom of LP branch increase dramatically (at a time scale of the order of $1\,ps$). A 'relaxation bottleneck' has been highlighted in early theoretical and experimental works [185, 184] in the momentum region where the photonic fraction starts to increase: for $\delta < 0$ scattering processes by acoustic phonons are far too weak to populate the $\mathbf{k} \simeq 0$ region and generate a BEC. Instead direct scattering processes (X-X$\rightarrow$ X-LP) by the excitonic reservoir have been shown in [186, 153] to occur on a shorter time scale at high enough excitonic density, fast enough to populate significantly the polaritonic branch and trigger the BEC transition. The system however does not present anymore a thermal signature (even in the BEC regime) for these temperatures due to the strong non-equilibrium kinetic effects induced by losses.

Finally, at higher temperatures ($T_{\text{lat}} = 30 - 300\,K$) the previously mentioned relaxation bottleneck is suppressed: the thermal occupation of the phononic reservoir has for effect to stimulate the scattering processes of lower exciton-polaritons by acoustic phonons, which can then relax toward the bottom of the branch by dissipating energy into the lattice without requiring (X-X$\rightarrow$ X-LP) collisions. In this regime, thermalization is thought to be almost

completely assisted by acoustic phonons for any choice of detuning, and the measured temperature coincides then with the lattice one ($T_{\text{eff}} \simeq T_{\text{lat}}$), since the fast energy exchange processes between the excitonic and the phononic reservoirsz completely wash out heating effects induced by the pump.

In addition to exciton-polaritons, room-temperature BEC was observed also in purely photonic platforms [108] in absence of inter-particle interactions: there the associated mechanism for relaxation and the onset of coherence was related to energy exchange with a thermal bath of dye molecules. The emergence of a thermal signature was observed in [109] and the kinetic dynamics of equilibration was characterized in [169]. The theoretical analysis was provided in [107, 105, 106] and highlighted also in these experiments the role played by the external temperature. More recently, the formation of a true bi-dimensional photonic BEC in an harmonic trap was reported in [44] and the excellent agreement with thermodynamic predictions was confirmed.

1.1.3 Concluding remarks and motivations

We have reviewed the physics of the non-equilibrium Bose-Einstein Condensation of exciton-polaritons. After a brief reminder of the microscopic physics of exciton-polaritons, we have introduced the driven-dissipative Gross-Pitaevskii equation which allows to describe the photoluminescence spectrum of the elementary excitations of an incoherently pumped BEC. The last part of this section was dedicated to the kinetic mechanisms involved in the emergence of a BEC and thermal signatures in experiments involving an incoherent pumping. In particular, the role of exciton-exciton scattering and acoustical phonons in the emergence of thermal signatures has been described. Some controversial studies suggesting that longitudinal optical phonons might actually play a dominant part in some configurations were mentioned.

Apart from a few studies [209, 162, 25], the impact of non-Markovianity [21], which arises when a quantum system is coupled to a complex environment presenting some memory effects, has been the object of little direct attention in the exciton-polaritons community up to now. While non-Markovian effects are somehow implicitly included in most theoretical descriptions of the semi-classical kinetics of exciton-polariton condensation under the form of frequency-dependent transfer rates [153, 129] and thus strongly contribute to the emergence of thermal signatures steady-state, a full quantum description of an out-of-equilibrium non-Markovian BEC still remains to provide. This would be necessary inorder to correctly describe the non-equilibrium Bogoliubov spectrum, as dissipation and the frequency selectivity of polariton emission or loss processes could affect the low-energy relaxation dynamics of the BEC elementary excitations. In addition, the spectral broadening induced by dissipation, and its interplay with non-Markovian effects, might not allow to compute the exact correlation functions in the steady-state directly by mean of a (too) simple classical rate approach, which thus excludes the possibility of accessing the energy or momentum distribution.

In Chap. 4 we present our first contribution to these research lines by developing a a simplified but already fully quantum and non-Markovian model for a weakly interacting BEC. The formalism, based on a rather transparent quantum Langevin equation, allows simultaneously in the Bogoliubov regime to address dynamical effects such as the relaxation modes of the condensate, and to access information on quantum and classical fluctuations induced by interactions and the external noise. In particular, following a preliminary result in Sec. 2.4, we unveil an alternative mechanism leading to the apparent emergence of an equilibrium signature in an open quantum system in contact with several non-Markovian non-equilibrated reservoirs.

1.2 Strongly correlated photons in cavity arrays

This section draws an overview of the physics of strongly interacting photons. One of the long-standing goals in that research area is the stabilization of strongly correlated phases such as the Mott Insulator of Fractional Quantum Hall states, which have been only observed by now in an equilibrium context and never in driven-dissipative photonic platforms. We will briefly describe some of the various platforms and explain how they allow to engineer

photonic Hamiltonians suited for the investigation of strong correlations. We will then move to the dissipative case where a drive of some kind has to be included in order to refill the many-body state: after reviewing the widely studied coherent drive scheme and explaining why it does not allow to stabilize incompressible quantum phases, we will present the most recent theoretical proposals in that direction.

1.2.1   Photon Blockade

An essential step toward the stabilization of strongly correlated photonic fluids consists in reaching the so-called *"photon-blockade"*, where photons start behaving as impenetrable particles. More specifically, a single-mode photonic device, such as an optical cavity or microwave resonator, is said to be in the blockade regime whenever the optical nonlinearity $U/\hbar = \omega_{2,1} - \omega_{1,0}$ ($\omega_{N,N-1}$ being the transition frequency between the $N-1$ and N-photon Fock states) is much larger than the total dissipative linewidth Γ_{diss} (which sums all dissipative contributions, like losses, dephasing, pump etc.): the transition frequencies $\omega_{1,0}$ and $\omega_{2,1}$ for the injection of a first photon and a second one are shifted with respect to each other and well separated spectrally. In this regime a coherent laser field tuned on $\omega_{1,0}$ will be able to inject a single photon, but the entrance of a second one will be strongly inhibited since the corresponding process is non-resonant with the drive frequency.

The photon blockade, whose concept was first introduced in [86], was reached in many experimental contexts ranging from optical cavity QED [13], quantum dots [55, 157], microwave superconducting circuits [116], propagating photon beams coupled to a gas of Rydberg EIT atoms [155, 147]. Here we briefly describe the cavity QED and circuit QED platforms and then move to the discussion of the Jaynes Cummings model, which is the most simple theoretical model allowing to describe the emergence of photon blockade from the light-matter interaction. More extended discussion of cavity/circuit QED experimental platforms can be found in [127, 158, 75, 48, 40, 68]. The quantum simulation of many-body physics with strongly interacting photons in of circuit QED and cavity QED lattices is reviewed in [77, 192, 84, 144]

1.2.1.1   Cavity and circuit QED

Cavity QED studies the strong coupling dynamics between matter and light degrees of freedom in confined geometries. The fundamental contributions of Haroche and Wineland [75] allowed to gain unprecedented control on the quantum coherence properties of very small systems composed of a few atoms and photons.

In the first generation of experiments, photons are confined in a cavity consisting in a set of superconducting mirrors with very low transparency and absorption rate, and atoms are responsible for the nonlinear properties of the quantum optics device. While in exciton-polariton experiments the strategy for boosting photon-photon interactions was based on developing semiconducting materials with high $\chi^{(3)}$ optical nonlinearities (see Sec. 1.1), in cavity QED experiments these platforms also benefit of another essential contribution related to a much higher mirror confinement: in contrast with the vacuum configuration, each single photon can repeatedly interact with the embedded atoms due to its numerous roundtrips within the resonator, and the corresponding cross-section $\sigma = \mathcal{F}\sigma_0$ is strongly enhanced with respect to its vacuum counterpart σ_0 [54]. Indeed, the cavity finesse $\mathcal{F}$, which measures the quality of the optical device, and quantifies how many times light can bounce against the cavity mirrors before being absorbed or lost by transparency, can typically reach extremely high values [104] ($\sim 10^7$ with respect to $10^2 - 10^4$ in exciton-polariton experiments).

Over the last two decades, circuit QED platforms [68] (i.e., superconducting circuits) have emerged as an integrated analogue of Cavity QED. The basic elements of a circuit QED experiment are a transmission line resonator and a qubit (replacing respectively the photonic cavity and the atom) made of a superconducting material, and can be coupled to each other/driven by an external voltage source by mean of capacitive couplings [14]. The transmission line resonator is an effective LC quantum circuit, i.e., an harmonic oscillator hosting quantized electromagnetic excitations (microwave photons). While many architectures can be chosen to represent a qubit (i.e. an artificial atom) [40], the Cooper Pair Box (CPB) is probably one of the most representative examples: made of two-superconducting islands weakly coupled by tunnel effect, the CPB forms a Josephson junction which can be

described by two conjugate quantum variables, namely the charge imbalance $\Delta \hat{Q}$ and the order parameter dephasing $\Delta \hat{\phi}$ between the two electronic reservoirs. Due to the 2π periodicity in the dephasing potential $U(\phi)$ between the islands, this circuit element possesses strong nonlinear properties, and under suited conditions it can be well approximated by a two-level system linearly coupled to the resonator photonic mode.

Progressive improvements in the state-of-the art in both cavity and circuit QED allowed to limit decoherence effects and reach a level of isolation effects sufficient to perform quantum information tasks [127, 48], while maintaining simultaneously the ability to manipulate the quantum state of the system and extract information from it. Recently, the possibility of coupling several cavity QED and circuit QED elementary blocks into lattices has opened the possibility of investigating the quantum many-body physics of strong correlations [76, 84].

1.2.1.2 Jaynes-Cummings model

Cavity QED and Circuit QED architectures can be well described by the Jaynes-Cummings model [68], which encapsulates the most essential features of those complex setups into the form of a reduced quantum optics system, made of a single photonic mode interacting with a two-level (artificial-)atom:

$$H_{\text{JC}} = \omega_0 a^\dagger a + \omega_{\text{q}} \sigma^+ \sigma^- + g(\sigma^+ a + \sigma^- a^\dagger). \tag{1.14}$$

Here, ω_0 (resp. ω_{q}) is the frequency of the uncoupled photonic mode (resp. atomic transition frequency), and g is the strength of the light-matter coupling. This Hamiltonian is exactly solvable as it conserves the total excitation number $N = a^\dagger a + \sigma^+ \sigma^-$ [1]. Similarly to the case of semiconductor exciton-polaritons, once diagonalized the Hamiltonian, the photonic and atomic degrees of freedom are mixed into two polaritonic branches

$$
\begin{aligned}
|N, +\rangle &= \cos(\theta_N) |N - 1, e\rangle + \sin(\theta_N) |N, g\rangle \\
|N, -\rangle &= -\sin(\theta_N) |N - 1, e\rangle + \cos(\theta_N) |N, g\rangle \\
E_{N,\pm} &= N\omega_0 + \frac{\Delta}{2} \pm \frac{1}{2}\sqrt{4g^2 N + \Delta^2}
\end{aligned}
\tag{1.15}
$$

where $\Delta = \omega_{\text{at}} - \omega_0$ and $\tan(2\theta_N) = 2g\sqrt{N}/\Delta$. N represents the number of excitations in the system, and the notation $|N, g\rangle$ (resp. $|N - 1, e\rangle$) refers to the state containing N (resp. $N - 1$) photons where the two-level system is in the fundamental (resp. excited) state.

While the zero-detuning case $\Delta = 0$ is of high interest, as this choice of detuning is expected to provide the biggest optical nonlinearities, it is also more complex as it maximally mixes the photonic and atomic degrees of freedom. We will instead focus on the simpler configuration of a strong detuning, which will present more important analogies with the equilibrium framework in which the Mott Insulator physics was historically studied [59]. In the regime $\Delta \gg g$, the branch structure becomes:

$$
\begin{aligned}
|N, +\rangle &\simeq |N - 1, e\rangle \\
|N, -\rangle &\simeq |N, g\rangle \\
E_{N,\pm} &\simeq N\omega_0 + \frac{\Delta}{2} \pm \left(\frac{\Delta}{2} + \frac{g^2}{\Delta} N - \frac{g^4 N^2}{4\Delta^3} \right)
\end{aligned}
\tag{1.16}
$$

In this simple configuration, matter and photonic degrees of freedom nearly do not mixed and are well separated in energy. In particular the photonic branch $|N, g\rangle$ leads to the single site effective photonic Bose-Hubbard Hamiltonian

$$H_{\text{ph}}^{\text{eff}} = \tilde{\omega}_0 a^\dagger a + \frac{U}{2} a^\dagger a^\dagger a a, \tag{1.17}$$

where the cavity frequency $\tilde{\omega}_0 = \omega_0 + \frac{g^2}{\Delta}$ has been shifted by the presence of the atom, and the higher order term in the expansion gives rises to a positive Kerr nonlinearity $U \simeq \frac{g^4}{2\Delta^3}$ which represents effective photon-photon repulsive interactions. The photon blockade condition translates then into $\frac{g^4}{2\Delta^3} \gg \Gamma_{\text{diss}}$.

---

[1]this would not be the case in the ultra strong coupling regime [37, 38], where counter-rotating term need to be included and virtual photons can be created starting from a configuration where the EM field is in vacuum and the atom in the fundamental state
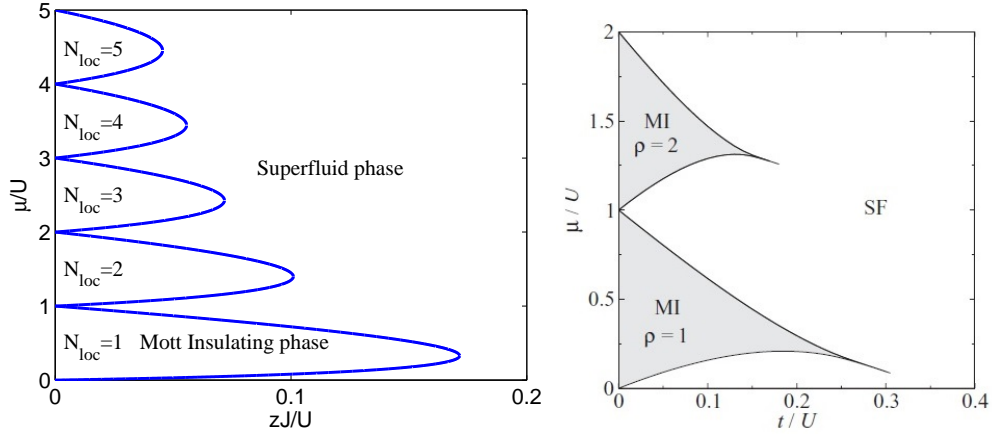
Figure 1.5: $T = 0$ equilibrium phase diagram of the Bose-Hubbard model. Left panel: Mean-Field phase diagram computed analytically in [59]. $z = 2d$ is the number of nearest neighbours of each lattice site, and d is the spatial dimension. Right panel: phase diagram for the 1D configuration computed exactly in [52] by mean of density matrix renormalization group (DMRG) simulations. Here $t = J$ is the tunneling constant. Right panel adpated from [52]

1.2.2 Isolated case: Mott-to-Superfluid transition

The Jaynes-Cummings single site physics described below serves as a building block for the investigation of the dynamic of strongly correlated photons [77, 84]: by setting ourselves in the previously described strong detuning regime $\Delta \gg g$ and coupling several of those units into a lattice structure, one is able to engineer a many-body photonic system whose Hamiltonian dynamics overlaps with the Bose-Hubbard (BH) model on a lattice

$$H_{\text{ph}}^{\text{BH}} = \sum_i \left[-\mu a_i^\dagger a_i + \frac{U}{2} a_i^\dagger a_i^\dagger a_i a_i \right] - J \sum_{\langle i,j \rangle} \left[a_i^\dagger a_j + hc \right]. \quad (1.18)$$

In optical cavities, the tunneling term takes place because of a finite overlap between the neighbouring cavity modes. In circuit-QED, it can be implemented by capacitively coupling adjacent transmission lines [84, 60]. In the latter platform, more complex terms such as a coupling to the nearest neighbour or long-range hopping [14] can be implemented. While the next subsection will focus on the non-equilibrium effects induced by dissipation, here we briefly review the well-known physics of the equilibrium BH model: we assume an isolated lattice in such a way that all the dynamics is provided by the Hamiltonian contribution given in Eq. (1.18).

The zero temperature phase diagram of such a model (shown in Fig. 1.5 in different geometries, and whose derivation in the mean-field regime can be found in App. A) has been studied in [59] and predicts the existence of two quantum phases separated by a quantum phase transition: the first one, called the Mott-Insulator, is incompressible, and the second is of a superfluid nature. The phase boundary is organizedas a series of 'lobes' whose internal parts contain the insulating regions, and the external part the superfluid one. Underlying the quantum phase transition is a commensurability effect between the lattice site and the particle number, associated to the effect of strong interactions: in the Mott phase, which presents an integer density $n = 1/2/3....$, the strong interaction blockade prevents particles to delocalize and is thus an obstacle to the generation of a long-range (or quasi long-range) order. The transition toward the superfluid phase can be driven either by adding extra-particles/holes leading to an incommensurate density, which is essentially induced by a change in the chemical potential μ, or by increasing the ability of particles to delocalize in spite of the blockade interaction U, which is done by increasing the tunneling constant J. These two types of quantum phase transitions belong to different universality classes [59, 51]: the one driven by a commensurability effect occurs at a generic point of the lobe (except the tip), while the other one driven by the quantum competition between tunneling

and interaction occurs precisely at the tip of the lobe.

While the phase diagram shown in Fig. 1.5 (left panel) results from a mean-field (MF) approach (which corresponds to the limit $z \to \infty$ where z is the number of nearest neighbors), the MI-SF transition has been predicted to be maintained for any spatial dimensions d: while in $d = 2, 3$ [27, 26] the superfluid region is accompagned by the emergence of a Bose-Einstein Condensate and is characterized by the presence of long-range order $\phi = \langle a_i \rangle$, in $d = 1$ [114, 52] only algebraic order subsists and the $T = 0$ phase transition is connected to the BKT (Berezinsky-Kosterlitz-Thouless) physics of a two-dimensional Bose system at finite temperature [111]. In the latter case, the shape of the phase boundary is significantly altered with respect to MF predictions, as shown in the right panel of Fig. 1.5.

Historically, the concept of Mott-Insulator was first introduced in a fermionic context by Neville Francis Mott in [138] who explained why, due to the blockade effect related to electronic interactions, certain materials predicted to be metallic by the band theory could not actually conduct electricity. The bosonic counterpart of the MI was successfully observed much more recently in ultra-cold atomic gases trapped in optical lattices in several geometries [70, 179, 182], and its transition toward the superfluid phase was characterized at the single atomic level in [8]. In the non-equilibrium photonic context it still represents a hot challenge: as we will see in the next subsection, the presence of dissipative losses highly complexifies the simple equilibrium description introduced here.

One finally mentions that the physics of the Mott-to-superfluid transition is not restricted to the Bose-Hubbard model: the multi-site extension of the Jaynes-Cummings model, namely the Jaynes-Cummings Hubbard (JCH) model, has been predicted to feature a very similar phase diagram [69, 4] also in the polaritonic configuration of zero detuning $\Delta = 0$, where atomic and photonic degrees of freedom are strongly coupled. Another variation consists in coupling the photonic modes of the various sites to anharmonic oscillators instead of two-level systems. This configuration, which naturally arises in lattices of semiconducting micropillars when strongly coupling a single cavity mode to an excitonic excitation [1], can also be realized in circuit-QED platforms by using qubits configured in the transmon regime [68]. Although the BH and the JCH model have been found to belong the same universality classes [110, 82], they generally do not overlap as the JCH model rather maps onto a two-species BH model. A comparative study [72] pointed out observables allowing to distinguish the two models, and identified the regime of parameters where they do instead overlap.

1.2.3 Driven-dissipative case

We now move to the more realistic driven-dissipative framework, where loss processes and the drive responsible for the injection of new photons inside the setup are not neglected anymore. Due to decoherence effects induced by the environment, the dynamics of the density matrix ρ is not Hamiltonian and can be described instead, e.g, by a quantum master/Redfield equation

$$\partial_t \rho = -i \left[H_{\mathrm{ph}}, \rho \right] + \mathcal{L}_{\mathrm{l}}[\rho] + \mathcal{L}_{\mathrm{pump}}[\rho], \tag{1.19}$$

where a Lindblad contribution

$$\mathcal{L}_{\mathrm{l}}[\rho] = \frac{\Gamma_{\mathrm{l}}}{2} \sum_i \left[2a_i \rho a_i^\dagger - a_i^\dagger a_i \rho - \rho a_i^\dagger a_i \right] \tag{1.20}$$

allows to implement the effect of losses. The term $\mathcal{L}_{\mathrm{pump}}[\rho]$ is left unspecified as we will study the effect of several class of pump schemes.

We will focus first on the simplest scheme consisting in a coherent drive. As we will see this scheme is not suited for the purpose of stabilizing incompressible quantum phases and thus we will move to more recent promising proposals involving non-Markovian engineered reservoirs, such as frequency-dependent pump schemes or the proposal of engineering artificial chemical potential by mean of a modulated coupling to a thermal environment. Even though such strategy has emerged only very recently in the context of the many-body physics with light, the potential quantum reservoir engineering, which consists in building a specific architecture designed to simulate the effect of some desired dissipative (Markovian or non-Markovian) quantum Liouvillian superoperator, has already been explored in many physical situations: at the level of a few particles, it can be useful in order to protect from decoherence

effects a superposition between two quantum states at a few particle level [140, 96], or to generate stable entanglement [200, 203]. In cold atoms, its use has been suggested in order to explore novel out-of-equilibrium competing effects between dissipative and hamiltonian dynamics [50].

1.2.3.1 Coherent pump

We first briefly review the case of a coherent pump which has been most widely addressed in the litterature [30, 192, 193, 115, 125]. In this case $\mathcal{L}_{\mathrm{pump}}(t)[\rho] = -i\left[H_{\mathrm{coh}}(t), \rho\right]$ represents a time-dependent additional Hamiltonian contribution

$$H_{\mathrm{coh}}(t) = F \sum_i \left[e^{i\omega_{\mathrm{L}} t} a_i + e^{-i\omega_{\mathrm{L}} t} a_i^\dagger \right], \tag{1.21}$$

which can be obtained physically by directly driving the system with a coherent/classical signal (e.g., a monochromatic laser field in the optical configuration [29, 76], or a capacitively coupled external voltage source in the circuit-QED platform [14, 60]).

Coherent pump schemes have proven particularly suited for the the spectroscopy of photonic many-body transitions [30, 194]: if E_N is the energy of a given N-photon eigenstate of H_{ph}, by changing the frequency ω_{L} the pump is able to address an N-photon resonance starting from vacuum whenever the condition

$$E_N = N\omega_{\mathrm{L}} \tag{1.22}$$

is satisfied. In [30] this method was put forward as a criterion to probe the fermionization of strongly interacting photons in the Tonks-Girardeau regime [67] in finite size lattices, since in the fermionic regime the resonances should be shifted in a very characteristic and easily identifiable manner with respect to the case of non-interacting bosons, due to the different momenta quantization rules [122].

However, one can understand intuitively that such a scheme is not suited to guide a strongly interacting many-body system close to an incompressible quantum phase with a perfectly defined photon number such as a Mott-Insulator state, due to the symmetry between the single-photon emission/injection events caused by the coherent pump Eq. (1.21): as an example, in the limit of impenetrable bosons where the nonlinearity U is very large compared to other energy scales (Γ_1, F) involved in the problem, the steady-state population will be at most $1/2$ (in analogy with a coherently driven two-level atom) for large enough driving strength $F \gg \Gamma_1$ and in particular will not reach any non-zero integer value, in stark contrast with our expectation $n = 1$ in the equilibrium case. Correspondingly, due to a Rabi oscillation effect the density will maintain important fluctuations and the steady-state will present a large number of excitations, precluding the possibility to observe any low-temperature effects.

Actually, the driven-dissipative Bose-Hubbard model with a coherent pump has been widely studied in the literature within the last years [115, 125], and it has been shown that it leads to a rich non-equilibrium phenomenology significantly differing from the one of the equilibrium Bose-Hubbard model [59, 179, 15]: in particular, it involves an hysteretic first order phase transition of gas/liquid type between two coherent phases characterized respectively by a low and high density (but not integer nor fluctuationless), with a bistable region separating the two phases. Optical bistability, which is a well-known effect of classical nonlinear optics [19, 146] and is already well understood for weakly interacting photonic systems such as exciton-polaritons [6, 172, 66], has been recently observed for the first time in a Circuit-QED experiment presenting relatively strong photon blockade [60]. Finally a recent theoretical study [62] has drawn a strong connection between this photonic non-equilibrium model, and the equilibrium physics of spins under a magnetic field (the low-density and high-density phases corresponding to different effective magnetization states).

1.2.3.2 Incoherent non-Markovian pumping

The restrictive possibilities for the investigation of strongly correlated photonic states in coherently driven cavity arrays has led a part of the community to search for alternative strategies during the years of my PhD. Among the various proposals, non-Markovian (i.e.

frequency-dependent) incoherent pump schemes have been put forward as promising candidates for the quantum simulation of incompressible quantum phases.

In the context of the many-body physics of strongly interacting photons, the first proposal [97] regarded the possibility of stabilizing Fractional Quantum Hall states of light in presence of an artificial gauge field. This work predicted a surprising performance where the occupancy of the degenerate ground-state (a lattice analogue to the Laughlin state) could reach values over 95%. While the calculations in [97] were done in special photonic lattices [98] engineered in such a way to present flat bands in analogy with the flat Landau levels in the continuum version, a very recent proposal [195] has extended these ideas to the continuum case, with a potential applicability in novel platforms [168]. Our initial work [119], which was in preparation at the moment of the publication of [97] and applied for the first time such kind of scheme to the Bose-Hubbard model, demonstrated the possibility of stabilizing a very localized $n = 1$ photonic Mott-Insulator state. It was afterwards followed by many other studies [126, 12], and the initial scheme was further refined in [118] in order to stabilize Mott Insulators robust against tunneling with arbitrary densities. This section is dedicated to the review of the works [97, 195] regarding the FQH physics (the description of all the proposals [119, 126, 12, 118] applied to the BH model will be the subject of Chapter 2 and Chapter 3).

Under suitable conditions of weak dissipation, the non-Markovian dynamics of an open quantum system can described at the lowest order in the coupling with the environment by a time-local quantum master equation of the form Eq. (1.19). As we will discuss in Chapter 2, in this regime the term of Eq. (1.19)) responsible for the frequency-dependent pump can be expressed as a superoperator in the non-standard Lindblad form

$$\mathcal{L}_{\text{pump}}[\rho] = \frac{\Gamma_{\text{em}}^0}{2} \sum_i \left[\tilde{a}_i^\dagger \rho a_i + a_i^\dagger \rho \tilde{a}_i - a_i \tilde{a}_i^\dagger \rho - \rho \tilde{a}_i a_i^\dagger \right]. \tag{1.23}$$

where $\tilde{a}_i^\dagger$ (resp. $\tilde{a}_i = [\tilde{a}_i^\dagger]^\dagger$) is a modified creation (resp. annighilation) operator implementing the presence of a frequency-dependent emission spectrum $\mathcal{S}_{\text{em}}(\omega)$, (see Secs. 2.2.2,2.2.3 for more details on the derivation and the mathematical expressions involved in Eq. (1.23)).

This scheme differs in many important manners with respect to the case of a coherently driven array: first, it is gauge invariant and does not break explicitly the $U(1)$ symmetry, secondly it is completely irreversible in the sense that the incoherent pumping term Eq. (1.23) only allows for the injection of new photons inside the system and precludes re-absorption. In order to obtain this irreversibility, two main strategies were put forward: the first one [97] involves a shadow lattice parametrically coupled to the main lattice; the second one [88, 119, 126, 195], maybe more intuitive, relies on embedded inverted two-level emitters (atoms or qubits). In the latter case the non-Markovianity of photonic emission arises from the interplay between bounded distribution of transition frequencies of the emitters and the spectral broadening induced by an irreversible pumping of the emitters in their excited state. While in the optical regime the inversion of population can be obtained in analogy with a laser by mean of an hidden third atomic level [170], a strategy was proposed in circuit-QED [126] relying on the coupling of the emitter (a transmon qubit) to a very lossy resonator tuned on the transition from the first to the second qubit excited stated.

The interplay between the frequency-dependent photonic pumping Eq. 1.23 and Markovian losses allows to transfer probability between various many-body eigenstates of the engineered Hamiltonian H_{ph} with the following rates

$$T_{f \to f'} = \mathcal{S}_{\text{em}}(\omega_{f',f}) \sum_i |\langle f| a_{\text{i}} |f'\rangle|^2, \tag{1.24}$$

$$T_{f' \to f} = \Gamma_{\text{l}} \sum_i |\langle f| a_{\text{i}} |f'\rangle|^2. \tag{1.25}$$

Here $\omega_{f',f} = \omega_{f'} - \omega_f$ is the energy jump between two eigenstates $|f\rangle$ and $|f'\rangle$ of H_{ph} with respectively N and $N+1$ particles (describing, e.g., a BH or a JCH model, or a more complex one featuring a gauge field for the investigation of FQH effects). In stark contrast with the previously described coherent pump scheme, the spectrum $\mathcal{S}_{\text{em}}(\omega)$ does not appear in $T_{f' \to f}$ (which corresponds to a process reducing the total particle number) due to the irreversibility of the photonic pumping: this provides the ability to fully control the relative strength of
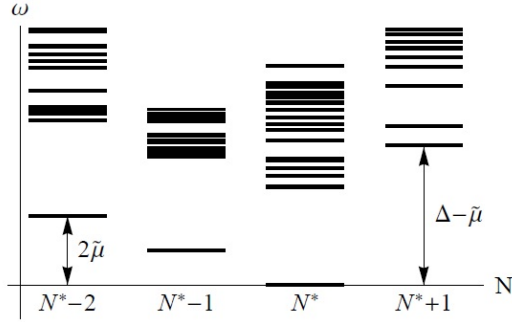
Figure 1.6: Generic energy level diagram of bosons in the lowest Landau level interacting by mean of a contact potential. The system allows for gapless addition of particles $N \leq N^*$. In absence of edges, hole excitations are completely degenerate. States with $N > N^*$ and excited states belonging to an higher band are separated by a gap Δ. Adapted from [97].

the transition rates in function of the energy jumps, and makes incoherent non-Markovian schemes particularly suited candidates to guide the photonic density matrix toward specific eigenstates such as the Hamiltonian ground-state.

Except from [118], all the proposals [97, 119, 126, 12, 195] considered a *"narrow bandpass emission spectrum"* of a Lorentzian type

$$\mathcal{S}_{\text{em}}^{\text{Lorentzian}}(\omega) = \Gamma_{\text{em}}^0 \frac{(\Gamma_{\text{p}}/2)^2}{(\omega - \omega_{\text{at}})^2 + (\Gamma_{\text{p}}/2)^2}. \tag{1.26}$$

While this choice of spectrum revealed functional for the stabilization of Fractional Quantum Hall states in the continuum and well-chosen lattices, we will see in Chapter. 2 that its efficiency is restricted to very specific many-body systems presenting in particular a flat band structure. In [118], we investigated the potential of more complex tailored spectra for the stabilization of generic quantum phases at zero temperature: this will be the subject of Chapter 3.

We now briefly explain why in [97, 195], an important fidelity with the Hamiltonian ground-state can be obtained with this choice of pump spectrum: while [195] directly considers the continuum configuration, in [97] the special choice of lattice structure [98] leads to the presence of analogous flat Landau levels and allows to reproduce the Fractional Hall physics [59] at filing $\nu = 1/k$ (k being some arbitrary integer): for any particle number N, all states belonging to the lowest energy submanifold coincide with the lowest Landau level (LLL), and the gapped ground-state with $N = N^*$ photons corresponds to the Laughlin state (see Fig. 1.6). In addition, due to the absence of edges and of a confining potential (the lattice is assumed to possess periodic boundary conditions), hole excitations (made of $1/\nu$ quasi-holes) corresponding to states with $N < N^*$ are massively isoenergetic: they do not have any dispersion nor interact. Finally, states belonging to the higher energy bands, as well as states with $N > N^*$, are energetically separated by a gap Δ of the order of the minimum between the on-site interaction strength U and the cyclotron energy $\hbar\omega_B$: in the limit $U \ll \hbar\omega_B$, they are quasi-particle excitations where several photons overlap spatially, and for $\hbar\omega_B \ll U$ they correspond to states where at least one photon belongs to the first excited Landau level.

Regarding the pump parameters, on one hand the ratio $\Gamma_{\text{em}}^0/\Gamma_l$ has to be set much higher than unity so that resonant transitions are dominated by pump processes. On the other hand the linewidth Γ_{p} of the frequency-dependent photonic emission spectrum has to be chosen small enough with respect to the many-body gap Δ in such a way that non-resonant transitions will be on contrary dominated by losses:

$$\frac{\Gamma_{\text{em}}^0}{\Gamma_l} \frac{(\Gamma_{\text{p}}/2)^2}{\Delta^2 + (\Gamma_{\text{p}}/2)^2} \ll 1. \tag{1.27}$$

Thus, by tuning the Lorentzian emission spectrum on the transition energy required to remove an hole excitation, the pump allows for a very efficient refilling toward the Laughlin state, and does not populated states with $N > N^*$ photons as the many-body gap Δ

shifts the transition. Still, one could possibly imagine to populate a state above the gap with $N < N^*$ photons during a loss process[2] in that case the Lorentzian pump would not be able to bring back the system toward the ground-state as it would involve at least one non-resonant transition. Luckily for this specific system, a very weak matrix element $\langle f | a_i | f' \rangle \simeq 0$ strongly suppresses the transition toward those states during a loss event (it vanishes exactly in the continuum limit for local interactions). As a consequence, the Laughlin state is very well self-stabilized by the dynamics.

While [97] assumed periodic boundary conditions which are more convenient mathematically but might not be realistic in most experimental platforms, the recent work [195] highlighted the role played by the presence of the confining potential $V_{\text{ext}}(\mathbf{r})$, which leads to the presence of edges and has for effect to lift the degeneracy between the various hole excitations. For a realistic choice of $V_{\text{ext}}(\mathbf{r})$, this complexifies the refilling process, as some excitations (especially those close to the edge) might fall out of the emission bandwidth of the Lorentzian spectrum $\mathcal{S}_{\text{em}}^{\text{Lorentzian}}(\omega)$ and undergo less efficient refilling. Deep in the bulk however, these effects are less important and the system properties should map on the $T = 0$ predictions provided by the Laughlin wavefunction.

1.2.3.3 Artificial chemical potential for light

In parallel to strategies based on incoherent non-Markovian pumping schemes, an orthogonal although very generic approach was proposed in [74] in order to cool down a photonic dissipative system toward an equilibrium-like low-T steady-state with an engineered and controllable chemical potential.

The concept of a non-zero chemical potential μ for photons is highly non-trivial since photons are not conserved particles: a photonic system (with time-dependent density matrix $\rho(t)$) and a thermal bath (with Hamiltonian H_B and initial thermal density matrix $\rho_B = \frac{1}{Z_B} e^{-\beta H_B}$) of absorbing/emitting degrees of freedom (e.g., atoms, qubits or transmission lines) are generally coupled to each other by mean of a time-independent Hamiltonian contribution of the form

$$H_I = \Omega_I \sum_j (a_j + a_j^\dagger) B_j, \tag{1.28}$$

where a_j is an annihilation photonic operator in a mode labelled by the index j, and B_j is some bath operator. For a weak enough coupling Ω_I, the reservoir dynamics can be traced out and the photonic density matrix is then expected to reach a Gibbs ensemble with zero chemical potential

$$\rho_{\text{ph}}^\infty = \lim_{t \to +\infty} \rho_{\text{ph}}(t) = e^{-\beta H_{\text{ph}}} \tag{1.29}$$

(where H_{ph} is the photonic Hamiltonian), and the photonic statistics follows thus the *"Planck law"* for the black-body radiation.

The conceptual novelty of [74] is to implement a time-dependent coupling with the reservoir

$$H_I(t) = 2\Omega_I \cos(\mu t) \sum_j (a_j + a_j^\dagger) B_j, \tag{1.30}$$

(in units of $\hbar = 1$) which the authors propose to engineer in a circuit-QED setup by mean of a Josephson junctions Wheatstone bridge modulated by a time-dependent magnetic flux. The bath is made of transmission lines containing a large number of internal modes so to reproduce a complex thermal environment with a continuum of frequencies.

In the rotating frame provided by the unitary transformation $U(t) = e^{-i\mu t N}$ (where N is the total photon number operator), the new photonic Hamiltonian can be written as $H_{\text{ph}} - \mu N$ and the bath Hamiltonian is left unchanged. Under the assumption that the modulation frequency μ is much higher than the frequency scales of the reservoir modes, one can perform the rotating-wave approximation (RWA) and the coupling term takes then the time-independent form of Eq. (1.28):

$$\begin{aligned} U^\dagger(t) H_I(t) U(t) &= \Omega_I \sum_j (a_j + a_j^\dagger + e^{-i2\mu t} a_j + e^{2i\mu t} a_j^\dagger) B_j \\ &\simeq \Omega_I \sum_j (a_j + a_j^\dagger) B_j. \end{aligned} \tag{1.31}$$

---

[2]Since loss processes are Markovian and can thus either cool or heat the system with equal efficiency

If there is no external source of losses, this dynamics then leads the photonic statistics toward a Gibbs ensemble with a-non-trivial chemical potential

$$\rho_{\mathrm{ph}}^{\infty} = e^{-\beta(H_{\mathrm{ph}} - \mu N)}. \tag{1.32}$$

In the more realistic case where external sources of losses are included, one has that the transition rates take the form

$$T_{f \to f'} = \mathcal{S}_{\uparrow}(\omega_{f',f}) \sum_i |\langle f| a_{\mathrm{i}} |f'\rangle|^2, \tag{1.33}$$

$$T_{f' \to f} = [\mathcal{S}_{\downarrow}(\omega_{f',f}) + \Gamma_{\mathrm{l}}] \sum_i |\langle f| a_{\mathrm{i}} |f'\rangle|^2, \tag{1.34}$$

where $|f\rangle$ and $|f'\rangle$ are two-photonic eigenstates of H_{ph} separated by the transition energy $\omega_{f',f}$ with respectively $N-1$ and N photons, $\mathcal{S}_{\uparrow}(\omega)$ and $\mathcal{S}_{\downarrow}(\omega)$ are respectively the frequency-dependent rates for photonic injection and absorption processes by the parametrically coupled reservoir, and Γ_{l} is the photonic loss rate (approximated by a Markovian contribution). The parametric equilibrium condition for the external reservoir translates into $\mathcal{S}_{\uparrow}(\omega) = e^{-\beta(\omega - \mu)} \mathcal{S}_{\downarrow}(\omega)$.

In the general case this model is not expected to lead to thermal statistics as the detailed balance relation $T_{f \to f'}/T_{f' \to f} = e^{-\beta(\omega_{f'f} - \mu)}$ is not verified. However one sees that if the external losses are kinetically dominated by absorption processes in such a way that $\mathcal{S}_{\downarrow}(\omega) \gg \Gamma_{\mathrm{l}}$, then this model can be be very well approximated by an equilibrium one, and has then that the steady-state density matrix $\rho_{\Sigma}^{\infty} \simeq e^{-\beta(H_{\Sigma} - \mu N)}$ is thermal-like again.

This scheme appears thus to be well suited for the stabilization of nearly equilibrium quantum phases in driven-dissipative photonic platforms. The feasibility of its experimental implementation is still an open question due to the relative complexity of the environment and the parametric coupling scheme.

1.2.4 Concluding remarks and motivations

We have introduced several promising platforms for the investigation of strong correlations in photonic experiments, and shown how it is theoretically possible to reproduce in engineered architectures the dynamics of important many-body models such as the Bose-Hubbard model, which have been largely studied in isolated systems but are still mostly unexplored in open quantum systems. In view of stabilizing incompressible quantum phases with light such as MI of FQH states, we have described the main proposals for the refilling of the photonic population: while the simple coherent drive schemes appears not suited for this task, more recent methods based on non-Markovian engineered reservoirs appear to be the most promising.

Quantum reservoir engineering techniques can be found in many physical contexts ranging from trapped ions [154], single-resonator configurations in cavity QED [140] and circuit QED [96], linear optics [123], cold atoms [50], Rydberg gases [203], opto-mechanical systems [200]. However, the study of its potential for the stabilization of strongly interacting photon fluids is a very recent topic which has emerged during my PhD. The frequency dependence induced by non-Markovianity appears in particular as a precious tools, as it allows to enhance selectively some dissipative transitions between many-body eigenstates, and might allow to access low temperature physics in this new physical context.

The method developed in [74] by Hafezi et al. (which we presented in Sec. 1.2.3.3) in order to simulate a chemical potential for light appears to be well suited for that purpose. However, due to the necessity of building a complex ensemble of long transmission lines maintained at a well-defined temperature and of engineering a modulated coupling to the many-body system, the realizability of such proposal might be unrealistic with current technologies. In this Thesis we investigate the simpler direction of engineering frequency-dependent pumping and/or losses by mean of smaller non-Markovian reservoirs (as was shown in Sec. 1.2.3.2), which can be implemented by mean of a reduced number of additional degrees of freedoms. This is the object of Chapters 2 and 3.

1.3   Conclusions and perspectives

We have reviewed the non-equilibrium physics of photon quantum fluids. The first part of our discussion regarded the weakly interacting regime and focused on experiments in exciton-polaritons. After briefly reviewing the driven-dissipative dynamics of a non-equilibrium exciton-polariton BEC, we moved to the discussion of the kinetics for the emergence of long range order and (in some cases) thermal signatures. The second part was dedicated to the strong blockade regime: After explaining how interesting many-body Hamiltonian can be engineered in those structures, we discussed the more realistic many-body problem involving also dissipative effects: the promises of non-Markovian reservoir engineering in view of stabilizing strongly correlated photon fluids were highlighted.

Although this concept has not been widely addressed (or sometimes in an hidden manner) in the framework of many-body physics with light, it appears that *"non-Markovianity"* (i.e., the non-trivial spectral properties of the external environement) play a key role in most of the phenomenology we have described in this introductory Chapter. Non-Markovian effects are indeed known to be strongly involved in the equilibration kinetics of open quantum systems [169, 124, 210]: in particular, the Kennard-Stepanov relation $\mathcal{S}_{\mathrm{em}}(\omega)/\mathcal{S}_{\mathrm{l}}(\omega) = e^{-\beta\omega}$ [102, 180], which provides a necessary relation between the emission and absorption spectrum for the equilibration of a photonic device, automatically implies the existence of frequency-dependent dissipative processes.

Memory effects associated to non-Markovianity have been explored in many other physical contexts: from a quantum information perspective, a quantitative measure of the degree of non-Markovianity and connections with the back flow of information were drawn in [20, 207]. Such back flow was shown to hinder the ability (called Quantum Darwinism) of a quantum system to redundantly imprint information on its state in the external environment [211, 65]. Non-Markovian effects have also been put forward in quantum technologies as a tool for optimal control operations [139] and quantum error corrections [96], and appear to play a key role in the protection of entanglement in quantum biochemical processes [188].

The next Chapters of this thesis are adapted from my research work during this PhD. In particular, in Chapters 2 and 3 we will explore more thoroughly the potential of non-Markovian schemes for the stabilization of incompressible quantum phases and the quantum simulation of zero temperature equilibrium physics with light. Chapter 4 will be dedicated to the analysis of the emergence of analogous thermal properties in generic non-Markovian driven-dissipative quantum systems.

Chapter 2

Strongly interacting photons under a frequency-dependent incoherent pump with a narrow bandpass spectrum

2.1 Introduction

Until now, most theoretical studies aiming at the investigation of strong correlations in driven-dissipative photonic lattices focused on schemes based on the use of a coherent drive to refill the photonic population [30, 192, 193, 115, 125]. This approach might appear as the simplest one from both experimental and conceptual points of view, as it only requires shining a resonant classical signal on a photonic architecture (e.g., light coming from a laser in cavity QED architectures, or an electric voltage capacitively coupled to a superconducting circuit), and proved useful in order to probe spectroscopically the many-body transitions of strongly interacting Hamiltonians [30]. However, as explain Sec. 1.2.3.1, this method is unlikely to be suited for the stabilization of incompressible quantum phase such as Fractional Quantum Hall [193, 194] and Mott-Insulator states with a perfectly defined energy and photon number.

In this chapter we follow a different direction, and focus on the possibility of implementing a novel non-Markovian (i.e., frequency-dependent) incoherent pump scheme in order to tackle the open problem of the stabilization a Mott Insulator photonic state in a dissipative Bose-Hubbard photonic model. Frequency-dependent incoherent pumping schemes, however relatively absent from the literature until recently in the physical context of strongly interacting photons in driven-dissipative resonator arrays, have been put forward over the last few years as novel candidates for the quantum simulation of new many-body physics with light. As discussed in last chapter in Sec. 1.2.3.2, one of the most striking potential applications of this approach the possibility of stabilizing Fractional Quantum Hall states in photonic architectures [97, 195]. While next chapter will focus on more complex frequency dependencies involving tailored reservoirs, here we investigate the simplest case of a *"narrow bandpass"* emission spectrum of a Lorentzian shape:

$$\mathcal{S}_{\mathrm{em}}^{\mathrm{Lorentzian}}(\omega) = \Gamma_{\mathrm{em}}^0 \frac{(\Gamma_{\mathrm{p}}/2)^2}{(\omega - \omega_{\mathrm{at}})^2 + (\Gamma_{\mathrm{p}}/2)^2}, \tag{2.1}$$

Our initial proposal [119] represents the first attempt of applying such kind of scheme to the Bose-Hubbard model, and demonstrated the possibility of stabilizing a pure photonic Mott-Insulator state (in a regime of weak inter-cavity hopping), which is another cornerstone of the low-temperature physics of strongly correlated quantum systems. Following the same philosophy, a more recent proposal [126] based on a slightly different implementation (although providing similar non-Markovian photonic dynamics), reached comparable conclusions. Our most recent manuscript [12] characterized the Mean-Field phase diagram of

such a model and unveiled a phase transition driven by a commensurability effect, from a photonic Mott state toward a coherent superfluid-like state of light.

This chapter is organized as follow: we introduce in Sec. 2.2 a quantum optics scheme in an array of driven-dissipative nonlinear resonators with embedded incoherently pumped two-level emitters. Projective methods are used to eliminate the emitter dynamics and write a generalized master equation for the photonic degrees of freedom only, where the frequency-dependence of gain introduces non-Markovian features. As a first step, in Sec. 2.3, we look at the various steady-state features in a single cavity configuration: for weak nonlinearities, this pumping scheme provides exotic optical bistability effects, not induced by the presence of a coherent incident pump, but rather by the frequency dependence of the non-Markovian gain medium. In the blockade regime, this scheme allows for the selective generation of Fock states with a well-defined photon number, which is an essential step toward the stabilization of strongly correlated many-body phases with photons. We then move to the investigation of the phenomenology in the many-cavity configuration: in Sec. 2.4 we analyse some general properties and show that the steady-state presents thermal properties when the emission spectrum is broad with respect to Hamiltonian frequency-scales. In Sec. 2.5 we briefly discuss an exotic mechanism leading to the emergence of coherence in presence of finite interactions. In Sec. 2.6 we analyse the steady-state properties in the strong blockade regime: first, we confirm the existence of a Mott phase for weak inter-cavity hopping. We show however that this state is not fully robust, as for a hopping constant exceeding the spectral emission linewidth, the commensurability condition on density is not sustainable anymore and holes are generated with the system, and analyse the one-body correlations close to the Mott regime. Finally, in Sec. 2.7, we investigate the Gutzwiller Mean-Field phase diagram of such a system. and unveil a Mott-to-Superfluid phase transition triggered by the same proliferation of hole excitations involved in the depletion of the MI state. We find that, at a critical value of the inter-cavity photon hopping, the system undergoes a second-order nonequilibrium phase phase transition (of a Mott-to-Superfluid type) associated with the spontaneous breaking of the $U(1)$ symmetry. Unlike the equilibrium case, the transition is always driven by commensurability effects for this model, and not by the competition between photon hopping and optical nonlinearity. The corresponding phase boundary is characterized numerically, and also accessed also analytically in the specific case of the Hard-Core regime.

All the results of this Chapter come from Refs. [119, 12]. Results from the beginning of this Chapter until Sec. 2.5 are adapted from the work [119], of which the author of this Ph. D thesis is the first and main author. Results from Sec. 2.6.1 until the end of this Chapter are adapted from the collaborative work [12] of which Alberto Biella is the first author. All simulations of [12] were performed by Alberto Biella and Florent Storme, while the author of this PhD thesis provided part of the analytical contributions and physical predictions.

2.2 The physical system and the effective photonic non-Markovian description

2.2.1 The model

We consider a driven-dissipative Bose-Hubbard model for photons in an array of M coupled nonlinear resonators/cavities of natural frequency ω_{cav}. The experimental platform can be a superconducting circuit or a cavity QED one. In units such that $\hbar = 1$, the Hamiltonian for the isolated system dynamics has the usual form [84, 29, 76, 144]:

$$H_{\text{ph}} = \sum_{i=1}^{M} \left[\omega_{\text{cav}} a_i^\dagger a_i + \frac{U}{2} a_i^\dagger a_i^\dagger a_i a_i \right] - \sum_{\langle i,j \rangle} \left[J a_i^\dagger a_j + hc \right]. \tag{2.2}$$

The resonators are coupled via tunneling processes with amplitude J, and we do not specify at this stage the spatial dimensionality nor the periodicity of this arrangement. Each cavity is assumed to contain a Kerr nonlinear medium, which induces effective repulsive interactions between photons in the same cavity with an interaction constant U proportional to the Kerr nonlinearity $\chi^{(3)}$. Dissipative phenomena due the finite transparency of the mirrors and

absorption by the cavity material are responsible for a finite lifetime of photons, which naturally decay at a rate Γ_l.

The key novelty of this model with respect to earlier work consists in the different mechanism that is proposed to compensate for losses and replenish the photon population. Instead of a coherent pumping or a very broad-band amplifying laser medium, we consider a configuration where a set of N_{at} two-level emitters with a bare transition frequency $\omega_{at}^{(n)}$ is present in each cavity. Each emitter, which can be an atom or a qubit depending on the chosen experimental platform, is coupled to the resonator with a Rabi frequency Ω_R and is assumed to be strongly incoherently pumped toward its excited state at a rate Γ_p: as we already anticipate, due to the interplay between the emitter pumping and the Rabi coupling to the cavity mode, each emitter provides an incoherent frequency-dependent photonic emission centered at the transition frequency $\omega_{at}^{(n)}$. The irreversible optical pumping in the excited state can be obtained, by analogy with laser physics, by using a third energy level of the emitter (not mentioned in this simplified description) with fast decay toward the first excited state. Our choice of two different physical mechanisms for nonlinearity and pumping (for example, two different types of two-level systems) allows us to to tune independently photonic interactions and emission.

The free evolution of the emitters and their coupling to the cavities are described by the following Hamiltonian terms,

$$H_{at} = \sum_{i=1}^{M} \sum_{n=1}^{N_{at}} \omega_{at}^{(n)} \sigma_i^{+(n)} \sigma_i^{-(n)} \tag{2.3}$$

$$H_I = \Omega_R \sum_{i=1}^{M} \sum_{n=1}^{N_{at}} \left[a_i^\dagger \sigma_i^{-(n)} + a_i \sigma_i^{+(n)}) \right] : \tag{2.4}$$

the emitter transition frequency $\omega_{at}^{(n)}$ is assumed to be in the vicinity (but not necessarily resonant) with the cavity mode and the emitter-cavity coupling is assumed to be weak enough $\Omega_R \ll \omega_{at}^{(n)}, \omega_{cav}$ to be far from the ultra-strong coupling regime [37, 38] and from phase transition of a superradiant type [201, 143, 10, 149].

As usual, the dissipative dynamics under the effect of the pumping and decay processes can be described in terms of a master equation for the density matrix ρ_{tot} of the whole emitter-cavity system,

$$\partial_t \rho_{tot} = \frac{1}{i} \left[H_{ph} + H_{at} + H_I, \rho_{tot} \right] + \mathcal{L}(\rho_{tot}), \tag{2.5}$$

where the different dissipative processes are summarized in the Lindblad super-operator $\mathcal{L} = \mathcal{L}_l + \mathcal{L}_p + \mathcal{L}_\gamma$, with

$$\mathcal{L}_l(\rho_{tot}) = \frac{\Gamma_l}{2} \sum_{i=1}^{M} \left[2a_i \rho_{tot} a_i^\dagger - a_i^\dagger a_i \rho_{tot} - \rho_{tot} a_i^\dagger a_i \right] \tag{2.6}$$

$$\mathcal{L}_p(\rho_{tot}) = \frac{\Gamma_p}{2} \sum_{i=1}^{M} \sum_{l=1}^{N_{at}} \left[2\sigma_i^{+(l)} \rho_{tot} \sigma_i^{-(l)} - \sigma_i^{-(l)} \sigma_i^{+(l)} \rho_{tot} - \rho_{tot} \sigma_i^{-(l)} \sigma_i^{+(l)} \right], \tag{2.7}$$

$$\mathcal{L}_\gamma(\rho_{tot}) = \frac{\gamma}{2} \sum_{i=1}^{M} \sum_{l=1}^{N_{at}} \left[2\sigma_i^{-(l)} \rho_{tot} \sigma_i^{+(l)} - \sigma_i^{+(l)} \sigma_i^{-(l)} \rho_{tot} - \rho_{tot} \sigma_i^{+(l)} \sigma_i^{-(l)} \right], \tag{2.8}$$

describing respectively the photon losses the emitter pumping and some possible spontaneous decay of the emitters. The $\sigma_i^{\pm(n)}$ operators are the usual raising and lowering operators for the two-level n-th emitter in the i-th cavity.

In this Chapter, we will consider the simplest configuration in which all emitters have the same transition frequency $\omega_{at}^{(n)} = \omega_{at}$, which as we will see, will lead to a narrow bandpass emission spectrum of Lorentzian shape (A different arrangement of the emitters frequencies leading to a more elaborated tailored emission spectrum will be the subject of next Chapter.). While theoretically, in this simple configuration a single atom per cavity ($N_{at} = 1$) should be enough to generate the frequency-dependent photonic emission, experimentally several

emitters might be needed in order to reach the desired photonic amplification. We introduce the detuning $\delta = \omega_{\mathrm{cav}} - \omega_{\mathrm{at}}$ of the bare cavity frequency with respect to the emitter transition frequency.

In the following, we shall concentrate on a regime in which the pumping of the emitters is much faster than any other sources of dissipations (emitter spontaneous decay, photonic injection and loss processes). First, this assumption implies that $\gamma \ll \Gamma_{\mathrm{p}}$ and thus the relaxation of emitters in their ground-state is a negligible process. In [119] thus, we fully neglected the term $\mathcal{L}_\gamma$, while our most recent work [12] included it for the sake of completeness of the physical description, and checked it did not bring any relevant contributions (the various simulations within this chapter involving this term will mention it). Secondly, we have thus that $\Gamma_{\mathrm{l}} \ll \Gamma_{\mathrm{p}}$, implying that photonic losses do not have the time to occur over the re-pumping time scale $1/\Gamma_{\mathrm{p}}$. While this will allow some mathematical simplifications, we will of course not neglect the effect of photonic losses which have a dramatic impact on the long time dynamics and are an essential feature of our physical description.

Most importantly, we assume to be in a weak emitter-cavity coupling regime $\sqrt{N_{\mathrm{at}}}\Omega_R \ll \Gamma_{\mathrm{p}}$, where the emitters are immediately repumped to their excited state after having injected a photon into the cavity: in this regime, an emitter having decayed to the ground state does not have the time to reabsorb any photon before being repumped to its excited state. In this regime, complex cavity-QED effects such as Rabi oscillations do not take place and the photon emission takes place in an effectively irreversible way. Under this constraint, we will be allowed to eliminate the two-level emitters dynamics from the problem and write an effective photonic master equation [21, 63] involving only the cavity degrees of freedom. We note that the condition $\Omega_R \ll \Gamma_{\mathrm{p}}$ assumed in presence of a single atom is not sufficient, as the Rabi coupling Ω_R is expected to be enhanced by a superradiant collective behavior [49] of the emitter reservoir which behaves then as a single macroscopic harmonic oscillator (for $N_{\mathrm{at}} \gg 1$) with effective Rabi coupling $\sqrt{N_{\mathrm{at}}}\Omega_R$ [1].

2.2.2 Projective methods for the derivation non-Markovian master equations

Here we provide a brief review of the projective methods developed in [142, 213] used for the derivation of non-local Master equations which includes the effect of non-Markovian processes. More complex methods involving convolutionless non-Markovian master equations can be found in [174, 173] (as we will be focusing in our work on a weak coupling regime the two approaches will be equivalent). Our discussion is based on the textbook [21].

2.2.2.1 General Formalism

We consider a quantum system $\mathcal{M}$ which undergoes dissipative processes. As it is not isolated, its state can not be described by a wave function but by a density matrix ρ_{tot} evolving according to the master equation:

$$\partial_t \rho_{\mathrm{tot}} = \mathcal{L}(\rho_{\mathrm{tot}}(t)), \qquad (2.9)$$

where $\mathcal{L}$ is some linear "super-operator" acting on the space of density matrices. Given an arbitrary initial density matrix $\rho_{\mathrm{tot}}(t_0)$, the density matrix ρ_{tot} at generic time t is equal to $\rho_{\mathrm{tot}}(t) = e^{\mathcal{L}(t-t_0)}\rho_{\mathrm{tot}}(t_0)$.

Now we are only interested in some partial information of the density matrix, which can represent some physical subsystem. This can be described by a projection operation on the density matrix $\mathcal{P}\rho_{\mathrm{tot}}$. We call $\mathcal{Q} = \mathbb{1} - \mathcal{P}$ the complementary projector. In order to describe the dynamics of $\mathcal{P}\rho_{\mathrm{tot}}$, we decompose the Lindblad operator $\mathcal{L}$ in two parts $\mathcal{L}_0$ and $\delta\mathcal{L}$ such that:

$$\begin{cases} \mathcal{L} = \mathcal{L}_0 + \delta\mathcal{L} \\ \mathcal{P}\mathcal{L}_0\mathcal{Q} = \mathcal{Q}\mathcal{L}_0\mathcal{P} = 0 \\ \mathcal{P}\,\delta\mathcal{L}\,\mathcal{P} = 0. \end{cases} \qquad (2.10)$$

---

[1] In the configuration where atoms are detuned with respect to each other (see for example next Chapter) this severe constraint might be relaxed, as atoms with very different frequencies are not able to couple collectively to the cavity. The condition $\sqrt{N_{\mathrm{at}}}\Omega_R \ll \Gamma_{\mathrm{p}}$ will be replaced then by the weaker assumption that the effective photon emission rate $\mathcal{S}_{\mathrm{em}}(\omega)$ (introduced in next section) will have to be much smaller than the pumping rate at any frequency: $\Gamma^0_{\mathrm{em}} \ll \Gamma_{\mathrm{p}}$ where $\Gamma^0_{\mathrm{em}} = \mathrm{Max}_\omega \mathcal{S}_{\mathrm{em}}(\omega)$.

Such a decomposition is always possible. In our case, $\mathcal{L}_0$ will contain in particular all photonic Hamiltonian contributions, and $\delta\mathcal{L}$ will contain in particular all contributions related to the atom-photon Rabi coupling Ω_R.

Then we define a generalised interaction picture for the density matrix and for generic superoperators $\mathcal{A}$ with respect to the evolution described by the free $\mathcal{L}_0$ and the initial time t_0:

$$\begin{cases} \hat{\rho}_{\text{tot}}(t) = e^{-\mathcal{L}_0(t-t_0)}\rho_{\text{tot}}(t) \\ \hat{\mathcal{A}}(t) = e^{-\mathcal{L}_0(t-t_0)}\mathcal{A}e^{\mathcal{L}_0(t-t_0)}. \end{cases} \tag{2.11}$$

As discussed in [21], we can get an exact closed master equation for the projected density matrix in the interaction picture

$$\partial_t \mathcal{P}\hat{\rho}_{\text{tot}}(t) = \int_{t_0}^t dt' \Sigma(t,t')\mathcal{P}\hat{\rho}_{\text{tot}}(t'), \tag{2.12}$$

which translates to

$$\partial_t \mathcal{P}\rho_{\text{tot}}(t) = \mathcal{L}_0(\rho_{\text{tot}}(t)) + \int_{t_0}^t dt' \tilde{\Sigma}(t-t')\mathcal{P}\rho_{\text{tot}}(t') \tag{2.13}$$

in the Schrodinger picture. In the interaction picture, the self energy operator Σ is defined as:

$$\begin{aligned} \Sigma(t,t') &= \sum_{n=2}^{\infty} \int_{t'}^t \int_{t'}^{t_1} .. \int_{t'}^{t_{n-1}} dt_1..dt_n \\ &\quad \mathcal{P}\delta\hat{\mathcal{L}}(t)\mathcal{Q}\delta\hat{\mathcal{L}}(t_1)\mathcal{Q}\delta\hat{\mathcal{L}}(t_2)...\mathcal{Q}\delta\hat{\mathcal{L}}(t_n)\mathcal{Q}\delta\hat{\mathcal{L}}(t')\mathcal{P} \end{aligned} \tag{2.14}$$

and results from the coherent sum over the processes leaving from $\mathcal{P}$, remaining in $\mathcal{Q}$ and then coming back finally to $\mathcal{P}$. In the Schrodinger representation, we have:

$$\tilde{\Sigma}(t-t') = e^{\mathcal{L}_0(t-t_0)}\Sigma(t,t')e^{-\mathcal{L}_0(t'-t_0)} = \Sigma(0,t'-t)e^{\mathcal{L}_0(t-t')}. \tag{2.15}$$

We call $\tau_c = 1/\Delta\omega$ the characteristic decay time/inverse linewidth for the self energy $\tilde{\Sigma}(t-t')$, which corresponds in general to the correlation time of the bath, and we estimate the rate of the dissipative processes induced by the perturbation $\delta\mathcal{L}$ and acting on the projected density matrix $\mathcal{P}\rho$ as $\Gamma \sim \int_0^{\infty} d\tau \Sigma(0,-\tau)$. In our proposal one has $\tau_c = 1/\Gamma_p$ and $\Gamma = \Gamma_{\text{em}}^0$, where Γ_{em}^0 is the maximum photonic emission rate (it will be deduced a posteriori by derivation of the photonic projected master equation). We put ourselves in the weak coupling regime in which the evolution of the projected density matrix in the interaction picture is almost constant over that time τ_c, i.e., $\Gamma \ll \Delta\omega$ (this will the case for us as we assumed $\Omega_R \ll \Gamma_p$). Furthemore, if $t - t_0 \gg \tau_c$ then the integral in Eq. (2.12) can be extended from $-\infty$ to t. From this equation and from (2.15), by going back in the Schrodinger picture we get an equation of evolution for the density matrix which is local in time:

$$\partial_t \mathcal{P}\rho_{\text{tot}}(t) = \left[\mathcal{L}_0 + \int_0^{\infty} d\tau \Sigma(0,-\tau)\right]\mathcal{P}\rho_{\text{tot}}(t) = \mathcal{L}_{\text{eff}}\mathcal{P}\rho_{\text{tot}}(t), \tag{2.16}$$

with

$$\mathcal{L}_{\text{eff}} = \mathcal{L}_0 + \int_0^{\infty} d\tau \Sigma(0,-\tau). \tag{2.17}$$

It is worth stressing that while the bath is Markovian with respect to the dissipative processes induced by the perturbation $\int_0^{\infty} d\tau \Sigma(0,-\tau)$, no Markovian approximation has been made with respect to the dynamics due to $\mathcal{L}_0$, which can still be fast. For the specific system under consideration in this work, this means that the emission rate Γ_{em}^0 will have to be slow with respect to the gain bandwidth set by the atomic pumping rate Γ_p [2]. However no restriction is to be imposed on the parameters U, J and $\omega_{\text{cav}} - \omega_{\text{at}}$ of the Hamiltonian, which can be arbitrarily large. This means that the physics can be strongly non-Markovian with respect to the Hamiltonian photonic dynamics.

---

[2]We will also have $\Gamma_l \ll \Gamma_p$ but for the physical reason that Γ_l should be comparable or small with respect to Γ_{em}^0 in order to obtain a non-negligible photonic population

2.2.2.2 Application to the photonic driven-dissipative array

With the notation of our proposal of implementation, the system $\mathcal{M}$ will correspond to the whole {photons+emitters} system. We choose the projector in the form

$$\mathcal{P}\rho_{\mathrm{tot}} = \left|\{e_i^{(n)}\}\right\rangle\left\langle\{e_i^{(n)}\}\right| \otimes \mathrm{Tr}_{\mathrm{at}}(\rho_{\mathrm{tot}}), \tag{2.18}$$

where we performed a partial trace over the embedded atoms in all cavities, and then made the tensor product of the density matrix and the atomic density matrix with all atoms in the excited state. We chose this particular projector because in the weak photon-emitter coupling regime, we expect the emitters to be repumped almost immediately after having emitted a photon in the resonator array, and thus to be most of the time in the excited state. Moreover this projection operation gives us direct access to the exact photonic density matrix $\mathrm{Tr}_{\mathrm{at}}(\rho_{\mathrm{tot}})$, and thus we do not lose any information on photonic statistics.

With the notation of the previous section we have:

$$\mathcal{L}(\rho_{\mathrm{tot}}) = -i\left[H_{\mathrm{ph}} + H_{\mathrm{at}} + H_{\mathrm{I}}, \rho_{\mathrm{tot}}\right] + \mathcal{L}_{\mathrm{diss}}(\rho_{\mathrm{tot}}), \tag{2.19}$$

with

$$\mathcal{L}_{\mathrm{diss}} = \mathcal{L}_{\mathrm{p}} + \mathcal{L}_{\mathrm{l}}, \tag{2.20}$$

where the emitter spontaneous decay contribution has been neglected as explained in Sec. 2.2.1. We decompose $\mathcal{L}$ in two contributions. The first one is

$$\mathcal{L}_0(\rho_{\mathrm{tot}}) = -i\left[H_{\mathrm{ph}} + H_{\mathrm{at}}, \rho_{\mathrm{tot}}\right] + \mathcal{L}_{\mathrm{l}}(\rho_{\mathrm{tot}}) - \mathcal{A}(\rho_{\mathrm{tot}}) + \mathcal{P}\mathcal{A}\mathcal{Q}(\rho_{\mathrm{tot}}) \tag{2.21}$$

where

$$\mathcal{A}(\rho_{\mathrm{tot}}) = \frac{\Gamma_{\mathrm{p}}}{2}\sum_{i=1}^{L}\sum_{n=1}^{N_{at}}\left[\sigma_i^{-(n)}\sigma_i^{+(n)}\rho_{\mathrm{tot}} + \rho_{\mathrm{tot}}\sigma_i^{-(n)}\sigma_i^{+(n)}\right]. \tag{2.22}$$

The last term in the expression of Eq. (2.21) comes from the fact that the pumping term $\mathcal{A}$ in $\mathcal{L}_0$ does not verify the condition (2.10): as a result, we have to remove the part unfixed by projector and put it in the other operator :

$$\delta\mathcal{L}(\rho_{\mathrm{tot}}) = -i\left[H_{\mathrm{I}}, \rho_{\mathrm{tot}}\right] + \frac{\Gamma_{\mathrm{p}}}{2}\sum_{i=1}^{L}\sum_{n=1}^{N_{at}}2\sigma_i^{+(n)}\rho_{\mathrm{tot}}\sigma_i^{-(n)} - \mathcal{P}\mathcal{A}\mathcal{Q}(\rho_{\mathrm{tot}}). \tag{2.23}$$

These two operators then satisfy to the conditions (2.10), and we can apply the projection method to get the evolution of $\mathcal{P}\rho(t)$, that is of $Tr_{\mathrm{at}}(\rho)(t)$. More precisely, we compute the first non-vanishing contribution to the self energy integral $\int_0^\infty d\tau \Sigma(0,-\tau)$ in powers of the weak parameters $\sqrt{N_{\mathrm{at}}}\Omega_R/\Gamma_{\mathrm{p}}$ and $\Gamma_{\mathrm{l}}/\Gamma_{\mathrm{p}}$, and derive thus the expression for the effective dissipator (2.17). All details of the derivation can be found in App. B.

2.2.3 A non-Markovian effective photonic master equation

Under the constraints $\sqrt{N_{\mathrm{at}}}\Omega_R, \Gamma_{\mathrm{l}} \ll \Gamma_{\mathrm{p}}$, the projective methods sketched in the previous section allow to trace out the atomic degrees of freedom and to derive the following photonic master equation:

$$\partial_t\rho = -i\left[H_{\mathrm{ph}}, \rho(t)\right] + \mathcal{L}_{\mathrm{l}} + \mathcal{L}_{\mathrm{em}}, \tag{2.24}$$

with

$$\mathcal{L}_{\mathrm{l}} = \frac{\Gamma_{\mathrm{l}}}{2}\sum_{i=1}^{M}\left[2a_i\rho a_i^\dagger - a_i^\dagger a_i\rho - \rho a_i^\dagger a_i\right], \tag{2.25}$$

$$\mathcal{L}_{\mathrm{em}} = \frac{\Gamma_{\mathrm{em}}^0}{2}\sum_{i=1}^{M}\left[\tilde{a}_i^\dagger\rho a_i + a_i^\dagger\rho\tilde{a}_i - a_i\tilde{a}_i^\dagger\rho - \rho\tilde{a}_i a_i^\dagger\right]. \tag{2.26}$$

describing photonic losses and emission processes, respectively. While the loss term has a standard Lindblad form at rate Γ_{l}, the emission term keeps some memory of the emitters

dynamics as it involves modified lowering and raising operators

$$\tilde{a}_i \;\; = \;\; \frac{\Gamma_{\rm p}}{2} \int_0^\infty d\tau \, e^{(-i\omega_{\rm at}-\Gamma_{\rm p}/2)\tau} a_i(-\tau), \tag{2.27}$$

$$\tilde{a}_i^\dagger \;\; = \;\; [\tilde{a}_i]^\dagger \tag{2.28}$$

which contain the photonic hamiltonian dynamics during the emitter re-pumping

$$a_i(\tau) = e^{iH_{\rm ph}\tau} \, a_i \, e^{-iH_{\rm ph}\tau} : \tag{2.29}$$

indeed, in the limit we are considering in which photonic losses are slow with respect to the pumping rate of the emitters, those dissipative process can be neglected over the integration time $\propto 1/\Gamma_{\rm p}$.

The Fourier-like integral in Eqs. (2.27),(2.28) is responsible for the frequency selectivity of the emission, as the emission rate will be maximum when the free evolution of $a_i(\tau)$ occurs at a frequency close to the emitters one $\omega_{\rm at}$. A deeper physical insight on those modified jump operators can be obtained by looking at their matrix elements in the basis of eigenstates of the photonic hamiltonian: we consider two eigenstates $|f\rangle$ (resp. $|f'\rangle$) with N (resp. $N+1$) photons and energy ω_f (resp. $\omega_{f'}$). After elementary manipulations, we see that the emission amplitude follows a Lorentzian law as a function of the detuning between the frequency difference of the two photonic states $\omega_{f'f} = \omega_{f'} - \omega_f$ and the emitters transition frequency $\omega_{\rm at}$,

$$\langle f| \, \tilde{a}_i \, |f'\rangle \;\; = \;\; \frac{\Gamma_{\rm p}/2}{-i(\omega_{f'f} - \omega_{\rm at}) + \Gamma_{\rm p}/2} \, \langle f| \, a_i \, |f'\rangle, \tag{2.30}$$

$$\langle f'| \, \tilde{a}_i^\dagger \, |f\rangle \;\; = \;\; \frac{\Gamma_{\rm p}/2}{+i(\omega_{f'f} - \omega_{\rm at}) + \Gamma_{\rm p}/2} \, \langle f'| \, a_i^\dagger \, |f\rangle .. \tag{2.31}$$

Upon insertion of Eq. (2.30) into the master equation (2.24), one can associate the real part of Eq. (2.30) to an effective emission rate

$$\mathcal{S}_{\rm em}(\omega_{f'f}) = \Gamma_{\rm em}^0 \frac{(\Gamma_{\rm p}/2)^2}{(\omega_{f'f} - \omega_{\rm at})^2 + (\Gamma_{\rm p}/2)^2}, \tag{2.32}$$

with a Lorentzian frequency dependence, while the imaginary part can be related to a frequency shift of the photonic states under the effect of the population-inverted emitters. This interpretation becomes the clearest in the secular approximation, as in this regime the Master Eq. (2.24) can be rewritten in the equivalent form containing a Lindblad contribution with the frequency-dependent emission rate given by Eq. (2.32), as well as an additional an Hamiltonian correction encapsulating the effect of the imaginary part of Eq. (2.30) (see App. C for the explicit form of the Master equation and the corresponding derivation).

The width of the Lorentzian is set by the pumping rate $\Gamma_{\rm p}$, that is by the autocorrelation time $\tau_{\rm p} = 1/\Gamma_{\rm p}$ of the emitter seen as a frequency-dependent emission bath. The peak emission rate exactly on resonance is equal to

$$\Gamma_{\rm em}^0 = N_{\rm at}\Gamma_{\rm em}^{\rm at} = \frac{4N_{\rm at}\Omega_R^2}{\Gamma_{\rm p}} . \tag{2.33}$$

While being in the regime $\Gamma_{\rm p} \gg \sqrt{N_{\rm at}}\Omega_R$ is a posteriori equivalent to the assumption that the photonic emission rate is much slower than the emitters repumping rate ($\Gamma_{\rm em}^0 \ll \Gamma_{\rm p}$), no constraint need being imposed on the parameters J, U and $\delta = \omega_{\rm cav} - \omega_{\rm at}$ of the photonic Hamiltonian, which can be arbitrarily large: this will allow for important non-Markovian effects. Whereas an extension of our study to the $\Gamma_{\rm l} \gtrsim \Gamma_{\rm p}$ regime would only introduce technical complications, entering the $\Gamma_{\rm em}^0 \gtrsim \Gamma_{\rm p}$ regime is expected to dramatically modify the physics, as emitters could exchange photons with the cavity at such a fast rate that they do not have time to be repumped to the excited state in between two emission events. As a result, reabsorption processes and Rabi oscillations would be then possible, and nonlinear saturation effects related to the anharmonic nature of the two-level systems would become relevant. Entering this regime would considerably complicate the theoretical description and is beyond the scope of this work.

2.3 Single cavity physics

In this section we focus on the single cavity physics of the non-Markovian theory derived in Sec. 2.2.3. After showing explicitely the analytical solution for the steady-state of Eq. (2.24) in this particular configuration, we investigate the steady-state properties for different strengths of photon-photon interactions. The main result of this section is given in Sec. 2.3.3, where we demonstrate the possibility of stabilizing photonic Fock states in the strong blockade regime.

2.3.1 Single cavity solution

A special attention will be paid to the steady-state ρ_∞ of the effective photonic non-Markovian master equation (2.24):

$$0 = -i\left[H_{\mathrm{ph}}, \rho_\infty\right] + \mathcal{L}_{\mathrm{l}}\left(\rho_\infty\right) + \mathcal{L}_{\mathrm{em}}\left(\rho_\infty\right). \tag{2.34}$$

In our specific case of a single cavity, the photonic states are labelled by the photon number N and have an energy

$$\omega_N = N\omega_{\mathrm{cav}} + \frac{1}{2}N(N-1)U. \tag{2.35}$$

Correspondingly, the $N \to N+1$ transition has a frequency

$$\omega_{N+1,N} = \omega_{\mathrm{cav}} + NU, \tag{2.36}$$

and the corresponding photon emission rate is

$$\mathcal{S}_{\mathrm{em}}(\omega_{N+1,N}) = \Gamma_{\mathrm{em}}^0 \frac{(\Gamma_{\mathrm{p}}/2)^2}{(\omega_{N+1,N} - \omega_{\mathrm{at}})^2 + (\Gamma_{\mathrm{p}}/2)^2}. \tag{2.37}$$

As no coherence can exist between states with different photon number N, the stationary density matrix is diagonal in the Fock basis, $\rho_\infty = \delta_{N,N'}\pi_N$ with the populations π_N satisfying

$$(N+1)\Gamma_{\mathrm{l}}\pi_{N+1} - (N+1)\mathcal{S}_{\mathrm{em}}(\omega_{N+1,N})\pi_N + N\mathcal{S}_{\mathrm{em}}(\omega_{N,N-1})\pi_{N-1} - N\Gamma_{\mathrm{l}}\pi_N = 0, \tag{2.38}$$

where the two last terms of course vanish for $N = 0$. As only states with neighboring N are connected by the emission/loss processes, detailed balance is automatically enforced in the stationary state, which imposes the simple condition on the populations,

$$(N+1)\Gamma_{\mathrm{l}}\pi_{N+1} - (N+1)\mathcal{S}_{\mathrm{em}}(\omega_{N+1,N})\pi_N = 0 \tag{2.39}$$

which is straightforwardly solved in terms of a product,

$$\pi_N = \pi_0 \prod_{M=0}^{N-1} \frac{\mathcal{S}_{\mathrm{em}}(\omega_{M+1,M})}{\Gamma_{\mathrm{l}}} = \left(\frac{\Gamma_{\mathrm{em}}^0}{\Gamma_{\mathrm{l}}}\right)^N \prod_{M=0}^{N-1} \frac{(\Gamma_{\mathrm{p}}/2)^2}{(\omega_{M+1,M} - \omega_{\mathrm{at}})^2 + (\Gamma_{\mathrm{p}}/2)^2}\pi_0. \tag{2.40}$$

2.3.2 A non-Markovian induced optical bistability

We now investigate the weakly interacting regime in a single cavity configuration (namely $U \ll \Gamma_{\mathrm{p}}$).

First, for a vanishing nonlinearity $U = 0$, all transition frequencies $\omega_{N+1,N}$ are equal to the bare cavity frequency ω_0 and the populations of the different N states have a constant ratio

$$\frac{\pi_{N+1}}{\pi_N} = \frac{\Gamma_{\mathrm{em}}^0}{\Gamma_{\mathrm{l}}} \frac{(\Gamma_{\mathrm{p}}/2)^2}{\delta^2 + (\Gamma_{\mathrm{p}}/2)^2}, \tag{2.41}$$

where we remind that $\delta = \omega_{\mathrm{cav}} - \omega_{\mathrm{at}}$. For weak pumping and/or large detuning, one has

$$\Gamma_{\mathrm{em}}^0 \frac{(\Gamma_{\mathrm{p}}/2)^2}{\delta^2 + (\Gamma_{\mathrm{p}}/2)^2} < \Gamma_{\mathrm{l}}, \tag{2.42}$$
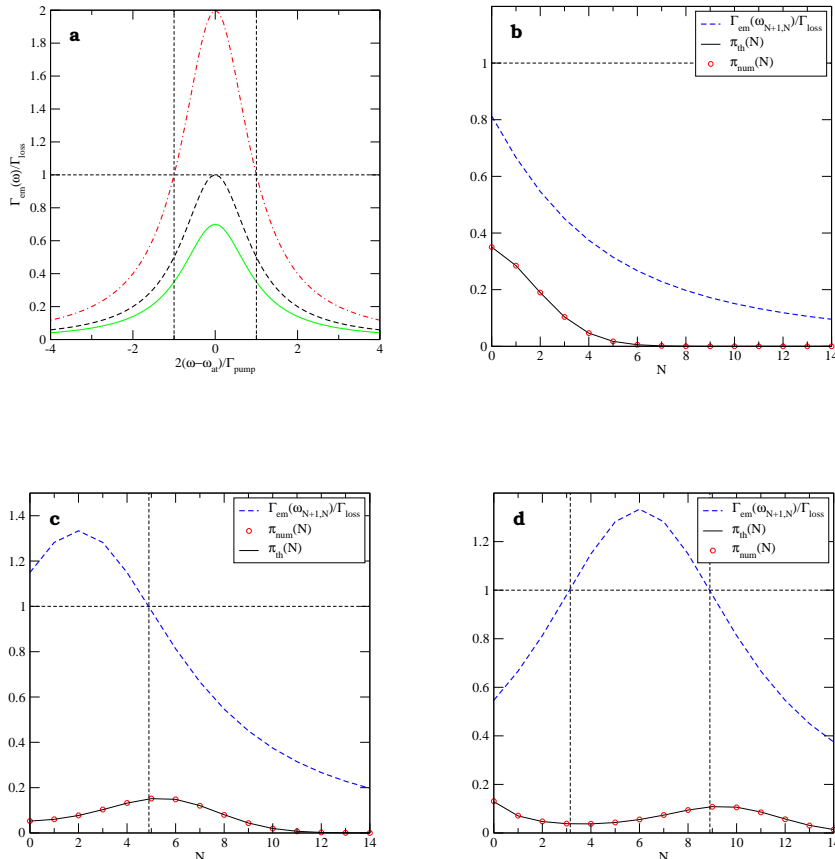
Figure 2.1: (a) Emission vs. loss rate as a function of the detuning from the emitters frequency ω_{at}: the three curves are for peak emission Γ_{em}^0 larger (red dash-dotted), equal (black dashed), smaller (green solid) than the loss rate Γ_{l}. (b-d) Populations π_N of the N-photon state as a function of N in the three cases $\omega_2 \leq \omega_{\mathrm{cav}}$ (b), $\omega_1 \leq \omega_{\mathrm{cav}} \leq \omega_2$ (c), $\omega_{\mathrm{cav}} \leq \omega_1$ (d). In the three panels, the open dots are the numerical results of the photon-emitter theory, while the solid line is the prediction of the analytical purely photonic theory; the dashed curves show the ratio $\mathcal{S}_{\mathrm{em}}(\omega_{N+1,N})/\Gamma_{\mathrm{l}}$ as a function of N. Parameters: $\delta/U = 4$ (b), -2 (c), -6 (d). In all panels, $2U/\Gamma_{\mathrm{p}} = 0.2$, $2\Gamma_{\mathrm{l}}/\Gamma_{\mathrm{p}} = 0.0006$, $2\Omega_R/\Gamma_{\mathrm{p}} = 0.02$.

so the density matrix for the cavity shows a monotonically decreasing thermal occupation law. For strong pumping and close to resonance, one can achieve the regime where the emission overcompensates losses and the cavity mode starts being strongly populated:

$$\Gamma_{\mathrm{em}}^0 \frac{(\Gamma_{\mathrm{p}}/2)^2}{\delta^2 + (\Gamma_{\mathrm{p}}/2)^2} > \Gamma_{\mathrm{l}}. \tag{2.43}$$

The transition between the two regimes is the usual laser threshold, but our mathematical description Eq. (2.24) does not include the standard gain saturation mechanism that usually serves to stabilize laser oscillation above threhsold [63, 170]: the population would in fact show a clearly unphysical monotonic growth for increasing N, as no mechanism limiting the efficiency of emission has been included. Physically, those saturations terms would provide from a limited efficiency of the atomic optical repumping scheme: for an high enough photon number, stimulated emission leads to a non-vanishing occupancy of the atomic ground-state which should reduce the photon emission rate as well as induce the presence of a re-absorption term in the purely photonic master equation (2.24). Mathematically, these corrections would correspond to higher order contributions in $\sqrt{N_{\mathrm{at}}}\Omega_{\mathrm{at}}/\Gamma_{\mathrm{p}}$ (not included here) in the series expansion of the self energy (2.14) involved in the derivation of Eq. (2.24). As we will see now, the presence of a finite interaction U and its interplay with the frequency-dependent emission will provide an alternative saturation mechanism which will regularize
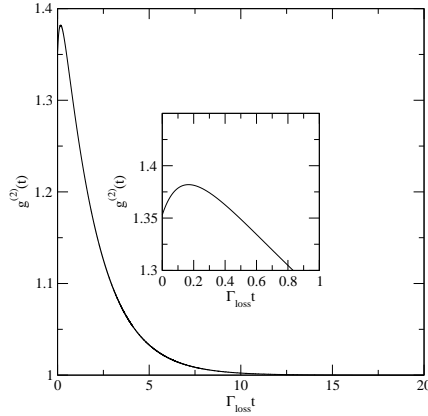
Figure 2.2: Purely photonic simulation of the two-time coherence function $g^{(2)}(\tau)$ in the weakly nonlinear regime. Parameters $U/\Gamma_\mathrm{p} = 0.1$, $\Gamma_\mathrm{l}/\Gamma_\mathrm{p} = 0.03$, $\Gamma_\mathrm{em}^0/\Gamma_\mathrm{p} = 0.04$, $\delta = -6U$ as in Fig.2.1(d).

the steady-state above threshold.

Indeed, for $U > 0$ the effective transition frequency depends on the number of photons,

$$\omega_{N+1,N} = \omega_\mathrm{cav} + NU \geq \omega_\mathrm{cav}, \tag{2.44}$$

so the gain condition

$$\frac{\Gamma_\mathrm{em}^0}{\Gamma_\mathrm{l}} \frac{(\Gamma_\mathrm{p}/2)^2}{(\omega_{N+1,N} - \omega_\mathrm{at})^2 + (\Gamma_\mathrm{p}/2)^2} \geq 1 \tag{2.45}$$

can be satisfied in a finite range of photon numbers only, as it is illustrated in Fig. 2.1 a). As a consequence, the presence of an increasing number of photons in the cavity is able to progressively blue shift the transition frequencies which ultimately fall out of the amplifying frequency domain (defined as $\mathcal{S}_\mathrm{em}(\omega) \ll \Gamma_\mathrm{l}$) above a critical photon number N^*, and even a weak nonlinearity U is able to stabilize the system for any value of Γ_em^0 (in spite of the absence of any gain saturation mechanism).

For $\Gamma_\mathrm{em}^0 < \Gamma_\mathrm{l}$, losses always dominate. For $\Gamma_\mathrm{em}^0 > \Gamma_\mathrm{l}$, the amplification condition is instead satisfied in a range of frequencies $[\omega_1, \omega_2]$ around ω_at. Under the weak nonlinearity condition $U \ll \Gamma_\mathrm{p}$, the $[\omega_1, \omega_2]$ range typically contains a large number of transition frequencies $\omega_{N+1,N}$ at different N. Three different regimes can then be identified depending on the position of the cavity frequency ω_cav with respect to the $[\omega_1, \omega_2]$ range.

(i) If $\omega_2 \leq \omega_\mathrm{cav}$, then the gain condition is never verified, and the population π_N shown in Fig.2.1(b) is a monotonically decreasing function of N: in this regime, the state of the cavity field is very similar to a thermal state, as it usually happens in a laser below threshold. (ii) If $\omega_1 \leq \omega_\mathrm{cav} \leq \omega_2$, the population π_N shown in Fig.2.1(c) is an increasing function for small N, shows a single maximum for $N \simeq \bar{N} = (\omega_2 - \omega_\mathrm{cav})/U$, and finally monotonically decreases for $N > \bar{N}$.

The phenomenology is the richest in the regime (iii) where $\omega_\mathrm{cav} \leq \omega_1$. In this case, for small N the population π_N decreases from its initial value π_0 until the nonlinearly shifted frequency enters in the gain interval for $N \simeq \bar{N}' = (\omega_1 - \omega_\mathrm{cav})/U$. After this point π_N starts increasing again until it reaches a local maximum at $N \simeq \bar{N} = (\omega_2 - \omega_\mathrm{cav})/U$. Finally, for even larger N it begins to monotonically decrease. An example of this behaviour is shown in Fig.2.1(d).

The existence of two well separate local maxima at $N = 0$ and $N \simeq \bar{N}$ in the photon number distribution π_N suggests that the incoherently driven nonlinear resonator exhibits a sort of bistable behaviour: when it is prepared at one maximum of the photon number distribution π_N, the system is trapped in a metastable state localized in a neighborhood of this maximum for a macroscopically long time. Switching from one metastable state to the other results is only possible as a result of a large fluctuation, so it has a very low probability, typically exponentially small in the photon number difference between the two metastable states.

This bistable behavior is clearly visible in the temporal dependence of the delayed two-photon correlation function

$$g^{(2)}(\tau) = \frac{\langle a^\dagger(t)\, a^\dagger(t+\tau)\, a(t+\tau)\, a(t) \rangle_{ss}}{\langle a^\dagger(t)\, a(t)\rangle_{ss} \langle a^\dagger(t+\tau)\, a(t+\tau)\rangle_{ss}} \; : \tag{2.46}$$

that is plotted in Fig. 2.2: at short times, the value of $g^{(2)}$ is determined by a weighted average of the contribution of the two maxima according to the stationary π_N. After a quick transient of order $1/\Gamma_{(em/l)}$, which corresponds to a fast local equilibration of the probability distribution around each of its maxima, the $g^{(2)}$ correlation function slowly decays to its asymptotic value 1 on a much longer time-scale mainly set by the exponentially long switching time from one maximum to the other

It is worth emphasizing that the present mechanism for optical bistability bears important differences from the dispersive or absorptive optical bistability phenomena discussed in textbooks [19, 146], i.e., in the case we presented in Sec. 1.2.3.1 of strongly interacting photons with a coherent drive [115, 125]: on one hand there is some analogy to dispersive optical bistability in the sense that the intensity-dependence of the refractive index is responsible for a frequency shift of the cavity resonance; on the other hand the frequency-selection is not provided by the resonance condition with a monochromatic coherent incident field, but rather by the competition between frequency-dependent incoherent emission and Markovian losses.

2.3.3 Photonic Fock states, premises of an incompressible quantum fluid of light

We now focus on the photon blockade regime $U \gg \Gamma_{\mathrm{p}}$, for which the nonlinearity is so large that a change of photon number by a single unity has a sizable effect on the emission rate $\mathcal{S}_{\mathrm{em}}(\omega_{N+1,N})$.

The ensuing physics is most clear in the regime when the maximum emission rate is large but only a single transition fits within the emission lineshape: these assumptions are equivalent to imposing that

$$\frac{\Gamma_{\mathrm{em}}^0}{\Gamma_{\mathrm{l}}} \gg 1 \qquad \text{and} \qquad \frac{\Gamma_{\mathrm{em}}^0}{\Gamma_{\mathrm{l}}} \frac{\Gamma_{\mathrm{p}}^2}{U^2} \ll 1 \tag{2.47}$$

with the further condition that the emission is resonant with the $N_0 \to N_0 + 1$ transition,

$$\omega_{\mathrm{at}} = \omega_{\mathrm{cav}} + N_0 U. \tag{2.48}$$

As a result, only this last transition is dominated by emission, while all others are dominated by losses.

In the strong blockade regime, the bimodal stationary distribution π_N of Fig. 2.1 d) becomes therefore sharply peaked at two specific values, $N = 0$ and at $N = N_0$. Examples of this physics are illustrated in Fig. 2.3: the two peaks are always clearly visible, but depending on the parameters their relative height can be tuned to different values almost at will. It is however important to note that having a sizeable stationary population in the $N = N_0$ peak requires quite extreme values of the parameters as population would naturally tend to accumulate at $N = 0$ and this difficulty turns out to be exponentially harder for larger N_0.

The physics underlying this behaviour can be easily explained in terms of the asymmetry in the switching mechanisms leading from $N = 0$ to $N = N_0$ and viceversa. The former process requires in fact a sequence of several unlikely emission events from $N = 0$ to $N = N_0 - 1$ as emission is favoured only in the last step. On the other hand, decay from $N = N_0$ occurs as a consequence a single unlikely loss event from $N = N_0 - 1$ to $N = N_0 - 2$: as soon as the system is at $N = N_0 - 2$, it will quickly decay to $N = 0$.

The rate Γ_{acc} of such an accident can be estimated as follows: the probability that the system in $N = N_0 - 1$ decays to $N = N_0 - 2$ is a factor $(N_0 - 1)\Gamma_{\mathrm{l}}/(N_0\Gamma_{\mathrm{em}}^0)$ smaller than the one of being repumped to $N = N_0$. As the rate at which the system decays from $N = N_0$ to $N_0 - 1$ is approximately equal to $N_0\Gamma_{\mathrm{l}}$, one finally obtains

$$\Gamma_{acc} = N_0\Gamma_{\mathrm{l}}\frac{(N_0 - 1)\Gamma_{\mathrm{l}}}{N_0\Gamma_{\mathrm{em}}^0} \ll N_0\Gamma_{\mathrm{l}}. \tag{2.49}$$
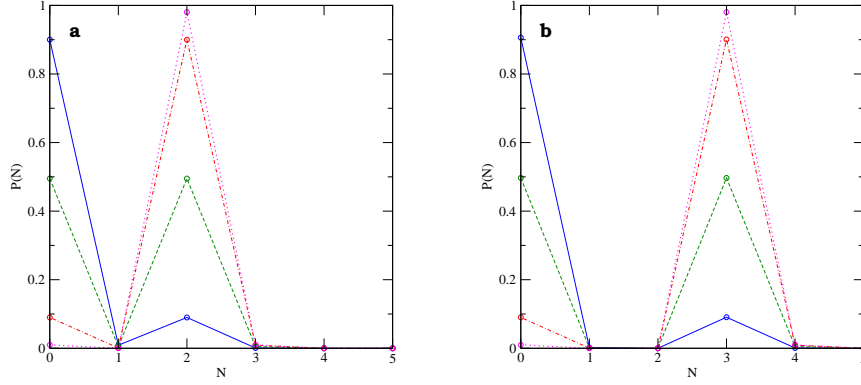
Figure 2.3: Selective generation of a $N_0 = 2$ photon (upper panel) and $N_0 = 3$ photon (lower panel) Fock state: Population π_N as a function of N for different pumping parameters. The points are the result of a purely photonic simulation, the lines are a guide to the eye. Left panel parameters: for all curves $\delta = -U$, $2\Omega_R/\Gamma_p = 0.01$, and then for each particular curve $2\Gamma_l/\Gamma_p = 2\,10^{-5}$ (blue solid line), $2\,10^{-6}$ (green, dashed line), $2\,10^{-7}$ (red, dash-dotted line), $2\,10^{-8}$ (magenta, dotted line). $2U/\Gamma_p = 10^{3/2}$ (blue solid line), 10^2 (green, dashed line), $10^{5/2}$ (red, dash-dotted line), 10^3 (magenta, dotted line). Right panel parameters: for all curves $\delta = -U$, $2\Omega_R/\Gamma_p = 0.01$, and then $2\Gamma_l/\Gamma_p = 5\,10^{-8}$ (blue solid line), $5\,10^{-9}$ (green, dashed line), $5\,10^{-10}$ (red, dash-dotted line), $5\,10^{-11}$ (magenta, dotted line). $2U/\Gamma_p = 2\,10^{5/2}$ (blue solid line), $2\,10^3$ (green, dashed line), $2\,10^{7/2}$ (red, dash-dotted line), $2\,10^4$ (magenta, dotted line). The goal of these choices of parameters was to control the steady-state ratios $P(N+1)/P(N) = 10^{-2}$ and $P(N)/P(0) = 0.1, 1, 10, 100$ (blue, green, red, magenta).

This longer time scale $\tau_{acc} = \Gamma_{acc}^{-1}$ is clearly visible in the long tail of the time-dependent $g^{(2)}(t)$ that is plotted in the left panel of Fig. 2.4. The quick feature at very short times corresponds to the emission rate Γ_{em}^0.

From a slightly different perspective, we can take advantage of the slow rate of accidents Γ_{acc} to selectively prepare a metastable state with $N = N_0$ photons even in parameter regimes where the $N = 0$ state would be statistically favoured at steady-state. Though the state will eventually decay to $N = 0$, the lifetime of the metastable $N = N_0$ state can be long enough to be useful for interesting experiments: The idea to prepare the state with N_0 photons is to inject a larger number $N > N_0$ of photons into the cavity: the system will quickly decay to the $N = N_0$ state where the system remains trapped with a lifetime Γ_{acc}^{-1}.

The efficiency of this idea is illustrated in the right panel of Fig.2.4 where we plot the time evolution of the most relevant populations π_N. The initially created state with $N = N_{in}$ photons quickly decays, so that population accumulates into $N = N_0$ on a time-scale of the order of Γ_l; the eventual decay of the population towards $N = 0$ will then occur on a much longer time set by Γ_{acc}. It is worth noting that this strategy does not require that the initial preparation be number-selective: it will work equally well if a wide distribution of N_{in} are generated at the beginning, provided a sizable part of the distribution lies at $N > N_0$. Furthermore, this idea removes the need for extreme parameters such as the ones used in Fig.2.3 to obtain a balance between $\pi(N)$ and $\pi(0)$: as a result, the difficulty of creating a (metastable) state of N_0 photons is roughly independent of N_0.

Following on an alternative approach, the characteristic time scale τ_{acc} could be further enhanced by adding a second type of emitters whose transition frequency is tuned to quickly and selectively emit photons on the $N - 2 \to N - 1$ transition. In this way, the accident rate can be efficiently reduced to $\Gamma_{acc}^{(2)} \simeq \Gamma_l \left(\Gamma_l/\Gamma_{em}^0\right)^2 \ll \Gamma_{acc}$. By repeating the mechanism on k transitions, one can suppress the accident rate in a geometrical way to $\Gamma_{acc}^{(k)} \simeq \Gamma_l \left(\Gamma_l/\Gamma_{em}^0\right)^k \ll \Gamma_{acc}$. Finally, the Fock state with N_0 photons can be fully stabilized to an infinite lifetime and no problem of metastability if N_0 different emitter species are included so to cover all transitions from $N = 0$ to $N = N_0$. This idea is explored in the next Chapter where we analysed, among other features, the single-cavity steady-state in presence of a tailored square-shaped emission spectrum allowing to cover all photonic transitions and fully stabilize arbitrary Fock states with an high efficiency.
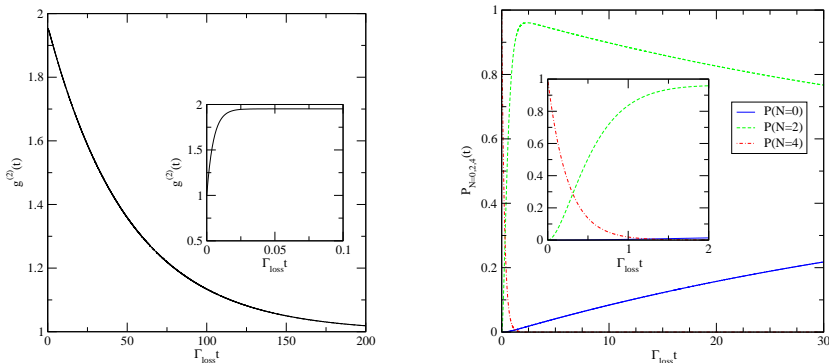
Figure 2.4: Left panel: Purely photonic simulation of the two-time coherence function $g^{(2)}(\tau)$ for a strongly nonlinear regime in a (metastable) $N_0 = 2$ photon selection regime. The inset shows a magnified view of the short time region. Parameters: $2U/\Gamma_{\mathrm{p}} = 100$, $2\Gamma_{\mathrm{l}}/\Gamma_{\mathrm{p}} = 2\,10^{-3}$, $2\Gamma^0_{\mathrm{em}}/\Gamma_{\mathrm{p}} = 0.2$, $\delta = -U$; in the language of Fig.2.3, the present parameters would correspond to a regime where the $N = 0, 2$ states are almost equally occupied. Right panel: Preparation of the metastable state at $N_0 = 2$ starting from a $N = 4$ $\pi(4)$ (red dot-dashed) $\pi(2)$ (green dashed) $\pi(0)$ (blue solid). Same parameters as in Fig.2.3.

These results show the potential of this novel photon number selection scheme to obtain light pulses with novel nonclassical properties: for instance, upon a sudden switch-off of the cavity mirrors, one would obtain a wavepacket containing an exact number of photons sharing the same wavefunction. With respect to the many other configurations discussed in the recent literature to produce N-photon Fock states and photon bundles [128, 163, 145], our proposal has the advantage of giving a deterministic preparation of a N-photon Fock state in the cavity, which can then be manipulated to extract light pulses with the desired quantum properties.

2.4 A preliminary result on pseudo-thermalization

After having discussed a number of interesting features that occur in the simplest case of a single-cavity, we are now in a position to start attacking the far richer many-cavity case. Before moving to the discussion of the Mott Insulator physics (which will be the subject of Sec. 2.6), we discuss some general properties of the steady-state not relying particularly on the specific choice of a Hamiltonian H_{ph}. In particular we unveil an exotic *"pseudo-thermalization"* effect occuring in the weakly non-Markovian regime where Hamiltonian energy scales are relatively small with respect to the linewidth Γ_{p} of the emission spectrum.

2.4.1 Markovian regime: infinite temperature state

We begin by considering the Markovian limit of the theory, which is recovered for $\Gamma_{\mathrm{p}} = \infty$, i.e. for a frequency-independent gain. In this case, the emission term of the master equation for photons Eq. (2.26) reduces to the usual Lindblad form

$$\mathcal{L}_{\mathrm{em}} = \frac{\Gamma^0_{\mathrm{em}}}{2} \sum_{i=1}^{L} \left[2a^\dagger_i \rho a_i - a_i a^\dagger_i \rho - \rho a_i a^\dagger_i \right]. \tag{2.50}$$

For a single cavity, the stationary state is immediately obtained as

$$\pi_N = \frac{1}{1 - \frac{\Gamma^0_{\mathrm{em}}}{\Gamma_{\mathrm{l}}}} \left(\frac{\Gamma^0_{\mathrm{em}}}{\Gamma_{\mathrm{l}}} \right)^N; \tag{2.51}$$

a necessary condition for stability for this system is of course that $\Gamma^0_{\mathrm{em}} < \Gamma_{\mathrm{l}}$. For $\Gamma^0_{\mathrm{em}} > \Gamma_{\mathrm{l}}$ amplification would in fact exceed losses and the system display a laser instability: while a correct description of gain saturation is beyond the purely photonic theory, the full atom-cavity theory would recover for this model the standard laser operation [63, 21].

For larger arrays of L sites, a straightforward calculation shows that in the Markovian limit the stationary matrix keeps a structureless form,

$$\rho_\infty = \frac{1}{Z} \left(\frac{\Gamma_{\text{em}}^0}{\Gamma_{\text{l}}} \right)^{\hat{N}}, \tag{2.52}$$

where $\hat{N} = \sum_i a_i^\dagger a_i$ is the total photon number operator, and

$$Z = \frac{1}{\left(\sum\limits_N \left(\frac{\Gamma_{\text{em}}^0}{\Gamma_{\text{l}}} \right)^N \right)^L}. \tag{2.53}$$

The validity of this result can be verified straightforwardly: on one hand, ρ_∞ can be expreessed as a series expansion in powers of $\hat{N}$ and thus trivially commutes with the particle number preserving Hamiltonian H_{ph}. On the other hand, $\rho_\infty = \frac{1}{Z} \prod_i \left(\frac{\Gamma_{\text{em}}^0}{\Gamma_{\text{l}}} \right)^{a_i^\dagger a_i}$ can be written as a product of the local solutions of the single site driven-dissipative problem, and thus also cancels the full dissipator: $\left[\mathcal{L}_{\text{em}} + \mathcal{L}_{\text{l}} \right] (\rho_\infty) = 0$: one has thus that $-i \left[H_{\text{ph}}, \rho_\infty \right] + \left[\mathcal{L}_{\text{em}} + \mathcal{L}_{\text{l}} \right] (\rho_\infty) = 0$.

This exact analytical result shows that independently of the number of cavities and the details of the Hamiltonian, in the Markovian limit the density matrix in the stationary state corresponds to an effective Grand-Canonical ensemble at infinite temperature $\beta_{\text{eff}} = 0$ with a fugacity $z = e^{\beta_{\text{eff}} \mu} = \Gamma_{\text{em}}^0 / \Gamma_{\text{l}}$ determined by the pumping and loss conditions only: the steady-state does not display much interesting physics as it is Hamiltonian independent, and all states $|f\rangle$ of a given N-photon sub-manifold are equally populated. In the particular case of the Bose-Hubbard model, the steady state does not depend neither on the tunneling amplitude J nor on the photon-photon interaction constant U.

2.4.2   Effective Grand-Canonical distribution in a weakly non-Markovian regime

The situation changes as soon as some non-Markovianity is included in the model. In this section we start from the weakly non-Markovian case where all relevant transitions adding one photon have a narrow distribution around the bare cavity frequency, $|\omega_{f'f} - \omega_{\text{cav}}| \ll \Gamma_{\text{p}}$ (i.e., $U, J \ll \Gamma_{\text{p}}$ in the specific case of the BH model), and show that in this regime the steady-state presents artificial thermal properties.

2.4.2.1   Secular regime

We start by assuming a secular limit where photonic dissipative processes are very slow with respect to Hamiltonian dynamics (i.e., $U, J \gg \Gamma_{\text{em}}^0, \Gamma_{\text{l}}$ in the specific case of the BH model), so that the non-diagonal terms of the density matrix in the photonic hamiltonian eigenbasis oscillate at a fast rate and are thus effectively decoupled from the (slowly varying) populations. In this limit, we can safely assume that all coherences vanish and we can restrict our attention to the populations. This somehow critical approximation will be justified a posteriori in the next subsection, where we treat perturbatively the coupling of populations to coherences and show both analytically and numerically that in the weakly markovian regime, their contribution is of higher order in the 'non-markovianity' parameter $1/\Gamma_{\text{p}}$ and therefore can be safely neglected.

Under these assumptions, the transfer rate on the $|f'\rangle \to |f\rangle$ transition where one photon is lost from $N + 1$ to N has a frequency-independent form

$$T_{f' \to f} = \Gamma_{\text{l}} \left| \langle f | a_i | f' \rangle \right|^2, \tag{2.54}$$

while the reverse emission process depends on the detunings $\Delta_{f'f} = \omega_{f'f} - \omega_{\text{cav}}$ and $\delta = \omega_{\text{cav}} - \omega_{\text{at}}$ as

$$
\begin{aligned}
T_{f \to f'} &= \Gamma_{\text{em}}^0 \left| \langle f' | a_i^\dagger | f \rangle \right|^2 \frac{(\Gamma_{\text{p}}/2)^2}{(\Delta_{f'f} + \omega_{\text{cav}} - \omega_{\text{at}})^2 + (\Gamma_{\text{p}}/2)^2} \\
&\simeq \tilde{\Gamma}_{\text{em}}^0 \left| \langle f |' a_i^\dagger | f \rangle \right|^2 \left[1 - \beta_{\text{eff}} \Delta_{f'f} + \mathcal{O} \left(\Delta_{f'f} \right)^2 \right],
\end{aligned} \tag{2.55}
$$

with

$$\tilde{\Gamma}^0_{\text{em}} = \frac{(\Gamma_{\text{p}}/2)^2}{(\omega_{\text{cav}} - \omega_{\text{at}})^2 + (\Gamma_{\text{p}}/2)^2} \Gamma^0_{\text{em}}, \tag{2.56}$$

$$\beta_{\text{eff}} = \frac{2(\omega_{\text{cav}} - \omega_{\text{at}})}{(\omega_{\text{cav}} - \omega_{\text{at}})^2 + (\Gamma_{\text{p}}/2)^2}. \tag{2.57}$$

In this expression, the weakly non-Markovian regime is characterized by having $|\beta_{\text{eff}}\Delta_{f'f}| \ll 1$: in this case, the square bracket in Eq. (2.55) can be replaced with no loss of accuracy by an exponential function of $\Delta_{f'f}$

$$1 - \beta_{\text{eff}}\Delta_{f'f} \simeq e^{-\beta_{\text{eff}}\Delta_{f'f}}, \tag{2.58}$$

which immediately leads to a Grand-Canonical form of the stationary density matrix

$$\rho_\infty = \frac{1}{\Xi} e^{\beta_{\text{eff}}\hat{N}\mu} e^{-\beta_{\text{eff}}H} : \tag{2.59}$$

indeed, in the secular approximation the quantum dynamics is well described by a diagonal classical stochastic process representing the probability transfer between the various eigenstates of H_{ph}, and the probability distribution provided by Eq. (2.59) verifies the detailed balance condition

$$T_{f'\to f}\pi_{f'} - T_{f\to f'}\pi_f = \left|\langle f'|\, a^\dagger \,|f\rangle\right|^2 \left[\Gamma_{\text{l}} \frac{1}{\Xi} \left(\frac{\tilde{\Gamma}^0_{\text{em}}}{\Gamma_{\text{l}}} e^{\beta_{\text{eff}}\omega_{\text{cav}}} \right)^{N+1} e^{-\beta_{\text{eff}}\omega_{f'}} + \right.$$
$$\left. - \tilde{\Gamma}^0_{\text{em}} e^{-\beta_{\text{eff}}\left(\omega_{f'f} - \omega_{\text{cav}}\right)} \frac{1}{\Xi} \left(\frac{\tilde{\Gamma}^0_{\text{em}}}{\Gamma_{\text{l}}} e^{\beta_{\text{eff}}\omega_{\text{cav}}} \right)^{N} e^{-\beta_{\text{eff}}\omega_f} \right] = 0. \tag{2.60}$$

Here the effective chemical potential

$$\mu = \frac{1}{\beta_{\text{eff}}} \log\left(\frac{\tilde{\Gamma}^0_{\text{em}}}{\Gamma_{\text{l}}} \right) + \omega_{\text{cav}} \tag{2.61}$$

and an effective temperature $T_{rmeff} = 1/\beta_{\text{eff}}$ (in units of $k_{\text{B}} = 1$) are artificial parameters depending on the spectral properties of the various reservoirs. Most remarkably, even if each transition involves a small deviation $\Delta_{f',f} \ll T_{\text{eff}}$ from the bare cavity frequency ω_{cav}, the cumulative effect of many such deviations can have important consequences for large photon numbers, so to make the stationary distribution strongly non-trivial (leading in particular, to dynamical stability above the lasing threshold: the emergence of Bose-Einstein Condensation in this context is the subject of Chap. 4). Remarkably, both positive and negative temperature configurations can be obtained from Eq. (2.57) just by tuning the peak emission frequency ω_{at} either below or above the bare cavity frequency ω_{cav}.

However it is crucial to keep in mind that this thermal-like distribution does not arises from any true thermalization process, but is a consequence of the specific form chosen for the pumping and dissipation: a subtle interplay between the frequency dependence of losses and emission processes allows to mimic the effect of a single thermalized bath in a local spectral region around ω_{cav}. This novel effect, that we choose to call *"pseudo-thermalization"*, implies that under very specific conditions, a quantum system in contact with an highly non-thermal environment can present all the properties of a thermalized system, at least at a static level. In order to complete this statement, one should also check the validity of the Fluctuation Dissipation theorem (FDT) [113] which allow to assess the level of thermalization also at a dynamical level (We will explore at length these aspects in Chapter. 4). A numerical test of pseudo-thermalization for a two-resonator system with a strong pumping $\Gamma_{\text{p}} \gg U, J$ and a large enough photon number so to induce appreciable nonlinear effects is shown in Fig. 2.5. The results of this comparison are displayed in the left and central panels: excellent agreement between an exact resolution of the photonic master equation and the grand canonical ensemble ansatz is found in both the average photon number and the first-order coherence. At higher $U \simeq \Gamma_{\text{p}}$ predictible deviations from the thermal predictions
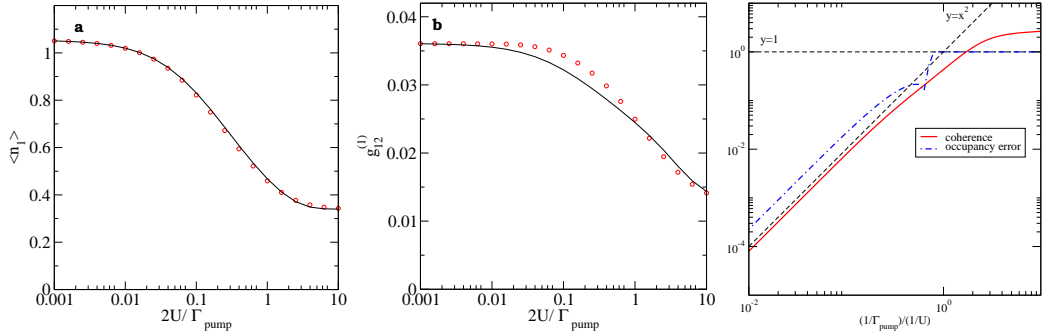
Figure 2.5: Left and center panels: average number of photons $n_1 = \langle a_1^\dagger a_1 \rangle$ (left) and spatial coherence $g_{1,2}^{(1)} = \langle a_1^\dagger a_2 \rangle / \langle a_1^\dagger a_1 \rangle$ (center) in a two cavity system with small U/Γ_p and J/Γ_p as a function of the non linearity U at fixed Γ_p. In red dots, exact resolution of the photonic master equation, and in black solid line the grand canonical ensemble ansatz. Parameters : $2J/\Gamma_\mathrm{p} = 0.02$, $2\Gamma_1/\Gamma_\mathrm{p} = 0.002$, $2\Gamma_\mathrm{em}^0/\Gamma_\mathrm{p} = 0.0014$, $2\delta/\Gamma_\mathrm{p} = 0.6$. Right panel: purely photonic simulation of the relative quantum coherence between two arbitrarily chosen two-photon eigenstates $\rho_{ij}/\sqrt{\rho_{ii}\rho_{jj}}$ as a function of $1/\Gamma_\mathrm{p}$ (the result does not depend on the specific eigenstates considered). As expected, this coherence vanishes in $1/\Gamma_{pump}^2$ in the Markovian limit $1/\Gamma_\mathrm{p} \to 0$. The value above 1 for large $1/\Gamma_\mathrm{p}$ signals breakdown of positivity of the density matrix as we move out of the validity regime of the purely photonic master equation. Parameters: $J/\Gamma_1 = 1$, $\Gamma_\mathrm{em}^0/\Gamma_1 = 0.5$, $\delta = -\Gamma_1$, $U/\Gamma_1 = 2$.

are found as we fall out of the weakly non-Markovian approximation. In particular, the deviations at increasing U/Γ_p become more quickly visible in the first order coherence $g_{1,2}^{(1)}$ since, in contrast with $\langle n_1 \rangle$, the non-vanishing value $g_{1,2}^{(1)} \simeq 0.036 \propto J/\Gamma_\mathrm{p}$ obtained at $U = 0$ already stems from the thermal signature arising from non-Markovian effects (at $T = \infty$, i.e., in the Markovian case, one would have $g_{1,2}^{(1)} = 0$).

The presence of a thermal signature strongly relies on the assumption that the Hamiltonian frequency scales (U, J for the BH model) are weak with respect to the gain medium emission linewidth Γ_p. This implies automatically that the resulting effective temperature T_eff is also large with respect to the U and J, and that pseudo-thermalization is valid only in the semi-classical regime, at least for our specific choice of a Lorentzian frequency-dependence emission spectrum. In a further study by [171] (which recovered independently our initial result), the author proposed to extend the detailed balance relation to a broader frequency range by engineering more complex reservoirs of emitters: theoretically, this improvement would allow in particular to lift the constraint of an hot temperature and access thus the quantum regime. However, while [171] was focusing on engineering rather hot artificial temperatures in view of accelerating the kinetics of quantum annealing operations in quantum circuits, a direct experimental application of this method to the stabilization of equilibrium-like strongly correlated quantum phases appears less realistic: indeed in the proposal of [171] reproducing the effect of a low temperature $T_\mathrm{eff} \ll U, J$ would necessarily involve an extremely large number of emitters and would be technologically challenging. An alternative approach allowing to reproduce the effect of a zero temperature involving relatively simple reservoirs will be the subject of next Chapter.

2.4.2.2 Beyond the secular approximation

In the weakly non-Markovian regime, the validity of the effective Grand-Canonical description can be extended outside the secular approximation according to the following arguments. As a first step, we decompose the master equation as

$$\frac{d\rho}{dt} = [\mathcal{M}_0 + \delta\mathcal{M}]\rho, \tag{2.62}$$

where the super-operators $\mathcal{M}$ and $\delta\mathcal{M}$ act on the density matrix ρ as

$$\mathcal{M}_0[\rho] = -i\,[H,\rho] + \frac{\Gamma_1}{2}\sum_{i=1}^{k}\left[2a_i\rho a_i^\dagger - a_i^\dagger a_i\rho - \rho a_i^\dagger a_i\right] + \frac{\tilde{\Gamma}_{\text{em}}^0}{2}\sum_{i=1}^{k}\left[\hat{a}_i^\dagger\rho a_i + a_i^\dagger\rho\hat{a}_i - a_i\hat{a}_i^\dagger\rho - \rho\hat{a}_i a_i^\dagger\right],$$
(2.63)

and

$$\delta\mathcal{M}[\rho] = \frac{\tilde{\Gamma}_{\text{em}}^0}{2}\sum_{i=1}^{k}\left[\delta a_i^\dagger\rho a_i + a_i^\dagger\rho\delta a_i - a_i\delta a_i^\dagger\rho - \rho\delta a_i a_i^\dagger\right],$$
(2.64)

$$\tilde{a}_i^\dagger = \frac{\tilde{\Gamma}_{\text{em}}^0}{\Gamma_{\text{em}}^0}\left(\hat{a}_i^\dagger + \delta a_i^\dagger\right).$$
(2.65)

Here,

$$\langle f'|\,\hat{a}_i^\dagger\,|f\rangle = \left(e^{-\beta_{\text{eff}}\Delta_{f'f}} - i\frac{\omega_{\text{cav}}-\omega_{at}}{\Gamma_{\text{p}}}\right)\langle f'|\,a_i^\dagger\,|f\rangle$$
(2.66)

contains the real part of the Fourier transform of the memory kernel of Eq. (2.31) up to first order in $\Delta_{f',f}$,

$$\langle f'|\,\delta a_i^\dagger\,|f\rangle \underset{\Gamma_{\text{p}}\to\infty}{=} \langle f'|\,a_i^\dagger\,|f\rangle\left(-i\frac{\Delta_{f'f}}{\Gamma_{\text{p}}} + \mathcal{O}\left(\frac{\Delta_{f',f}}{\Gamma_{\text{p}}}\right)^2\right).$$
(2.67)

contains the first order correction related to the imaginary part as well as all the remaining higher order contributions we did not include in Eq. (2.66). We can straightforwardly show by an exact calculation (not relying on the secular approximation), that the grand canonical distribution is a steady state of this modified $\mathcal{M}_0$ operator,

$$\mathcal{M}_0(e^{-\beta_{\text{eff}}(H_{\text{ph}}-\hat{N})}) = 0.$$
(2.68)

As the correction term $\delta\mathcal{M}$ vanishes in the Markovian limit proportionally to $1/\Gamma_{\text{p}}$, we can calculate the lowest order correction to the steady state induced by the perturbation $\delta\mathcal{M}$, which implies computing $\delta\mathcal{M}(e^{-\beta_{\text{eff}}(H_{\text{ph}}-\hat{N})})$: we easily show that the first order corrections in Eq. (2.67) are purely imaginary so that populations are perturbed only to second order in $\Delta_{f'f}/\Gamma_{\text{p}}\sim\beta_{\text{eff}}\Delta_{f'f}$. In our Markovian limit, these corrections then vanish even if we perform simultaneously the Markovian and thermodynamic limit. Secondly, coherences (which are exactly zero in the Markovian case, see Sec. 2.4.1) should be then proportional to $\Delta_{f'f}/\Gamma_{\text{p}}$. However, we have shown in App. D by computing the off-diagonal elements of $\delta\mathcal{M}(e^{-\beta_{\text{eff}}(H_{\text{ph}}-\hat{N})})$ that the linear contribution to coherences $\propto \frac{\Delta_{f'f}}{\Gamma_{\text{p}}}$ exactly vanishes when we sum over all sites of the system. We conclude thus that in the weakly non-Markovian limit, coherences between eigenstates of the hamiltonian are quadratic in $\Delta_{f'f}/\Gamma_{\text{p}}$ and therefore remain very small even out of the secular approximation .

As a further verification of this analytical argument, in the right panel of Fig. 2.5 we have shown the Γ_{p} dependence of the coherence between an arbitrary pair of two-photon states as well as the error in the population of an arbitrary eigenstate, between the true steady state and the grand canonical distribution. As expected on analytical grounds, both these quantities scale indeed as Γ_{p}^{-2}.

From these arguments, we conclude that the breakdown of the secular approximation which occurs in the thermodynamic limit where the spectrum become continuous should not affect the pseudo-thermalization of the steady state in the weakly non-Markovian regime of large Γ_{p}. Even if the steady-state is not modified, we however expect that the relatively strong dissipation will significantly affect the the system dynamics. A complete study of the physics of pseudo-thermalization (where we verify in particular the validity of the fluctuation-dissipation theorem also at a dynamical level) is the subject of Chapter 4.

2.5 An unexpected interaction-driven mechanism for quantum coherence

We discuss briefly in this section an exotic non-equilibrium effect occurring for zero detuning $\omega_{\text{cav}}=\omega_{\text{at}}$ [red dashed lines in Fig. 2.6(a-c)]. In panel (c) we see that the non-negligible

value of $2J/\Gamma_p$ is responsible for a significant spatial coherence between the two sites, which attains a maximum value $g_{12}^{(1)} \approx 0.26$ for an interaction strength $2U/\Gamma_p \simeq 0.16$ of the same order of magnitude as the tunnel coupling $2J/\Gamma_p = 0.2$. The quite unexpected appearance of this coherence in a $M = 2$ cavity configuration can be understood as follows: on one hand, in the absence of tunneling $J = 0$, all the dynamics is local and we do not expect any spatial coherence. On the other hand, in the absence of interparticle interactions $(U = 0)$ and for zero detuning $\omega_{cav} = \omega_{at}$, photonic symmetric and antisymmetric states are equally close to the pump resonance (albeit with opposite detuning) so they should be equally populated and one do not expect any coherence also in that case.

The origin of this mechanisms comes from the fact that, in presence of both tunneling and small interactions (i.e. for $J, U \neq 0$ and $U \ll J$), the energy of all eigenstates (symmetric/anti-symmetric states with various photon numbers) is perturbatively shifted in the upward direction by (small) interactions U. As a result, symmetric states, which are below the emitter transition frequency ω_{at}, get closer to resonance and become more populated than the anti-symmetric ones, which get farther to the resonance and are thus depleted (respectively, for an attractive interaction $U < 0$ one would expect to populate more the anti-symmetric state and favour sign alternation of the wave function between neighbouring sites). Moreover, no coherence is expected also in blockade regime $U \gg J, \Gamma_p$: since photons almost do not overlap spatially, the energy shift induced by interaction transition frequencies becomes very weak, and thus symmetric and antisymmetric states are no longer discriminated. As a consequence, one expects that a maximum of the coherence is obtained when interactions and tunneling are of the same magnitude, $U \approx J$: this result is clearly visible in panel Fig. 2.6(c).

This exotic effect is reflected in the steady-state occupancy of the different eigenstates shown in Fig. 2.6(d) for the maximum coherence point, where one can see that those which possess an overall positive coherence and weaker kinetic energy are the most populated ones. Even though the nonlinearity is only active for states with at least two photons, it is interesting to note that also in the single-photon manifold the antisymmetric state is less populated than the symmetric one. This population unbalance is inherited from the one in the above-lying $N > 1$ states, as the decay preferentially occurs into the symmetric state.

This effect of interaction-induced coherence does not have a clear equivalent in equilibrium physics for which states with low-energy states are always favoured with respect to excited ones. Understanding its implication in an infinite lattice, regarding in particular the underlying mechanism for non-equilibrium condensation at zero detuning has been postponed to a future study, as we decided during my thesis to focus on the many-body physics in the strong blockade regime

2.6 Non-equilibrium physics in the blockade regime $U \gg \Gamma_p$

Extending the photon-number selectivity idea to the many-cavity case, we now look for many-body states that resemble a Mott insulator [76, 59] in the strongly nonlinear regime $U \gg \Gamma_p$. As in the single cavity case (see Sec. 2.3.3), the strong pumping $\Gamma_{em}^0 \gg \Gamma_l$ would favour a large occupations of sites, but is counteracted by the effect of the nonlinearity $U \gg \Gamma_p$ and the choice of detuning $\delta = 0$ which set an upper bound to the occupation: the pump process which consists in adding a second photon on top of an already existing is strongly suppressed.

2.6.0.1 Mott states in the weak tunneling regime $J \ll \Gamma_p$

In the zero-tunneling $J = 0$ case, we fully recover the single cavity physics and our scheme predictably leads to the formation of a perfect Mott state with one photon per site. As discussed in Sec. 2.3.3, a similar stabilization procedure for larger integer densities $n \geq 2$ could be made possible by adding several emitters species on resonance with the different photonic transitions below n in order to avoid metastability issues of the Mott state. An improved version of the scheme presented in Sec. 2.2 allowing for the stabilization of Mott states with arbitrary n will be introduced in the next Chapter.
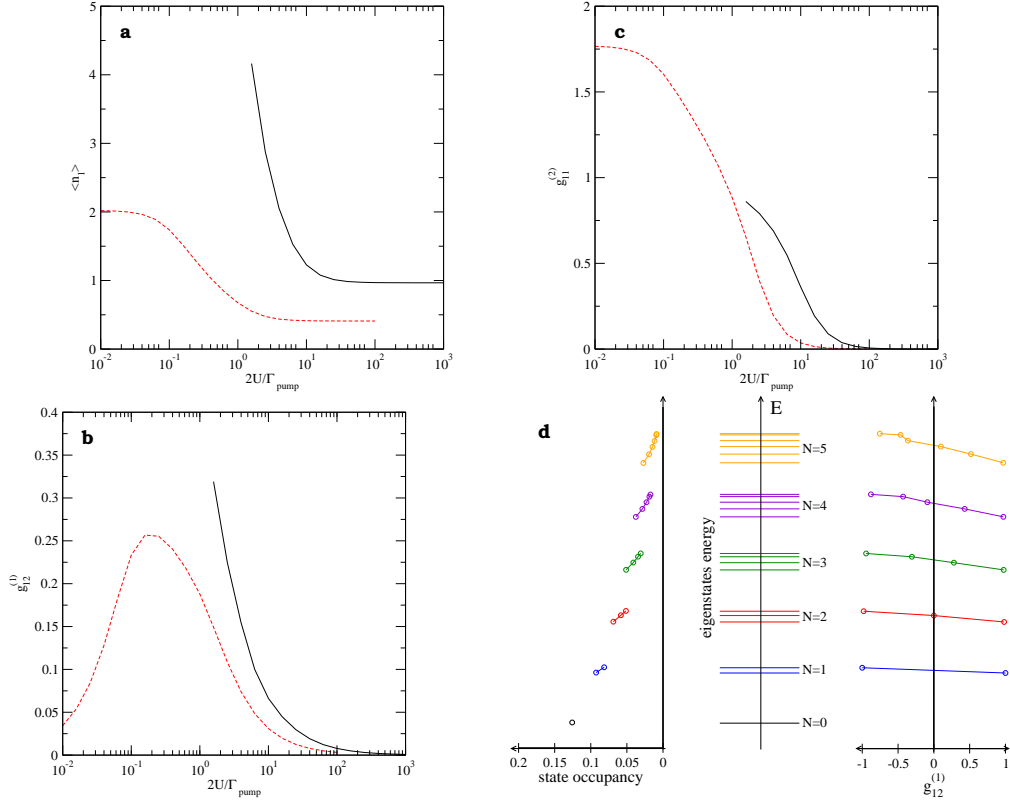
Figure 2.6: Purely photonic simulations of steady-state observables as a function of $2U/\Gamma_{\mathrm{p}}$ in a two-cavity system: (a) average number of photons $n_1 = \langle a_1^\dagger a_1 \rangle$, (b) one-site two-body correlation function $g_{1,1}^{(2)} = \langle a_1^\dagger a_1^\dagger a_1 a_1 \rangle = \langle n_1(n_1 - 1) \rangle$, (c) inter-site one-body correlation function $g_{1,2}^{(1)} = \langle a_1^\dagger a_2 \rangle / \langle a_1^\dagger a_1 \rangle$. Parameters: $2J/\Gamma_{\mathrm{p}} = 0.2$, $2\Gamma_1/\Gamma_{\mathrm{p}} = 0.002$, $2\Gamma_{\mathrm{em}}^0/\Gamma_{\mathrm{p}} = 0.06$, $\omega_{\mathrm{at}} = \omega_{\mathrm{cav}}$ (solid black line). Red dashed line, same simulation with a weaker $2\Gamma_{\mathrm{em}}^0/\Gamma_{\mathrm{p}} = 0.00144$. Panel (d), from left to right : state occupancy, energy and two site spatial coherence of the different eigenstates of the hamiltonian, at the maximum coherence point $2U/\Gamma_{\mathrm{p}} = 0.16$ of the red dashed line.

We now move to the more complex case of a weak but non-vanishing tunneling constant $J \ll \Gamma_{\mathrm{p}} \ll U$. Since $J \lll U$, photons are still unable to overcome photon blockade by tunneling and quantum processes involving particle exchange are largely suppressed. In particular, the eigenstate of the photonic Hamiltonian H_{ph} corresponding to the Mott Insulator (with $N = M$ photons) is completely localized: photons are almost perfectly pinned on a single site. Another consequence of having a weak tunneling is that all transitions frequencies $\omega_{\mathrm{cav}} - \epsilon_k$ (with $-2J < \epsilon_k < 2J$) from hole excited states with momentum k toward a completely saturated Mott-state have almost resonant values with the pump frequency $\omega_{\mathrm{at}} = \omega_{\mathrm{cav}}$ and fall within the emission frequency range (since $J \ll \Gamma_{\mathrm{p}}$). As a consequence, if one loses a photon starting from a completely filled Mott state with exactly one photon per site, the strong pump ($\Gamma_{\mathrm{em}}^0 \gg \Gamma_1$) will inject immediately a new photon and remove the corresponding hole excitation. In conclusion, one expects that in this regime the steady-state will still be a perfect Mott-state with a well-defined $n = 1$ number of photons per cavity.

This intuition is confirmed in Fig. 2.6(a-c) (black lines) where we can see clear signatures of the desired Mott state with one particle per site: for an high emission rate Γ_{em}^0 and a strong nonlinearity $U/\Gamma_{\mathrm{p}} \gg 1$, the steady-state average number of photons [panel a)] and the probability of double occupancy [panel (b)] respectively tends to 1 and 0. Finally the one-body coherence between two neighbouring sites also tends to 0 [panel c)], confirming the photonic localization effect. Based on this preliminary analysis, we can already make some claims on the structure of the non-equilibrium phase diagram of our model. As for $J = 0$ one can efficiently create a Fock state in each cavity, we expect that for small J the

system will remain in a sort of Mott state.

Finally, one would like to comment that, while simulations of Fig. 2.6 were done at the early beginnings of this Ph.D project for a very small system consisting in $M = 2$ coupled cavities, all the steady-state features described in this section were recovered in more extended lattices (see, e.g., Fig. 2.7) by using improved numerical methods.

2.6.1   Tunneling-induced depletion of the Mott state

In this subsection we investigate the effect of higher values of the tunneling constant ($J \geq \Gamma_p$), with a particular focus regarding the stability of the Mott-Insulating state. Numerical results and physical discussions are based on the collaborative work[12] for which the author of this Ph. D thesis provided contributions regarding physical predictions in the various regimes of parameters. Numerical simulations were performed by Alberto Biella and Florent Storme, and are based on the study of the master equation Eq. (2.5) of Sec. 2.2.1 associated to the full emitter+photon description. This model, although corresponding to a significantly bigger Hilbert space than the purely photonic one, is of a full Markovian type: this allowed to exploit powerful numerical methods such as corner-space renormalization [58] and matrix product operators techniques (MPO) [198, 214] in order to access the steady-state properties in larger 1D chains with open boundary conditions.

As we have seen in Sec. 2.6.0.1, for strong emission rate ($\Gamma_{em}^0 \gg \Gamma_l$), strong interaction-induced particle number selectivity ($U \gg \Gamma_p$) and weak tunneling ($J \ll \Gamma_p$), one can stabilize localized Mott-like states in a many cavity configuration: for a weak photonic single-particle bandwidth $\sim J$ compared to the emission linewidth Γ_p, hole excitations generated by photonic loss processes fall in resonance with the emitters and are immediately refilled by the pump, which brings back the many-body state toward the Mott state. Moreover, in this configuration, since tunneling is extremely weak with respect to the interaction ($J \ll \Gamma_P \ll U$), it does not allow to overcome the photon blockade potential barrier, and the particles are perflectly pinned on each site, i.e., fully localized.

However, the situation is expected to become more complex when J becomes of the order of Γ_p: in this regime, some hole excitation states start to be necessarily off-resonant with respect to the pump emission range. In consequence the pump does not inject photons at all energies and thus is not able to sustain a commensurate lattice filling: one expect the steady-state to possess a density n weaker than unity, and thus to be characterized by the presence of holes excitations.

This feature is confirmed by Fig. 2.7 (upper panels) where we show (for a 1D chain and various system sizes M) the average photon density $n = \left\langle a_i^\dagger a_i \right\rangle$ (left panel) and its variance $\Delta n^2 = \sum_i \Delta n_i^2 / M$ (right panel) as a function of the hopping J: while a Mott-state with fluctuationless density $n = 1$ appears to be stable for $J \ll \Gamma_p$, for higher tunneling values n starts to decrease and fluctuations in the density become important. Ultimately, for very strong hopping ($J \gg \Gamma_p$) the density goes progressively to 0 since only a few momentum states are in resonance with the pump. In addition to destabilizing the Mott state in the $J \gg \Gamma_p$ regime, fluctuations in the density as well as in the momentum of the generated hole excitations are responsible for a non-vanishing entropy $\mathcal{S} = -\langle \ln(\rho) \rangle > 0$, which is the signature of a statistical mixture. This is in stark contrast with the localized region ($J \ll \Gamma_p$), in which the photon-emitter density-matrix appears to be a pure quantum state: $\rho_{i,\infty} \simeq |1 \uparrow\rangle \langle 1 \uparrow|$.

The underlying mechanism of this instability of the Mott state can be well captured (even quantitatively) at an Hard-Core bosons level of description (namely, photons can be considered as fully impenetrable particles), since it occurs in a regime of parameters in which $J \simeq \Gamma_p \ll U$ is still negligible with respect to U (this is precisely the case in Fig. 2.7, where $U/J = +\infty$). This confirms our intuition according to which this change of behaviour is not physically related to some effect of competition between tunneling and interaction, but rather by an interplay between the tunneling and the frequency-dependence of the pump.

The main remaining question regards the nature of the quantum phases in both parameter regimes ($J \ll \Gamma_p$) and ($J \geq \Gamma_p$). Since the excess holes in the depleted $n < 1$ region do not suffer from the photon blockade and can delocalize via tunneling, one expects that they might allow to establish long range order (resp. quasi long range order depending on the spatial dimension), triggering thus a phase transition toward a coherent Bose-Condensed
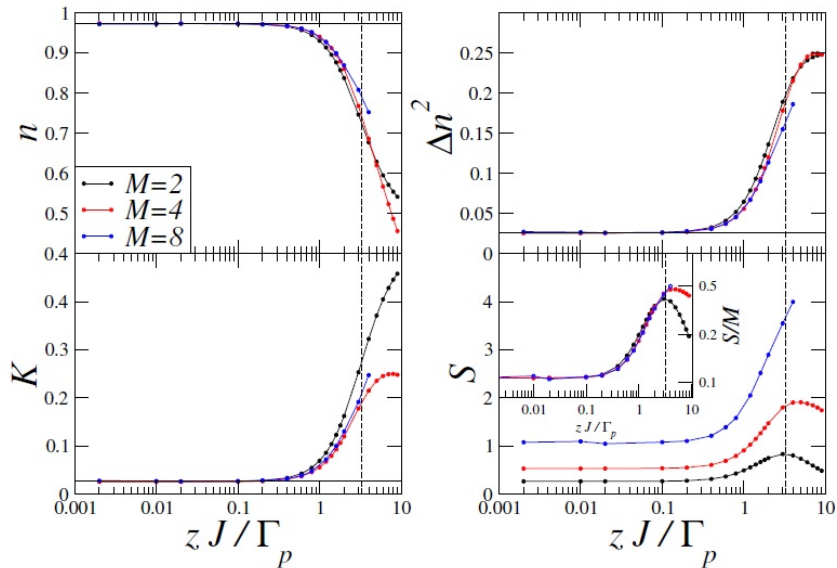
Figure 2.7: Top panels: the average photon density n in the steady-state (left panel) and its variance Δn^2 (right panel) as a function of zJ/Γ_{p} ($z = 2$ is the number of nearest neighbors). Bottom panels: steady-state value of the pseudo-compressibility $\kappa = \Delta n^2/n$ (left panel) and of the entropy (right panel) as a function of J/Γ_{p} in the hard-core limit ($U/J = +\infty$). The simulations were performed for periodic 1D chains for different system sizes M, as indicated in the legend. The solid horizontal lines are the single-cavity values ($J = 0$) of the quantity under consideration. Steady-state properties obtained by Florent Storme using corner-space renormalization methods [58]. The dashed vertical lines denote the critical hopping rates predicted by the Gutzwiller mean-field theory. The parameters are set as $\omega_{\mathrm{at}} = \omega_{\mathrm{cav}} - zJ$, $\Gamma_{\mathrm{l}}/\Gamma_{\mathrm{p}} = \gamma/\Gamma_{\mathrm{p}} = 10^{-3}$, $\Omega_{\mathrm{R}}/\Gamma_{\mathrm{p}} = 10^{-1}$.

state (resp. superfluid-like state). This specifically non-equilibrium phase transition from a Mott state to a superfluid phase was observed numerically and characterized at a Mean-Field level by Alberto Biella, and is the object of the Sec. 2.7.

Analysing this mechanism in the Bose-Hubbard case allows to understand why such a feature did not appear to be an hindrance for the stabilization of photonic Fractional Hall states with a similar frequency-dependent pump scheme [97, 195]. The FQH was indeed predicted in both proposals to be stable even for relevant values of the hopping term thanks to the presence of flat photonic bands. Indeed, the proposal of [97] involved a more complex lattice structure (originally introduced in [98]) specifically conceived in order to mimic the continuum physics of the FQH effect [59, 195], and featuring in particular flat photonic bands analogous to Landau levels even in presence of non-vanishing interactions.

2.6.2 Spatial correlations close to the Mott phase

Here we provide some preliminary results on the one-body correlations in a regime of relatively weak tunneling (J small with respect to Γ_p but non-negligible). The analytical calculation is based on somehow heuristic arguments as it involves an ansatz for the photonic density matrix in the hard-core limit in a 1D chain, and can not be taken as a definitive derivation of the steady-state properties. However we found, by comparing our predictions to our numerical results, that this ansatz allowed to capture important phenomenological features regarding the (small) deviations from the Mott state, such as the scaling of the coherence length λ in the ratio J/Γ_{p} (for a finite J, λ is expected to be non-zero due to the generation of a small number of hole excitations). For this reason I decided to include this discussion in my thesis.

2.6.2.1 Ansatz for the steady-state density matrix

In analogy with the equilibrium physics of hard-core bosons in one dimension [67, 122], we suppose that the steady-state is fermionized, i.e., that the photonic density matrix is diagonal in the fermionic momentum basis, up to a unitary Jordan-Wigner transformation U which antisymmetrizes the bosonic density matrix:

$$\rho^{\mathrm{F}} = U\rho^{\mathrm{B}}U^{-1}, \quad \rho^{\mathrm{F}} = \otimes_k \rho_k^{\mathrm{F}}. \tag{2.69}$$

The bosonic and fermionic annihilation operators are related through the unitary relation

$$a_j^{\mathrm{F}} = e^{i\pi(\sum_{l<j}\hat{n}_l)}Ua_j^{\mathrm{B}}U^{-1}, \tag{2.70}$$

where the value of the local particle number operator $\hat{n}_l = \hat{n}_l^{\mathrm{B/F}}$ is left unchanged by the unitary transformation. In the simple case of free bosons, no ansatz would be required as the momentum distribution of the steady-state of Eq. 2.24 can be exactly calculated analytically:

$$
\begin{aligned}
n_k^{\mathrm{B},0} &= \frac{1}{\frac{\Gamma_1}{\mathcal{S}_{\mathrm{em}}(\omega_{\mathrm{cav}}+\epsilon_k)} - 1} \\
&= \frac{1}{\frac{\Gamma_1}{\Gamma_{\mathrm{em}}^0}\left[\left(\tilde{\delta}+2\epsilon_k/\Gamma_{\mathrm{p}}\right)^2 + 1\right] - 1},
\end{aligned} \tag{2.71}
$$

where $\tilde{\delta} = 2(\omega_{\mathrm{cav}} - \omega_{\mathrm{at}})/\Gamma_p$ and $\epsilon_k = -2J\cos(k)$. Thus, in the Hard-Core regime, one would be tempted to choose the following ansatz for the Fermionic non-equilibrium distribution:

$$
\begin{aligned}
n_k^{\mathrm{F}} &= \frac{1}{\frac{\Gamma_1}{\mathcal{S}_{\mathrm{em}}(\omega_{\mathrm{cav}}+\epsilon_k)} + 1} \\
&= \frac{1}{\frac{\Gamma_1}{\Gamma_{\mathrm{em}}^0}\left[\left(\tilde{\delta}+2\epsilon_k/\Gamma_{\mathrm{p}}\right)^2 + 1\right] + 1}.
\end{aligned} \tag{2.72}
$$

The idea of this ansatz comes from the analogy with the equilibrium Bose-Einstein and Fermi distributions $n_k^{\mathrm{B,eq}} = \frac{1}{e^{\beta(\omega_{\mathrm{cav}}+\epsilon_k-\mu)}-1}$, $n_k^{\mathrm{F,eq}} = \frac{1}{e^{\beta(\omega_{\mathrm{cav}}+\epsilon_k-\mu)}+1}$ and their relation to the validity of the detailed balance relation $\mathcal{S}_{\mathrm{em}}^{\mathrm{eq}}(\omega_{\mathrm{cav}}+\epsilon_k)/\mathcal{S}_1^{\mathrm{eq}}(\omega_{\mathrm{cav}}+\epsilon_k) = e^{\beta(\omega_{\mathrm{cav}}+\epsilon_k-\mu)}$ (or Kennard-Stepanov [102, 180] relation) between the photonic emission and loss spectra whenever the external environment is thermal. The analytical function

$$g(z) = \frac{1}{\frac{\Gamma_1}{\Gamma_{\mathrm{em}}^0}\left[\left(\tilde{\delta}+z\right)^2 + 1\right] + 1} \tag{2.73}$$

of the complex variable z possesses two conjugated poles z_0 and z_0^*, where $z_0 = -\tilde{\delta} + i\sqrt{1 + \frac{\Gamma_{\mathrm{em}}^0}{\Gamma_1}}$. We find that $g(z)$ can be thus decomposed as a sum of two singular components and then easily expanded in power series:

$$
\begin{aligned}
g(z) &= \frac{\Gamma_{\mathrm{em}}^0}{\Gamma_1(z_0^*-z_0)}\left[\frac{1}{z_0-z} - \frac{1}{z_0^*-z}\right] \\
&= \frac{\Gamma_{\mathrm{em}}^0}{\mathrm{Im}(z_0)\Gamma_1}\frac{1}{R}\sum_{n=0}^{\infty}\sin[(n+1)k_0]\left(\frac{-z}{R}\right)^n,
\end{aligned} \tag{2.74}
$$

with $k_0 = -\frac{\pi}{2} + \mathrm{Arctan}\left(\frac{\tilde{\delta}}{\sqrt{1+\frac{\Gamma_{\mathrm{em}}^0}{\Gamma_1}}}\right)$ and $R = \sqrt{\tilde{\delta}^2 + 1 + \frac{\Gamma_{\mathrm{em}}^0}{\Gamma_1}}$. One obtains thus for the momentum distribution

$$n_k^{\mathrm{F}} = n_0\sum_{n=0}^{\infty}\frac{\sin[k_0(n+1)]}{\sin[k_0]}\left[\frac{4J/\Gamma_{\mathrm{p}}}{R}\right]^n\cos(k)^n, \tag{2.75}$$

where

$$n_0 = \frac{\Gamma_{\mathrm{em}}^0}{\mathrm{Im}(z_0)\Gamma_{\mathrm{l}}}\frac{\sin[k_0]}{R} = \frac{1}{\frac{\Gamma_{\mathrm{l}}}{\Gamma_{\mathrm{em}}^0}\frac{(\omega_{\mathrm{cav}}-\omega_{\mathrm{at}})^2+(\Gamma_{\mathrm{p}}/2)^2}{(\Gamma_{\mathrm{p}}/2)^2}+1} \tag{2.76}$$

is the photonic density at steady-state for $J = 0$. This expression for n_0 obtained from the ansatz is also analytically exact as one can verify it by studying the exactly solvable $J = 0$ case.

2.6.2.2   Fermionic one-body spatial autocorrelation

From the fermionic momentum distribution Eq. (2.72), it is possible to the compute by Fourier transform the fermionic one-body autocorrelation in spatial coordinates :

$$\left\langle a_{i+r}^{\mathrm{F}\dagger}a_i^{\mathrm{F}}\right\rangle = \int_{-\pi}^{\pi}\frac{dk}{2\pi}e^{-ikr}n_k^{\mathrm{F}}. \tag{2.77}$$

Using the series expansion Eq. (2.75) in power of the kinetic energy, one has that $\left\langle a_{i+r}^{\mathrm{F}\dagger}a_i^{\mathrm{F}}\right\rangle$ can be rewritten as

$$\left\langle a_{i+r}^{\mathrm{F}\dagger}a_i^{\mathrm{F}}\right\rangle = n_0 \sum_{n\geq r}\frac{\sin[k_0(n+1)]}{\sin(k_0)}\left[\frac{2J/\Gamma_{\mathrm{p}}}{R}\right]^n\int_{-\pi}^{\pi}\frac{dk}{2\pi}e^{-ikr}\underbrace{\cos(k)^n}_{=\left(\frac{e^{ik}+e^{-ik}}{2}\right)^n}, \tag{2.78}$$

where the the contributions $r < n$ are not present in the sum, as the integral in the right side is non-zero only for $n \geq r$. Since we are focusing on the weak tunneling regime $\frac{2J/\Gamma_{\mathrm{p}}}{R} \ll 1$, we keep only the lowest power of J in the serie expansion, which corresponds to $n = j$:

$$\begin{aligned}\left\langle a_{i+r}^{\mathrm{F}\dagger}a_i^{\mathrm{F}}\right\rangle &\simeq& n_0\frac{\sin[k_0(r+1)]}{\sin(k_0)}\left[\frac{2J/\Gamma_{\mathrm{p}}}{R}\right]^r\underbrace{\int_{-\pi}^{\pi}\frac{dk}{2\pi}e^{-ikr}\left(e^{ik}+e^{-ik}\right)^r}_{=1}\\ &=& n_0\frac{\sin[k_0(r+1)]}{\sin(k_0)}e^{-r/\lambda_F}, \end{aligned}\tag{2.79}$$

The fermionic autocorrelation thus spatially decays exponentially with a correlation length λ_F which is given by

$$1/\lambda_{\mathrm{F}} = \ln\left(\frac{\Gamma_p\sqrt{1+\tilde{\delta}^2+\frac{\Gamma_{\mathrm{em}}^0}{\Gamma_{\mathrm{l}}}}}{2J}\right), \tag{2.80}$$

and scales as $1/\ln\left(\frac{\Gamma_p}{J}\right)$ for vanishing J.

2.6.2.3   Photonic one-body spatial autocorrelation

The true photonic correlations are related to the fermionic correlations in the following way:

$$\left\langle a_{i+r}^{\dagger}a_i\right\rangle = \left\langle a_{i+r}^{\mathrm{F}\dagger}e^{i\pi\sum_{i<l<i+r}n_l^{\mathrm{F}}}a_i^{\mathrm{F}}\right\rangle, \tag{2.81}$$

where $n_l^{\mathrm{F}} = a_l^{\mathrm{F}\dagger}a_l^{\mathrm{F}}$ is the fermionic number operator on the site l. Since the fermionic steady-state is gaussian, the Wick theorem [56] could be applied to calculate this function. However in the generic case this would involve a very complex series expansion. For a very weak J the situation is much simpler, since the fermionic distribution is nearly momentum independent and the particles are almost localized with the corresponding spatial density $\left\langle n_l^{\mathrm{F}}\right\rangle = n_0$. To compute this complex correlation function, one can keep only the lowest order contribution in J/Γ_{p} in the series expansion related to the application of the Wick theorem, leading to the expression:

$$\left\langle a_{i+r}^{\dagger}a_i\right\rangle =\simeq \left\langle a_{i+r}^{\mathrm{F}\dagger}a_i^{\mathrm{F}}\right\rangle\prod_{i<l<i+r}\left\langle e^{i\pi\hat{n}_l}\right\rangle. \tag{2.82}$$

The local expectation value verifies $\left\langle e^{i\pi\hat{n}_l} \right\rangle = \pi^{n_l=0} - \pi^{n_l=1} \simeq 1 - 2n_0$: it is is positive for hole-dominated statistics ($n_0 < 1/2$), i.e., for $\mathcal{S}_{\text{em}}(\omega_{\text{cav}}) < \Gamma_{\text{l}}$, and negative for particle-dominated statistics ($n_0 > 1/2$), i.e., for $\mathcal{S}_{\text{em}}(\omega_{\text{cav}}) > \Gamma_{\text{l}}$. We note that the factor $\left\langle e^{i\pi\hat{n}_l} \right\rangle$ is not involved in the calculation of $\left\langle a^{\dagger}_{i+r} a_i \right\rangle$ for $r = 0$, 1.

We deduce thus the final expression for the photonic one-body spatial correlation for weak tunneling: expectedly for $r = 0$, one has that $\left\langle a^{\dagger}_i a_i \right\rangle = n_0$ is the photonic density calculated at zero-tunneling, while for $r \geq 1$ it still presents an exponential decaying behaviour:

$$\left\langle a^{\dagger}_{i+r} a_i \right\rangle_{r \geq 1} = \begin{cases} \frac{2n_0 J/\Gamma_{\text{p}}}{R} \frac{\sin[k_0(r+1)]}{\sin(k_0)} e^{-(r-1)/\lambda_B}, & \text{for} \quad n_0 < 1/2 \\ \frac{2n_0 J/\Gamma_{\text{p}}}{R} \frac{\sin[(k_0+\pi)(r+1)]}{\sin(k_0)} e^{-(r-1)/\lambda_B}, & \text{for} \quad n_0 > 1/2 \end{cases} \tag{2.83}$$

For a positive (resp. negative) detuning δ, the nearest neighbor correlation $\left\langle a^{\dagger}_{i+1} a_i \right\rangle$ is positive (resp. negative) independently of the density n_0, and is followed by a strong decay of $\left\langle a^{\dagger}_{i+r} a_i \right\rangle$ in modulus at higher distances $r > 1$: this indicates that a positive (resp. negative) detuning privileges momentum states close to $k = 0$ (resp. $k = \pi$), in agreement with our basic intuition. However the behaviour of the sign of $\left\langle a^{\dagger}_{i+r} a_i \right\rangle$ is less trivial when $r > 2$ and appears to be depending on whether $n_0 < 1/2$ or $n_0 > 1/2$.

The inverse correlation length is given by

$$1/\lambda = \ln\left(\frac{\Gamma_p \sqrt{1 + \tilde{\delta}^2 + \frac{\Gamma^0_{\text{em}}}{\Gamma_1}}}{2\left|1 - 2n_0\right| J} \right): \tag{2.84}$$

λ maintains the same scaling in J/Γ_{p} as the fermionic correlation length λ_{F} and is slightly shorter, due to a scrambling induced by sign changes when crossing intermediary particles. The exponential decay of correlations and the logarithmic scaling in J/Γ_{p} of the inverse correlation length λ^{-1} are confirmed by the MPO simulations for finite 1D chains shown in Fig. 2.8.

The behaviour $\left\langle a^{\dagger}_{i+r} a_i \right\rangle \propto (J/\Gamma_{\text{p}})^r$ is in agreement with the idea that the steady-state can be accessed perturbatively starting from a localized Mott state for a weak ratio J/Γ_{p}, as delocalizing a photon over r sites requires a process of order-r. The fact that $\lambda \to 0$ for very high $\Gamma^0_{\text{em}}/\Gamma_1$ is also conform to our intuition, as a strong emission rate would be able to pump new photons at all momenta and thus saturate the Mott state, even in the regime in which the kinetic energy $\propto J$ is large enough to shift the transition away from the core $\propto \Gamma_{\text{p}}$ of the Lorentzian emission spectrum.

While these observations encourage us to think that the fermionization hypothesis is not meaningless and does provide some insight on the steady-state properties, we recognize that our results in this direction are still speculative. Understanding under which conditions hard-core bosons can behave as free fermions also in an open quantum system with particle losses and pumping is a complex question which will be addressed in a future study.

2.7 Gutzwiller Mean-Field phase diagram

In this section, we investigate the mean-field phase diagram of the full Markovian model of Sec. 2.2.1 containing all emitters and photonic degrees of freedom. The MF phase diagram should also coincide with the one of the effective photonic non-Markovian description presented in Sec. 2.2.3 (although we do not have access to direct tools allowing to address the non-Markovian problem). All physical discussions and numerical results of this section provide from our most recent work [12]. Numerical simulations were performed by Alberto Biella, and are based on a Gutzwiller Mean-Field (MF) description (which represents formally the limit $z \to \infty$ of an infinite number of nearest neighbours) of the full Markovian emitter+photon dynamics given by Eq. (2.5) of Sec. 2.2.1 .

2.7.1 Method

One starts by assuming a factorized and translational-invariant ansatz for the time-dependent density matrix $\rho_{MF}(t) = \bigotimes_i \rho_i(t)$, where $\rho_i = \rho_j \ \forall i, j$. This approximation is justified
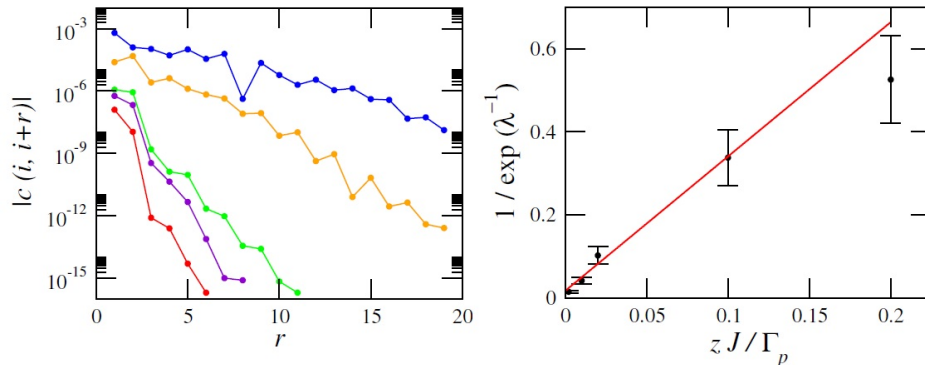
Figure 2.8: Left panel: Spatial decay of the correlation function $c(i, i+r) = \left\langle a_{i+r}^\dagger a_i \right\rangle$ (as defined in Eq. 2.83) at steady-state in function of the distance r for $M = 20$ sites computed by mean of the MPO algorithm, for several value of the tunneling J and zero detuning $\omega_{\text{at}} = \omega_{\text{cav}}$.. Correlators have been chosen in a symmetric way with respect to the center of the chain. $zJ/\Gamma_{\text{p}} = 0.002, 0.01, 0.02, 0.1, 0.2$ (red, violet, green, orange and blue line respectively). The other parameters are set as in Fig. 2.7. Right panel: The correlation length λ obtained fitting $c(i, i+r)$ with an exponentially decaying function. The red line is the scaling predicted by Eq. (2.84).

physically by the fact that for a large number of nearest neighbors, the physics becomes essentially the one of a single site coupled dynamically to a mascroscopic external classical field (the condensate), and additional non-local quantum correlations between two-specific neighboring sites are negligible. By inserting this ansatz in the master equation Eq. (2.5), and by keeping only most relevant terms in $1/z$ (more details on this procedure can be found, e.g., in Ref. [191]), we get an effective master equation

$$\partial_t \rho_i = \frac{1}{i} \left[H_{MF}(t), \rho_i \right] + \mathcal{L}(\rho_i), \tag{2.85}$$

where $\mathcal{L} = \mathcal{L}_{\text{l}}^{(i)} + \mathcal{L}_{\text{p}}^{(i)} + \mathcal{L}_{\gamma}^{(i)}$ is the sum of all local dissipative processes on the i-th site (photonic losses, two-level emitters pumping and spontaneous decay). The Mean-Field Hamiltonian $H_{\text{MF}}(t) = H_{\text{loc}}^{(i)} + H_{\text{tun}}(t)$ is the sum of

$$H_{\text{loc}} = \omega_{\text{cav}} a_i^\dagger a_i + \omega_{\text{cav}} \sigma^+ \sigma^- + \Omega_{\text{R}} \left(a^\dagger \sigma_i^- + a_i \sigma_i^+ \right) \tag{2.86}$$

which contains all local contributions of the total photon-emitter Hamiltonian (we assumed here the presence of $N_{\text{at}} = 1$ two-level emitter per site) of Sec. 2.2.1 on the i-th site, and

$$H_{\text{tun}}(t) = -zJ \left\langle a_i \right\rangle (t) a_i^\dagger + hc \tag{2.87}$$

is the time-dependent Mean-Field contribution which has to be computed self-consistently according to $\left\langle a_i \right\rangle (t) = \text{Tr} \left[\rho_i(t) a_i \right]$. The steady-state of Eq. (2.85) was reached dynamically by mean of a fourth-order Runge-Kutta integration method. The fact that this theory completely decouples the various sites i associated to the translational invariance allow us to use the simplified notations $a_i \to a$, $\sigma_i^- \to \sigma^-$.

This approach has been used extensively in order to determine the phase diagram of a wide range of driven-dissipative quantum systems [192, 191, 93, 16, 125]. It is exact in the limit of an infinite number of nearest neighbours (i.e., for long range hopping, or an infinite number of spatial dimensions), while for a more realistic configuration it has to be taken as a qualitative description encapsulating some features of the phase transition.

Renormalization group methods [206, 89, 187] allow to provide more insight on the conditions of validity of the Mean-Field description: above some upper-critical spatial dimension d_+ (which depends on the symmetries of the problem) MF theories provide exact predictions regarding the critical exponents, which describe the long range and low-frequency behaviour of the system close to a second order phase transition point. On the opposite below d_+, MF descriptions become inaccurate as it is necessary to include higher order couplings terms
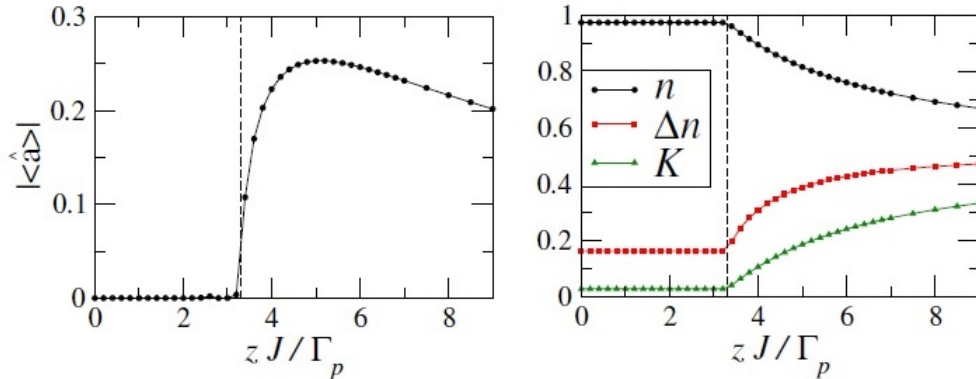
Figure 2.9: The order parameter $|\langle a \rangle|$ (left panel), the number of photons n, its variance Δn and the compressibility K (right panel) of the steady-state of Eq. cite as a function of zJ/Γ_{p} in the hard-core limit ($U/J = +\infty$). Here $\Gamma_{\mathrm{l}}/\Gamma_{\mathrm{p}} = \gamma/\Gamma_{\mathrm{p}} = 10^{-3}$, $\Omega_{\mathrm{R}}/\Gamma_{\mathrm{p}} = 10^{-1}$ and $\omega_{\mathrm{at}} = \omega_{\mathrm{cav}}$. The dashed vertical line signals the predicted critical value of J (see App. B).

going beyond a simple Gaussian field theory. Ultimately, under a lower-critical dimension d_{-}, no spontaneous symmetry breaking phenomenon is expected to occur [136] and phase transitions are usually replaced by smooth crossovers. An important exception to this statement is the 2D Bose Gas where the Bose-Einstein Condensation is replaced by a superfluid BKT transition[111] related to the unbinding of topological defects with opposite charges.

These considerations, although historically pretty clear for equilibrium systems, need for our purpose to be reframed in the context of non-equilibrium physics. One points out that being at thermal equilibrium can be understood as a special symmetry inside the Keldysh action [187, 95] of an underlying field theory [5, 175]. Thus, being out-of-equilibrium consists in breaking this symmetry, which can give rise to new universality classes differing from equilibrium ones both at a dynamical [176] and static level [2]. Remarkably, it has been predicted that arbitrary small deviations from equilibrium should have a dramatic impact on the structure of spatial and temporal correlations in lower dimensional systems [2, 199, 80]. For our model, providing information on the impact of non-equilibrium processes on long range correlations and critical properties would require to simulate numerically quantum problems over very large space scales, and goes beyond our MF level of description which should be thus understood as a description of the phenomenology at intermediary distances.

2.7.2   A Mott-to-Superfluid non-equilibrium phase transition

In this subsection, we describe the properties of the various phases of the model of Sec. 2.2.1 within our MF framework. As we have seen in Sec. 2.6.1, the Mott-like states obtained for strong emission rate ($\Gamma_{\mathrm{em}}^{0} \gg \Gamma_{\mathrm{l}}$), strong interaction ($U \gg \Gamma_{\mathrm{p}}$) and weak tunneling ($zJ \ll \Gamma_{\mathrm{p}}$) become unstable when one increases the tunneling constant as soon as one reaches the regime $zJ \geq \Gamma_{\mathrm{p}}$: off-resonant hole excitations start to proliferate within the steady-state and benefit from a strong mobility as they do no suffer from the effect of photon blockade. If those excitations are generated with enough energy selectivity, one expects that they could trigger a phase transition toward an ordered phase (of a Superfluid-like or Bose-Condensed type depending on the number of spatial dimensions). This intuition is confirmed at Mean-Field level by Fig. 2.9, where we show the value of the mean-field order parameter $\langle a \rangle (t)$, the photon density n, its fluctuations Δn and the pseudo-compressibility compressibility $\kappa = \Delta n^2 / n$ [3] in the steady-state in the hard-core limit ($U/J = +\infty$). We observe a clear second-order phase transition at a critical hopping $zJ_c^{HC}/\Gamma_{\mathrm{p}} \simeq 3.3$ breaking the $U(1)$ symmetry. The properties of the various phases can be summarized as follows.

For $J < J_c^{HC}$, the mean-field order parameter $\langle a \rangle (t)$ takes a vanishing value at steady-state, so the system is in a normal phase. Moreover, the steady-state single-site density

---

[3]It is equal to the static compressibility in the equilibrium case (where according to the FDT theorem, density response to a change of chemical potential is related to density fluctuations) and under the requirement of vanishing non-local correlations, so deep inside the Mott phase ($zJ \ll \Gamma_{\mathrm{p}}$).
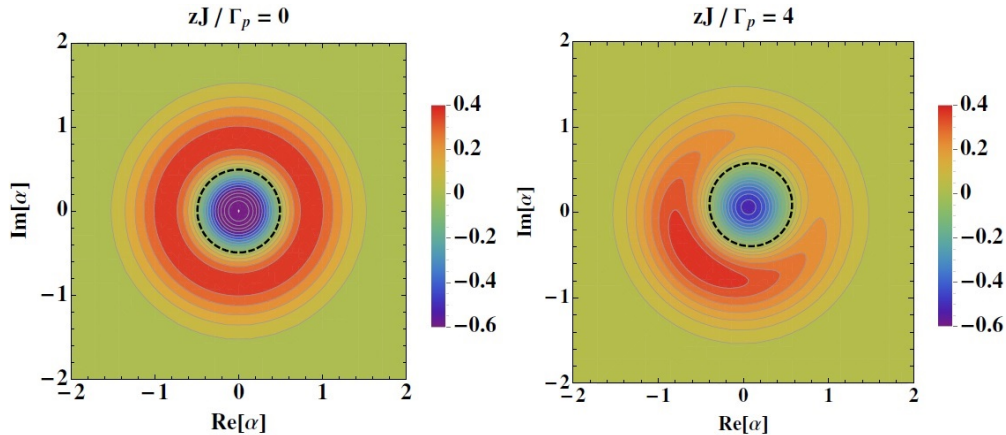
Figure 2.10: Contour plot of the steady-state Wigner distribution $W(\alpha)$ in the Mott-like (left panel) and coherent phase (right panel). Each contour denotes a variation of 0.05 of the value of $W(\alpha)$. The black dashed contour encircles the region with $W(\alpha) < 0$. The parameters are set as in Fig. 2.9.

matrix $\rho_{i,\infty}$ can very well represented by

$$\rho_{i,\infty} \simeq |1\uparrow\rangle\langle 1\uparrow|, \tag{2.88}$$

and is characterized by an almost unity density $n \simeq 1$ and very weak density variations ($\simeq 3\%$ probability of not being in the Fock state $|1\rangle$): the steady-state is in a Mott-Like phase. The non-vanishing value for fluctuations is related to the finite choice of parameters of Fig. 2.9 (chosing too extreme parameters would have induced a very large time scale separation, and rendered unfeasible the time-dependent numerical simulation): while a finite ratio $\Gamma_{\rm em}^0/\Gamma_1$ is responsible for weak (but non-zero) probability leakage out of the desired steady-state, for $\Gamma_{\rm em}^0/\Gamma_1 \to \infty$ one would stabilize a perfect $n = 1$ Mott-state.

For $J > J_c^{HC}$, the system enters a coherent phase, where the steady-state maintains an oscillatory behaviour in the non-vanishing order parameter

$$\langle a\rangle (t) = |\langle a\rangle| e^{-i\omega_L t}, \tag{2.89}$$

were ω_L is a lasing frequency spontaneously chosen by the system. Although those simulations where done in the Hard-Core limit ($U = +\infty$), the Mott-phase instability appears to occur at a finite critical hopping J_c and is always accompanied by a decrease of density n, which indicates that hole excitations are responsible for the superfluid-like nature of the steady-state. Similarly to what was observed for finite size simulations in Fig. 2.7, the spontaneously broken phase is also characterized by the emergence of non-vanishing particle number fluctuations Δn and pseudo-compressibility κ (we also observed a non-zero entropy $\mathcal{S}$ in that phase).

The remaining time-dependence in the coherent phase related to the spontaneous breaking of the gauge symmetry is a simple effect also present in equilibrium Bose-Einstein condensates (where $\langle a\rangle (t) = |\langle a\rangle| e^{-i\mu t}$), which does not present any particular surprise. However highly non-trivial persistent oscillatory behaviours of local measurable observables (the absolute phase can not be measured) can be observed in other non-equilibrium configurations: while a no-go theorem precluding the observation of a *"time crystal"* [205] spontaneously breaking the time translational symmetry in isolated equilibrated systems has been formulated in [202], its realizability has been predicted in periodically driven isolated systems [53, 103] and observed very recently in [36, 212]. In driven-dissipative systems this phenomena is well-know under the name of *"limit-cycle phase"*: highly non-trivial oscillatory behaviours without any equilibrium counterpart have been predicted theoretically in open systems such as the self-induced modulation of density patterns in circuit-QED devices [87] and Rydberg atoms [121], the Bose-condensed fraction and light field in hybrid atom-optics quantum systems [148], as well as the magnetization [32] in spin systems,

It is possible to gain more information on the statistics of both Mott and coherent phases
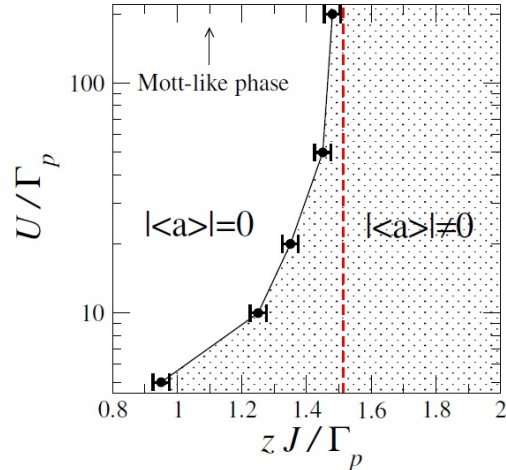
Figure 2.11: Mean-field steady-state phase diagram in the $\{U/\Gamma_{\rm p}, zJ/\Gamma_{\rm p}\}$ plane. The white area corresponds to the region of the parameters for which $|\langle a \rangle| = 0$ while in the dotted region the $U(1)$ symmetry is spontaneously broken and the steady-state exhibits limit-cycle $(|\langle a \rangle| > 0)$. Here Here $\Gamma_{\rm l}/\Gamma_{\rm p} = \gamma/\Gamma_{\rm p} = 10^{-2}$, $\Omega_{\rm R}/\Gamma_{\rm p} = 10^{-1}$ and $\omega_{\rm at} = \omega_{\rm cav}$. The dashed vertical line denotes critical hopping rate predicted by the Gutzwiller stability analysis for Hard-Core bosons $zJ_c^{HC}/\Gamma_{\rm p} = 1.51$.

by looking at the Wigner quasi-probability distribution [75]

$$W(\alpha) = \frac{2}{\pi} \text{Tr} \left[\rho_{i\infty} \mathcal{D}(\alpha) e^{ia^\dagger a} \mathcal{D}^\dagger(\alpha) \right] \tag{2.90}$$

where $\mathcal{D}(\alpha) = e^{\alpha a - \alpha^* a^\dagger}$ is the deplacement operator and the prefactor comes from the normalization condition $\int_{\mathbb{C}} d^2\alpha W(\alpha) = 1$. Since the two quadratures of the quantum field $X = \frac{1}{\sqrt{2}}(a + a^\dagger)$ and $P = \frac{1}{\sqrt{2}}\frac{(a - a^\dagger)}{i}$ do not commute, they can not be measured altogether and thus W can not be understood as a probability distribution in the classical phase space $\{X, P\}$ (W can even be negative in some regions for very quantum states). However, for strongly occupied semiclassical states where quantum fluctuations are less relevant, W ultimately has the meaning of a probability distribution.

As we can see in Fig. 2.10, the Wigner distribution is perfectly phase invariant deep in the Mott phase. The steady-state is almost a one-photon Fock state: this strong non-classicality appears under the form of a large domain around $\alpha = 0$ where W takes negative values. Above the critical coupling $(J > J_c^{HC})$ the steady-state has a broken symmetry and so has the Wigner distribution. Note that the asymmetric part of the Wigner function rather possesses positive values, reflecting the fact that the Bose-Einstein Condensate on top of the Mott state is a large populated coherent state of quasi-classical nature (this is especially true for the Mean-Field theory/for long range hopping).

2.7.3 Phase diagram

Here we discuss the properties of the phase boundary associated to the phase transition introduced in Sec. 2.7.2. As a first step we study the position of of the phase boundary in function of the interaction parameter U (shown in Fig. 2.11). The transition occurs at any numerically accessible values of the interaction parameters U. On one hand, the critical hopping J_c remains finite even in the Hard-Core regime and thus does not scale proportionally with U, highlighting the non-equilibrium nature of the phase transition, which does not rely in a fondamental manner on the interplay between interaction and tunneling, but is rather related to the generation of hole excitations at non-resonant energies with the pump (a more advanced driven-dissipative non-Markovian scheme allowing to recover all equilibrium features is the subject of the next Chapter). On the other hand at rather weak $U \simeq \Gamma_{\rm p}$ the transition threshold J_c appears to be lowered. We believe that this is related to two different physical mechanisms: first, the lowered value J_c is related to the

loss of commensurability, as for $U \simeq \Gamma_{\rm p}$ the emission of a second photon on top of an already existing one is not inhibited anymore by the blockade effect. Secondly for a finite U/J, the competition between delocalization and photon blockade might also start playing a non-negligible role and contribute to trigger the transition.

Fig. 2.11 shows the phase diagram only for values of the Kerr nonlinearity above $U/\Gamma_{\rm p} = 5$: for very weak interactions, the number of photons per site is very high above the lasing threshold ($\Gamma_{\rm em}^0/\Gamma_{\rm l} > 1$) and so is the required dimension of the corresponding Hilbert space $\mathcal{H}$, making the numerical simulation unworkable. While providing a full quantum description in this range of parameters at a numerical level is beyond the scope of our work, the weakly nonlinear regime can however can be understood at a mean-field level: for vanishing interactions, the dynamical instability occurs precisely at the lasing threshold $\Gamma_{\rm em}^0/\Gamma_{\rm l} = 1$. For an high enough spatial dimension d, any arbitrary weak hopping constant J is enough thus to favour a single momentum mode (the most amplified one) which will be macroscopically occupied and lead to the formation of a Bose-Einstein Condensate. One expects thus the critical hopping J_c to go to 0 in the weakly interacting regime $U/\Gamma_{\rm p} \to 0$. In Chapter 4, we will proceed to a complete theoretical study of the non-Markovian model introduced in this chapter focusing on the case of a weakly interacting BEC, which we will treat analytically by mean of an alternative approach based on a quantum Langevin formalism. At lower dimensions d the physics is expected to be sensitively different: in $d = 2$ the BEC transition should be replaced at intermediary spatial scales by BKT-like phase transition [111]. At very long spatial scales however, non-equilibrium effects highlighted in [2, 199] will probably play an important role and the transition is likely to be replaced by a very sharp crossover. This will be also the case in $d = 1$, where a Luttinger liquid-like phenomenology [64] and the formation of quasi-condensate [137] with a very large (but still finite) coherence length are expected. The study of low dimension physics in the regime of weak interactions will be the subject of a future work.

We now move to the discussion of the Hard-Core regime which allows to capture fondamental aspects of the phase transition: since superfluidity is essentially carried by holes in the strongly interacting regime $U/\Gamma_{\rm p}$, the presence of a finite contact interaction U can be seen somehow as a perturbation complexifying the physical discussion. For $U = +\infty$, the model given by Eq. (2.85) is considerably simplified as it corresponds to the driven-dissipative theory of two coherently coupled spins one-half

$$H_{\rm MF}(t) = \omega_{\rm cav}\Sigma^+\Sigma^- + \omega_{\rm cav}\sigma^+\sigma^- + \Omega_{\rm R}\left(\Sigma^x\sigma^x + \Sigma^y\sigma^y\right) - \frac{zJ}{2}\left(\Sigma^x\left\langle\Sigma^x\right\rangle + \Sigma^y\left\langle\Sigma^y\right\rangle\right) \quad (2.91)$$

where Σ^z is the photonic spin operator (at most one photon on each site is authorized), and σ^z is the emitter spin operator. It becomes then possible to compute analytically the shape of the Gutzwiller Mean-Field phase boundary, according to the following procedure [32, 191]: since the emitter+photon model of Sec. 2.2 is purely Markovian, it is possible to derive directly equations of motions for all time-dependent correlators starting from the Mean-Field master equation Eq. (2.85):

$$\frac{d\left\langle\theta\right\rangle(t)}{dt} = i\left\langle[H_{\rm MF}(t),\theta]\right\rangle(t) + \left\langle\bar{\mathcal{L}}(\theta)\right\rangle(t), \quad (2.92)$$

where θ is a generic operator, $\bar{\mathcal{L}} = \Gamma_{\rm l}\bar{\mathcal{D}}(a,\theta) + \Gamma_{\rm p}\bar{\mathcal{D}}(\sigma^+,\theta) + \gamma\bar{\mathcal{D}}(\sigma^-,\theta)$ and

$$\bar{\mathcal{D}}(\mathcal{O},\theta) = \frac{1}{2}\left[2\mathcal{O}^\dagger\theta\mathcal{O} - \mathcal{O}^\dagger\mathcal{O}\theta - \theta\mathcal{O}^\dagger\mathcal{O}\right] \quad (2.93)$$

is a modified dissipator acting on the operator θ instead of the density matrix, where left and right operators have been inverted. Since we are considering spins one-half, an infinite hierarchy of coupled equations is avoided: indeed, higher order correlations (e.g. $\left\langle\sigma^x\sigma^y\right\rangle$ or $\left\langle\sigma^x\sigma^y\Sigma^x\right\rangle$) can always be re-expressed as a sum of average values involving at maximum one spin operator of a single specie (e.g., $\left\langle\sigma^z\right\rangle$) or two spin operators of different species (e.g., $\left\langle\sigma^z\Sigma^x\right\rangle$), and one only needs to compute a finite number of these average values (there are 15 different correlators in total in our case). This leads to the following finite set of equations (where we have shown only the equations of motions for the photonic spin degrees
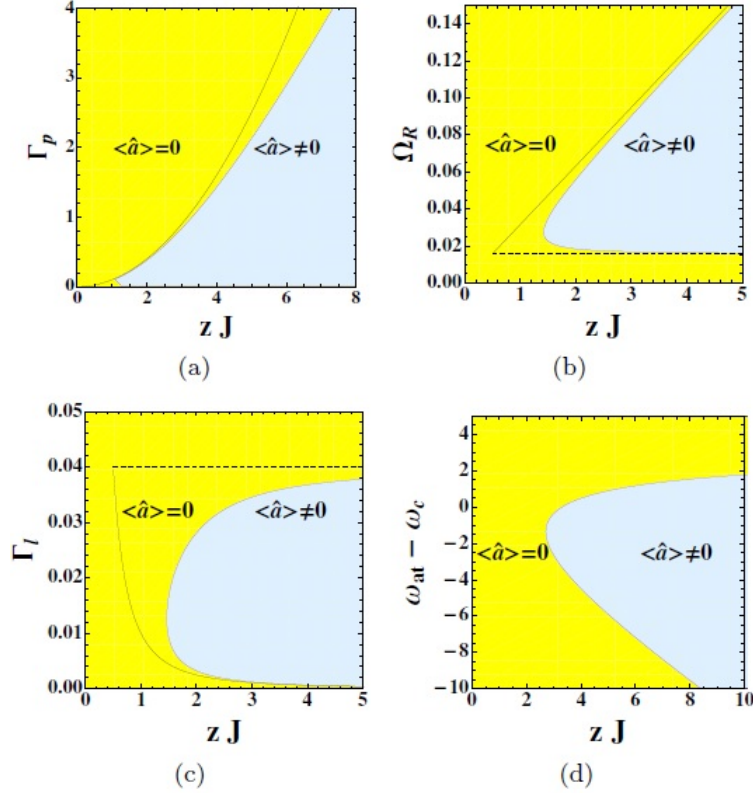
Figure 2.12: Results of the Gutzwiller mean-field stability analysis in the hard-core regime $(U/J = +\infty)$. The yellow area denotes the region where $|\langle a \rangle| = 0$ is stable, while the light blue area is the region where the solution $|\langle a \rangle| = 0$ is unstable and the symmetry is broken. When not varying them, we fixed the parameters as $\Gamma_l/\Gamma_p = \gamma/\Gamma_p = 10^{-3}$, $\Omega_R/\Gamma_p = 10^{-1}$ and $\omega_{at} = \omega_{cav}$. The solid lines [panels a)-c)] are the predictions for the critical hopping rate given by Eq.   which well approximates the phase boundary in the $\Gamma_{em}^0/\Gamma_l \to \infty$ limit (see Eq.). The dashed horizontal lines [panels b)-c)] denotes the lasing threshold at $\Gamma_{em}^0/\Gamma_l = 1$.

of freedom):

$$
\begin{aligned}
\frac{d\langle\Sigma^x\rangle(t)}{dt} &= \frac{\omega_{cav}}{2}\langle\Sigma^y\rangle(t) - \Omega_R\langle\sigma^y\Sigma^z\rangle(t) + zJ\langle\Sigma^y\rangle(t)\langle\Sigma^z\rangle(t) - \frac{\Gamma_l}{2}\langle\Sigma^x\rangle(t) \\
\frac{d\langle\Sigma^y\rangle(t)}{dt} &= -\frac{\omega_{cav}}{2}\langle\Sigma^x\rangle(t) + \Omega_R\langle\sigma^x\Sigma^z\rangle(t) - zJ\langle\Sigma^x\rangle(t)\langle\Sigma^z\rangle(t) - \frac{\Gamma_l}{2}\langle\Sigma^y\rangle(t) \\
\frac{d\langle\Sigma^z\rangle(t)}{dt} &= \Omega_R\left[\langle\sigma^y\Sigma^x\rangle(t) - \langle\sigma^x\Sigma^y\rangle(t)\right] - \Gamma_l\langle\Sigma^x\rangle(t) \\
&\quad \dots
\end{aligned}
\tag{2.94}
$$

For $J = 0$, the set of equations (2.94) is completely linear and can be analytically inverted. This leads to a unique steady-state solution which always verifies $\langle\Sigma^x\rangle_\infty = \langle\Sigma^y\rangle_\infty = \langle\sigma^x\rangle_\infty = \langle\sigma^y\rangle_\infty = 0$ due to the $U(1)$ symmetry. For a finite J, the $J = 0$ non-condensed solution is still valid, since the nonlinear perturbations $\propto J\langle\Sigma^{x/y/z}\rangle$ vanish in the set of equations 2.94 in absence of SSB. In order to analyze its dynamical stability, one linearizes the system of coupled equations around the $J = 0$ solution, and computes the eigenvalues of the resulting Jacobian Matrix. If the real part of one of its eigenvalues becomes positive for certain values of the parameters $(J, \delta, \Omega, \Gamma_l...)$ then the single-cavity fixed point is dynamically unstable: this defines the stability domain of the Mott-like phase. Outside the Mott region, Eqs. (2.94) presents a continuous set of limit-cycle solutions (with oscillatory phases) due to the broken symmetry. No analytical solution can be found there, as the system of equations (2.94) is intrinsically nonlinear in the superfluid region.

The stability domain obtained analytically from this approach is given in Fig. 2.12. Its

shape can be understood quite well according to the following physical argument: in order to be in a coherent hole-superfluid phase, the conduction band needs to be large enough in such a way that some off-resonant hole excitations are generated (with a certain selectivity in momentum and frequency), leading thus to the inequality

$$\Gamma_{\text{em}}^0 \frac{(\Gamma_{\text{p}}/2)^2}{(E_J + \omega_{\text{cav}} - \omega_{\text{at}})^2 + (\Gamma_{\text{p}}/2)^2} \leq \Gamma_{\text{l}}, \tag{2.95}$$

where E_J either equals $-zJ_c^{HC}$ or $+zJ_c^{HC}$ (depending on the positive or negative choice for the detuning). At the same time, under the lasing threshold we do not expect that a dynamical instability leading to the emergence macroscopic coherence can occur, so the dynamical amplification condition

$$\Gamma_{\text{em}}^0 \geq \Gamma_{\text{l}} \tag{2.96}$$

needs to be verified.

These two conditions can be re-expressed in function of the microscopic photon-emitter parameters of Sec. 2.2.1 as $\Gamma_{\text{em}}^0 = \frac{4\Omega_{\text{at}}^2}{\Gamma_{\text{p}}}$. In the zero detuning case ($\omega_{\text{at}} = \omega_{\text{cav}}$), for example, one finds that the superfluid domain can be estimated according to the two inequalities:

$$zJ_c^{HC} \quad \geq \quad \sqrt{\frac{\Gamma_{\text{p}}}{\Gamma_{\text{l}}}}\Omega_R, \tag{2.97}$$

$$\Omega_R \quad \geq \quad \frac{\sqrt{\Gamma_{\text{l}}\Gamma_{\text{p}}}}{2}. \tag{2.98}$$

The tunneling selectivity condition Eq. (2.97) is shown in solid line in Fig. 2.12 (panels a)-c)), while the lasing condition Eq. (2.98) is shown in dashed line(panels b),c)). The very good qualitative agreement between this estimate (providing even exact orders of magnitude) and the true analytical solutions (obtained by the full calculation of the stability domain according to the procedure described below) make us feel confident about the robustness of our interpretation of the physical mechanisms underlying the transition. As could be expected, the exact phase boundary kind of interpolates the two conditions Eq. (2.97) and Eq. (2.98).

2.8 Conclusions

We have introduced a novel quantum optics scheme in an array of driven-dissipative non-linear resonators with embedded incoherently pumped two-level emitters, and by mean of projective methods, we could eliminate the emitter dynamics and wrote an effective photonic master equation where the non-Markovian properties of emission are highlighted. In this chapter, the focus was set on the many-body phenomenology arising from the simple configuration for which the resulting emission spectrum is of a narrow bandpass type and more precisely of Lorentzian shape, which is obtained in the case where all emitters possess the same frequency. Simulations for the first part of this chapter were done using the projected non-Markovian photonic master equation, and simulations in the second part were based on the full {photons+emitters} microscopic model.

As a first step we focused on the steady-state properties of this model in a single cavity configuration, and showed that this scheme leads to exotic bistability effects, but more importantly allows for the stabilization of photonic Fock state in a strongly repulsive regime, which is a key step toward the stabilization of strongly correlated quantum phases in photonic platforms. Then, by investigating the many cavity configuration, we confirmed the existence of a Mott phase for weak tunneling, and unveiled an instability mechanism occurring when the hopping constant becomes comparable to the emission linewidth leading to a depletion of the Mott states and increased fluctuations. The scaling of the correlation length in the region presenting deviations from the Mott state has been predicted by mean of a fermionized ansatz for the steady-state, and found to fit with the numerical predictions.

The last part of our study was related to the phase diagram of this model within a Gutzwiller Mean-Field framework. We showed that while the Mott-phase was stable at weak tunneling, the depletion mechanism mentioned earlier was accompanied by a phase transition led by commensurability effects toward a coherent phase reminiscent of the Superfluid or

Bose-condensed phase of the equilibrium model. This result is significant as the MI-SF transition had never been predicted quantum optics in any previous study including the effect of dissipation. The stability domain of the two phases was computed numerically and also accessed analytically in the specific case of the Hard-core regime, and its shape could be reproduced qualitatively by mean of a simple ansatz encapsulating the mechanisms underlying the instability.

The two works [119, 12] highlighted the promises of implementing non-Markovian reservoirs in optical devices in view of stabilizing strongly correlated photonic phases. Still, the specific non-equilibrium features obtained in the case of a narrow bandpass emission spectrum could be seen as a remaining hindrance toward the quantum simulation of equilibrium physics. A more advanced non-Markovian scheme involving reservoirs with tailored spectra, allowing for the stabilization of robust Mott states with arbitrary integer density, and more generally for the quantum simulation of the ground-state of many-body Hamiltonians in driven-dissipative photonic lattices is the subject of next Chapter.

Chapter 3

Stabilizing strongly correlated photon fluids with tailored non-Markovian reservoirs

3.1 Introduction

In this chapter, we present our results regarding the possibility of stabilizing incompressible quantum states with light such as the celebrated Mott-Insulator phase, and more generally of quantum simulating zero-temperature equilibrium physics, by mean of a novel non-Markovian pump scheme. With respect to the previous chapter our scheme is based on the use of more complex tailored reservoirs for pumping and losses, leading to broad bandpass dissipative spectra.

In last Chapter, we have introduced a photonic model in a driven-dissipative array of nonlinear resonators featuring a *frequency-dependent incoherent pump* in order to stabilize interesting incompressible photonic phases. Our scheme is based on the insertion of two-level emitters with an inversion of population enforced by the presence of an incoherent drive [119, 12]. The narrow bandpass frequency spectra (typically Lorentzian ones)

$$\mathcal{S}_{\text{em}}^{\text{Lorentzian}}(\omega) = \Gamma_{\text{em}}^0 \frac{(\Gamma_{\text{p}}/2)^2}{(\omega - \omega_{\text{at}})^2 + (\Gamma_{\text{p}}/2)^2} \tag{3.1}$$

we have considered as a first step the configuration where all emitters transition frequencies take the identical value ω_{at}. As was discussed in the introductory Chapter 1 (Sec. 1.2.3.2) such scheme appears well suited to observe Fractional Quantum Hall effects [97] under the requirement of flat photonic bands [98]. Its potential for quantum error correction operations was also highlighted in [96]. In Chapter 2 we validated the possibility of stabilizing strongly localized $n = 1$ Mott insulator states. However as was discussed, the use of a narrow bandpass spectrum does not appear suitable to explore the physics of competing effects between interactions and tunneling in the dissipative photonic Bose-Hubbard model, as we have shown that its efficiency is restricted to the regime for which the photonic hopping is extremely weak compared to the interaction ($J \ll \Gamma_{\text{p}} \ll U$). Namely, it was demonstrated that even relatively weak values of the hopping amplitude ($J \sim \Gamma_{\text{p}}$) result in a proliferation of holes inside the Mott state, which then undergoes a transition toward a coherent superfluid-like phase with incommensurate density $n < 1$. A slightly different scheme based on a two-photon coherent drive combined with frequency-dependent losses was recently proposed in [22] and featured somehow comparable results.

The origin of these difficulties for this class of models comes from the fact that the overall shape of a Lorentzian function has only a single tunable parameter, namely its linewidth Γ_{p}, which simultaneously determines the widths of its core and its tails, i.e., the frequency domains where it takes respectively strong and weak values. For example, such a spectral

shape does not allow to select a broad band of energies while excluding undesired transitions above a certain energy cutoff, which is the role of the interplay between a chemical potential and temperature in equilibrium physics, and might be of critical importance for our purpose.

In order to reproduce the equilibrium phenomenology of the Mott-Insulator-to-superfluid phase transition in the novel physical context of driven-dissipative photonic systems, it is thus essential to develop new pumping schemes that allow to refill holes across a wide bandwidth, while maintaining simultaneously a strong selectivity above some characteristic frequency. An interesting first step in this direction was discussed in Sec. 1.2.3.3 where a relatively complex protocol was proposed to implement the idea of an engineered chemical potential for light in a circuit-QED platform. For suitably chosen equilibration rates with the engineered reservoir, photons may effectively thermalize to a statistical distribution with the desired thermodynamic parameters. Due to the necessity of building a complex thermal environment with a controlled parametric coupling to the desired many-body system, implementing such a proposal could potentially reveal a hard challenge.

In this Chapter we follow a different and potentially much simpler path of proposing the use of non-Markovian incoherent baths with tailored emission and loss spectra, to cool strongly correlated photonic systems toward ground-state-like steady states with a tunable effective chemical potential, on a longer run, observe interesting phase transitions. In analogy with Chapter 2, a non-Markovian incoherent pump with a "square-shaped" tailored emission spectrum

$$\mathcal{S}_{\text{em}}^{\text{tailored}}(\omega) \propto \int_{\omega_-}^{\omega_+} d\omega' \frac{\Gamma_{\text{p}}/2}{(\omega - \omega')^2 + (\Gamma_{\text{p}}/2)^2} \qquad (3.2)$$

could be engineered in a simple yet realistic manner by using population-inverted two-level emitters with a broad distribution of transition frequencies, homogeneous over the interval $[\omega_-, \omega_+]$. A similar scheme with a wide frequency distribution of absorbers and/or additional lossy cavities could be used to implement tailored frequency-dependent losses. As we will see, several experimental strategies allow to reproduce the effect of such reservoirs while reducing the number of required emitters and absorbers to a few units, making this scheme readily implementable with state-of-the art quantum technologies.

The structure of the Chapter is the following. In Sec.3.2, we introduce a first physical model based on the implementation of a non-Markovian pump scheme with tailored emission spectrum. In Sec.3.3, we discuss the equilibrium-like properties of the non-equilibrium steady-state for this model, and briefly review the single cavity physics demonstrating that this scheme allows for the stabilization of arbitrary photonic Fock states. Then in Sec. 3.4, by applying our scheme to the paradigmatic case of the one-dimensional (1D) BH model, we numerically show how a square-like emission spectrum allows to stabilize Mott-Insulator-like states with an arbitrary integer and fluctuationless photon density which are robust against tunneling and losses. For higher tunneling amplitudes or a change in the effective chemical potential (the two cases leading respectively to integer and non-integer values for the photonic density), our finite-size system exhibits a crossover towards a coherent state reminiscent of the Mott insulator-to-superfluid transition of equilibrium systems. In addition to the overall agreement with the equilibrium physics, in Sec. 3.5 we unveil and characterize novel non-equilibrium processes leading to entropy generation and deviations from a zero temperature state in some specific regions of the parameters space. In order to overcome this entropic transition and be able to perform a full quantum simulation of the whole phase diagram of the Bose-Hubbard model, in Sec. 3.6 we extend the initial model by adding frequency-dependent losses. We anticipate and confirm numerically that in this way the steady-state fully overlaps with the Hamiltonian ground-state for all choices of parameters. In Sec. 3.7, we discuss a possible experimental implementation of both models: after a brief reminder of the microscopic model introduced in the last Chapter in the case of a Lorentzian emission spectrum, we draw several simplification strategies in view of a future realization of tailored non-Markovian reservoirs.

All the results of this Chapter are based on the publication [118], of which the author of this thesis is the first and main author.
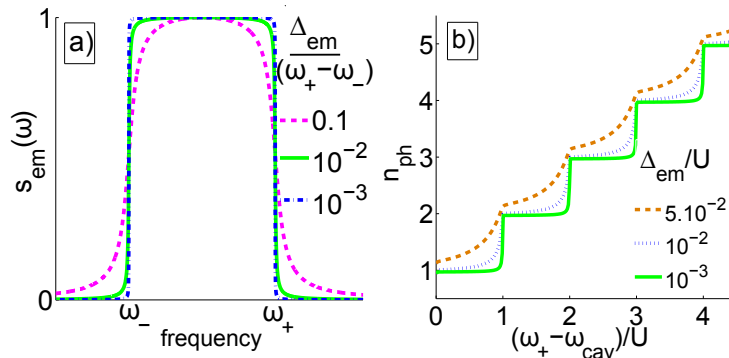
Figure 3.1: Panel a): Plot of the "square-shaped" emission spectrum $s_{em}(\omega)$ defined in (3.11) for various values of Δ_{em}. Panel b): Average photon number n_{ph} as a function of $\mu = \omega_+ - \omega_{cav}$ (i.e. varying ω_{cav}) for a single site system with various values of Δ_{em}. Parameters of panel b): $\Gamma_{em}^0/U = 3.10^{-4}$, $\Gamma_l/U = 10^{-5}$, $\omega_-/U = -40$.

3.2 The model

In this Chapter, we consider a driven-dissipative Bose-Hubbard model for strongly interacting photons in an array of L coupled nonlinear cavities ($\hbar = 1$):

$$H_{ph} = \sum_{i=1}^{L} \left[\omega_{cav} a_i^\dagger a_i + \frac{U}{2} a_i^\dagger a_i^\dagger a_i a_i \right] - \sum_{\langle i,j \rangle} J a_i^\dagger a_j, \qquad (3.3)$$

where a_i ($a_i^\dagger$) are bosonic annihilation (creation) operators for photons in the i-th cavity. As usual, J is the tunneling amplitude between neighboring cavities and U is the on-site interacting energy.

We will focus on the weakly-dissipative regime, in which photonic losses and emission processes (of respective rates $\sim \Gamma_l$ and $\sim \Gamma_{em}^0$) are slow with respect to the bath memory time scales. In contrast with the previous Chapter, here we provide directly the photonic Redfield master equation [21, 63] for the density matrix ρ providing non-Markovian dynamic

$$\partial_t \rho(t) = -i \left[H_{ph}, \rho(t) \right] + \mathcal{L}_l \left[\rho(t) \right] + \mathcal{L}_{em} \left[\rho(t) \right], \qquad (3.4)$$

while in Sec. 3.7 we will discuss several possibilities for experimental implementation. While losses are assumed to be Markovian and therefore modeled by a usual Lindblad term

$$\mathcal{L}_l[\rho] = \frac{\Gamma_l}{2} \sum_{i=1}^{L} \mathcal{D}[a_i; \rho] \qquad (3.5)$$

with $\mathcal{D}[\mathcal{O}; \rho] = 2\mathcal{O}\rho\mathcal{O}^\dagger - \mathcal{O}^\dagger\mathcal{O}\rho - \rho\mathcal{O}^\dagger\mathcal{O}$, the key ingredient of this model is to use a frequency-dependent incoherent pump, so that the emission term

$$\mathcal{L}_{em}[\rho] = \frac{\Gamma_{em}^0}{2} \sum_{i=1}^{L} \left[\tilde{a}_i^\dagger \rho a_i + a_i^\dagger \rho \tilde{a}_i - a_i \tilde{a}_i^\dagger \rho - \rho \tilde{a}_i a_i^\dagger \right] \qquad (3.6)$$

does not have a standard Lindblad form and involves modified lowering ($\tilde{a}_i$) and raising ($\tilde{a}_i^\dagger \equiv [\tilde{a}_i]^\dagger$) operators:

$$\frac{\Gamma_{em}^0}{2} \tilde{a}_i = \int_0^\infty d\tau \, \Gamma_{em}(\tau) a_i(-\tau). \qquad (3.7)$$

Here, the kernel

$$\Gamma_{em}(\tau) = \theta(\tau) \int \frac{d\omega}{2\pi} \mathcal{S}_{em}(\omega) e^{-i\omega\tau} \qquad (3.8)$$

takes into account the reservoir emission spectrum $\mathcal{S}_{em}(\omega)$, while the $a_i(t)$ operators are defined in the interaction picture with respect to the photonic Hamiltonian, $a_i(\tau) = e^{iH_{ph}\tau} a_i e^{-iH_{ph}\tau}$. Thus, considering two eigenstates $|f\rangle$ (resp. $|f'\rangle$) of the photonic

Hamiltonian with N (resp. $N + 1$) photons and energy ω_f (resp. $\omega_{f'}$), the matrix element of the modified jump operators equals

$$\langle f | \, \tilde{a}_i \, | f' \rangle = \frac{2}{\Gamma^0_{\mathrm{em}}} \Gamma_{\mathrm{em}}(\omega_{f'f}) \, \langle f | \, a_i \, | f' \rangle \,, \tag{3.9}$$

with $\omega_{f'f} = \omega_{f'} - \omega_f$ and

$$\Gamma_{\mathrm{em}}(\omega) = \frac{1}{2} \mathcal{S}_{\mathrm{em}}(\omega) - i\delta_l(\omega) \tag{3.10}$$

is the Fourier transform of the memory kernel $\Gamma_{\mathrm{em}}(\tau)$. While the magnitude of the Lamb-shift $\delta_l(\omega)$ stemming from the imaginary part of $\Gamma_{\mathrm{em}}(\omega)$ is typically small as compared to the emission linewidth $\propto \Delta_{\mathrm{em}}$ and Hamiltonian parameters U, J and thus does not bring important physical effects, the real part $\mathcal{S}_{\mathrm{em}}(\omega)/2$ is physically essential as it provides the frequency-dependent emission rate (this can be seen most clearly in App. C where we derive a Lindblad reformulation of Eq. 3.4 in the secular approximation). Further extension of the model including additional non-Markovian losses will be discussed in Sec. 3.6 .

As was discussed in the introduction and in the previous Chapter, the physics and the phase diagram of this driven-dissipative model critically depend on the specific choice of the emission spectrum. In contrast with our previous works [119, 12] in which the emission spectrum was Lorentzian, we will focus here on the study of a "square-shaped" spectrum $\mathcal{S}_{\mathrm{em}}(\omega) = s_{\mathrm{em}}(\omega)\Gamma^0_{\mathrm{em}}$, where

$$s_{\mathrm{em}}(\omega) = \mathcal{N} \int_{\omega_-}^{\omega_+} d\omega' \frac{\Delta_{\mathrm{em}}/2}{(\omega - \omega')^2 + (\Delta_{\mathrm{em}}/2)^2} \tag{3.11}$$

is shown in Fig.3.1 a) and the normalization constant $\mathcal{N}$ is set such that $s_{\mathrm{em}}\left(\frac{\omega_+ + \omega_-}{2}\right) = 1$. From the figure, one sees that $\mathcal{S}_{\mathrm{em}}(\omega)$ maintains an almost constant value Γ^0_{em} all over a frequency domain $[\omega_-, \omega_+]$, and decays smoothly with a power law outside this interval over a frequency scale Δ_{em}.

While Sec. 3.7 will be devoted to the discussion of several strategies for experimental implementation, basing ourselves on the microscopic model of Sec. 2.2 of last Chapter one can already see that this kind of emission spectrum could be obtained by coupling the various lattice sites to two-level emitters with an incoherent pumping in the excited state at a rate $\Gamma_{\mathrm{p}} = \Delta_{\mathrm{em}}$, and whose transition frequencies are uniformly distributed over the interval $[\omega_-, \omega_+]$ (the Lorentzian spectrum would be then recovered when $\omega_- = \omega_+$). As we will see in Sec. 3.7.2.2, the number of emitters required to reproduce this distribution can be reduced to a few units.

The main advantage of this scheme with respect to the case of a narrow bandpass emission spectrum of last Chapter, is that it allows to select a particular band of energies $[\omega_-, \omega_+]$ (in order to engineer low-T like steady-state, it will be a lower band of energy) while excluding transitions falling out this particular interval (in our case we will be interested in excluding high energy transitions): this will allow the Mott state to develop robustness against tunneling since, in contrast with the case of the Lorentzian spectrum, photons with a broad range of kinetic energies ($\sim J$) can now be injected without emitting undesired excitations above the many-body band gap ($\sim U$). For our purpose, the upper cutoff ω_+ will be the key ingredient to stabilize the desired steady-states: in Sec.3.3, we will show that the detuning $\omega_+ - \omega_{\mathrm{cav}}$ plays the role of a chemical potential for photons. On the other hand, the lower cutoff will be set to a far red-detuned frequency, in such a way to cover all required transitions below the upper cutoff ω_+. Typically, a value of $\omega_+ - \omega_-$ of the order of a few times U (which sets the characteristic transition energy between several photonic bands) is enough.

As we will see, in order to be able to target certain many-body transitions (and avoid in particular to pump new photons above the energy band gap), frequency-dependent emission processes will need to verify the selectivity condition $\Delta_{\mathrm{em}} \ll U$. Finally, the weak dissipation condition that we assumed at the beginning of this section translates into $\Gamma_{\mathrm{l}}, \Gamma^0_{\mathrm{em}} \ll \Delta_{\mathrm{em}}$. Understanding whether this latter inequality is required on physical grounds, or is only a mathematical artefact required for the validity of Redfield equation Eq. (3.4) which could be lifted experimentally, is a complex question that we will address in a future study. Nonetheless, we can conclude that the validity of our approach strongly relies on a net
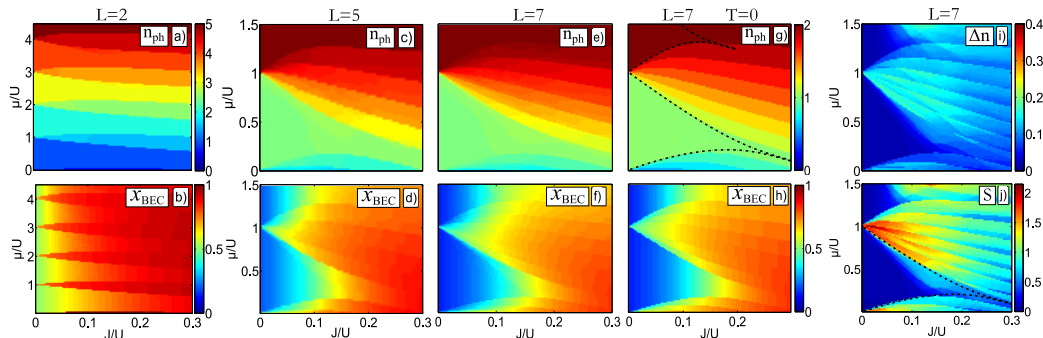
Figure 3.2: Steady-state properties for a limit choice of parameters. Panels a),c),e) [resp. panels b),d),f)] Average steady-state photon number per site $n_{\rm ph}$ (resp. condensed fraction $x_{\rm BEC}$), for $L = 2, 5, 7$ respectively. Panel g) [resp. panel h)]: Average $n_{\rm ph}$ (resp. $x_{\rm BEC}$) in a $T = 0$ equilibrium system, for $L = 7$. Panel i) [resp. panel j)]: steady-state particle number relative fluctuations Δn [resp. entropy $S = -\langle \ln(\rho_\infty) \rangle$], for $L = 7$. In panel g) and j) dash dotted black lines indicate the MPS $T = 0$ prediction for the first Mott lobes. Parameters used in all panels (except g,h): $\Gamma_{\rm l}/\Gamma_{\rm em}^0 = 10^{-3}$, $U/\Delta_{\rm em} = 10^6$, $\Gamma_{\rm em}^0/\Delta_{\rm em} = 10^{-2}$, $\omega_+ = 0$, $\omega_-/\Delta_{\rm em} = -4 \times 10^7$. Cutoff in particle number per site $N_{\rm max} = 6$ [Panels a),b)] and $N_{\rm max} = 3$ [panels c)-j)]

time-scale separation between photonic loss/emission processes (and their associated lamb-shifts) and Hamiltonian ones. The various required inequalities can summarized as following: $\Gamma_{\rm l}, \Gamma_{\rm em}^0 \ll \Delta_{\rm em} \ll U \le (\omega_+ - \omega_-)$ (we will see that they can be verified by state-of-the-art parameters in superconducting circuits [159]).

3.3 Steady-state equilibrium-like properties

In this section we predict some general properties of the steady-state ρ_∞ of the Master Eq. (3.4) and draw a connection between ρ_∞ and the $T = 0$ equilibrium prediction for the Hamiltonian $H_{\rm ph}$.

As a first step, it is essential to gain more insight on the effect of dissipation in our model. One of the main consequences of being in the weakly dissipative regime $\Gamma_{\rm l}, \Gamma_{\rm em}^0 \lll U, J$ (J is also much larger than $\Gamma_{\rm l}, \Gamma_{\rm em}^0$ if we set a reasonable coupling strength between the various lattice resonators) is that emission and loss processes are not strong enough to build coherent superpositions between pure quantum states with different energies: during time evolution (and thus also at steady-state) the density matrix remains almost diagonal in the eigenbasis of $H_{\rm ph}$ (this was always perfectly confirmed by our simulations when we compared the results obtained by mean of the secular approximation to the exact numerical predictions). One could possibly argue that $H_{\rm ph}$ might present some degeneracies: however most of those are accidental, and the corresponding states are usually very dissimilar and are not coupled by mean of elementary processes such as particle losses or injections processes [1]. The remaining degeneracies are connected to the underlying symmetries of the many-body problem: in our case the reflection symmetry plays an important role, as it implies that states with opposite total momenta (e.g., two counter-propagating hole excitations) possess equal energies. However, due to the translational invariance of the problem, starting from homogeneous initial conditions the density matrix must maintain this invariance and thus can not present off-diagonal elements between those states during its further evolution.

With that picture in mind, the evolution of Master. Eq. (3.4) can be understood physically as a near classical/'diagonal' stochastic problem: the main effect of dissipative processes is to transfer probability between various eigenstates of $H_{\rm ph}$. The corresponding transfer efficiency is provided by the Fermi Golden rule: given two eigenstates $|f\rangle$ (resp. $|f'\rangle$) of the photonic Hamiltonian with N (resp. $N + 1$) photons and energy ω_f (resp. $\omega_{f'}$), the transition rates $T_{f \to f'}$ and $T_{f' \to f}$ between those two states are two completely independent

---

[1] This might be not true in the thermodynamic limit for the Goldstone mode, but our finite-size simulation could not address this issue

quantities with different frequency dependencies

$$T_{f \to f'} \quad = \quad \mathcal{S}_{\mathrm{em}}(\omega_{f',f}) \sum_i |\langle f | a_{\mathrm{i}} | f' \rangle|^2, \tag{3.12}$$

$$T_{f' \to f} \quad = \quad \Gamma_{\mathrm{l}} \sum_i |\langle f | a_{\mathrm{i}} | f' \rangle|^2. \tag{3.13}$$

This ability to control the relative strength of the transition rates in the function of the energy jumps will allow us to guide the photonic density matrix toward particular eigenstates of the Hamiltonian.

Our intuition is already confirmed in a single cavity geometry, as the scheme introduced in this work readily allows to stabilize pure Fock states with arbitrary photon number: indeed, in Fig. 3.1 b) we observe a plateau structure with successive jumps between integer values of the steady-state photon number [2], with a smooth (resp. sharp and discontinuous) transition for $\Delta_{\mathrm{em}}/U \gtrsim 1$ (resp. $\Delta_{\mathrm{em}}/U \ll 1$) between the various steps. The physical quantity $\omega_+ - \omega_{\mathrm{cav}}$ manifestly plays a similar role as the chemical potential in equilibrium physics [59] but with a mechanism differing from the scheme presented in Sec. 1.2.3.3.

Pushing the analogy with equilibrium forward, we find that the specific shape of the pump spectrum [Fig. 3.1 a)] allows to drive large many-cavity systems toward a steady state closely related to a $T = 0$ state (and thus to overcome the fragility against tunneling pointed out in [119] for Lorentzian pumps). To see this, let us set a strong emission at resonance $\Gamma_{\mathrm{em}}^0 \gg \Gamma_{\mathrm{l}}$, while maintaining a sharp cut-off at the edges of the spectrum $\Delta_{\mathrm{em}} \ll U$, in such a way to strongly favor (resp. block) $f \to f'$ transitions between states (with N and $N+1$ photons) verifying $\omega_{f'f} \leq \omega_+$ (resp. $\omega_{f'f} \geq \omega_+$). Under those constraints, the transition rates follow the condition

$$\frac{\mathcal{T}_{f \to f'}}{\mathcal{T}_{f' \to f}} \simeq \frac{\Gamma_{\mathrm{em}}^0}{\Gamma_{\mathrm{l}}} \theta(\omega_+ - \omega_{f'f}) \quad \begin{cases} \ggg 1 & \text{if } \omega_{f'f} < \omega_+ \\ \lll 1 & \text{if } \omega_{f'f} > \omega_+ \end{cases},$$

that closely resembles a $T = 0$ detailed-balance relation

$$\left. \frac{\mathcal{T}_{f' \to f}}{\mathcal{T}_{f \to f'}} \right|_{\mathrm{eq}} = e^{\beta(\omega_+ - \omega_{f'f})} \tag{3.14}$$

with $\beta \to +\infty$. One may thus expect the many-body steady-state to be very close to the ground state $|\mathrm{GS}\rangle$ of the rotating frame effective Hamiltonian

$$H_{\mathrm{eff}} \quad = \quad H_{\mathrm{ph}} - \omega_+ N \tag{3.15}$$

$$= \quad \sum_{i=1}^{L} \left[-\mu a_i^\dagger a_i + \frac{U}{2} a_i^\dagger a_i^\dagger a_i a_i \right] - \sum_{\langle i,j \rangle} J a_i^\dagger a_j,$$

i.e., a $T = 0$ state with chemical potential $\mu = \omega_+ - \omega_{\mathrm{cav}}$. Defining $\tilde{\omega}_{f'f} = \omega_{f',f} - \omega_+$ as the transition energy between the two eigenstates defined previously, calculated this time by mean of H_{eff}, one has that $\frac{\mathcal{T}_{f \to f'}}{\mathcal{T}_{f' \to f}} \simeq \frac{\Gamma_{\mathrm{em}}^0}{\Gamma_{\mathrm{l}}} \theta(-\tilde{\omega}_{f'f})$: emission processes are strongly enhanced (resp. suppressed) for photonic transitions reducing (resp. increasing) the energy of the new effective Hamiltonian H_{eff}, and thus indeed tend to guide probability toward its ground-state.

In the next sections, we will show that this agreement with equilibrium physics is generally robust for most choices of system parameters, but subtle signatures of the deviations from the detailed balance condition (3.14) can appear in some specific regions. These new non-equilibrium features will be discussed at length in Sec. 3.5. A way to suppress them by adding extra frequency-dependent losses is then introduced and characterized in Sec. 3.6 in view of quantum simulation applications.

3.4 Numerical results for finite periodic chains

As the sophisticated numerical techniques used in [92, 12] are not straightforwardly applicable to non-Markovian problems, we had to base our study on a direct numerical calculation

---

[2]We checked that particle number fluctuations were strongly suppressed.

of the steady-state density matrix $\rho_\infty \equiv \rho(t \rightarrow +\infty)$ by looking for a zero of the Redfield super-operator on the right-hand side of Eq. (3.4) for mesoscopic one-dimensional chains. While a complete study of larger systems in possibly higher dimensionality is postponed to future work addressing e.g. the critical properties of possible phase transitions, our approach turned out to be sufficient to anticipate and understand the behaviour of experimentally relevant systems.

For system sizes going up to $L = 5$ sites, a complete numerical calculation was possible. Above 5 sites, we had to perform the secular approximation and discard fast oscillating terms in the master equation: for very weak dissipation and in absence of relevant degeneracies of the photonic Hamiltonian, the diagonal terms of the density matrix in the Hamiltonian eigenbasis are in fact not coupled to off-diagonal terms, and the latter can be neglected when computing the steady state. As this approximation is generally accurate for weak dissipation but may be problematic in the presence of degeneracies, we have numerically checked on chains of $L = 3, 4, 5$ sites that it indeed gives indistinguishable results from the exact solution for small systems sizes.

In order to facilitate the reader, we start our discussion in Sec. 3.4.1 from a limit case of parameters for which the physics is most transparent [Fig. 3.2]. As a second step, in Sec. 3.4.2 we will then assess the robustness and actual observability of our predictions by considering parameters inspired to state-of-the-art experimental devices [Fig. 3.3].

3.4.1 Idealized parameters

In order to present the physics in a cleanest way, we first discuss the occurrence of the insulator-like state and its transition towards a superfluid-like state for an idealized set of parameters where the loss rate Γ_l is extremely small as compared to the interaction energy U. This allows to keep all other parameters well spaced in magnitude and largely satisfy the inequalities. Calculations showing the robustness of our conclusions for realistic parameters of state-of-the-art circuit-QED devices are presented in the next subsection.

The steady-state photon density $n_{ph} = \langle N \rangle / L$ and the Bose-condensed fraction $x_{BEC} = \langle n_{k=0} \rangle / \langle N \rangle$ (where $\langle O \rangle \equiv \text{Tr}(O\rho_\infty)$) are given in Fig. 3.2 [panels a)-f)] for several system sizes L, and are compared to the $T = 0$ equilibrium predictions for $L = 7$ sites [panels g), h)]. Even though one does not expect a true Bose-Einstein Condensation/Bose-Enstein Condensate (BEC) for an infinite 1D chain [136], still x_{BEC} provides physical insight on the long-range coherence properties of our finite-size system.

Apart from the presence of small corrections that will be discussed below, the qualitative agreement between the observables calculated for the driven-dissipative steady state and the $T = 0$ prediction of the equilibrium BH model is very good: first, we observe for increasing μ a series of insulating-like regions with successive integer values of the density n_{ph} and a small x_{BEC}. Within these regions, the photonic density does not depend on the Hamiltonian parameters ω_{cav} and J, and fluctuations in the total photon number are suppressed to $\Delta n \equiv \sqrt{\langle N^2 \rangle - \langle N \rangle^2} / \langle N \rangle \simeq 10^{-2}$ [Fig. 3.2 i)]: this is a sort of non-equilibrium form of incompressibility.

These insulating regions closely follow the shape of the phase boundary [panel g)] predicted for a $T = 0$ equilibrium 1D system (the so-called Mott lobes [59, 114]), that we obtained by means of matrix-product-states (MPS) simulations with $L = 200$ sites (see [114] for details on the approach): the agreement for the first lobe is excellent, while the deviations for the second lobe are due to a numerical cutoff in the maximum particle number per site $N_{max} = 3$ used in the steady-state calculation.

Secondly, the insulating regions are separated by coherent regions with non-integer density, reminiscent of the equilibrium superfluid phase where excess particles/holes do not suffer from the photon blockade and can delocalize via tunneling: the condensed fraction is important and eventually reaches the maximal value $x_{BEC} = 1$ at high J, indicating a full coherence over the finite system.

3.4.2 Realistic parameters

While Fig.3.2 focused on a limit case of parameters in order to validate the theoretical viability of our approach, Fig. 3.3 confirms the actual feasibility of our proposal and the
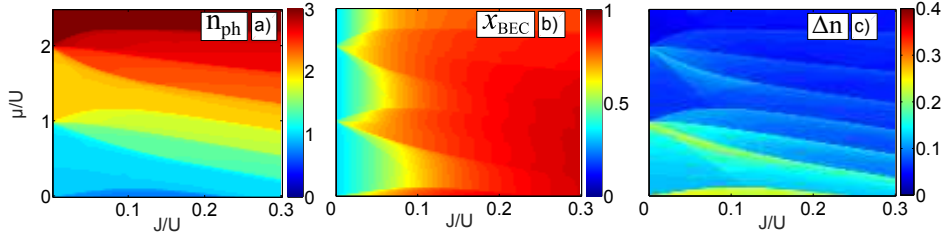
Figure 3.3:   Steady-state properties for $L = 3$, for state-of-the-art parameters in circuit QED. Panel a): average photon number per site n_{ph}. Panel b): condensed fraction x_{BEC}. Panel c): relative fluctuations of the total particle number Δn. Parameters inspired from circuit-QED systems [126, 159]: $U = 200 \times 2\pi\mathrm{MHz}$, $\Delta_{\mathrm{em}} = 0.5 \times 2\pi\mathrm{MHz}$, $\Gamma_{\mathrm{em}}^0 = 30 \times 2\pi\mathrm{kHz}$, $\Gamma_{\mathrm{l}} = 1 \times 2\pi\mathrm{kHz}$. In order to be able to correctly see the higher lobes, we had to increase the maximum allowed number of particles per site to $N_{\mathrm{max}} = 4$, and correspondingly to reduce the system size to $L = 3$.

overall robustness of our predictions for state-of-the-art parameters in circuit-QED systems [126, 159].

The main consequence of the finite ratios Δ_{em}/U and $\Gamma_{\mathrm{em}}^0/\Gamma_{\mathrm{l}}$ is in fact a weak but appreciable value of particle number fluctuations, and could be seen as the non-equilibrium counterpart of the effect of a finite temperature T_{eff}. For a low-T equilibrium state with $\{J/U = 0, \mu/U = 1/2\}$ (which is the point of the first lobe with highest energy gap and thus predictably at low temperature the one with the weakest fluctuations) and restricting the partition function $Z_{th} \simeq 1 + e^{\beta\mu} + e^{\beta(2\mu - U)}$ to the most relevant Fock states $N = 0, 1, 2$, one finds that the particle number fluctuations can be connected to the temperature through the following relation

$$kT = \frac{U}{2} \frac{1}{\ln\left(\frac{2}{\Delta n^2}\right)}.$$ (3.16)

A rough estimate for a sort of effective temperature for our non-equilibrium system can then be extracted by inserting in this formula the value $\Delta n \sim 0.13$ found in Fig. 3.3 c). This gives a quite low value $T_{\mathrm{eff}} \simeq 0.1\, U$. The steady-state effective temperature should be even lower away from $\{J/U = 0, \mu/U = 1/2\}$ for the specific parameters choice of Fig. 3.3 c), since the resulting fluctuations are rather independent from tunneling and only change by a factor ~ 1.5 across the transition line (in contrast to the equilibrium case where fluctuations dramatically increase when the many-body gap closes). Still, based on the low value of T_{eff}, one can thus expect that it will be possible to catch the effect of quantum fluctuations (or crossover) for current state-of-the-art parameters, at least on some intermediate length scale. We stress that this effective temperature presented here represents a mere attempt of assessing the amount of fluctuations at steady-state, and should not be confused with the one deriving from the pseudo-thermalization effect discussed in Sec. 2.4 and Chap. 4 (although there might be some connections between the two quantities).

3.4.3   Finite-size effects

Even though there is a quite good overall agreement of the non-equilibrium calculations to the well-known physics of the equilibrium system in the thermodynamic limit [59, 114], a careful observer can still notice in Fig. 3.2 some significant discrepancies, in particular with the $T = 0$ prediction for the phase boundary [dash dotted line in Fig. 3.2 g)]. As a first step, it is therefore important to first assess which features are likely to be finite-size effects and which ones might instead signal some new physics.

The most prominent such features are that in Fig. 3.2 [b), d), f)] the insulating regions do not close completely to form lobes but rather end with a stripe, x_{BEC} is not exactly zero even at very weak J, and all observables present a smooth crossover for increasing tunneling instead of a sharp transition at the tip of the lobe (which is not present here). Comparing these panels, one notices that both the width of the stripes and the condensed fraction inside the insulating region decreases as $1/L$ for increasing system sizes (actually for $J = 0$ one has precisely $x_{\mathrm{BEC}} = 1/L$). The fact that a similar behaviour is found in the finite size
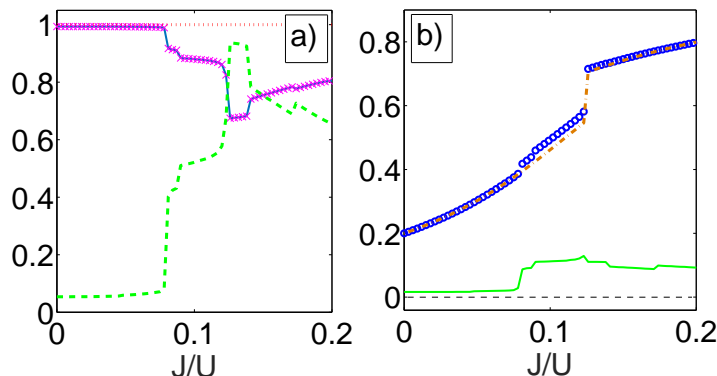
Figure 3.4: Steady-state statistical properties for $L = 5$ at fixed $\mu = 0.55\,U$. Panel a): fidelity $\mathcal{F}$ between the steady state and the Hamiltonian ground state (blue solid line), occupancy π_0 of the most populated state $|\psi\rangle_+$ (purple crosses), overlap $|\langle\psi_+|GS\rangle|^2$ between the ground state and the most populated state (red dot line), entropy S (green dash line). Panel b): number fluctuations Δn (green solid line) and condensed fraction (blue circles), compared to the $T = 0$ equilibrium value (orange dash-dot line). Same parameters as in Fig. 3.2. In order to be able to perform exact diagonalization of the Liouvillian and avoid using the secular approximation, we had to choose a smaller system size $L = 5$ as compared to Fig. 3.4.

equilibrium plot of Fig. 3.2 g) is therefore a strong indication of the finite-size origin of this effect: the scaling for the width of the stripes is related to the fact that for a finite-size system a given eigenstate can remain the ground-state for a finite range of parameters, even if this one would belong to the continuum in the thermodynamic limit. One can notice actually between the two lobes the presence of $L - 1$ other stripes (with precisely rational density values $n = N/L$ in the $T = 0$ case), consistently with the fact that one needs to add L bosons on top of a $n = 1$ Mott Insulator in order to move to $n = 2$. The $1/L$ value for the Bose-Condensed fraction deep in the Mott lobe is a direct consequence of the fact that the MI is fully localized for $J = 0$, and thus has a uniform momentum distribution ($n(k) = n/L$ for any momentum k).

If one could take the infinite system size limit, a tempting conjecture would be that all these discrepancies should in fact disappear, recovering clean Mott lobes surrounded by a superfluid (and possibly also Bose-condensed depending on the dimensionality) phase. However, as we are going to discuss in the next Section, a more careful analysis allows to unveil another kind of deviations, which signals a much richer non-equilibrium phenomenology.

3.5 Non-equilibrium features

The most remarkable such feature is highlighted in the plots of the particle number fluctuations and of the entropy shown in Fig. 3.2(i,j): While in most parts of the insulating region the steady state presents an almost vanishing entropy $S = -\langle\ln(\rho_\infty)\rangle$ [Fig. 3.2 j)] and can thus be well approximated by a pure quantum state (as for a $T = 0$ equilibrium state), this is not the case in some regimes of parameters in the vicinity of the transition line where the entropy S acquires a significant positive value slightly before the jump in the particle number and in the condensate fraction at the equilibrium superfluid transition.

The present section is dedicated to the characterization of this novel entropic transition and to the description of the non-equilibrium mechanisms underlying it. Since this phenomenon could be seen as an hindrance in the prospect of quantum simulating the ground-state of the Bose-Hubbard Hamiltonian, in Sec. 3.6 we will put forward a further extension of the optical scheme that is able to remove this deviation from equilibrium.

To quantitatively characterize these non-equilibrium features, we looked at the fidelity $\mathcal{F} = \langle GS|\,\rho_\infty\,|GS\rangle$ between the steady state ρ_∞ and the Hamiltonian ground state $|GS\rangle$ and at the steady-state occupancy π_0 of the most populated state $|\psi_+\rangle$ [3].

---

[3] To avoid possible artifacts such as the preferential choice of the steady-state eigenbasis, all these physical
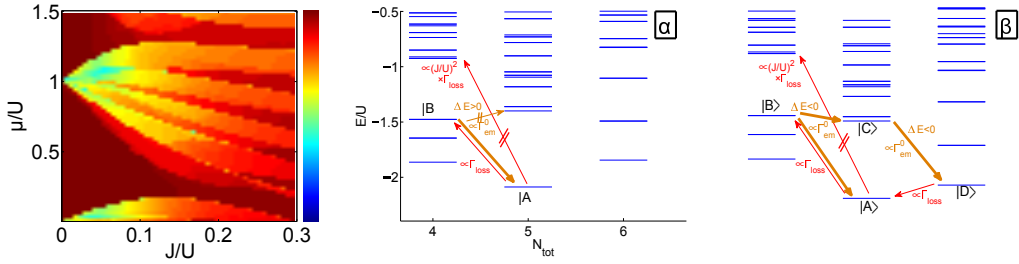
Figure 3.5: Left panel: Occupancy π_0 of the most populated quantum state at steady state for a 5 sites system. Central (resp. right) panel: spectrum of H_{eff} at the values $J/U = 0.1$ and $\mu/U = 0.38$ (resp. $\mu/U = 0.55$) indicated by the point $[\alpha]$ (resp. $[\beta]$) in the left panel. Parameters used: $\Gamma_l/\Gamma_{\text{em}} = 10^{-3}$, $U/\Delta_{\text{em}} = 10^6$, $\Gamma^0_{\text{em}}/\Delta_{\text{em}} = 10^{-2}$, $\omega_+ = 0$, $\omega_-/\Delta_{\text{em}} = -4 \cdot 10^7$.

As one can see in Fig. 3.4a), the transition takes the form of a discontinuous jump in entropy from a 99% pure quantum state toward a statistical mixture above some critical J_c, located within an insulating region at a small but finite distance from the equilibrium transition line [Fig. 3.2 j)]. Note that this jump is present even for finite sizes L, and just gets smoother for the state-of-the-art parameters of Fig. 3.3. In the pure region $\mathcal{F} = \pi_0 \simeq 0.993$ are close to unity, indicating that ρ_∞ can be well approximated by the pure state $|GS\rangle \langle GS|$ (not the case in the entropic region). In both regions, $|\langle \psi_+ | GS \rangle|^2 = 1$ (within machine precision), $\mathcal{F}$ and π_0 take identical values, so the most populated state $|\psi_+\rangle$ is precisely equal to the Hamiltonian ground state at any value of J (at least for the precise value of μ in Fig. 3.4 a)). Looking at the observable x_{BEC} [Fig. 3.4 b)], the pure (resp. entropic) region is characterized by negligible (resp. small) deviations from equilibrium, and very weak fluctuations $\Delta n \simeq 0.016$ (resp. non-zero $\Delta n \simeq 0.13$).

This effect can be understood as a consequence of the departure of the pump and loss rates from a true detailed balance relation: the emission spectrum is in fact not exponential in the frequency but rather decays with a power law above ω_+ and most importantly saturates at the value Γ^0_{em} below ω_+. A physical interpretation of the underlying microscopic mechanism is illustrated in Fig. 3.5 and Fig. 3.6. In the left panel of Fig. 3.5, we plot the occupancy π_0 of the most populated quantum state of the density matrix at steady state. In the central and right panels, we show the spectrum of the underlying Hamiltonian evaluated at two points $[\alpha]$ and $[\beta]$ separated by a small variation of μ for which the entropy is respectively zero and non-zero.

From the previous discussion, one expects that the steady state occupation be concentrated in the ground state $|GS\rangle = |A\rangle$ of H_{eff}, i.e., a (weakly delocalized) Mott state with 1 photon per site. However looking at the spectrum of many-body quantum states for the choice of parameters indicated as $[\beta]$ (right panel of Fig. 3.5), we note that, starting from $|A\rangle$ which contains $N_{tot} = 5$ photons in total, the system can lose one photon and arrive in a state $|B\rangle$ with $N_{tot} - 1$ photons containing one hole excitation. Then, the pump re-injects a new photon and brings the system into a doublon-hole excited quantum state $|C\rangle \neq |A\rangle$ with N_{tot} photons such that $E_C < E_B$. Since the spectrum has a square shape, the pump can bring the system toward both the ground state $|A\rangle$ and $|C\rangle$ with comparable efficiencies $\propto \Gamma^0_{\text{em}}$. There is one last doublon excited state $|D\rangle$ with $N_{tot} + 1$ photons and energy E_D such that $E_D < E_C$ so the excited N_{tot} photon state $|C\rangle$ is unstable and gets quickly pumped toward $|D\rangle$ where it gets trapped for a while as no state with higher photon number and lower energy exists, until one photon gets slowly lost and the system goes back to the ground state $|A\rangle$.

This mechanism explains why we observe, in the steady state, a significantly non-zero entropy as well as a photonic density slightly bigger than in the ground state. Of course, if the emission rate were exponentially dependent in the energy jump and the detailed balance condition was verified, the re-pumping process toward $|C\rangle$ would not be relevant since its efficiency will be dynamically overwhelmed by the process bringing the system back toward

---

quantities were computed for $L = 5$ by exact steady-state calculation without using the secular approximation.
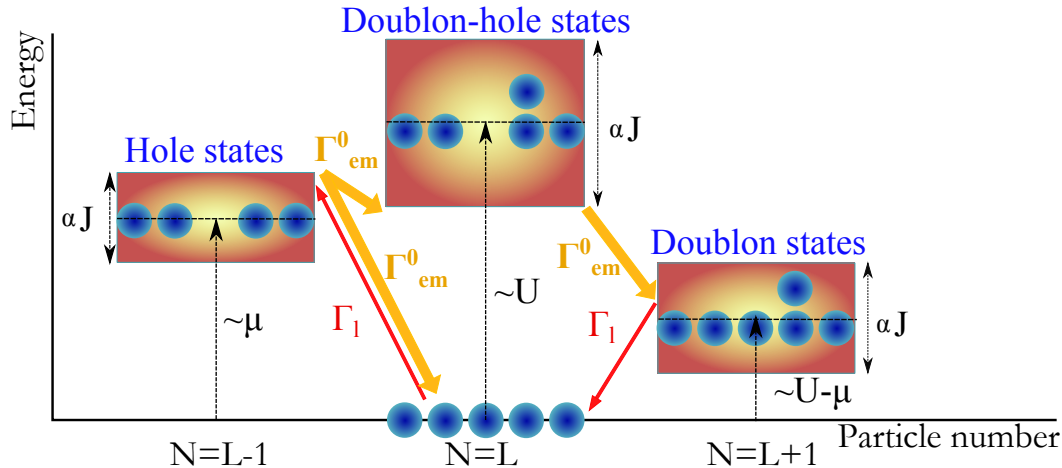
Figure 3.6: Sketch of the non-equilibrium scenario in the thermodynamic limit: above a critical hopping J_c, the hole and doublon-hole energy bands start overlapping and are thus coupled by emission process (which are only enhanced for transition diminishing the total energy computed with H_{eff}). This allows for a probability leakage toward doublon states after a photon loss event. Turning back toward the ground-start requires an additional slow photon loss event.

the ground state $|A\rangle$. As a result, no significant trapping of population into excited states would occur.

In contrast, for the choice of parameters indicated as $[\alpha]$ and illustrated in the central panel of Fig. 3.5, the ground state $|A\rangle$ is well isolated dynamically, as the only energetically authorized transition after creating a single hole excitation is to go back into the Mott ground state of N_{tot} photons. Of course there exist states with $N_{tot}-1$ photons in an higher energy band which would allow the kind of processes described earlier. However those states correspond to highly excited states (e.g., an hole combined with a doublon-hole) and have a much smaller overlap $\propto J/U$ with the state $a_i |A\rangle$ in which we removed one photon to the ground state. The effective rate of this process is thus of the order of $(J/U)^2 \Gamma_1 \sim \Gamma_1/100$ and induces a negligible leak out of $|A\rangle$. As a consequence the steady state is almost pure, and corresponds very well to the Mott-like ground state. The sharpness of the transition between the two regimes at the α, β points is set by the edge linewidth of the order of $\Delta_{\text{em}} = \Gamma_{\text{p}} \ll U$.

Even though our interpretation of the effect is related to the level crossing between discrete hole and doublon-hole excited states of a finite system, we expect that a similar effect will occur in the thermodynamic limit (as illustrated in Fig. 3.6) when the continuous energy bands of the hole excitations and doublon-hole excitations start to overlap above some tunneling $J = J_c$. Such an overlap can of course not happen when J is relatively small with respect to U since, for the first lobe for example, the hole band is separated from the ground-state by an energy $E^{hole} \simeq \mu \leq U$ while the doublon-hole one is separated by $E^{hole}_{doublon} \simeq U$. As a consequence, a critical value J_c exist for this non-equilibrium channel to open up. Below this value, the Mott phase is expected to remain robust even in the thermodynamic limit. Whether this unexpected feature will affect the phase diagram in a dramatic manner (e.g., by destabilizing ordered phases [2] and/or giving rise to novel exotic ones [93, 87, 92]) is a complex question that goes beyond the scope of this work and will be addressed in forthcoming works.

3.6 An improved scheme for a full quantum simulation of the ground-state

In this section we introduce a further extension of the non-Markovian model of Sec. 3.2 with the specific purpose of countering the effect of the non-equilibrium processes presented in Sec. 3.5, which induce a probability leakage out of the ground-state. This improved scheme
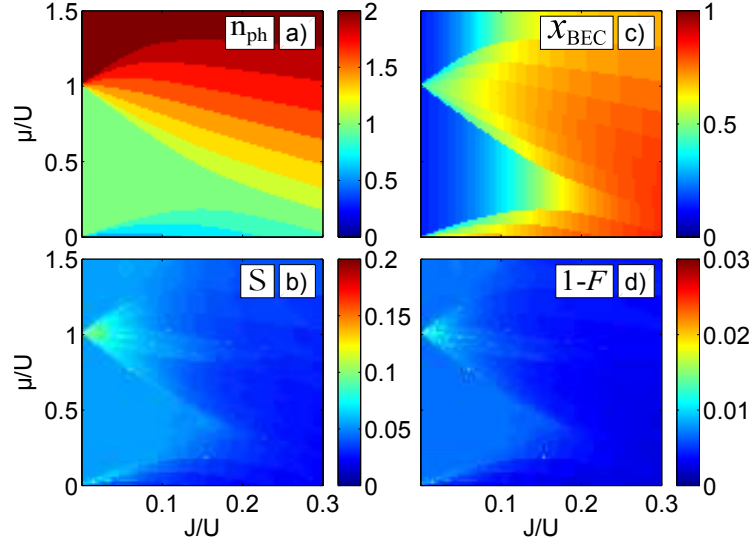
Figure 3.7: Steady-state properties using frequency-dependent losses with a square-spectrum in addition to frequency-dependent emission. Simulations were done for a $L = 7$ sites periodic chain. Panel a) (resp. panel c): Average steady-state photon number per site $n_{\rm ph}$ (resp. condensed fraction $x_{\rm BEC}$). Panel b): steady-state entropy. Panel d): $1 - \mathcal{F}$, where $\mathcal{F} = \langle GS | \rho_\infty | GS \rangle$ is the fidelity of the steady-state density matrix ρ_∞ with the ground-state $|GS\rangle$ of the Hamiltonian $H_{\rm eff}$, i.e, a $T = 0$ state of chemical potential μ. Same parameters as in Fig. 3.2 except for the additional frequency-dependent losses: $\Gamma_{\rm L}^0 = \Gamma_{\rm em}^0$, $\omega_{\rm L} - \omega_{\rm cav} = \omega_+ - \omega_-$ and $\Delta_{\rm L} = \Delta_{\rm em}$.

is based on the introduction of extra frequency-dependent losses in addition to the natural Markovian ones.

3.6.1 The model

We consider the following dynamics for the photonic density matrix

$$\partial_t \rho(t) = -i\left[H_{\rm ph}, \rho(t)\right] + \mathcal{L}_{\rm l}\left[\rho(t)\right] + \mathcal{L}_{\rm em}\left[\rho(t)\right] + \mathcal{L}_{\rm L}^{\rm (add)}\left[\rho(t)\right], \tag{3.17}$$

where the Hamiltonian and dissipative contributions $H_{\rm ph}$, $\mathcal{L}_{\rm l}\left[\rho(t)\right]$ and $\mathcal{L}_{\rm em}\left[\rho(t)\right]$ are left unchanged with respect to Sec. 3.2.

Similarly to emission, the additional frequency-dependent loss term

$$\mathcal{L}_{\rm L}^{\rm (add)}\left[\rho(t)\right] = \frac{\Gamma_{\rm L}^0}{2} \sum_{i=1}^{L} \left[\bar{a}_i \rho a_i^\dagger + a_i \rho \bar{a}_i^\dagger - a_i^\dagger \bar{a}_i \rho - \rho \bar{a}_i^\dagger a_i\right]. \tag{3.18}$$

involves modified lowering ($\bar{a}_i$) and raising ($\bar{a}_i^\dagger \equiv [\bar{a}_i]^\dagger$)
operators

$$\frac{\Gamma_{\rm L}^0}{2} \bar{a}_i = \int_0^\infty d\tau \, \Gamma_{\rm L}(\tau) a_i(-\tau), \tag{3.19}$$

where

$$\Gamma_{\rm L}(\tau) = \theta(\tau) \int \frac{d\omega}{2\pi} \mathcal{S}_{\rm L}(\omega) e^{-i\omega\tau}. \tag{3.20}$$

$\mathcal{S}_{\rm L} = s_{\rm L}(\omega)\Gamma_{\rm L}^0$ is the frequency-dependent loss rate, which we also choose to be of a square shape as the emission term of Sec. 3.2, by setting

$$s_{\rm L}(\omega) = \mathcal{N}' \int_{\omega_+}^{\omega_{\rm L}} d\omega' \frac{\Delta_{\rm L}/2}{(\omega - \omega')^2 + (\Delta_{\rm L}/2)^2} \tag{3.21}$$

where the normalization constant $\mathcal{N}'$ is set such that $s_{\rm L}\left(\frac{\omega_+ + \omega_{\rm L}}{2}\right) = 1$. Note the different choice for the loss frequency domain $[\omega_+, \omega_{\rm L}]$ (instead of $[\omega_-, \omega_+]$ for emission).

As will be discussed in Sec. 3.7, frequency-dependent losses with the desired spectral profile could be obtained by coupling our system to absorbers with transition frequencies uniformly distributed over $[\omega_+, \omega_L]$ and a strong dissipative decay $\Gamma_\downarrow = \Delta_L$ toward the ground-state.

We will choose strongly enhanced frequency-dependent losses with respect to the Markovian ones: $\Gamma_L^0 \gg \Gamma_l$. Similarly to the emission spectrum, the upper cutoff ω_L is not the most important feature and will be set to a very far blue-detuned frequency: $\omega_L - \omega_{cav} \gg U, J \geq 0$. Likewise, we will have $\Delta_L \ll U$, $\omega_L - \omega_+$. All these conditions can be naturally satisfied, e.g., by mimicking the choice of parameters for emission: $\Gamma_L^0 = \Gamma_{em}^0$, $\omega_L - \omega_+ = \omega_+ - \omega_-$ and $\Delta_L = \Delta_{em}$.

3.6.2 Steady-state properties

In analogy to the frequency-dependent emission, the main effect of the frequency-dependent losses is to strongly enhance transitions removing a photon with a frequency above ω_+. As a result, both non-Markovian emission and loss processes strongly accelerate transitions between many-body eigenstates which reduce the total energy computed using the effective Hamiltonian of Eq. (3.15). Thus, the only quantum state for which both emission and losses are strongly suppressed (i.e., for which only natural Markovian losses are present) is the ground-state $|GS\rangle$ of H_{eff} (with N_{tot} photons), since it does not have states with $N_{tot} - 1$ and $N_{tot} + 1$ photons with lower energy.

As a consequence, the ground-state $|GS\rangle$ has a long life time $\sim 1/\Gamma_l \gg 1/\Gamma_{(em/L)}^0$, while all remaining eigenstates have a short life-time $\sim 1/\Gamma_{(em/L)}^0$. This important property was not ensured by the original scheme introduced in Sec. 3.2, for which some lowest-excited states with $N_{tot} + 1$ photons (e.g. the $|D\rangle$ state of Fig. 3.5) were long lived and could only relax with a slow rate $\sim \Gamma_l \ll \Gamma_{em}^0$ towards $|GS\rangle$. This is the main reason for which this scheme shows a significant entropy in some regions of the parameter space. The new scheme including frequency-depedent losses solves this issue and is expected to be well suited to efficiently stabilize the ground state independently of the system parameters.

This statement based on simple physical arguments is confirmed in Fig. 3.7 where we see that the steady-state average values of n_{ph} and x_{BEC} [panels a) and c)] are completely undistinguishable from the $T = 0$ predictions of Fig. 3.2 [panels g) and h)]. We checked that this was also the case for higher order correlations. Even more remarkably, the steady-state ρ_∞ has a very low entropy [panel b)], and its fidelity $\mathcal{F}$ with the ground-state is very close to unity [panel d)] for any choice of parameters μ and J, indicating thus that we are indeed stabilizing a pure quantum state coinciding with the ground-state: $\rho_\infty = |GS\rangle\langle GS|$.

In contrast with the original scheme, there appears to be no real physical limitations to how close the steady-state can be to the ground-state $|GS\rangle$. We have in fact verified that the very small non-vanishing values for entropy (between 0.05 and 0.12) and deviations of the fidelity $\mathcal{F}$ from unity (between 0.002 and 0.012) were a mere consequence of the finite choice of the dissipative parameters, and could be further reduced by orders of magnitude by improving the frequency selectivity $\Delta_{(em/L)}/U$ of emission and losses and the ratios $\Gamma_{(em/L)}/\Gamma_l$.

The fact that this improved scheme succeeds to stabilize the ground-state of the Bose-Hubbard model everywhere in the $\{\mu/U, J/U\}$ parameter space independently of the details of the underlying many-body physics (which is significantly different in the $J \ll U$ or $J \gg U$ cases) is a strong indication of its robustness and flexibility. We are therefore confident that this scheme can be efficiently applied to the quantum simulation of the zero temperature physics of a wide range of Hamiltonians.

3.7 Experimental proposal

3.7.1 Ideal configuration

Following our proposal of the last Chapter, a natural approach to engineer the non-Markovian pump introduced in Eq. (3.6) would be to insert a large number $N_{at} \gg 1$ of two-level emitters into each cavity, whose evolution and coupling to the cavity field are described by

Hamiltonian terms of the form

$$H_{\mathrm{at}} = \sum_{i=1}^{L} \sum_{n=1}^{N_{\mathrm{at}}} \omega_{\mathrm{at}}^{(n)} \sigma_i^{+(n)} \sigma_i^{-(n)} \tag{3.22}$$

$$H_I = \Omega_R \sum_{i=1}^{L} \sum_{n=1}^{N_{\mathrm{at}}} (a_i^\dagger \sigma_i^{-(n)} + \mathrm{h.c.}). \tag{3.23}$$

Accordingly, each emitter is incoherently pumped in the excited state at a rate Γ_{p}, which is modelled by the Lindblad term

$$\mathcal{L}_{\mathrm{p,at}}[\rho_{\mathrm{tot}}] = \frac{\Gamma_{\mathrm{p}}}{2} \sum_{i=1}^{L} \sum_{n=1}^{N_{\mathrm{at}}} \mathcal{D}[\sigma_i^{+(n)}; \rho_{\mathrm{tot}}], \tag{3.24}$$

so that the total (cavity+emitters) density matrix ρ_{tot} obeys the master equation:

$$\begin{aligned} \partial_t \rho_{\mathrm{tot}}(t) &= -i \left[H_{\mathrm{ph}} + H_{\mathrm{at}} + H_I, \rho_{\mathrm{tot}}(t) \right] \\ &\quad + \mathcal{L}_{\mathrm{l}}[\rho_{\mathrm{tot}}(t)] + \mathcal{L}_{\mathrm{p,at}}[\rho_{\mathrm{tot}}(t)]. \end{aligned} \tag{3.25}$$

For sufficiently strong pump rate Γ_{p}, the pump induces an almost perfect inversion of population in the emitters. As a result, these undergo irreversible cycles in which they are immediately re-pumped after emitting a photon in the cavity and reabsorption processes are suppressed. Such a pumping can be implemented for instance by coherently driving the emitter into a third level, from which it quickly decays towards the excited state of the active transition as often done in practical laser devices and discussed in [126].

In contrast with the proposal of last Chapter, where the choice of a unique emitter frequency leaded to a Lorentzian-shape profile for emission

$$\mathcal{S}_{\mathrm{em}}^{\mathrm{Lorentzian}}(\omega) = N_{\mathrm{at}} \Gamma_{\mathrm{em}}^{(\mathrm{at})} \frac{(\Gamma_{\mathrm{p}}/2)^2}{(\omega - \omega_{\mathrm{at}})^2 + (\Gamma_{\mathrm{p}}/2)^2} \qquad \left(\Gamma_{\mathrm{em}}^{(\mathrm{at})} = \frac{4\Omega_R^2}{\Gamma_{\mathrm{p}}} \right), \tag{3.26}$$

the transition frequencies $\omega_{\mathrm{at}}^{(n)}$ of the different emitters are assumed now to be uniformly distributed over the interval $[\omega_-, \omega_+]$ in order to engineer a broadband tailored emission spectrum: the summation over the contribution of all emitters across their uniform frequency distribution $[\omega_-, \omega_+]$ yields the desired square-shaped spectrum

$$\mathcal{S}_{\mathrm{em}}^{\mathrm{tailored}}(\omega) = N_{\mathrm{at}} \Gamma_{\mathrm{em}}^{(\mathrm{at})} \frac{1}{\omega_+ - \omega_-} \int_{\omega_-}^{\omega_+} d\omega' \frac{(\Gamma_{\mathrm{p}}/2)^2}{(\omega - \omega')^2 + (\Gamma_{\mathrm{p}}/2)^2}. \tag{3.27}$$

of Eq. (3.11) and Fig. 3.1 a), with an edge width equal to $\Delta_{\mathrm{em}} = \Gamma_{\mathrm{p}}$. For $\Gamma_{\mathrm{p}} = \Delta_{\mathrm{em}} \ll \omega_+ - \omega_-$, we obtain for the maximum emission rate $\Gamma_{\mathrm{em}}^0 = 2\pi N_{\mathrm{at}} \Omega_R^2 / (\omega_+ - \omega_-)$.

Technically speaking, under the constraints $\sqrt{N_{\mathrm{at}}}\Omega_R, \Gamma_{\mathrm{l}} \ll \Gamma_{\mathrm{p}}$, we can use the projective methods [21] presented in Sec. 2.2.2 to trace out the emitter degrees of freedom (see Sec. B for the details of the derivation) and write a closed master equation for the photonic density matrix in the form of Eq. (3.4) with $\mathcal{S}_{\mathrm{em}}(\omega)$ given by Eq. (3.11).

The frequency-dependent loss term introduced in Sec. 3.6 can be implemented in a analogous manner: instead of using inverted emitters with a strong pumping toward the excited state, a possibility would be to couple our system to absorbers (or photonic resonators) with transition frequencies uniformly distributed over $[\omega_+, \omega_{\mathrm{L}}]$, and a very strong dissipative decay $\Gamma_\downarrow = \Delta_{\mathrm{L}}$ toward the ground-state (resp. vacuum state).

3.7.2 Possible simplification strategies

At a first glance, the physical implementation of the scheme may appear as a quite challenging task, as it involves coupling a large number of different emitters to each resonator. In the following part of this section, we are going to explain how this scheme may be simplified and made accessible to state-of-the-art technology.
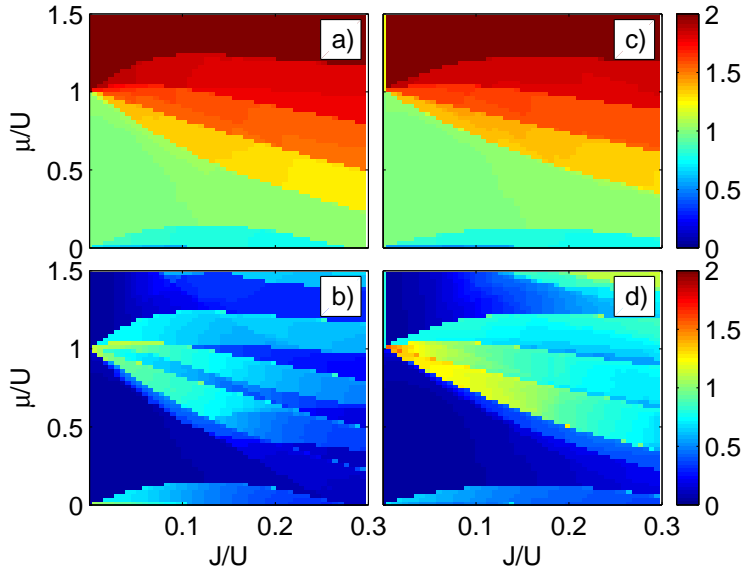
Figure 3.8: Steady-state properties using only one or two emitting sites in different geometries. Panel a) (resp. c)) show the steady-state average density n_{ph}, and panel b) (resp. d)) the entropy for a $L = 4$ sites system with periodic boundary conditions with emitters localized on the first two sites (resp. an open chain with emitters only on first site). Same parameters as in Fig. 3.2 except for the stronger emission rate to compensate the reduced number of emitting sites: $\Gamma_{\mathrm{em}}^0/\Delta_{\mathrm{em}} = \frac{L}{2} \times 10^{-2}$ in panels a), b) (resp. $L \times 10^{-2}$ in panels c),d)). A smaller lattice of $L = 4$ sites had to be used because of the broken translational invariance.

3.7.2.1   Pumping a few sites only

As a first idea, following a suggestion of [126], we argue that a pumping mechanism restricted to one or two sites only is sufficient to stabilize the same steady-state that one would obtain if emitters were present on all sites.

Indeed, when a photon is lost starting from a state $|f\rangle$, a sort of "hole" is created in a local region of the fluid. Due to tunneling, this hole can travel along the chain at a significant group velocity that typically scales as $v_g \sim J \gg \Gamma_\mathrm{l}, \Gamma_{\mathrm{em}}^0$ and is thus able to expand over a large number of sites before undergoing decoherence or additional dissipative effects. Because of this delocalisation effect, a large number of sites (not only the one where the initial loss process took place) feel the presence of the hole and are able to replenish the original many-body state $|f\rangle$ by injecting a new photon.

As pointed out in [126], in case of large lattices, hole excitations (in particular low-momentum ones with slow group velocities) might not have the time to travel and reach the emitting site before suffering from additional dissipative processes. In this case, it is enough to introduce many regularly spaced emitting sites in the bulk of the chain. Of course, the single-site emission rate has to be correspondingly increased in order to compensate the reduced number of emitters and maintain the same total emission power. Finally, attention must be paid so to avoid the emitter being located at the node of the wave function of some hole states, which would block the re-emission of a new photon. Indeed, due to reflection symmetry, generated hole wave packets possess a symmetric momentum distribution and therefore must be seen as a superposition of cosine-like standing waves.

We conclude that for a periodic chain where the location of those nodes is not fixed due to the absence of edges, embedding emitters in two neighboring sites is enough to have all hole states quickly replenished, as confirmed in Fig. 3.8 [panels a),b)] which features steady-state properties which are undistinguishable from those of Fig. 3.2 obtained by pumping all sites. For the most relevant experimental configuration of open boundary conditions, this issue of nodes in the wave-function can be avoided in a simple manner by setting the emitting site at one of the chain extremities, where the nodes can not be located [Fig. 3.8 c),d)] (for open boundaries, a single particle/hole wave function presents nodes at the extremities only in a
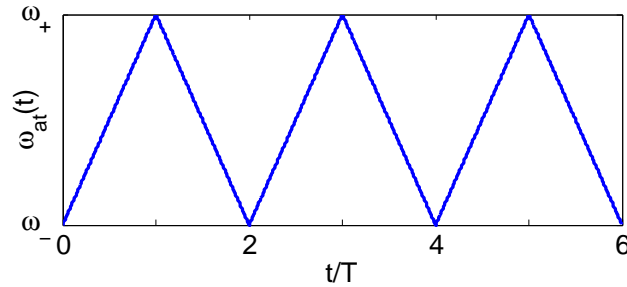
Figure 3.9: Temporal profile of the time-dependent emitter transition frequency required to mimic the square-shaped emission spectrum

continuum configuration, not for a lattice).

3.7.2.2 Temporally-modulated emitter frequency

Along different lines, a dramatic reduction of the number of required emitters can be obtained by making a single emitter to mimic the effect of a square spectrum. In the original proposal presented in Sec. 3.7.1, each single emitter provides a Lorentzian contribution (Eq. (3.26)) to the emission spectrum and the square spectrum of Eq. (3.11) is recovered upon integration over a uniform distributed of emitter frequencies within the interval $[\omega_-, \omega_+]$.

The goal of this subsection is to show how a wide distribution of emitters can be imitated by temporally modulating the transition frequency of a single emitter. In order to get a uniform distribution, one needs a constant modulation speed $v_\omega = |\frac{d\omega_{\mathrm{at}}}{dt}|$ (leading to the time-dependent profile of Fig. 3.9). Under suitable conditions described below, the resulting time-averaged emission spectrum then has the desired shape

$$
\begin{aligned}
\mathcal{S}_{\mathrm{em}}^{(av)}(\omega) &= \frac{\Gamma_{\mathrm{em}}^{\mathrm{at}}}{T} \int_t^{t+T} dt \, \frac{(\Gamma_{\mathrm{p}}/2)^2}{(\omega - \omega_{\mathrm{at}}(t))^2 + (\Gamma_{\mathrm{p}}/2)^2} \\
&= \frac{\Gamma_{\mathrm{em}}^{\mathrm{at}}}{\omega_+ - \omega_-} \int_{\omega_-}^{\omega_+} d\tilde{\omega} \, \frac{(\Gamma_{\mathrm{p}}/2)^2}{(\omega - \tilde{\omega})^2 + (\Gamma_{\mathrm{p}}/2)^2},
\end{aligned}
\tag{3.28}
$$

where $T = \frac{(\omega_+ - \omega_-)}{v_\omega}$ is the frequency modulation half-period. A similar idea was experimentally implemented in [81] to obtain a square spectrum field by modulating a classical source in time. This technique allowed to spectrally probe the different photonic levels of a single mode cavity coupled to a far-off-resonance emitter, and thus to demonstrate a dispersive blockade effect.

Such a simplification strategy, which drastically reduces the number of emitters required in order to reproduce a square emission spectrum, would apply also for the implementation of the frequency-dependent losses, as one could couple the system to a single absorber (resp. resonator) whose transition frequency is temporally modulated over the interval $[\omega_+, \omega_{\mathrm{L}}]$.

General considerations: While a full numerical study is postponed to a future work, one can already see on physical grounds that in order to avoid spurious effects, several conditions must be met. First, v_ω should be fast enough for photons not to be lost within a modulation half-period T, which imposes that $\frac{1}{T} = \frac{v_\omega}{\omega_+ - \omega_-} \gg \Gamma_{\mathrm{l}}$. If this condition is not satisfied, the scheme fails to stabilize a quasi time-independent steady-state and the system keeps performing wide oscillations.

As a second requirement, v_ω should be slow enough that well-defined edges are maintained at the extremes of the spectrum and uncontrolled heating effects are avoided. Provided $v_\omega \ll \Gamma_{\mathrm{p}}^2$, the resulting frequency-dependent emission is expected to converge toward the exact square spectrum of Fig. 3.1 a) with edges possessing a width $\Delta_{\mathrm{em}} = \Gamma_{\mathrm{p}}$. Otherwise, one expects that $1/\sqrt{v_\omega}$ becomes then the dominant limiting time scale in the memory kernel of Eq. (3.8) and the effective edge linewidth increases as $\Delta_{\mathrm{em}}^{\mathrm{eff}} \propto \sqrt{v_\omega}$. This additional broadening can be tolerated as long as one remains in the frequency-selectivity regime $\Delta_{\mathrm{em}}^{\mathrm{eff}} \ll U$.

These two constraints can be simultaneously satisfied for weak enough losses. As we have seen in Sec. 3.2, $\omega_+ - \omega_-$ should be at least equal to a few times the interaction strength U,
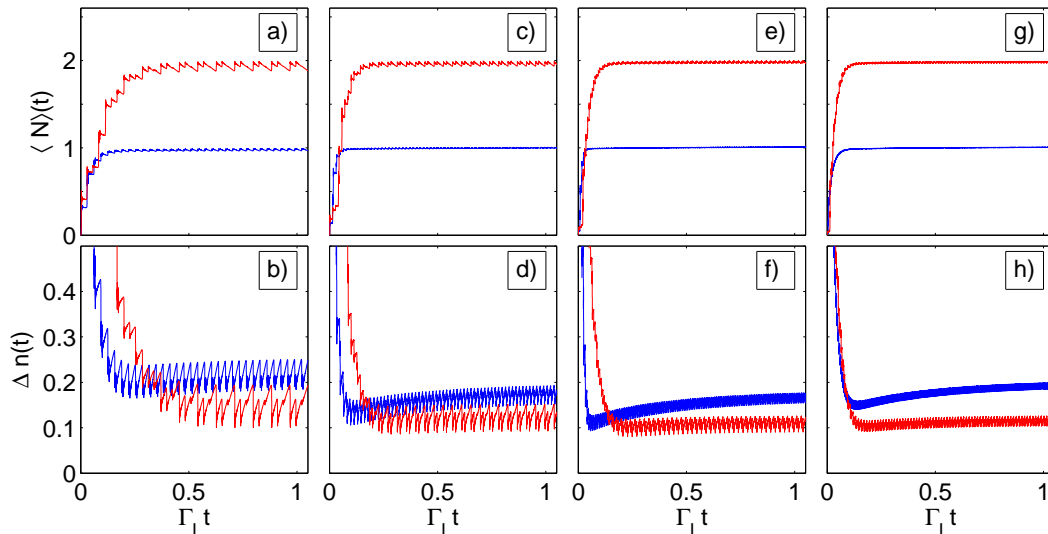
Figure 3.10: Time evolution of a single cavity configuration using a single temporally modulated emitter to mimic the effect of a square emission spectrum. Different panels from left to right refer to increasing values of the modulation speed $v_\omega = \left|\frac{d\omega_{at}}{dt}\right|$. The blue (resp. red) lines correspond to a single photon (resp. two photon) Fock state stabilization. Upper panels: average photon number $\langle N \rangle (t)$. Lower panels: relative fluctuations of the total particle number $\Delta n(t) = \sqrt{\langle N^2 \rangle (t) - \langle N \rangle^2 (t)}/\langle N \rangle (t)$. The photon-emitter Rabi coupling Ω_R was chosen for each modulation speed in such a way to set the stationary value of the photon number close the desired occupation number: $\langle N \rangle (t) \simeq_{t\to\infty} 1$ (resp. 2). Parameters inspired from state-of-the-art in circuit-QED systems [126, 159]: $U = 200 \times 2\pi$MHz, $\Gamma_p = 0.5 \times 2\pi$MHz, $\Gamma_l = 1 \times 2\pi$kHz. For the blue (resp. red) lines $\mu = \omega_+ - \omega_{cav} = U/2$ (resp. $3U/2$), and $\omega_+ - \omega_- = 0.6\,U$ (resp. $1.6\,U$). Choice for the modulation speed, from left to right: $v_\omega = 7.5 \times (2\pi$MHz$)^2$, $15 \times (2\pi$MHz$)^2$, $30 \times (2\pi$MHz$)^2$, $50 \times (2\pi$MHz$)^2$. Corrispondingly for the blue lines, from left to right $\Omega_R = 0.83 \times 2\pi$Hz, $0.9 \times 2\pi$Hz, $0.97 \times 2\pi$Hz, $1.07 \times 2\pi$Hz (resp. for the red lines $\Omega_R = 1 \times 2\pi$Hz, $1.07 \times 2\pi$Hz, $1.15 \times 2\pi$Hz, $1.24 \times 2\pi$Hz).

and $\Gamma_p = \Delta_{em}$ is a tunable parameter which will have to verify $\Delta_{em}/U \ll 1$: one concludes that a very small $\Gamma_l/U \lll 1$ allows to simultaneously satisfy both conditions. For realistic parameters a compromise between the two opposite constraints must be found. In that prospect, a good strategy may be to use several emitters spanning different sub-intervals of the spectral range $[\omega_-, \omega_+]$: in this way, the modulation speed $\left|\frac{d\omega_{at}}{dt}\right|$ required to cover the whole interval $[\omega_-, \omega_+]$ within the finite photon lifetime $1/\Gamma_l$ would in fact be reduced, which would help fulfilling the two constraints.

Numerical checks: Some first numerical results validating this conclusion as well as our intuition on how to optimize the performance of this scheme are presented in Fig. 3.10 for a very simplified single-cavity model, where we investigate the possibility of stabilizing a single-photon (resp. two-photon) Fock state by setting $\mu = U/2$ (resp. $\mu = 3U/2$) in the middle of the first (resp. second) Mott lobe, and we compared the resulting performance between several modulation speeds $v_\omega = \left|\frac{d\omega_{at}}{dt}\right|$.

As was predicted, for low modulation speeds (panels a)-d)), losses occuring within the modulation half-period $T = (\omega_+ - \omega_-)/v_\omega$ of the modulated emitter can not be neglected, and thus the density maintains measurable oscillatory behaviour, a true steady-state is not fully reached and fluctuations are substantial. For an optimal modulation speed (panels e),f)), using state-of-the art parameters of circuit QED, we obtained a minimized value for the particle number relative fluctuations $\Delta n \simeq 0.17$ (resp. 0.12) for the first (resp.second) Fock state, leading to a probability $\pi \simeq \langle N^2 \rangle - \langle N \rangle^2$ of only 3% (resp. 5%) of not being in the desired Fock state, and an effective temperature $T_{eff} \simeq 0.12 \times U$ (resp. $0.14 \times U$): this is a very good level of performance, comparable to the results of Sec. 3.4.2 obtained by direct steady-state calculation of the master equation Eq. (3.4) using similar parameters (we had obtained $\pi = 1.7\%$ and $T_{eff} \simeq 0.10 \times U$ for the first lobe in the limit $J = 0$ of a single cavity). At higher modulation speeds (panels g),h)), as discussed previously, the

modulation-induced broadening is responsible for an increase of fluctuations as it leads to heating effects and undesired transitions toward Fock states with higher photon number.

As we can see, temporal variations of the density are slightly more important if we want to stabilize a Fock state with an higher photon number, since the emitter needs to travel over a broader range of frequencies, in order to protect all transitions from the vacuum until the desired occupation number, and thus losses are more important over the modulation time interval $T = (\omega_+ - \omega_-)/v_\omega$. As was explained earlier, this issue can be readily fixed by using several emitters spanning different frequency regions.

3.8 Conclusions and perspectives

In this Chapter, in order to tackle some inherent difficulties related to the use of the non-Markovian pump scheme with a narrow bandpass emission spectra, we have introduce a fully novel scheme based on more complex tailored reservoirs in order to stabilize strongly correlated photonic states. By focusing on the Bose-Hubbard model, our study confirmed the possibility of cooling down the many-body state toward a Mott-Insulator incompressible state with a perfectly defined (and arbitrary) integer density, robust against dissipative losses. Strikingly, the resulting state survives to the presence of an important hopping, which was not the case with a narrow bandpass spectrum. In a completely identical way to the equilibrium configuration, the Insulating state can be reshaped into a superfluid like state, characterized by strong non-local effects, either by changing the chemical potential or increasing the tunneling.

Depending on the specific values of the system and pumping parameters, the system behaviour can either closely resemble its equilibrium counterpart or show an unexpected transition to a non-equilibrium state characterized by a significant entropy. We related this deviation from equilibrium to the kinetic generation of doublon excitations, occurring when some specific high energy band start presenting some overlap. A strategy to circumvent this feature by adding frequency-dependent losses was proposed. Our numerical study confirmed for this new scheme the possibility for any choice of parameters of fully stabilizing the Hamiltonian ground-state, which has a much longer lifetime than all excited states.

In addition to observing the superfluid-insulator transition in a fluid of strongly interacting photons, our work demonstrates the possibility of quantum simulating zero-temperature equilibrium physics on a photonic platform. In addition, our scheme which can be implemented by mean of a relatively small of additional components with respect to current experiments, is readily accessible to the state-of-the-art technologies.

Future work will explore the possibility of exploiting the very non-equilibrium features to generate exotic many-body states and novel non-equilibrium phase transitions (It would be interesting to gain some insight on the nature of the novel entropic transition in the thermodynamic limit, which occurs in absence of frequency-dependent losses), as well as investigate the potential of our schemes to quantum simulate a wider range of many-body problems. Another research direction will be the development of novel analytical tools allowing to compute at a mean-field level the static and dynamical properties of strongly interacting driven-dissipative systems in presence of a non-Markovian environment, in order to address directly the systems properties in the thermodynamic limit.

Chapter 4

Pseudo-Thermalization effects in non-Markovian open quantum systems

4.1 Introduction

The dynamics of open quantum systems is often characterized by the presence of a complex external environment often modelled as a series of reservoirs [57, 24], which can implement a wide range of effects such as single particle/many-body losses, pump, dephasing [29, 76], or more exotic dissipative processes [50]. Our understanding of the conditions allowing for the emergence of analogous equilibrium properties in this physical context is still limited. Over the last decade, these problematics have become particularly relevant at an experimental level also in the quantum regime, as pioneering works in photonic devices have opened a whole new panel of research on the dynamics of non-equilibrium quantum fluids. Signatures of Bose-Einstein distributions, such as the presence of power-law infrared divergencies similar to the Rayleigh-Jeans distribution ($n_k \underset{k \to 0}{\propto} \frac{1}{k^2}$), and/or high-energy exponential tails of a Boltzmann type ($n_k \underset{k \to \infty}{\propto} e^{-\beta E_k}$), have been observed in several experiments involving photon and exciton-polariton non-equilibrium fluids [99, 9, 108, 101, 152, 169] and predicted by various models [153, 105, 34, 35]. If in the high-temperature regime [108, 101, 152, 169], the appearance of thermal correlations might be seen as something rather predictable since energy exchange with the thermal environment is occurring much faster than particle losses, in other classes of low-temperature exciton-polaritons [99, 9] and VCSEL [7] experiments, where non-equilibrium effects are expected to be kinetically dominant, the underlying mechanisms leading to emergence of an effective temperature differing from the one of the apparatus are less clear and subject to controversy.

From a theoretical point of view, phenomenological work has been done to quantify the distance from equilibrium for photonic systems [105, 106] and connections have been drawn between equilibrium and symmetries of the Keldysh action [5, 175]. Studies based renormalization group methods for non-equilibrium field theories have addressed the long-range and low-energy properties of quantum fluids [176, 177]. In particular, the important role played the spatial dimensionality in determining whether a driven-dissipative quantum system presents asymptotic pseudo-thermalization properties or not [2, 199, 80] was highlighted. More recently, the necessity of characterizing the dynamical properties was also pointed out in [33], which showed that a driven-dissipative quantum system could present at steady static equilibrium-like static correlations without verifying the Fluctuation-Dissipation Theorem (FDT) at a dynamical level.

In this Chapter, we want to push this last statement one step further: we argue that, under very specific conditions, an open quantum system can present all the attributes of an equilibrated system both at a static and a dynamic level (verifying in particular the FDT theorem), even though its environment is highly non-thermal: in a previous work [119] (see Sec. 2.4 of a previous chapter), we unveiled a novel 'pseudo-thermalization effect' under

the form of a preliminary result, where the impact of a single thermal bath is mimicked by coupling the system to several non-thermal and non-Markovian baths and the system apparently thermalizes: since the detailed balance relation [17, 190] is verified, the system is not able to perceive that the reservoirs are not equilibrated and ends up in a steady-state overlapping with a thermal state, with both temperature and chemical potential being artificial physical quantities depending on the various baths spectral properties. Following that work, the preliminary concept was deepened by [171], who suggested to engineer more complex reservoirs so to reproduce this effect over broader energy scales, and then obtain artificial and controllable temperatures in view of optimizing the performance of quantum annealers. Some hints suggest that the apparent emergence of thermal static properties in low-T exciton-polariton experiments [99, 9] might be related to pseudo-thermalization in some experimental configurations.

In both works [119, 171], the formalism was based on a quantum master equation formalism, which allowed to access static properties of the steady-state but not the dynamical ones such as multiple time correlators, and in particular did not allow to verify the validity of the Fluctuation Dissipation Theorem (FDT) [113]. Moreover, as all predictions were based on very general theoretical arguments, a full validation on a specific model still remains to provide. In this Chapter, we give a proof of pseudo-thermalization for the specific model of a weakly interacting BEC coupled to several non-Markovian reservoirs. We demonstrate in particular the validity of the FDT theorem. While this model was already introduced in Chapter 2 and Chapter 3 and formulated in terms of a quantum master equation, here we develop an alternative analytical approach based on a quantum non-Markovian Langevin formalism which keeps tracks of the bath dynamics and is physically very transparent, and allows in particular to access both static and dynamical properties of the steady state.

This Chapter is organized as follows: in Sec. 4.2 we introduce the general Langevin model and use Bogoliubov theory to linearize this theory around a mean-field solution, from which we demonstrate numerically the dynamical stability. We also derive an low-energy effective description, allowing to provide exact analytical expressions for the low-momentum Bogoliubov spectrum. In Sec. 4.3, we show that, for baths with arbitrary spectral shape, this model presents low-energy pseudo-thermalization both at a static and dynamical level: we demonstrate that not only static correlations overlap with their thermal counterpart at low energies, but that the FDT is also verified in that same frequency range. Moreover, if the non-thermal baths are suitably chosen so that the kinetics of the system verifies the Kennard-Stepanov (KS) relation (i.e. the detailed balance relation) at all energies, then the system undergoes artifical thermalization at all energies. In Sec. 4.4 we provide a derivation of the quantum Langevin model basing ourselves on the quantum optics model introduced in a previous Chapter in Sec. 2.2.1. We also explain how the Kennard-Stepanov relation could be engineered with this model, and how it might be naturally reproduced in exciton-polariton low-T experiments. In Sec.4.5 we give hint about how to break pseudo-thermalization and drive the system out-of-equilibrium by adding saturation and/or non-trivial momentum dependence to emission.

All the results of this Chapter are based on the preprint [120] (submitted for pubication), of which the author of this thesis is the first and main author.

4.2 Non-Markovian quantum-Langevin equation

In this section we present a reformulation based on a quantum Langevin formalism of the non-Markovian model for an driven-dissipative interacting Bose Gas which we already addressed in Chapters 2 and 3. Focusing on the weakly interacting case, in the BEC regime we study the mean-field solution of this model and use the Bogoliubov theory to study the dynamics of fluctuations. After demonstrating numerically the dynamical stability for a specific choice of the pump and loss spectra, we develop a low-energy effective theory so to access analytically the low-momentum collective modes of the condensate.

4.2.1 Model for a driven condensate

Let us consider a bosonic gas in d spatial dimensions, described by the annihilation and creation fields $\hat{\psi}(\mathbf{r})$ and $\hat{\psi}^\dagger(\mathbf{r})$. The evolution in time of these operators is described by the

non-Markovian quantum-Langevin equation

$$\frac{\partial \hat{\psi}}{\partial t}(\mathbf{r}, t) = -i\left[\omega_0 - \frac{\nabla^2}{2m} + g\hat{\psi}^\dagger(\mathbf{r}, t)\hat{\psi}(\mathbf{r}, t)\right]\hat{\psi}(\mathbf{r}, t) + \int_{t'} \Gamma(t')\hat{\psi}(\mathbf{r}, t - t') + \hat{\xi}(\mathbf{r}, t), \quad (4.1)$$

where $\int_t' \equiv \int_{-\infty}^{+\infty} dt'$, while ω_0 is the bare cavity frequency, m is the bosonic mass, $g > 0$ is the strength of the repulsive contact interaction, Γ is a memory kernel and $\hat{\xi}(\mathbf{r}, t)$ a zero-mean Gaussian quantum noise operator. Equation (4.1) resembles the Heisenberg equation for the motion of the operator $\hat{\psi}$ for an isolated interacting Bose gas. However, the dynamics described by Eq. (4.1) does not conserve energy and number of particles. Namely, the terms $\Gamma(t')$ and $\hat{\xi}(t)$ model the effect of frequency-dependent particle injection and losses dissipative processes. With respect to the previous Chapters, in addition to the non-Markovian emission $\mathcal{S}_{\text{em}}(\omega)$ our analysis will include the possibility of a non-trivial frequency dependence also the loss spectrum $\mathcal{S}_{\text{l}}(\omega)$.

With the Langevin formalism, the correlations of the noise operators $\hat{\psi}(\mathbf{r}, t)$, $\hat{\psi}^\dagger(\mathbf{r}, t)$ can thus be written as

$$\langle\hat{\xi}(t)\hat{\xi}^\dagger(t')\rangle = \int_\omega \mathcal{S}_{\text{l}}(\omega)\,e^{-i\omega(t-t')} \tag{4.2a}$$

$$\langle\hat{\xi}^\dagger(t)\hat{\xi}(t')\rangle = \int_\omega \mathcal{S}_{\text{em}}(\omega)\,e^{i\omega(t-t')}, \tag{4.2b}$$

with $\int_\omega \equiv \int_{-\infty}^{+\infty} d\omega/(2\pi)$, where the loss/pump power spectra $S_{l,p}(\omega) \geq 0$ are functions of ω. Likewise, Γ is expressed as

$$\Gamma(t) = \theta(t)\int_\omega \left[\mathcal{S}_{\text{em}}(\omega) - \mathcal{S}_{\text{l}}(\omega)\right]e^{-i\omega t}. \tag{4.3}$$

The Heaviside function $\theta(t)$ in Eq. (4.3) is needed in order to ensure causality: as a result, its presence implies the Kramers-Kronig relations between the real and imaginary parts of the Fourier transform $\Gamma(\omega) = \int_t e^{i\omega t}\Gamma(t)$, which can thus be written as

$$\text{Re}\left[\Gamma(\omega)\right] = \frac{1}{2}\left[\mathcal{S}_{\text{em}}(\omega) - \mathcal{S}_{\text{l}}(\omega)\right], \tag{4.4a}$$

$$\text{Im}\left[\Gamma(\omega)\right] = \text{PV}\int_{\omega'} \frac{\mathcal{S}_{\text{em}}(\omega') - \mathcal{S}_{\text{l}}(\omega')}{\omega - \omega'}. \tag{4.4b}$$

The power spectra $\mathcal{S}_{\text{em}}(\omega)$ and $\mathcal{S}_{\text{l}}(\omega)$ are assumed to be smooth functions of the frequency ω. In the following, we will restrict to the case in which there exists a range of frequencies $\omega_1 < \omega < \omega_2$ such that $\mathcal{S}_{\text{em}}(\omega) > \mathcal{S}_{\text{l}}(\omega)$ ("amplifying" region), and that $\mathcal{S}_{\text{em}}(\omega) < \mathcal{S}_{\text{l}}(\omega)$ outside this interval ("lossy" region). Accordingly, losses are perfectly balanced by pumping at the boundary of this interval, i.e., $\mathcal{S}_{\text{em}}(\omega_{1,2}) = \mathcal{S}_{\text{l}}(\omega_{1,2})$. We also define $\Delta_{diss} = \min(\text{FHWM}(\mathcal{S}_{\text{l}}), \text{FHWM}(\mathcal{S}_{\text{em}}))$ as the minimum of the full width at half maximum of the power spectra $\mathcal{S}_{\text{l}}(\omega)$ and $\mathcal{S}_{\text{em}}(\omega)$. It represents a characteristic frequency scale over which these power spectra change value and quantifies the non-Markovianity of the dynamics. We stress that the loss and emission power spectra $\mathcal{S}_{\text{l}}(\omega)$ and $\mathcal{S}_{\text{em}}(\omega)$ arise from the contact of the system with separate reservoirs, i.e., an absorbers/loss medium and an emitters/gain medium: as a consequence, $\mathcal{S}_{\text{l}}(\omega)$ and $\mathcal{S}_{\text{em}}(\omega)$ are assumed to be perfectly independent and completely tunable physical quantities. A microscopic derivation of the Quantum Langevin Equation (4.1) starting from the quantum optics model of Chapter 2 involving a photonic lattice and two-level emitters is presented in Sec. 4.4.

Finally we introduce the following quantity

$$\beta_{\text{eff}} \equiv \frac{1}{T_{\text{eff}}} \equiv \frac{S_{\text{l}}'(\omega_2) - S_{\text{em}}'(\omega_2)}{\mathcal{S}_{\text{em}}(\omega_2)} = \frac{d}{d\omega}\log\left[\frac{\mathcal{S}_{\text{l}}(\omega)}{\mathcal{S}_{\text{em}}(\omega)}\right]\Bigg|_{\omega=\omega_2}. \tag{4.5}$$

As we will see in Sec. 4.3, this model presents pseudo-thermalization properties at low energies for generic power spectra, and T_{eff} will play the role of an effective temperature. T_{eff} also scales like the linewidth of the power spectra Δ_{diss} and quantifies non-Markovianity, but unlike Δ_{diss} it is more sensitive to the local properties around ω_2. In the Markovian

limit, we have that $T_{\text{eff}}, \Delta_{diss} \to \infty$. On the contrary, for very steep power spectra (very coherent pump and/or loss processes), the dynamics is highly non-Markovian and we have that $T_{\text{eff}}, \Delta_{diss} \to 0$.

In analogy with what was already discussed in Sec. 2.4 in a previous chapter, here the physical origins of the pseudo-thermalization can be understood intuitively at a qualitative level: at ω_2 losses and pump exactly compensate ($\mathcal{S}_{\text{em}}(\omega_2) = \mathcal{S}_{\text{l}}(\omega_2)$), so this frequency will play for this model the role of the condensate frequency (while ω_1 will be unstable), and frequencies close to this value will correspond to low-energy excitations on top of the condensate. However, close to ω_2 , the pump and loss power spectra verify the following condition (see Eq. (4.5)):

$$\frac{\mathcal{S}_{\text{em}}(\omega_2 + \omega)}{\mathcal{S}_{\text{l}}(\omega_2 + \omega)} \underset{\omega \to 0}{\simeq} (1 - \beta_{\text{eff}}\omega + \mathcal{O}(\omega/\Delta_{\text{diss}})^2) \sim e^{-\beta_{\text{eff}}\omega}, \tag{4.6}$$

so the Kennard-Stepanov relation [102, 180] (which is a special form of equilibrium/detailed balance condition for the absorption and emission spectra in quantum optical systems) is asymptotically verified at low frequencies. Thus, as we will demonstrate in Sec. 4.3, steady-state low-energy properties are expected to be thermal.

Moreover, if we choose the emission and absorption spectra to verify exactly the Kennard-Stepanov relation

$$\frac{\mathcal{S}_{\text{em}}(\omega_2 + \omega)}{\mathcal{S}_{\text{l}}(\omega_2 + \omega)} = e^{-\beta_{\text{eff}}\omega}, \tag{4.7}$$

then the system should thermalize at all energies. Note that this can be obtained without the various baths being at thermal equilibrium, as we can tune independently the emission and loss power spectra $S_{(\text{l/em})}$ by changing the emitters and absorbers frequency distributions. In Sec. 4.4.1.2 we discuss how the the Kennard-Stepanov might be reproduced naturally in exciton-polariton low-T experiments by the loss power spectrum (related to mirror transparency) and the emission spectrum (related to the excitonic reservoir), in some experimetnal configurations where the scattering processes by longitudinal optical phonons are dominant..

All the results presented in the next sections regarding low-energy properties are general in the sense that they do not depend on the precise shape of the power spectra. Nonetheless, in order to substantiate the discussion, we performed numerical simulations for a specific choice of $\mathcal{S}_{(\text{l/em})}(\omega)$. For all the graphical representations we will thus consider the case of Markovian losses and a Lorentzian-shaped pump (see Fig. 4.1)

$$\mathcal{S}_{\text{l}}^{graph}(\omega) \equiv \Gamma_l, \tag{4.8a}$$

$$\mathcal{S}_{\text{em}}^{graph}(\omega) \equiv \Gamma_{\text{em}} \frac{(\Delta_{\text{diss}}/2)^2}{(\omega - \omega_{\text{em}})^2 + (\Delta_{\text{diss}}/2)^2}. \tag{4.8b}$$

where the use of the notation Δ_{diss} is consistent with the previous definition. We also define the detuning $\delta \equiv \omega_0 - \omega_{\text{em}}$ between the photonic and the pump frequency. Accordingly, we need to have $\Gamma_l < \Gamma_{\text{em}}$ in order to obtain an amplified range of frequencies and generate a condensate, and $\omega_{1,2}$ are the two solutions of $\frac{(\Delta_{\text{diss}}/2)^2}{(\omega - \omega_{\text{em}})^2 + (\Delta_{\text{diss}}/2)^2} = \frac{\Gamma_l}{\Gamma_{\text{em}}}$.

This choice of loss and emission power spectrum is naturally reproduced by our quantum optics proposal Sec. 4.4.1.1. Since it does not verify completely the Kennard-Stepanov relation, we do not expect it will lead to complete thermalization; however, it is well suited to investigate the effect of low-T pseudo-thermalization.

4.2.2 Non-interacting case

In this section we consider the case of a non-interacting Bose gas, i.e, we set the interaction strength g to 0. In this case, the Langevin equation Eq. (4.1) is linear and it can be solved exactly, for a given choice of $\Gamma(\omega)$. If a stationary state exists independent on the initial conditions (see discussion further below), one may evaluate the corresponding solution by
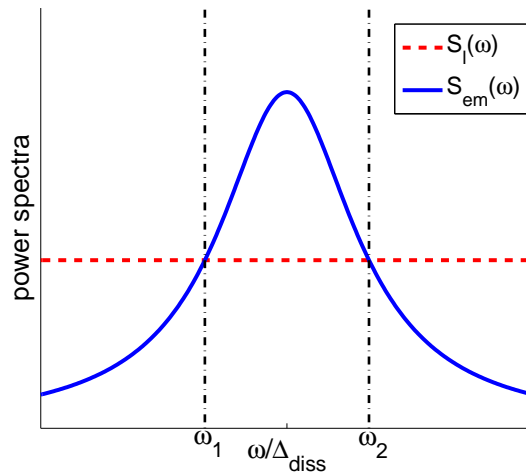
Figure 4.1: Power spectra for Markovian losses and Lorentzian shape pump

introducing the Fourier transforms

$$\hat{\psi}_{\mathbf{k}}(\omega) = \int_{\mathbf{r},t} \hat{\psi}(\mathbf{r},t) e^{i(\mathbf{k}\cdot\mathbf{r}-\omega t)}, \qquad (4.9\text{a})$$

$$\hat{\psi}_{\mathbf{k}}^{\dagger}(\omega) = \int_{\mathbf{r},t} \hat{\psi}^{\dagger}(\mathbf{r},t) e^{-i(\mathbf{k}\cdot\mathbf{r}-\omega t)} \left[\hat{\psi}_{\mathbf{k}}(\omega)\right]^{\dagger}, \qquad (4.9\text{b})$$

$$\hat{\xi}_{\mathbf{k}}(\omega) = \int_{\mathbf{r},t} \hat{\xi}(\mathbf{r},t) e^{i(\mathbf{k}\cdot\mathbf{r}-\omega t)}, \qquad (4.9\text{c})$$

$$\hat{\xi}_{\mathbf{k}}^{\dagger}(\omega) = \int_{\mathbf{r},t} \tilde{\xi}^{\dagger}(\mathbf{r},t) e^{-i(\mathbf{k}\cdot\mathbf{r}-\omega t)} = \left[\hat{\xi}_{\mathbf{k}}(\omega)\right]^{\dagger}, \qquad (4.9\text{d})$$

and by replacing them into Eq. (4.1): one thus finds that the value of $\hat{\psi}_{\mathbf{k}}(\omega)$ is given by

$$\hat{\psi}_{\mathbf{k}}(\omega) = \frac{i\hat{\xi}_{\mathbf{k}}(\omega)}{\omega - \omega_0 - \epsilon_{\mathbf{k}} - i\Gamma(\omega)}, \qquad (4.10)$$

with $\epsilon_{\mathbf{k}} = k^2/2m$. Note that, as a consequence of the absence of the non-linearity, all the modes $\mathbf{k}$ are decoupled. When $\hat{\psi}_{\mathbf{k}}(\omega)$ is transformed back in real time, it results in a linear combination of several modes $\omega_{\mathbf{k},n}$, corresponding to the poles of the denominator in Eq. (4.10) (assuming no branch-cuts), weighted with different amplitudes. For each value of $\mathbf{k}$, several solutions $\omega_{\mathbf{k},n}$ (labelled by the index n) may exist: this give rise to a branched spectrum of eigenfrequencies. The number of these branches depends on the peculiar choice of $\Gamma(\omega)$: these additional dispersions are related to the degrees of freedom which were traced out from the dynamical description of the bosonic fields $\hat{\psi}$ and are accounted for by $\Gamma(\omega)$.

The imaginary part $\text{Im}[\omega_{\mathbf{k},n}]$ corresponds to the inverse lifetime of the given mode: in order to have a dynamically stable mode, the condition $\text{Im}[\omega_{\mathbf{k},n}] < 0$ must be satisfied; this also implies that a dynamically stable stationary solution independent of the initial state exists, as any information on the initial state will vanish exponentially fast in time. On the contrary, if $\text{Im}[\omega_{\mathbf{k},n}] \geq 0$ for some values of $\mathbf{k}$ and n, the corresponding mode grows indefinitely in time, or it remains constant: in both cases, one cannot neglect the information about the initial state, thus invalidating the assumption that a stationary value independent on the initial state exist. For $\text{Im}[\omega_{\mathbf{k},n}] > 0$, the field $\hat{\psi}$ diverges exponentially in time, and thus the solution is physically meaningless: nonetheless, this feature may signal a dynamical instability of the non-interacting approximation of Eq. (4.1), and, as a result, the inclusion of non-linearity may be crucial.

For the specific choice of the power spectra, discussed in the previous Section, which admits an amplifying region $[\omega_1, \omega_2]$, one expects some eigenmodes to present dynamical instabilities. Qualitatively, if $\omega_0 + \epsilon_{\mathbf{k}}$ falls into the amplifying region (which is not necessarily

$[\omega_1, \omega_2]$, due to the presence of the imaginary part $\mathrm{Im}[\Gamma(\omega)]$ which induces a Lamb shift of the bare frequency), a dynamical instability is expected: while in a standard laser the instability would be controlled and ultimately stopped due to the presence of a saturated gain medium [170, 131], here those nonlinear terms where not included in our Langevin description. As was already discussed in a previous chapter in Sec. 2.3.2, we will recover below that the inclusion of a non-vanishing interaction strength $g \neq 0$ provides a non-standard saturation mechanism which prevents the unconstrained growth of dynamically unstable modes.

4.2.3   Interacting case: mean-field solution

We consider now the interacting solution of Eq. (4.1) for the interacting case $g \neq 0$. As a first level of approximation, we consider the classical limit of Eq. (4.1), which, in absence of a reservoir, corresponds to the well-known Gross-Pitaevskii description of a condensate [151]. This can be accomplished by replacing the quantum field $\hat{\psi}$ with a classical complex field ψ and by neglecting the quantum noise $\hat{\xi}$. The classical field ψ can be thus interpreted as the wave function of a condensate.

The validity of this approximation relies on the fact that the non-condensed fraction is assumed to be very small: this would have to be checked a posteriori by studying the effect of the fluctuations on the stability of the condensate solution (see Sec. 4.2.4). While in lower dimensions, fluctuations are expected to be dominant and thus preclude any such description[1], we expect that for high enough spatial dimension d condensation is possible [176, 177]. Thus, a weak interaction coupling g (inducing a weak quantum depletion), and a certain selectivity in frequency of the dissipation (limiting the generation of excitations of high energy) should be suitable conditions for the emergence of coherence in the system. The classical field $\psi(\mathbf{r}, t)$ thus obeys the following equation:

$$\frac{\partial \psi(\mathbf{r}, t)}{\partial t} = -i \left[\omega_0 - \frac{\nabla^2}{2m} + g|\psi(\mathbf{r}, t)|^2 \right] \psi(\mathbf{r}, t) + \int_\tau \Gamma(\tau)\psi(\mathbf{r}, t - \tau), \qquad (4.11)$$

which has the form of a driven-dissipative Gross-Pitaevskii equation with a memory kernel. We focus on spatially homogeneous solutions of the form

$$\psi(t) = \psi_0 \, e^{-i\omega_{\mathrm{BEC}} t}, \qquad (4.12)$$

which describe a condensate with infinite lifetime, frequency ω_{BEC} and density $n_0 = |\psi_0|^2$.

The non-condensed case $\psi_0 = 0$ is always a solution of Eq. (4.11), whose stability may be studied by linearizing Eq. (4.11) around it: this yields the linear equation studied in Sec. 4.2.2. As a result, the non-condensed solution is stable when the spectrum of the excitations lies outside the amplifying region, i.e., $\omega_0 + \epsilon_{\mathbf{k}} \geq \omega_2$. We will now show that non-trivial, condensed ($\psi_0 \neq 0$) solutions exist when the bare frequency lies below the upper-boundary of the amplifying region, i.e., $\omega_0 \leq \omega_2$. In this case, the interaction generates a blue-shift $\sim g n_0$ of the bosonic bare frequency ω_0, thus providing a natural saturation mechanism as the condensate frequency is spontaneously set at one of the boundaries of the amplifying region. In fact, by inserting Eq. (4.12) into Eq. (4.11), one finds

$$\omega_{\mathrm{BEC}} = \omega_0 + g|\psi_0|^2 + i\Gamma(\omega_{\mathrm{BEC}}) \qquad (4.13)$$

from which, by taking the real and the imaginary part and by using Eq. (4.4), one finds the two following equations for ω_{BEC} and $|\psi_0|^2$:

$$\mathcal{S}_{\mathrm{em}}(\omega_{\mathrm{BEC}}) = S_l(\omega_{\mathrm{BEC}}) \qquad (4.14a)$$

$$\omega_{\mathrm{BEC}} = \omega_0 + \mu + \delta_{\mathrm{L}}(\omega_{\mathrm{BEC}}), \qquad (4.14b)$$

where

$$\mu \equiv g|\psi_0|^2 \qquad (4.15)$$

is the mean-field self-interaction energy and

$$\delta_{\mathrm{L}}(\omega) = \mathrm{PV} \int_{\omega'} \frac{1}{\omega - \omega'} \left[\mathcal{S}_l(\omega') - \mathcal{S}_{\mathrm{em}}(\omega') \right] \qquad (4.16)$$

---

[1]Naively, one could possibly think about an alternative quasi-condensate description involving the phase and density degrees of freedom [137]. However in that situation the corresponding KPZ equation describing the non-equilibrium phase dynamics has been predicted to lead to strong long range fluctuations [2, 199]

corresponds to a Lamb shift of the condensate frequency due to the contact with the bath. From Eq. (4.14a), we deduce that the only solutions for the condensate frequency are: $\omega_{\text{BEC}} = \omega_{1,2}$. However, the solution ω_1 will be unstable, since the low energy excitations of the condensate will fall in the amplified region $[\omega_1, \omega_2]$ and undergo dynamical instability, thus we will not take into account this solution and consider in all the next sections the case $\omega_{\text{BEC}} = \omega_2$.

We finally remark that, unlike usual VCSEL [85] where stability is induced by a saturation effect of the pump (photonic emitters are 'two-level like' nonlinear systems which need some time to be repumped in the excited state), here stability is expected to be a consequence of the interplay between the frequency dependence of pumping and the progressive blue-shift $g|\psi_0|^2$ induced by interactions during the condensate growth, this until the condensate frequency reaches ω_{BEC} where pump and losses perfectly compensate.

4.2.4 Interacting case: Bogoliubov analysis of fluctuations

In order to study the stability of the condensate and to characterize the properties of its excitations, we express the bosonic field as

$$\hat{\psi}(\mathbf{r}, t) = \left[\psi_0 + \hat{\Lambda}(\mathbf{r}, t)\right] \mathrm{e}^{-i\omega_{\text{BEC}} t}, \tag{4.17}$$

where $\hat{\Lambda}(\mathbf{r}, t)$ is an operator describing the fluctuations above the condensate. Inserting this decomposition and the mean-field solution obtained from Eq. (4.14) into Eq. (4.1), and retaining terms up to the first order in the fields $\hat{\Lambda}(\mathbf{r})$, $\hat{\Lambda}^\dagger(\mathbf{r})$, one obtains

$$\frac{\partial \hat{\Lambda}(\mathbf{r}, t)}{\partial t} = -i\left[\hat{\Lambda}(\mathbf{r}, t), H_{\text{bog}}(t)\right] + \int_\tau \widetilde{\Gamma}(\tau)\hat{\Lambda}(\mathbf{r}, t-\tau) + \tilde{\xi}(\mathbf{r}, t) \tag{4.18}$$

where

$$H_{\text{bog}} = \int \mathrm{d}^d r \left\{ \hat{\Lambda}^\dagger(\mathbf{r})\frac{-\nabla^2}{2m}\hat{\Lambda}(\mathbf{r}) + \frac{\mu}{2}\left[2\hat{\Lambda}^\dagger(\mathbf{r})\hat{\Lambda}(\mathbf{r}) + \hat{\Lambda}(\mathbf{r})\hat{\Lambda}(\mathbf{r}) + \hat{\Lambda}^\dagger(\mathbf{r})\hat{\Lambda}^\dagger(\mathbf{r})\right] \right\} \tag{4.19}$$

is the Bogoliubov Hamiltonian, $\widetilde{\Gamma}$ is defined as

$$\widetilde{\Gamma}(t) = \mathrm{e}^{i\omega_{\text{BEC}} t}\Gamma(t) - \delta(t)\Gamma(\omega_{\text{BEC}}), \tag{4.20}$$

and $\tilde{\xi}(\mathbf{r}, t) = \mathrm{e}^{i\omega_{\text{BEC}} t}\xi(\mathbf{r}, t)$. After calculation of the commutator, the equation Eq. (4.18) can be rewritten as

$$\frac{\partial \hat{\Lambda}(\mathbf{r}, t)}{\partial t} = -i\left\{\frac{-\nabla^2}{2m}\hat{\Lambda}(\mathbf{r}, t) + \mu\left[\hat{\Lambda}(\mathbf{r}, t) + \hat{\Lambda}^\dagger(\mathbf{r}, t)\right]\right\} + \int_\tau \widetilde{\Gamma}(\tau)\hat{\Lambda}(\mathbf{r}, t-\tau) + \tilde{\xi}(\mathbf{r}, t). \tag{4.21}$$

The linear system 4.21 can be regarded as the driven-dissipative non-markovian counterpart of the Bogoliubov-de Gennes equations. Similarly to the equilibrium case, the field $\hat{\Lambda}(\mathbf{r}, t)$ and its hermitian conjugate $\hat{\Lambda}^\dagger(\mathbf{r}, t)$ are coupled by the interaction energy μ: this coupling is mediated by processes in which non-condensed particles are scattered into the condensate, and vice-versa. It is convenient to rewrite Eq. (4.18) in momentum and frequency space: in order to do this, we define the Fourier transform of the fields and noise operators as in Eq. (4.9). The correlations of the quantum noise operators in the momentum and frequency space are given by:

$$\langle \tilde{\xi}_{\mathbf{k}}(\omega)\tilde{\xi}_{\mathbf{k}'}^\dagger(\omega')\rangle = \delta_{\mathbf{k}-\mathbf{k}'}\, \delta_{\omega-\omega'}\mathcal{S}_{\text{l}}(\omega_{\text{BEC}} + \omega), \tag{4.22a}$$

$$\langle \tilde{\xi}_{\mathbf{k}}^\dagger(\omega)\hat{\xi}_{\mathbf{k}'}(\omega')\rangle = \delta_{\mathbf{k}-\mathbf{k}'}\, \delta_{\omega-\omega'}\mathcal{S}_{\text{em}}(\omega_{\text{BEC}} + \omega). \tag{4.22b}$$

with $\delta_{\mathbf{k}} \equiv (2\pi)^d\, \delta^{(d)}(\mathbf{k})$, $\delta_\omega \equiv 2\pi\delta(\omega)$. After taking the Fourier transform of Eq. (4.18), we obtain the following set of coupled equations :

$$\omega \begin{pmatrix} \hat{\Lambda}_{\mathbf{k}}(\omega) \\ \hat{\Lambda}_{-\mathbf{k}}^\dagger(-\omega) \end{pmatrix} = \mathcal{L}_{\mathbf{k}}(\omega) \begin{pmatrix} \hat{\Lambda}_{\mathbf{k}}(\omega) \\ \hat{\Lambda}_{-\mathbf{k}}^\dagger(-\omega) \end{pmatrix} + i \begin{pmatrix} \tilde{\xi}_{\mathbf{k}}(\omega) \\ \tilde{\xi}_{-\mathbf{k}}^\dagger(-\omega) \end{pmatrix}, \tag{4.23}$$

where the matrix $\mathcal{L}_{\mathbf{k}}(\omega)$ is given by

$$\mathcal{L}_{\mathbf{k}}(\omega) = \begin{pmatrix} \epsilon_k + \mu + i\widetilde{\Gamma}(\omega) & \mu \\ -\mu & -\epsilon_k - \mu + i\widetilde{\Gamma}^*(-\omega) \end{pmatrix}, \tag{4.24}$$

where $\widetilde{\Gamma}(\omega)$ is the Fourier transform of $\widetilde{\Gamma}(t)$ defined in Eq. (4.20), and it reads:

$$\widetilde{\Gamma}(\omega) = \Gamma(\omega + \omega_{\mathrm{BEC}}) - \Gamma(\omega_{\mathrm{BEC}}), \tag{4.25}$$

and we used the notation $\widetilde{\Gamma}^*(\omega) \equiv \left[\widetilde{\Gamma}(\omega)\right]^*$. The complex function $\widetilde{\Gamma}(\omega)$ represents the frequency dependent decay rate (real part) and lamb shift (imaginary part) of the fluctuations. $\widetilde{\Gamma}(\omega)$ vanishes for $\omega \to 0$, consistently with the fact that the condensate has an infinite lifetime (see Eq. (4.13)).

For later convenience, we define the correlation matrix $\mathcal{C}_{\mathbf{k}}(\omega)$

$$\delta_{\mathbf{k}-\mathbf{k}'}\,\delta_{\omega-\omega'}\,\mathcal{C}_{\mathbf{k}}(\omega) = \begin{pmatrix} \langle \hat{\Lambda}_{\mathbf{k}}(\omega)\hat{\Lambda}_{\mathbf{k}'}^{\dagger}(\omega') \rangle & \langle \hat{\Lambda}_{\mathbf{k}}(\omega)\hat{\Lambda}_{-\mathbf{k}'}(-\omega') \rangle \\ \langle \hat{\Lambda}_{-\mathbf{k}}^{\dagger}(-\omega)\hat{\Lambda}_{\mathbf{k}'}^{\dagger}(\omega') \rangle & \langle \hat{\Lambda}_{-\mathbf{k}}^{\dagger}(-\omega)\hat{\Lambda}_{-\mathbf{k}'}(-\omega') \rangle \end{pmatrix}, \tag{4.26}$$

which can be calculated by inverting Eq. (4.23), multiplying the solution by its hermitian conjugate and averaging over the noise correlation using Eq. (4.22) (see App. E for the details of the calculations).

4.2.5   Dynamical stability of excitations

In order to study the dynamical stability of the mean-field solution, it is necessary to check that the elementary excitations do not grow exponentially and have a finite lifetime. To this end, we derive from Eq. (4.23) the excitations spectrum by calculating frequencies $\omega_{\mathbf{k}}^i$ (with i some integer number used to label the excitation) which cancel out the determinant of the matrix $\omega - \mathcal{L}_{\mathbf{k}}(\omega)$ with $\mathcal{L}_{\mathbf{k}}(\omega)$ defined in Eq. (4.24). This leads us to the following condition on the frequency:

$$\left[\omega - \epsilon_k - \mu - i\widetilde{\Gamma}(\omega)\right]\left[\omega + \epsilon_k + \mu - i\widetilde{\Gamma}^*(-\omega)\right] + \mu^2 = 0. \tag{4.27}$$

Solutions with negative imaginary parts correspond to decaying excitations, while in presence of any instability, some solutions present a positive imaginary part. Since we are considering generic non-Markovian systems, $\widetilde{\Gamma}(\omega)$ can be any function verifying the Kramers-Kronig relations reported in Eq. (4.4), thus in general Eq. (4.27) may have a large number of solutions, and it may be not possible to solve it analytically.

In the case of Markovian losses and a Lorentzian spectrum Eq. (4.8), Eq. (4.27) becomes an algebraic equation which admits four different solutions, thus giving rise to four different branches by varying the momentum k which we computed numerically. In Fig. 4.2, these solutions are plotted successively for increased values of $\Gamma_{(l/\mathrm{em})}$, going at fixed ratio $\Gamma_l/\Gamma_{\mathrm{em}} = 0.3$ from a weakly-dissipative regime (upper panels) in which the spectral power $\Gamma_{(l/\mathrm{em})}$ are weak with respect to the linewidth Δ_{diss}, to a strong-dissipative regime (lower panels) in which they become comparable or higher. All other parameters (interaction g, mass m, detuning δ, linewidth Δ_{diss}) are left unchanged.

As a first observation, all imaginary parts of the frequencies are negative, so there is no instability (we checked this for other choice of parameters). Secondly, in the weak dissipative regime (panels a) and f)) the mode structure is typical of photonic driven-dissipative condensates [183, 208, 35, 29] and presents a sharp transition from purely damped modes to propagating ones. Also we observe two other branches of imaginary part Δ_{diss} and real parts $\pm(\omega_{BEC} - \omega_{\mathrm{em}})$: these additional frequencies account for the oscillation of bath degrees of freedom, which are hidden in the non-Markovianity of the Langevin equation and are nearly unaffected by the system dynamics due to the weak coupling (In a photonic language for the Lorentzian emission spectrum, the reservoir degrees of freedom responsible for the emission may be seen as two-level emitters of transition frequency ω_{em}). However, for stronger dissipation (other panels), the system and reservoir degrees of freedom are coupled and can not be treated separately, which can be seen in a clearest way by a deformation of the various
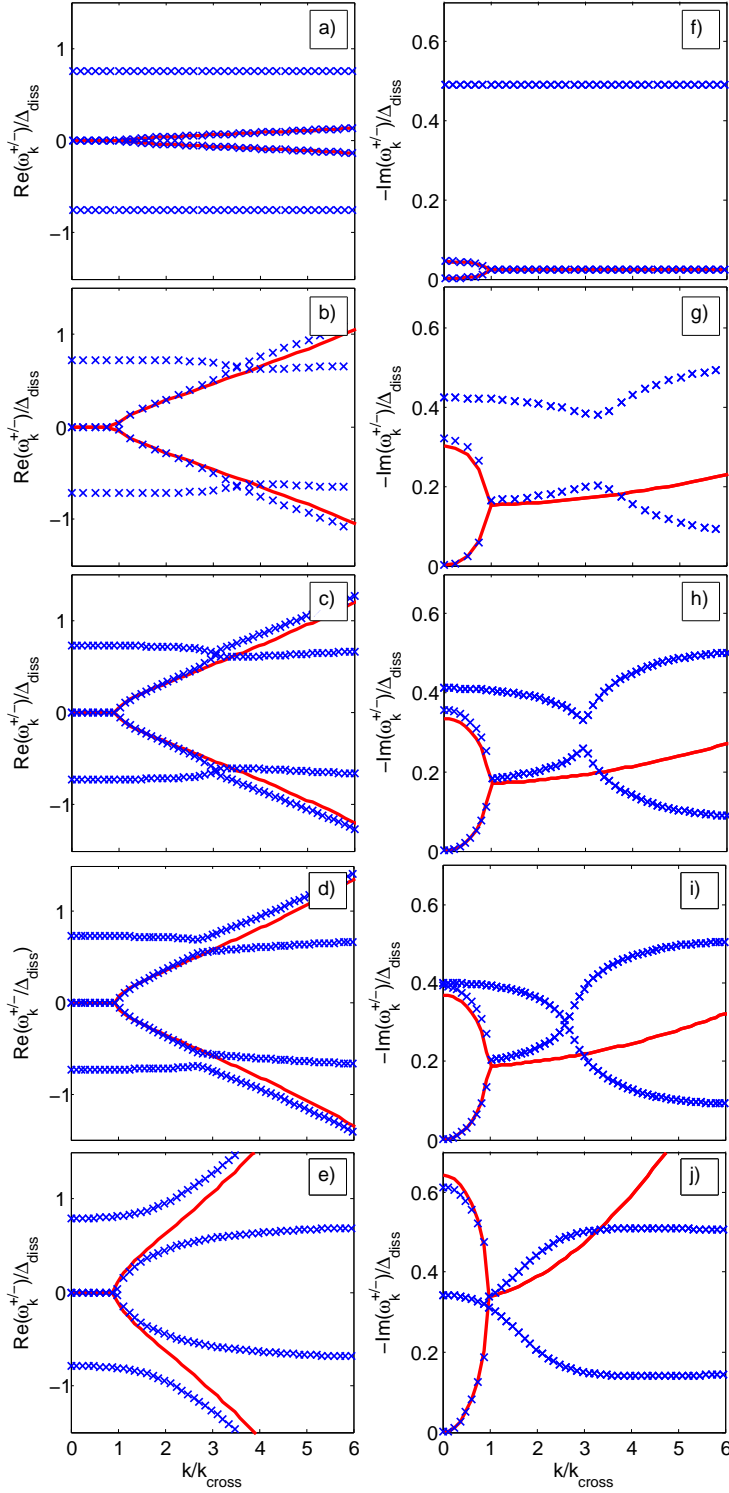
Figure 4.2: Excitation spectrum of the condensate in the case a Lorentzian emission spectrum (which can represent the emission by a two level atom), and Markovian losses (model defined in Sec.4.2.1). Left (resp. right) panel: real (resp. imaginary) part of the frequency in units of Δ_{diss} in function of the momentum k in units of k_{cross} defined as $|z_R|E_{k_{cross}} = z_I\mu$ (momentum at which the branching effect occurs). In blue crosses we plot exact numerical solutions of the full non-Markovian theory (Eq. 4.23)), and in red full lines the solutions given by the corresponding Markovian effective theory at low energies (Eq. (4.31)). From up to down panels, we investigate the transition between weak-dissipation to strong-dissipation. Parameters: for all panels, $m = 1$, $\delta/\Delta_{\text{diss}} = 0$, $\Gamma_l/\Gamma_{\text{em}} = 0.3$. From up to down, $\Gamma_{\text{em}}^0/\Delta_{diss} = 0.1$, 0.55, 0.6, 0.65, 1.

branches near the crossing point. Remarkably, a sharp transition from weak to strong coupling occurs between the panels c),h) and the panels d),i), inducing a change in excitation spectrum structure, as one moves from a situation of branch crossing to an avoided crossing: in this regime, the collective modes associated with the excitation spectrum couples the bosonic and the bath degrees of freedom, giving birth to a mixed quasi-excitation. In a photonic language, this suggests that some elementary excitations are of polaritonic nature.

4.2.6 Effective low-frequency Markovian dynamics

An effective time-local equation describing the dynamics for frequencies small enough with respect to Δ_{diss}: indeed, for $\omega \ll \Delta_{\text{diss}}$, the function $\widetilde{\Gamma}(\omega)$ defined in Eq. (4.23) can be linearized and approximated as $\widetilde{\Gamma}(\omega) \approx \omega \widetilde{\Gamma}'(0) = \omega \Gamma'(\omega_{\text{BEC}})$. As a result, the low-frequency limit of the Langevin equation Eq. (4.23) becomes:

$$\omega \hat{\Lambda}_{\mathbf{k}}(\omega) = z \left\{ \epsilon_k \hat{\Lambda}_{\mathbf{k}}(\omega) + \mu \left[\hat{\Lambda}_{\mathbf{k}}(\omega) + \hat{\Lambda}^\dagger_{-\mathbf{k}}(-\omega) \right] + i \overline{\xi}_{\mathbf{k}}(\omega) \right\}, \tag{4.28}$$

with the coefficient z defined as

$$z = \lim_{\omega \to 0} \left[\frac{\omega}{\omega - i\widetilde{\Gamma}(\omega)} \right] = [1 - i\Gamma'(\omega_{\text{BEC}})]^{-1}, \tag{4.29}$$

and the new noise operators $\overline{\xi}_{\mathbf{k}}(\omega)$ and $\overline{\xi}^\dagger_{\mathbf{k}}(\omega)$ are characterized by the correlations

$$\langle \overline{\xi}_{\mathbf{k}}(\omega) \overline{\xi}^\dagger_{\mathbf{k}'}(\omega') \rangle = \delta_{\mathbf{k}-\mathbf{k}'} \, \delta_{\omega-\omega'} \, \mathcal{S}_{\text{l}}(\omega_{\text{BEC}}), \tag{4.30a}$$

$$\langle \overline{\xi}^\dagger_{\mathbf{k}}(\omega) \overline{\xi}_{\mathbf{k}'}(\omega') \rangle = \delta_{\mathbf{k}-\mathbf{k}'} \, \delta_{\omega-\omega'} \, \mathcal{S}_{\text{em}}(\omega_{\text{BEC}}). \tag{4.30b}$$

Notice that the noise operators $\overline{\xi}_{\mathbf{k}}(\omega)$ and $\overline{\xi}^\dagger_{\mathbf{k}}(\omega)$ correspond to an effective classical noise, since their correlations do not depend on the order of the operators, as a consequence of Eq. (4.14a).

With respect, to a purely hamiltonian dynamics, all couplings in the commutator have been multiplied by the complex number z. The eigenmodes of Eq. (4.28) are given by

$$\omega_k^\pm = -i z_I \left(\epsilon_k + \mu \right) \pm \sqrt{z_R^2 E_k^2 - z_I^2 \mu^2}, \tag{4.31}$$

where $z = z_R - i z_I$, z_R and z_I are both real numbers, and $E_k = \sqrt{\epsilon_k(\epsilon_k + 2\mu)}$ is the equilibrium Bogoliubov energy for the Hamiltonian Eq. (4.19). We can already verify the dynamical instability of the mean-field solution for the choice of BEC frequency $\omega_{\text{BEC}} = \omega_1$, as this leads to a negative z_I (due to a change of sign in the derivative of the real part of $\Gamma(\omega)$ involved in Eq. (4.29)) and thus to a positive imaginary part in the low-momentum excitation spectrum in Eq. (4.31). This justifies definitively the choice $\omega_{\text{BEC}} = \omega_2$ (whose dynamical stability was already checked in 4.2.5).

The frequencies $\omega_k^\pm$, shown in Fig. 4.2 in red solid lines, closely resemble the spectrum of a polaritonic driven-dissipative condensate [183, 208, 35, 29], already described in Sec. 1.1.2.1: they are are imaginary for small momenta, which signals the purely diffusive nature of low-energy excitations, while they acquire a finite real part at higher momenta. In particular, for $k \to 0$ the branch ω_k^+ vanishes and therefore it can be identified with the (diffusive) Goldstone mode associated with the spontaneous breaking of the $U(1)$ symmetry. As was already discussed in the previous subsection, higher powers of ω present in Eq. (4.23) related to the non-Markovianity can generate additional modes not predicted by the effective low-energy theory Eq. (4.28), which can be observed in Fig. 4.2.

The validity of Eq. (4.28) for the study the long-range physics has to be checked a posteriori, by requiring the absolute value $|\omega_k^\pm|$ to be small with respect to Δ_{diss} for small k, so that it can be computed by mean of the low-energy effective theory Eq. (4.28). On the one hand, this condition is naturally satisfied for the Goldstone branch ω_k^+ for low enough momenta. On the other hand, the gapped branch ω_k^- verifies $|\omega_{k=0}^-| = 2 z_I \mu$, and therefore the gapped mode is correctly described by the Markovian low-frequency theory only if $2 z_I \mu \ll \Delta_{\text{diss}}$. According to Eq. (4.29), z scales as $\mathcal{S}_l(\omega_{BEC})/\Delta_{\text{diss}}$, so the gapped mode is

correctly described by the Markovian low-frequency theory only if $\hat{S}_l(\omega_{BEC})\mu \ll \Delta_{\mathrm{diss}}^2$: this is the case for very small power spectra (weak dissipation) or very small interaction energy μ. The validity of this analysis is illustrated in Fig.4.2 where we can see that, within the range of applicability of our theory described below, the theoretical prediction Eq. (4.31) for the Goldstone mode and the gapped mode always fits with the exact numerical predictions.

4.3 Pseudo-thermalization

In this section we give evidence for low-energy pseudo-thermalization for generic power spectra, both at static and dynamical level, by showing that the low-energy static correlations map on equilibrium ones, and demonstrating the validity of the FDT in the the low frequency regime. We also compute exactly the static correlations at all energies in the weakly dissipative regime. Finally, in the specific choice of reservoirs where the Kennard-Stepanov relation is exactly verified, we demonstrate the validity of FDT at all frequencies, and show that the steady-state in the weakly dissipative regime the steady-state is in a Gibbs ensemble.

4.3.1 Static correlations

A system presenting low-energy effective thermal properties should have steady state static properties similar to an equilibrium one, and look like a Gibbs ensemble at low-energies. In Sec.4.3.1.1, we give the low-energy expression for static correlations, both in the weak and strong dissipative regimes, while in Sec. 4.3.1.2 we give an exact analytical expression at all energies, only valid in the weak-dissipative regime .

4.3.1.1 Low energies

In this section we focus on the low energy regime $E_k \ll \Delta_{\mathrm{diss}}$. By using the expression derivated in Sec. E.1 for the frequency-correlation matrix $\mathcal{C}_k(\omega)$ defined in Eq. (4.26) and by restricting ourselves to the low-frequency regime using the procedure described in Sec. 4.2.6, we compute by Fourier transform the steady state values of the momentum distribution $n_k = \langle \hat{\Lambda}_{\mathbf{k}}^\dagger \hat{\Lambda}_{\mathbf{k}} \rangle$ and the anomaleous average $\mathcal{A}_k = \langle \hat{\Lambda}_{\mathbf{k}} \hat{\Lambda}_{-\mathbf{k}} \rangle$, at leading order for low energies (see App. E for the details of the calculation):

$$n_k \quad \simeq \quad \frac{T_{\mathrm{eff}}(\epsilon_{\mathbf{k}} + \mu)}{(E_{\mathbf{k}})^2}, \tag{4.32}$$

$$\mathcal{A}_k \quad \simeq \quad -\frac{T_{\mathrm{eff}}\,\mu}{(E_{\mathbf{k}})^2}, \tag{4.33}$$

where we remind that T_{eff} is defined in Eq. (4.5). These static correlations have to be compared to those obtained by doing a Bogoliubov calculation for a Bose gas at thermal equilibrium of temperature T_{eff} and chemical potential $\mu = g|\psi_0|^2$:

$$n_k^{\mathrm{th}} \quad = \quad \frac{1}{e^{\beta_{\mathrm{eff}} E_{\mathbf{k}}} - 1}(|u_{\mathbf{k}}|^2 + |v_{\mathbf{k}}|^2) + |v_{\mathbf{k}}|^2 \tag{4.34}$$

$$\underset{(\beta_{\mathrm{eff}} E_{\mathbf{k}}) \to 0}{\simeq} \quad \frac{T_{\mathrm{eff}}(\epsilon_{\mathbf{k}} + \mu)}{(E_{\mathbf{k}})^2},$$

$$\mathcal{A}_k^{\mathrm{th}} \quad = \quad 2\left(\frac{1}{e^{\beta_{\mathrm{eff}} E_{\mathbf{k}}} - 1} + \frac{1}{2}\right)u_{\mathbf{k}} v_{\mathbf{k}}^*, \tag{4.35}$$

$$\underset{(\beta_{\mathrm{eff}} E_{\mathbf{k}}) \to 0}{\simeq} \quad -\frac{T_{\mathrm{eff}}\,\mu}{(E_{\mathbf{k}})^2},$$

where u_k and v_k relate (in the case of an isolated Bose Gas at equilibrium) the annihilation operator $\hat{\Lambda}_{\mathbf{k}}$ to the phonon annihilation (resp. creation) operator $\hat{b}_{\mathbf{k}}$ (resp. $\hat{b}_{\mathbf{k}}^\dagger$) through the

Figure 4.3: Static properties of the condensate at steady state in the weak dissipative regime (i.e.,with the power spectra much smaller than Δ_{diss}) in the case of Lorentzian emission spectrum and Markovian losses (model defined in Sec.4.2.1). The left (resp. right) panels correspond to a detuning between the cavity and the atoms chosen to induce a weak (resp. strong) chemical potential μ with respect to the effective temperature T_{eff}. Upper panels: static correlations $n_{\mathbf{k}} = \langle \Lambda_{\mathbf{k}}^{\dagger} \Lambda_{\mathbf{k}} \rangle$ in function of the momentum $\mathbf{k}$ in units of $\mathbf{k}_{\text{th}}$ defined by $E(\mathbf{k}_{\text{th}}) = T_{\text{eff}}$, and in inset, their logarithm in function of the square momentum $\mathbf{k}^2$ in units of $\mathbf{k}_{\text{th}}^2$. In green squares we plot the steady state properties given by numerical calculations of the linearized Langevin equation (Eq. (4.23)) in the weak dissipative regime, in red lines with circles the results given by the Grand-Canonical ensemble (Eq. (4.34)), and in solid blue lines the analytical results given by the Fermi Golden's rule (Eq. (4.39)). Lower panels: the absolute error $n_k - n_k^{th}$ in green squares lines (resp. $n_k^{Fermi} - n_k^{th}$ in solid blue lines) between the numerical solution of the Langevin equation (resp. the analytical solution given by the Fermi's golden rule) and the thermal case, in function of the momentum $\mathbf{k}$ in units of $\mathbf{k}_{\text{th}}$. Parameters: for all panels, $m = 1$, $\Gamma_l/\Gamma_{\text{em}}^0 = 0.3$, $\Gamma_{\text{em}}/\Delta_{\text{diss}} = 10^{-2}$. Deduced quantity $T_{\text{eff}}/\Delta_{\text{diss}} = 0.55$. For the left (resp. right) panels: $\delta/\Delta_{\text{diss}} = 0.72$ (resp. -10). Deduced quantity $\mu/\Delta_{\text{diss}} = 4.6 \times 10^{-2}$ (resp. 10.8×10^0).

Bogoliubov transformation:

$$\hat{\Lambda}_k \quad = \quad u_{\mathbf{k}} \hat{b}_{\mathbf{k}} + v_{\mathbf{k}}^* \hat{b}_{\mathbf{k}}^\dagger, \tag{4.36}$$

$$u_{\mathbf{k}} \quad = \quad \frac{1}{2} \left[\sqrt{\frac{\epsilon_{\mathbf{k}}}{E_{\mathbf{k}}}} + \sqrt{\frac{E_{\mathbf{k}}}{\epsilon_{\mathbf{k}}}} \right], \tag{4.37}$$

$$v_{\mathbf{k}} \quad = \quad \frac{1}{2} \left[\sqrt{\frac{\epsilon_{\mathbf{k}}}{E_{\mathbf{k}}}} - \sqrt{\frac{E_{\mathbf{k}}}{\epsilon_{\mathbf{k}}}} \right]. \tag{4.38}$$

By comparing Eqs (4.32),(4.33) and Eqs. (4.34),(4.35), we note that the low-energy limit $\beta_{\text{eff}} E_{\mathbf{k}} \to 0$ of the driven-dissipative quantum Langevin model accurately presents thermal-like infrared behaviour (the so-called Rayleygh-Jeans distribution). Higher energies correlations are not expected although to be thermal, and due to the algebraic behaviour of the Lorentzian emission spectrum we do not expect in particular to see any exponential tails.

This analytical arguments can be verified in Fig.4.3 (resp. Fig. 4.4), where we plot the static correlations obtained by numerical resolution of the linearized Langevin equation for a Markovian loss spectrum and Lorentzian pump spectrum (Eq. (4.8)), in the weak-dissipative regime (resp. strong-dissipative regime), i.e, for Γ_{em}^0, $\Gamma_l \ll \Delta_{\text{diss}}$ (resp. Γ_{em}^0, Γ_l of the order of Δ_{diss}), and compare those correlations to thermal ones. We plotted the static correlations for two detunings δ of the bare frequency ω_0 with respect to the pump resonance ω_{em}, inducing different effective chemical potentials μ, which is a decreasing function of δ. Indeed, looking at Eq. (4.14b) and neglecting as a first step the Lamb shift, we see that increasing the frequency of the pump ω_{em} defined in Eq. (4.8), i.e., diminuishing the detuning $\delta = \omega_0 - \omega_{\text{em}}$, has for effect to increase ω_{BEC}, and thus to increase also the chemical potential μ. The case of a chemical potential weak (resp. strong) with respect to the effective temperature T_{eff} is plotted in the left (resp. right) panels. The upper panels correspond to the static correlations (with in insets their logarithm to check for any high-energy exponential tails), while in the lower panels we plot the absolute error $n_k - n_k^{th}$ between the solutions of the Langevin equations with respect to thermal predictions.

Expectedly, static correlations given by the numerical simulation of the Langevin equation (green squares) coincide with the equilibrium results (red circles and solid lines) at energies lower than the temperature (since T_{eff} scales as the spectra linewidth Δ_{diss} and is of the same order of magnitude), both in the weak and strong dissipative regimes. In particular, they diverge as $1/k^2$ at low momenta, and looking at the absolute errors we note the that the corresponding corrections to thermal equilibrium remain finite at low energies and thus surprisingly do not present any subsingular divergencies $\propto 1/k$, so effective thermal equilibrium seems also to be true also at the next leading order at a static level for this particular system.

However, as we expected, the pseudo-thermalization does not extend for a generic choice of power spectra at higher energy scales (see the logarithmic plot) as the Kennard-Stepanov relation is not valid in this energy range: in particular, while one can see in the Grand Canonical distribution the presence of exponential tails of a Boltzmann type in the panel a) of Fig.4.3 (approximately for momenta verifying $k/k_{\text{th}}^2 \le 20$, the kink at $k/k_{\text{th}}^2 = 20$ and the slower decay for higher momenta being related to the dominant vacuum fluctuations), such behaviour is not present in the driven-dissipative steady-state which rather features algebraic decay. This features is specifically related to the Lorentzian shape for the emission spectrum Eq. (4.8) chosen for numerical simulations. In the case of a big chemical potential $\mu > T_{\text{eff}}$ (see Fig.4.3 [panel c)]), the thermal distribution does not present exponential tails neither because the vacuum fluctuations which decay algebraically are dominant with respect to thermal fluctuation in the energy range $E_k \ge T_{\text{eff}}$.

4.3.1.2 Static correlations at all energies in the weakly dissipative regime

When the dissipation strength $\mathcal{S}_{(1/\text{em})}(\omega)$ is much weaker than the linewidth of the power spectra Δ_{diss}, it is possible to compute exactly the static correlations at all momenta (see
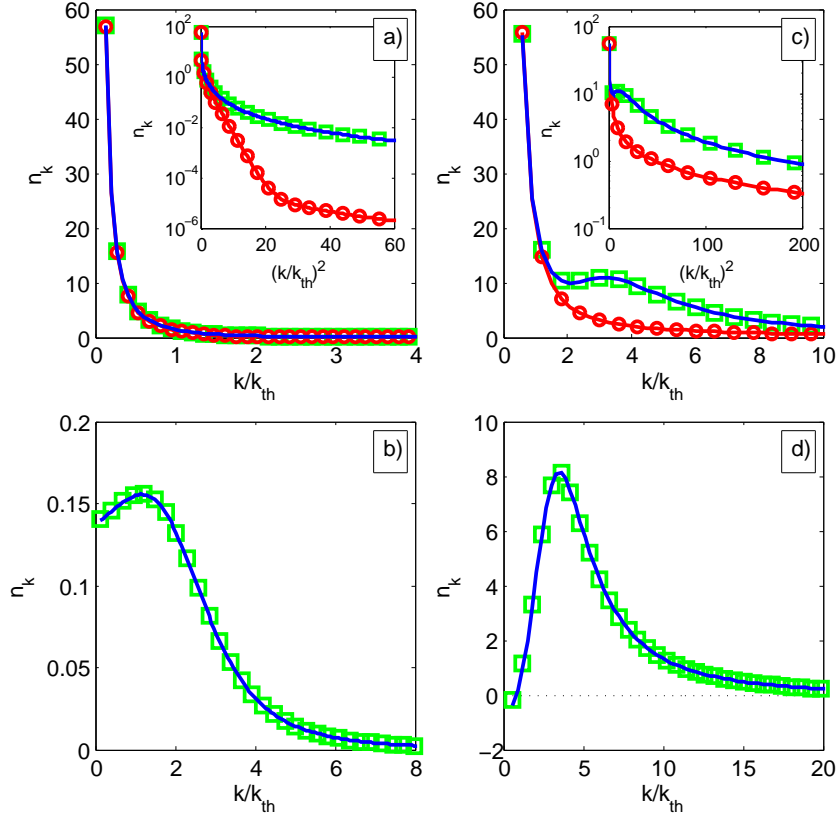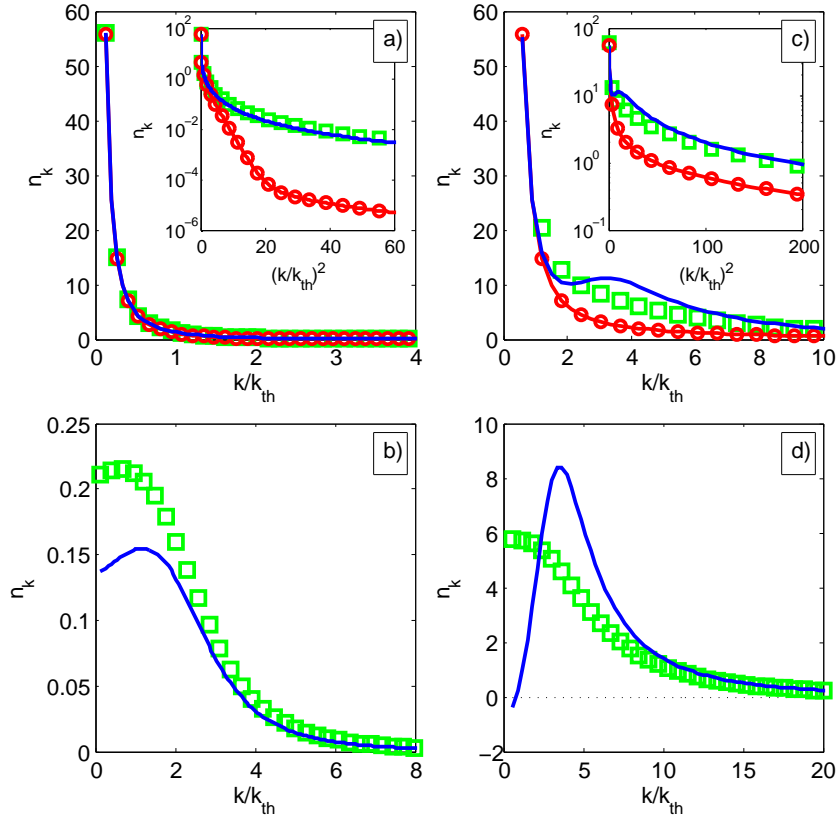
Figure 4.4: Static properties of the condensate at steady state in the strong dissipative regime (i.e. with the power spectra of the order of Δ_{diss}) in the case of Lorentzian emission spectrum and Markovian losses (model defined in Sec.4.2.1). The left (resp. right) panels correspond to a detuning between the cavity and the atoms chosen to induce a weak (resp. strong) chemical potential μ with respect to the effective temperature T_{eff}. Upper panels: static correlations $n_{\mathbf{k}} = \langle \Lambda_{\mathbf{k}}^{\dagger} \Lambda_{\mathbf{k}} \rangle$ in function of the momentum $\mathbf{k}$ in units of $\mathbf{k}_{\text{th}}$ defined by $E(\mathbf{k}_{\text{th}}) = T_{\text{eff}}$, and in inset, their logarithm in function of the square momentum $\mathbf{k}^2$ in units of $\mathbf{k}_{\text{th}}^2$. In green squares we plot the steady state properties given by numerical calculations of the linearized Langevin equation (Eq. (4.23)) in the strong dissipative regime, in red lines with circles the results given by the Grand-Canonical ensemble (Eq. (4.34)), and in solid blue lines the analytical results given by the Fermi Golden's rule (Eq. (4.39)). Lower panels: the absolute error $n_k - n_k^{th}$ in green squares lines (resp. $n_k^{Fermi} - n_k^{th}$ in solid blue lines) between the numerical solution of the Langevin equation (resp. the analytical solution given by the Fermi's golden rule) and the thermal case, in function of the momentum $\mathbf{k}$ in units of $\mathbf{k}_{\text{th}}$. Parameters: for all panels, $m = 1$, $\Gamma_l/\Gamma_{\text{em}} = 0.3$, $\Gamma_{\text{em}}^0/\Delta_{\text{diss}} = 1$. Deduced quantity $T_{\text{eff}}/\Delta_{\text{diss}} = 0.55$. For the left (resp. right) panels: $\delta/\Delta_{\text{diss}} = 0.92$ (resp. -10). Deduced quantity $\mu/\Delta_{\text{diss}} = 7.3 \times 10^{-2}$ (resp. 11.0×10^{0}).

below for a sketch of the derivation below):

$$n_{\mathbf{k}}^{\mathrm{F}} = \frac{1}{K(E_k)-1}(|u_{\mathbf{k}}|^2+|v_{\mathbf{k}}|^2)+|v_{\mathbf{k}}|^2, \tag{4.39}$$

$$\mathcal{A}_{\mathbf{k}}^{\mathrm{F}} = \left(\frac{1}{K(E_k)-1}+\frac{1}{2}\right)u_{\mathbf{k}}v_{\mathbf{k}}^*. \tag{4.40}$$

Comparing these expressions to Eqs. (4.34),(4.35), we see that the vacuum properties are left unchanged with respect to equilibrium statistics, while the Boltzmann factor $e^{\beta E_k}$ of the Bose Einstein phononic distribution in the Grand canonical ensemble has been replaced by the non-equilibrium factor:

$$K(E_k) = \frac{\mathcal{S}_l(\omega_{\mathrm{BEC}}+E_k)|u_k|^2+\mathcal{S}_{\mathrm{em}}(\omega_{\mathrm{BEC}}-E_k)|v_k|^2}{\mathcal{S}_{\mathrm{em}}(\omega_{\mathrm{BEC}}+E_k)|u_k|^2+\mathcal{S}_l(\omega_{\mathrm{BEC}}-E_k)|v_k|^2}, \tag{4.41}$$

giving thus rise to the modified Bose Einstein phonon distribution $\frac{1}{K(E_k)-1}$. The factor $K(E_k)$ can be interpreted as the ratio between the annihilation and creation rates (both induced by pumping and losses dissipative processes) of a single phononic excitation at the Bogoliubov energy E_k, and is calculated using the secular approximation (valid in the weakly dissipative regime). The phonon distribution and average occupation number are a consequence of detailed balance between states with $N_{\mathbf{k}}$ and $N_{\mathbf{k}}-1$ phonons of momentum $\mathbf{k}$. We note that if the pumping and loss rates verify the Kennard-Stepanov condition Eq. (4.7), one recovers the equilibrium Boltzmann factor $K(E_k) = e^{\beta E_k}$: as expected the system is fully thermal at all energies, and its density matrix at steady-state is a Grand-Canonical ensemble. In the general case by using Eq. (4.5) we note that $K(E_k) \underset{E_k\to 0}{\sim} 1-\beta_{\mathrm{eff}}E_k \sim e^{-\beta_{\mathrm{eff}}E_k}$: this provides us another confirmation that low-energy static properties should be thermal.

Static correlations of Eqs. (4.39),(4.40) computed under the secular approximation are shown in solid blue lines in the upper panels of Fig. 4.3 (resp. Fig. 4.4) and compared with the numerical results Langevin equation in the weak (resp. strong) dissipative regime. In the lower panels we plot the absolute error $n_k^{Secular}-n_k^{th}$ between the solution given by the secular approximation and the thermal distribution. We note absolutely no difference between the exact numerical solution and $n_k^{Secular}$. Expectedly, in the strong-dissipative regime they coincide only at low momenta ($E_k \ll T_{\mathrm{eff}}$) (up to a finite error, which is small with respect to the divergency in $1/k^2$), and do not provide exact results at higher momenta.

We now justify the expression Eqs. (4.39),(4.40) for the static correlations in the weak dissipative regime $\mathcal{S}_{\mathrm{em}},\mathcal{S}_l \ll \Delta_{\mathrm{diss}}$ by applying the secular approximation: we consider dissipation as a "classical" stochastic process inducing transitions in the system S between the hamiltonian eigenstates populations, i.e., the diagonal coefficients of the bosonic density matrix $\rho_S = \mathrm{Tr}_{\mathcal{B}}(\rho)$ (which corresponds to the partial trace of the full density matrix ρ over the various baths) in the eigenbasis of the Bogoliubov hamiltonian H_{bog} (defined in Eq. (4.19)). These eigenstates are defined in the equilibrium phononic basis: $\otimes_{\mathbf{k}}|N_{\mathbf{k}}\rangle$, where $\mathbf{k}$ is the momentum and $N_{\mathbf{k}}$ is the occupation number of the phonon of momentum $\mathbf{k}$. The phonon annihilation and creation operators $\hat{b}_{\mathbf{k}}$ and $\hat{b}_{\mathbf{k}}^\dagger$ are related to the particle annihilation and creation operators $\hat{\Lambda}_{\mathbf{k}}$ and $\hat{\Lambda}_{\mathbf{k}}^\dagger$ by the Bogoliubov transformation Eq. (4.36).

Phonon annihilation rate: Let us calculate as a first step the phononic annihilation rate. Starting from a state with $N_{\mathbf{k}}$ phonons of momentum $\mathbf{k}$ and Bogoliubov energy energy E_k, one can remove one phonon through two processes:

- First, one can remove a phonon by losing a particle of momentum $\mathbf{k}$. The total energy removed to the system is $\omega_{\mathrm{BEC}}+E_k$. This leads to the partial rate:

$$\mathcal{T}^{(l)}(N_{\mathbf{k}} \to N_{\mathbf{k}}-1) = \mathcal{S}_l(\omega_{\mathrm{BEC}}+E_k)\left|\langle N_{\mathbf{k}}-1|\hat{\Lambda}_{\mathbf{k}}|N_{\mathbf{k}}\rangle\right|^2$$

$$= \mathcal{S}_l(\omega_{\mathrm{BEC}}+E_k)N_{\mathbf{k}}|u_k|^2. \tag{4.42}$$

Starting from a wave-function calculation, this expression could have been alternatively recovered by mean of the Fermi's Golden rule [73].

- However, due to the presence of counter-rotating terms in the Bogoliubov theory, it is also possible to remove a phonon by pumping a particle of momentum $-\mathbf{k}$. The total

energy added to the system in that case is $\omega_{\text{BEC}} - E_k$, i.e, the mean-field energy of a single photon, minus the energy of the phonon excitation. Thus the corresponding rate is:

$$
\begin{aligned}
\mathcal{T}^{(p)}(N_{\mathbf{k}} \to N_{\mathbf{k}} - 1) &= \mathcal{S}_{\text{em}}(\omega_{\text{BEC}} - E_k) \left| \langle N_{\mathbf{k}} - 1 | \hat{\Lambda}_{\mathbf{k}}^{\dagger} | N_{\mathbf{k}} \rangle \right|^2 \\
&= \mathcal{S}_{\text{em}}(\omega_{\text{BEC}} - E_k) N_{\mathbf{k}} |v_k|^2.
\end{aligned} \tag{4.43}
$$

The total phonon loss rate is thus:

$$
\mathcal{T}^{(tot)}(N_{\mathbf{k}} \to N_{\mathbf{k}} - 1) = \mathcal{S}_l(\omega_{\text{BEC}} + E_k) N_{\mathbf{k}} |u_k|^2 + \mathcal{S}_{\text{em}}(\omega_{\text{BEC}} - E_k) N_{\mathbf{k}} |v_k|^2. \tag{4.44}
$$

Phonon creation rate: One can calculate similarly the phonon total creation rate. Starting from a state with $N_k - 1$ phonons of momentum $\mathbf{k}$ and Bogoliubov energy energy E_k, one can add one phonon by pumping a new particle (the total energy added to the system is thus $\omega_{\text{BEC}} + E_k$) or by losing a particle (the total energy lost is $\omega_{\text{BEC}} - E_k$). After a calculation very similar to the previous paragraph, one obtains the following expression:

$$
\mathcal{T}^{(tot)}(N_{\mathbf{k}} - 1 \to N_{\mathbf{k}}) = \mathcal{S}_{\text{em}}(\omega_{\text{BEC}} + E_k) N_{\mathbf{k}} |u_k|^2 + \mathcal{S}_l(\omega_{\text{BEC}} - E_k) N_{\mathbf{k}} |v_k|^2. \tag{4.45}
$$

Phonon probability distribution: The ratio between the phonon annihilation and creation rates is given by

$$
\begin{aligned}
K(E_k) &= \frac{\mathcal{T}^{(tot)}(N_{\mathbf{k}} \to N_{\mathbf{k}} - 1)}{\mathcal{T}^{(tot)}(N_{\mathbf{k}} - 1 \to N_{\mathbf{k}})} \\
&= \frac{\mathcal{S}_l(\omega_{\text{BEC}} + E_k)|u_k|^2 + \mathcal{S}_{\text{em}}(\omega_{\text{BEC}} - E_k)|v_k|^2}{\mathcal{S}_{\text{em}}(\omega_{\text{BEC}} + E_k)|u_k|^2 + \mathcal{S}_l(\omega_{\text{BEC}} - E_k)|v_k|^2}.
\end{aligned} \tag{4.46}
$$

Because dissipation processes can remove or add only one phonon of momentum $\mathbf{k}$ at a time and do not affect simultaneously the other momenta, one deduces that at steady state, the probabilities $\pi(..., N_{\mathbf{k}} - 1, ...)$ and $\pi(..., N_{\mathbf{k}}, ...)$ of having $N_{\mathbf{k}} - 1$ and $N_{\mathbf{k}}$ phonons of momentum $\mathbf{k}$ (leaving the occupation numbers other momenta $\mathbf{k}'$ unchanged) verify the following detailed balance relation :

$$
\pi(N_{\mathbf{k}} - 1) = K(E_k)\pi(N_{\mathbf{k}}). \tag{4.47}
$$

One deduces that the probability distribution is

$$
\pi(N_{\mathbf{k}}) = \frac{1}{1 - K(E_k)^{-1}} K(E_k)^{-n}, \tag{4.48}
$$

and that the average phonon occupation number is

$$
n_{\mathbf{k}}^{(phonon)} = \frac{1}{K(E_k) - 1}. \tag{4.49}
$$

Doing a Bogoliubov transformation Eq. (4.36), one obtains the momentum static distribution and anomaleous averages Eqs. (4.39),(4.40).

More on the validity of the secular approximation: As we already saw, in Fig. 4.3 we notice absolutely no difference between the numerical results of the Langevin equation in the weak dissipative regime and the solution given by the secular approximation, which appears to be valid at all momenta. This makes us confident that the prediction Eqs. (4.39),(4.40) should be robust and work for a wide range of pump and loss power spectra. Still, it would be interesting to establish a full justification of the validity of this approach based on more theoretical grounds: As a first step, we note that for high energy modes ($E_{\mathbf{k}} \gg \mathcal{S}_{l/\text{em}}$) we are in the natural range of validity the secular approximation, and dissipation has the effect of a classical process coupling only diagonal coefficients of the density matrix, so our approach should be valid. However, the potential problem arise for very low energy modes ($E_{\mathbf{k}} \lessapprox \mathcal{S}_{l/p}$) in the thermodynamic limit, where dissipation is theoretically fast enough to induce coherences between the eigenstates and does not couple anymore only populations. While we had already formulated in a previous chapter (Sec. 2.4.2.2) a proof
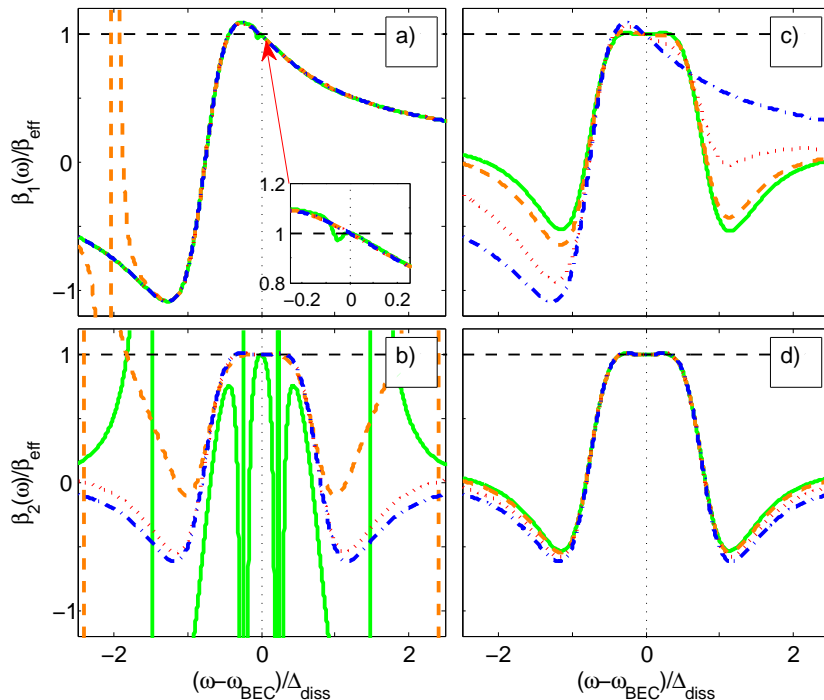
Figure 4.5: Test of the FDT/KMS relations for various sets of parameters. Upper (resp. lower) panels: plot of the frequency dependent effective temperature $\beta_{1,\text{eff}}(\mathbf{k}, \omega)$ (resp. $\beta_{1,\text{eff}}(\mathbf{k}, \omega)$) defined in Eq. (4.5) for a Lorentzian pump and Markovian losses (which is the model of Chap. 2), in function of the frequency $\omega - \omega_{\text{BEC}}$ in units of Δ_{diss}, and for various momenta $\mathbf{k}$. Panels a),b) (resp. c),d)) use the same parameters as in the panels a),b) (resp. c),d)) of Fig. 4.3. For each panel, the various curves corresponds to increasing momenta chosen in such a way that the corresponding Bogoliubov spectrum spans all energy below and above the resulting effective temperature $T_{\text{eff}} = 0.54\Delta_{\text{diss}}$: $k/k_{\text{th}} = 0.18$ for the green solid line, $k/k_{\text{th}} = 3.65$, for the orange dashed line, $k/k_{\text{th}} = 9.1$ for the red dotted line, $k/k_{\text{th}} = 54.7$ for the blue dash-dotted line

that the secular approximation is accurate in some conditions, our initial derivation implicitly assumed that the dissipative coupling between the various hamiltonian eigenstates remained finite at any momenta and did not take into account infra-red divergent behaviours induced by the presence of the widely populated phononic branch and strong vacuum fluctuations ($\propto |u_k|^2$).

Here, apart from the excellent numerical agreement observed in Fig. 4.3, we do not have yet any direct argument justifying that the secular approximation could be directly applied in that energy range to compute the steady-state properties. Still, we point out that we have already computed exactly the asymptotic behaviour of static correlations Eqs. (4.32),(4.33) in Sec. 4.3.1.1 in the regime $E_{\mathbf{k}} \ll \Delta_{\text{diss}}$, and thus also for $E_{\mathbf{k}} \stackrel{\sim}{\ll} \mathcal{S}_{l/p}$ (since $\mathcal{S}_{l/p} \ll \Delta_{\text{diss}}$): we have shown that their dominant singular contribution $\propto 1/k^2$ coincides with the thermal prediction Eqs. (4.34),(4.35) and thus also with the prediction Eqs. (4.39),(4.40) provided by the secular approximation. This does not explain unfortunately why the secular approximation led exact results at all momenta (as can be seen in Fig. 4.3), and in particular why sub-singular corrections $\propto 1/k$ (nor offset corrections $\propto 1$) are not present. A full theoretical proof will be the subject of a future work.

4.3.2 Effective temperature from FDT

A remarkable consequence of equilibrium which involves dynamical quantities is the so-called fluctuation-dissipation theorem [113], which provides a relationship between the linear response of a system to an external perturbation and the correlation of thermal fluctuations.

Let us define the symmetrized correlation (C) and response (R) functions for two arbi-

trary operators $\hat{A}$ and $\hat{B}$ as

$$iC(t - t') = \langle\{\hat{A}(t), \hat{B}(t')\}\rangle, \tag{4.50a}$$

$$iR(t - t') = \theta(t - t')\langle[\hat{A}(t), \hat{B}(t')]\rangle, \tag{4.50b}$$

where the time dependence of $\hat{A}(t)$ and $\hat{B}(t)$ is determined in the Heisenberg picture, while the average $\langle \ldots \rangle$ is taken over an equilibrium state at temperature T. As a consequence of equilibrium, C and R depend only on the time difference $t - t'$ and therefore we can define their Fourier transforms $C(\omega)/R(\omega) = \int_t e^{i\omega t} C(t)/R(t)$. The explicit form of the FDT then reads:

$$C(\omega) = 2\coth(\beta\omega/2)\,\mathrm{Im}[R(\omega)], \tag{4.51}$$

with $\beta = T^{-1}$. An alternative, fully equivalent formulation of the FDT is the so-called Kubo-Martin-Schwinger (KMS) [112, 135] condition:

$$S_{AB}(-\omega) = e^{-\beta\omega} S_{BA}(\omega), \tag{4.52}$$

where $S_{AB}(t) = \langle\hat{A}(t)\hat{B}\rangle$ and $S_{BA}(t) = \langle\hat{B}(t)\hat{A}\rangle$.

The FDT and KMS condition have often been used as a tool to probe the actual thermalization in classical and quantum systems, and to characterize the eventual departure from equilibrium [42, 61, 33]. In particular, from Eqs. (4.51) and (4.52) one can define an effective frequency-dependent temperature $T_{A,B,\mathrm{eff}}(\omega)$ such that FDT or KMS condition are satisfied: if the system is really at equilibrium, then $T_{A,B,\mathrm{eff}}(\omega)$ has a constant value T which corresponds to the thermodynamic temperature. On the other hand, if the system is out of equilibrium it will generically develop a non-trivial dependence on A, B and ω.

In the following, we discuss the effective temperatures obtained from the linearized equation Eq. (4.18): in this respect, we will consider the following ratios:

$$\frac{\langle\hat{\Lambda}_{\mathbf{k}}(\omega)\hat{\Lambda}_{\mathbf{k}}^\dagger\rangle}{\langle\hat{\Lambda}_{\mathbf{k}}^\dagger(\omega)\hat{\Lambda}_{\mathbf{k}}\rangle} = \frac{\mathcal{S}_{\mathrm{l}}(\omega_{\mathrm{BEC}} + \omega) + \mathcal{S}_{\mathrm{em}}(\omega_{\mathrm{BEC}} - \omega)A_k(\omega)}{\mathcal{S}_{\mathrm{em}}(\omega_{\mathrm{BEC}} + \omega) + \mathcal{S}_{\mathrm{l}}(\omega_{\mathrm{BEC}} - \omega)A_k(\omega)}, \tag{4.53}$$

$$\frac{\langle\hat{\Lambda}_{\mathbf{k}}(\omega)\hat{\Lambda}_{-\mathbf{k}}\rangle}{\langle\hat{\Lambda}_{\mathbf{k}}(-\omega)\hat{\Lambda}_{-\mathbf{k}}\rangle} = \frac{\mathcal{S}_{\mathrm{l}}(\omega_{\mathrm{BEC}} + \omega) + \mathcal{S}_{\mathrm{em}}(\omega_{\mathrm{BEC}} - \omega)B_k(\omega)}{\mathcal{S}_{\mathrm{em}}(\omega_{\mathrm{BEC}} + \omega) + \mathcal{S}_{\mathrm{l}}(\omega_{\mathrm{BEC}} - \omega)B_k(\omega)}, \tag{4.54}$$

where the functions $A_k(\omega)$ and $B_k(\omega)$ are explicitly reported in App. E.1. At thermal equilibrium, the value of the ratios (4.53) and (4.54) is fixed by Eq. (4.52) while, in the present case, they have a nontrivial dependence on ω and k, since the system is out of equilibrium.

We then define the effective (inverse) temperatures

$$\beta_{1,\mathrm{eff}}(\mathbf{k}, \omega) = \frac{\mathrm{d}}{\mathrm{d}\omega}\log\left[\frac{\langle\hat{\Lambda}_{\mathbf{k}}(\omega)\hat{\Lambda}_{\mathbf{k}}^\dagger\rangle}{\langle\hat{\Lambda}_{\mathbf{k}}^\dagger(\omega)\hat{\Lambda}_{\mathbf{k}}\rangle}\right], \tag{4.55}$$

$$\beta_{2,\mathrm{eff}}(\mathbf{k}, \omega) = \frac{\mathrm{d}}{\mathrm{d}\omega}\log\left[\frac{\langle\hat{\Lambda}_{\mathbf{k}}(\omega)\hat{\Lambda}_{-\mathbf{k}}\rangle}{\langle\hat{\Lambda}_{\mathbf{k}}(-\omega)\hat{\Lambda}_{-\mathbf{k}}\rangle}\right], \tag{4.56}$$

which are generic functions of k and ω which can be evaluated by using Eqs. (4.53) and (4.54). However, inserting the functional forms Eqs. (4.53), (4.54) into Eqs. (4.55), (4.56) we see that for $\omega \to 0$, both $\beta_{1,\mathrm{eff}}(k, \omega)$ and $\beta_{2,\mathrm{eff}}(k, \omega)$ tend toward the same k-independent value β_{eff} defined in Eq. (4.5), indicating that the KMS condition and the FDT are asymptotically verified at low frequencies.

Remarkably, if the system satisfies the Kennard-Stepanov relation

$$\mathcal{S}_{\mathrm{em}}(\omega_{\mathrm{BEC}} + \omega) = \mathcal{S}_{\mathrm{l}}(\omega_{\mathrm{BEC}} + \omega)e^{-\beta\omega}, \tag{4.57}$$

then $\beta_{1,\mathrm{eff}}(\mathbf{k}, \omega) = \beta_{2,\mathrm{eff}}(\mathbf{k}, \omega) = \beta$ for every value of ω and $\mathbf{k}$, i.e., the system is at full thermal equilibrium, even if the environment is highly non-thermal (see Sec. 4.4.1.2 for a physical made of non-thermal reservoirs verifying artificially the KS relation).

In Fig. 4.5, we plot the effective temperature $\beta_{1,\mathrm{eff}}(\mathbf{k}, \omega)$ (resp. $\beta_{2,\mathrm{eff}}(\mathbf{k}, \omega)$) in the left panel (resp. right panel) in function ω in units of Δ_{diss}, for various momenta $\mathbf{k}$. We

notice first that in the region $\omega \ll \Delta_{\text{diss}}$, these effective temperatures converge to the same value β_{eff} confirming thus the low-frequency validity of FDT, and that the system is effectively thermalized in that frequency range. Away from that region they have a non trivial, frequency-momentum dependent behaviour, so the system is globally not at equilibrium.

Strikingly, it appears that FDT is completely verified below a certain energy cutoff Δ_{therm} (for these precise simulations $\Delta_{\text{therm}} \simeq 0.05 \times \Delta_{\text{diss}} \simeq 0.1 \times T_{\text{eff}}$): for frequencies close enough to the condensate frequency $|\omega - \omega_{\text{BEC}}| \leq \Delta_{\text{therm}}$, we observe that excitations at any momenta feature frequency-dependent effective temperatures $\beta_{1/2}(\omega)$ presenting less than 5% deviation from the limit value β_{eff} (this error can be arbitrarily reduced by getting closer to ω_{BEC}). In particular, the green solid line in Fig. 4.5 b) shows the worst case scenario, which occurs to $\beta_2(\omega)$ in the limit $k \to 0$ (we have checked for any momenta that the singularities[2] of $\beta_2(\omega)$ can not get any closer to ω_{BEC}). As a consequence, all the low-energy elementary excitations of the condensate, whose counterpart in the isolated equilibrium case possesses a Bogoliubov energy $E_k \leq \Delta_{\text{therm}}$ will have their resonance located in the thermalized frequency window $[\omega_{\text{BEC}} - \Delta_{\text{therm}}, \omega_{\text{BEC}} + \Delta_{\text{therm}}]$ and will verify FDT at a very good level of approximation.

4.4 Derivation of the Langevin equation from a quantum optics microscopic model

In this section, we proceed to the derivation of the Langevin equation (4.1) in an array spatial geometry, starting from the microscopic quantum optics model introduced in Chapter 2 in Sec. 2.2.1 (up to some minors changes in notation). The physics we are considering does not depend much on whether space is considered as being discrete or a continuum.

Before moving to the derivation we remind the model in question: we consider a photonic driven-dissipative Bose-Hubbard lattice made of L nonlinear cavities coupled by tunneling. Each cavity possesses a natural frequency ω_0 and is assumed to contain a $\chi^{(3)}$ Kerr nonlinear medium, which induces effective repulsive interactions between photons lying in the same cavity. Dissipative phenomena due finite mirror transparency and absorption by the cavity material are responsible for (possibly non-Markovian) loss processes. We assume that a number N_{at} of two-level atoms are embedded in each cavity in order to inject new photons to compensate losses, and that the atomic transition $\omega_{\text{at}}^{(n)}$ frequencies possess some frequency distribution $\mathcal{D}(\omega)$. Each atom is strongly pumped at a rate Γ_{p} (its spontaneously decay is neglected), and is coupled to the cavity with a Rabi frequency Ω_{R}, which is assumed to be weak enough ($\Omega_{\text{R}} \ll \omega_{\text{at}}^{(n)}, \omega_0$) to be far from the ultra-strong coupling regime. The dissipative dynamics under the effect of the pumping and decay processes can be described in terms of the coupling of the photon-atom system to various reservoirs responsible for photonic losses and atomic pumping.

The system dynamics can be described as the hamiltonian of the photonic/atomic system plus an environment :

$$H = H_{\text{ph}} + H_{\text{at}} + H_{\text{bath}} + H_{\text{I}} \tag{4.58}$$

The Hamiltonian for the isolated photonic system has the usual Bose-Hubbard form :

$$H_{\text{ph}} = \sum_{i=1}^{L} \left[\omega_0 a_i^\dagger a_i + \frac{U}{2} a_i^\dagger a_i^\dagger a_i a_i \right] - \sum_{\langle i,j \rangle} \left[\hbar J a_i^\dagger a_j + hc \right] : \tag{4.59}$$

We assumed that the Kerr nonlinearity of thr cavity medium induces an on-site interaction term U. The free evolution of the atoms is described by the following Hamiltonian

$$H_{\text{at}} = \sum_{i=1}^{L} \sum_{n=1}^{N_{\text{at}}} \omega_{\text{at}}^{(n)} \sigma_i^{(n)+} \sigma_i^{(n)-}. \tag{4.60}$$

---

[2]Those are not actual singularities for a finite dissipation, while the resonance gets sharper and sharper in the weak dissipation limit

The baths, modelled as a reservoir of harmonic oscillators, are represented by the following Hamiltonian:

$$H_{\text{bath}} = \sum_{i=1}^{L} \sum_{m} \left[\omega_m b_i^{(m)\dagger} b_i^{(m)} - \sum_{n=1}^{N_{\text{at}}} \tilde{\omega}_m c_i^{(n,m)\dagger} c_i^{(n,m)} \right]. \tag{4.61}$$

The indices i, n, m account respectively for the cavity modes, the atoms, and the bath excitations. The full interaction hamiltonian, between photons, atoms and bath excitations is given by :

$$H_{\text{I}} = \Omega_{\text{R}} \sum_{i,n} \left[a_i^{\dagger} \sigma_i^{-(n)} + hc \right] + \sum_{i,m} g_m \left[a_i^{\dagger} b_i^{(m)} + hc \right] + \sum_{i,n,m} \tilde{g}_m \left[\sigma_i^{+(n)} c_i^{\dagger(n,m)} + hc \right]. \tag{4.62}$$

Unlike Chapter 2 and Chapter 3, the baths $b_i^{(m)}$ and $c_i^{(n,m)}$ accounting respectively for photonic losses and atomic pumping have been explicitly included in the microscopical description. We note that each atom is coupled to a different pumping bath, i.e, a different set of harmonic oscillators. This is due to the fact that atoms being spatially separated enough, are pumped incoherently with respect to each other. We assume both baths to be in the vacuum state at initial time

$$\left\langle b_i^{(m)\dagger} b_i^{(m)} \right\rangle (0) = \left\langle c_i^{(n,m)\dagger} c_i^{(n,m)} \right\rangle (0) = 0, \tag{4.63}$$

and to have a broad spectral function

$$\sum_{m} |g_m|^2 e^{-i\omega_m \tau} = \int_{\omega} \mathcal{S}_{\text{l}}(\omega) e^{-i\omega\tau} \tag{4.64}$$

$$\sum_{m} |\tilde{g}_m|^2 e^{-i\tilde{\omega}_m \tau} = \Gamma_{\text{p}} \delta(\tau), \tag{4.65}$$

where $\mathcal{S}_{\text{l}}(\omega)$ is the loss power spectra of a single cavity, and the atomic pumping processes are described as Markovian.

Remarkably, unlike the photonic field $a_i^{(m)}$ which is coupled to the bath by mean of a creation operator $b_i^{(m)\dagger}$, the atomic raising operator $\sigma_i^{+(n)}$ is coupled in an anti-rotating way to a creation operator $c_i^{\dagger(n,m)}$: since both bath are in the vacuum state, this means that $b_i^{(m)}$ can only induce photon losses, meaning the bath $c_i^{(n,m)}$ can only induce atomic excitation (this process is compatible with energy conservation as the harmonic oscillator $c_i^{(n,m)}$ possesses a negative frequency $\tilde{\omega}_m$). While such a reservoir might look a bit artificial at first glance, physically such an irreversible atomic pumping in the excited state can be obtained by mean of a third atomic level, not included in this level of description for simplicity purpose.

We make the further assumption that the effective atomic pumping rate Γ_{p} is big enough with respect to the Rabi Coupling Ω_{R}, in such a way that during dynamics atoms spend most of their time in the excited state and very little in the ground-state (To do so and maintain at the same time the photonic total emission rate fixed at the desired intensity, one can embed a large enough number of atoms within the whole system, while diminishing correspondingly their individual Rabi coupling Ω_{R} to the cavity mode). In consequence, a single atom will have a very weak probability to be in the ground-state, the effect of atomic saturation of the pump will be very reduced and atoms will behave as linear degrees of freedom. We can thus replace the spin matrix of each atomic two-level system by an 'inverse' harmonic oscillator whose vacuum state (resp. first occupied state) corresponds to the atomic excited state (resp. ground-state) : $a_{\text{at},i}^{(n)} \equiv \sigma_i^{(n)+}$. States of the harmonic oscillator with more than one excitation will be so rarely occupied that they will not contribute to the photonic dynamics.

We obtain thus the modified atomic and interaction Hamiltonians :

$$H_{\text{at}} = \sum_{i=1}^{N_{cav}} \sum_{k=1}^{N_{\text{at}}} (-\omega_{\text{at}}^{(n)}) a_{\text{at},i}^{(n),\dagger} a_{\text{at},i}^{(n)} + E_0 \tag{4.66}$$

where E_0 is a constant, and

$$H_{\text{I}} = \Omega_{\text{R}} \sum_{i,n} \left[a_i^{\dagger} a_{\text{at},i}^{(n),\dagger} + hc \right] + \sum_{i,m} g_m \left[a_i b_i^{(m)\dagger} + hc \right] + \sum_{i,n,m} \tilde{g}_m \left[c_i^{(n,m)\dagger} a_{\text{at},i}^{(n)} + hc \right] \tag{4.67}$$

In our description the harmonic oscillator $a_{\text{at},i}^{(n)}$ and the excitations bath $c_i^{(m)}$ both have a negative energy (respectively $-\omega_{\text{at}}^{(n)}$ and $-\tilde{\omega}_m$). After linearization of the atomic dynamics it is possible to derive an exact non-Markovian Langevin equation for the photonic quantum field, by reexpressing the Hamiltonian dynamics into the form of Heisenberg equations of motion for the various operators :

$$\partial_t a_i(t) = -i\left[a_i(t), H_{\text{ph}}(t)\right] - i\sum_m g_m^* \hat{b}_i^{(m)}(t) - i\Omega_{\text{R}}\sum_k a_{\text{at},i}^{(n)\dagger}(t) \tag{4.68}$$

$$\partial_t a_{\text{at},i}^{(n)\dagger}(t) = -i\omega_{\text{at}} a_{\text{at},i}^{(n)\dagger}(t) + i\sum_m c_i^{(n,m)\dagger}(t) + i\Omega_{\text{R}} a_i(t) \tag{4.69}$$

$$\partial_t b_i^{(m)}(t) = -i\omega_m b_i^{(m)}(t) - ig_m a_i(t) \tag{4.70}$$

$$\partial_t c_i^{(n,m)\dagger}(t) = -i\tilde{\omega}_m c_i^{(m)\dagger}(t) - i\tilde{g}_m a_{\text{at},i}^{(n)\dagger}(t) \tag{4.71}$$

Injecting the integrated equation (4.71) for the bath oscillators into the equation (4.69) for the atomic degrees of freedom, we obtain a Markovian quantum langevin equation for the atomic field coupled to the photonic field :

$$\partial_t a_{\text{at},i}^{(n)\dagger}(t) = \left(-i\omega_{\text{at}}^{(n)} - \frac{\Gamma_{\text{p}}}{2}\right) a_{\text{at},i}^{(n)\dagger}(t) + i\Omega_{\text{R}} a_i(t) + \hat{\xi}_{\text{at},i}^{(n)}(t) \tag{4.72}$$

with a Markovian quantum noise contribution related to atomic pumping :

$$\left\langle \hat{\xi}_{\text{at},i}^{(n)}(t+\tau)\hat{\xi}_{\text{at},i}^{(n')\dagger}(t)\right\rangle = \delta_{i,j}\delta_{n,n'}\Gamma_{\text{p}}\delta(\tau), \qquad \left\langle \hat{\xi}_{\text{at},i}^{(n)\dagger}(t+\tau)\hat{\xi}_{\text{at},i}^{(n')}(t)\right\rangle = 0. \tag{4.73}$$

Then, integrating Eqs. (4.72),(4.70) and injecting them in Eq. (4.68) we get for the photonic dynamics :

$$\partial_t a_i(t) = -i\left[a_i(t), H_{\text{ph}}(t)\right] - \int_{t'}\Gamma_{\text{l}}(t')a_i(t-t') + \hat{\xi}_{\text{l},i}(t) + \int_0^t ds\left(\sum_n \Omega_{\text{R}}^2 e^{(-i\omega_{\text{at}}^{(n)} - \frac{\Gamma_{\text{p}}}{2})(t-s)}a_i(s)\right)$$

$$- i\Omega_{\text{R}} e^{(-i\tilde{\omega}_m - \frac{\Gamma_{\text{p}}}{2})t}\sum_n a_{\text{at},i}^{(n),\dagger}(0) - i\Omega_{\text{R}}\int_0^t ds\sum_n e^{(-i\omega_{\text{at}}^{(n)} - \frac{\Gamma_{\text{p}}}{2})(t-s)}\hat{\xi}_{\text{at},i}^{(n)}(s), \tag{4.74}$$

where the expressions for the loss memory kernel and noise autocorrelations are described below.

4.4.1 Langevin equation: general form

At long time with respect to $1/\Gamma_{\text{p}}$, the time-dependent contribution $\propto e^{(-i\tilde{\omega}_m - \frac{\Gamma_{\text{p}}}{2})t}$ in Eq. (4.74) (which represents a memory of the initial conditions) vanishes, and we can also replace the boundaries in the various integrals by 0 and $+\infty$. We obtain then the final form for the photonic non-Markovian Langevin equation of Eq. (4.1)

$$\partial_t \hat{a}_i(t) = -i\left[\hat{a}_i(t), H_{\text{ph}}(t)\right] + \int_{-\infty}^{\infty}d\tau[\Gamma_{\text{em}}(\tau) - \Gamma_{\text{l}}(\tau)]\hat{a}_i(t-\tau) + \hat{\xi}_{\text{em},i}(t) + \hat{\xi}_{\text{l},i}(t) \tag{4.75}$$

where $\hat{\xi}_{\text{em},i}(t) = -i\Omega_{\text{R}}\int_{-\infty}^t ds\sum_n e^{(-i\omega_{\text{at}}^{(n)} - \frac{\Gamma_{\text{p}}}{2})(t-s)}\hat{\xi}_{\text{at},i}^{(n)}(s)$. The non-zero contributions for the two-points quantum noise autocorrelations can be summarized into :

$$\begin{aligned}\left\langle \hat{\xi}_{\text{l},i}(t+\tau)\hat{\xi}_{\text{l},j}^{\dagger}(t)\right\rangle &= \delta_{i,j}\int_\omega \mathcal{S}_{\text{l}}(\omega)e^{-i\omega\tau} \\ \left\langle \hat{\xi}_{\text{em},i}^{\dagger}(t+\tau)\hat{\xi}_{\text{em},j}(t)\right\rangle &= \delta_{i,j}\int_\omega \mathcal{S}_{\text{em}}(\omega)e^{+i\omega\tau}\end{aligned} \tag{4.76}$$

where $\Gamma_{\text{l}}(\tau) = \theta(\tau)\int_\omega \mathcal{S}_{\text{l}}(\omega)e^{-i\omega\tau}$ and $\Gamma_{\text{em}}(\tau) = \theta(\tau)\int_\omega \mathcal{S}_{\text{em}}(\omega)e^{-i\omega\tau}$. While the loss power spectrum $\mathcal{S}_{\text{l}}(\omega)$ is provided in Eq. (4.64), the emission power spectrum has the expression

$$\mathcal{S}_{\text{em}}(\omega) = \Gamma_{\text{em}}^{\text{at}}\int d\omega' \mathcal{D}(\omega')\frac{(\Gamma_{\text{p}}/2)^2}{(\omega - \omega')^2 + (\Gamma_{\text{p}}/2)^2}, \tag{4.77}$$

with $\Gamma_{\text{em}}^{\text{at}} = \frac{4\Omega_{\text{R}}^2}{\Delta_{\text{diss}}}$: as in Chapter 2 and Chapter 3, each atom is responsible a Lorentzian contribution to emission, the continuous sum of the various contributions then provides the full spectrum $\mathcal{S}_{\text{em}}(\omega)$.

4.4.1.1 First example: Markovian losses and Lorentzian emission spectrum

As a first example, we set ourselves in the configuration in which losses are Markovian processes, i.e., $\mathcal{S}_{\mathrm{em}}(\omega) = \Gamma_{\mathrm{l}}$, and all atomic transitions are equal to ω_{em}, in such a way that $\mathcal{D}(\omega) = N_{\mathrm{at}}\delta(\omega - \omega_{\mathrm{em}})$. In that case we obtain for the emission spectrum the Lorenzian form:

$$\mathcal{S}_{\mathrm{em}}(\omega) = N_{\mathrm{at}}\Gamma_{\mathrm{em}}^{\mathrm{at}} \frac{(\Delta_{\mathrm{diss}}/2)^2}{(\omega - \omega_{\mathrm{em}})^2 + (\Delta_{\mathrm{diss}}/2)^2}, \tag{4.78}$$

where we have set the value $\Gamma_{\mathrm{p}} = \Delta_{\mathrm{diss}}$ for the atomic pumping rate. This configuration leads to the specific model Eq. (4.8) introduced in Sec. 4.2, that we have chosen in order to perform numerical simulations along this Chapter.

4.4.1.2 Second example: artificial Kennard-Stepanov relation

Another option would be to engineer non-trivial distributions $\mathcal{D}(\omega)$ (which we could imagine to do in a fictious way by tuning all atoms to different frequencies, or by using several atomic species) of the atomic transition frequencies in such a way to simulate a Kennard-Stepanov relation. More specifically, we choose losses to be also Markovian $\mathcal{S}_{\mathrm{l}}(\omega) = \Gamma_{\mathrm{l}}$, and the particular form for the distribution of atomic transition frequencies:

$$\mathcal{D}(\omega) = \mathcal{D}_0 e^{\beta_{\mathrm{eff}}\omega}. \tag{4.79}$$

In that case the emission power spectrum becomes

$$\mathcal{S}_{\mathrm{em}}(\omega) = \mathcal{D}_0 \Gamma_{\mathrm{em}}^{\mathrm{at}} \int d\omega' e^{\beta_{\mathrm{eff}}\omega'} \frac{(\Gamma_{\mathrm{p}}/2)^2}{(\omega - \omega')^2 + (\Gamma_{\mathrm{p}}/2)^2}. \tag{4.80}$$

In the limit of a very weak pumping rate $\Gamma_{\mathrm{p}} \ll T_{\mathrm{eff}} = 1/\beta_{\mathrm{eff}}$, we recover the exponential-shaped emission spectrum:

$$\mathcal{S}_{\mathrm{em}}(\omega) = \Gamma_{\mathrm{em}} e^{\beta_{\mathrm{eff}}\omega}, \tag{4.81}$$

where $\Gamma_{\mathrm{em}} = \frac{\pi}{2}\mathcal{D}_0\Delta_{\mathrm{diss}}\Gamma_{\mathrm{em}}^{\mathrm{at}}$. The Kennard-Stepanov relation Eq. (4.7) is thus reproduced artificially even though the photonic environment is highly out-of-equilibrium. Of course a realistic realization of such emission spectrum would need to set an upper and lower cut-off to the emission frequency range to avoid any exponential divergencies. These cutoffs can be chosen to be very far away from the energy range where the interesting photonic many-body physics occurs. Theoretically, this emission spectrum (initially proposed in [171]) can be reproduced for an arbitrary low temperature: if necessary one can lower simultaneously the pumping rate $\Gamma_{\mathrm{p}} = \Delta_{\mathrm{diss}}$ and Ω_{R}, while increasing the number of atoms in order to stay within the previously described conditions of validity of the quantum Langevin equation (4.75). Concretely, for very low T_{eff} the engineering procedure might be become more complex as it requires an high number of emitters with a fine control on transition frequencies.

4.4.1.3 Pseudo-thermalization in exciton-polaritons low-T experiments

The artificial Kennard-Stepanov configuration mentioned in Sec. 4.4.1.2 might also be naturally reproduced in low-T exciton-polaritons experiments [99, 9]: while most theoretical works in the early literature [153, 129] have stressed on the impact of exciton-exciton scattering processes in the relaxation of polaritons into the bottleneck region of lower branch, more recent experimental observations [132] highlighted the important role played high energy longitudinal optical phonons. It appears that in some regimes those processes even constitute the dominant relaxation channel for polaritons.

Since the excitons (located in an higher energy with respect to the bottom of the polaritonic band) usually undergo fast collisions/energy exchanges processes and also possess a much longer lifetime than polaritons, the exciton reservoir is rather well thermalized (while polaritons might not thermalize) and can thus be described by a classical Boltzmann distribution $n_X(\epsilon_k) \propto e^{-\beta\epsilon_k}$ (excitons being very massive particles, their degree of degeneracy is usually very weak in those experiments).

One hand, since the LO phonons dispersion law is typically very flat and strongly located around the frequency ω_{LO} (in stark contrast with acoustic phonons who present a

light-cone), the LO phonon-assisted scattering processes excitons→polaritons maintain the full information on the excitonic energy distribution and 'copy and paste' it into the polariton injection rate (up to an energy shift $\hbar\omega_{\mathrm{LO}}$): in the hypothesis that LO phonon-assisted scattering processes are dominant, the polaritonic frequency-dependent injection rate should thus present an exponential frequency dependence ($\mathcal{S}_{\mathrm{em}}(\omega) \propto e^{-\beta_{\mathrm{eff}}\omega}$) at very a good degree of approximation. On the other hand, in that same picture, polariton→exciton recombination processes are strongly inhibited as they would involve the absorption of a phonon from the LO phononic reservoir, which can be approximated as being close to the vacuum state (LO phonons possessing a significantly higher energy ($\simeq 5meV$) than the typical temperatures ($\simeq 0.5meV$) in exciton-polaritons): as a consequence, polaritonic losses are by far dominated by mirror transparency effects, which are usually well represented by Markovian processes ($\mathcal{S}_{\mathrm{l}}(\omega) = \Gamma_{\mathrm{l}} + \mathcal{S}_{\mathrm{abs}}(\omega) \simeq \Gamma_{\mathrm{l}}$). One concludes that the Kennard-Stepanov relation $\mathcal{S}_{\mathrm{em}}(\omega)/\mathcal{S}_{\mathrm{l}}(\omega) \propto e^{-\beta_{\mathrm{eff}}\omega}$ might be artificially verified in that context, and polaritons be subject to pseudo-thermalization.

The measurement of thermal signatures in those experiments has to thus be interpreted carefully. In that prospect, it might be interesting to verify that polaritons are indeed equilibrated with excitons (i.e., their environment) in order to provide conclusions regarding a true thermalization or a pseudo-thermalization: one way to proceed would be to check the validity of the FDT associated to a pair of operators $\hat{A}(t)$ and $\hat{B}(t)$ (with the notations of Sec. 4.3.2) associated respectively to polariton and exciton degrees of freedoms, by measuring the corresponding frequency-dependent effective temperature.

4.5 How to break pseudo-thermalization

Expectedly, the low-energy pseudo-thermalization effect described in Sec. 4.3 is not a fully general properties of driven-dissipative quantum systems, since a wide class of models can not been cast into the form of the quantum Langevin Eq. (4.1) which only implements non-Markovian effects. In this section, we discuss a simple extension of Eq. (4.1) which allows to break the emergent equilibrium presented in Sec. 4.3. More specifically, we introduce a generalized Bogoliubov-de Gennes model at low energies and low momenta, with a complex kinetic energy and a complex chemical potential:

$$-i\omega\hat{\Lambda}_{\mathbf{k}}(\omega) = -i\left[z\epsilon_{\mathbf{k}}\hat{\Lambda}_{\mathbf{k}}(\omega) + \tilde{z}\mu\left(\hat{\Lambda}_{\mathbf{k}}(\omega) + \hat{\Lambda}^{\dagger}_{-\mathbf{k}}(-\omega)\right)\right] + \hat{\xi}_{neq,\mathbf{k}}(\omega). \qquad (4.82)$$

The noise auto correlation is

$$\langle\hat{\xi}_{neq,\mathbf{k}}(\omega)\hat{\xi}^{\dagger}_{neq,\mathbf{k}'}(\omega')\rangle = \langle\hat{\xi}^{\dagger}_{neq,\mathbf{k}}(\omega)\hat{\xi}_{neq,\mathbf{k}}(\omega')\rangle \qquad (4.83)$$

$$= \delta_{\mathbf{k}-\mathbf{k}'}\,\delta_{\omega-\omega'}\mathcal{S}_{\mathrm{l}}(\omega_{\mathrm{BEC}}),$$

and complex couplings are written in phase-modulus representation as $z = \rho e^{-i\theta}$, $\tilde{z} = \tilde{\rho}e^{-i\tilde{\theta}}$. This model is very similar to the low-energy model Eq. (4.28) derived in a previous section, except that the kinetic energy ϵ_k and the chemical potential μ have respectively been multiplied by two different complex numbers z and $\tilde{z}$ (while they were multiplied by the same complex in the low-energy theory Eq. (4.28). In Sec. 4.5.1 and Sec. 4.5.2 we will show that in case of alignement in the complex plane of these couplings (i.e., $\theta = \tilde{\theta}$), we obtain an effective equilibrium theory, while in the case of a misalignement, the steady state presents non-equilibrium features. Finally in Sec. 4.5.3, we will describe many ways to implement those modified complex couplings.

4.5.1 Static correlations

Analysing Eqs. (4.82),(4.83) we obtain the following expression for momentum distribution $n_k^{neq} = \langle\hat{\Lambda}^{\dagger}_{\mathbf{k}}\hat{\Lambda}_{\mathbf{k}}\rangle$ and the anomaleous average $\mathcal{A}_k^{neq} = \langle\hat{\Lambda}_{\mathbf{k}}\hat{\Lambda}_{-\mathbf{k}}\rangle$ (the derivation is very similar to the one made in App. E):

$$n_k^{neq} = \frac{|z\epsilon_k + \tilde{z}\mu|^2\mathcal{S}_{\mathrm{l}}(\omega_{\mathrm{BEC}})/2}{\left(\rho\sin(\theta)\epsilon_k + \tilde{\rho}\sin(\tilde{\theta})\mu\right)\rho\epsilon_k\left(\rho\epsilon_k + 2\cos(\theta-\tilde{\theta})\tilde{\rho}\mu\right)}, \qquad (4.84)$$

$$\mathcal{A}_k^{neq} = \frac{-(z^*\epsilon_k + \tilde{z}^*\mu)\tilde{z}\mu\mathcal{S}_{\mathrm{l}}(\omega_{\mathrm{BEC}})/2}{\left(\rho\sin(\theta)\epsilon_k + \tilde{\rho}\sin(\tilde{\theta})\mu\right)\rho\epsilon_k\left(\rho\epsilon_k + 2\cos(\theta-\tilde{\theta})\tilde{\rho}\mu\right)}. \qquad (4.85)$$

In the general case, it is not possible to further simplify those expression, and the steady state properties differs from the equilibrium statistics. However, considering the particular case in which the complex couplings z and $\tilde{z}$ are aligned in the complex plane, i.e., $\theta = \tilde{\theta}$, one obtains

$$n_k^{aligned} \quad = \quad \frac{\tilde{T}_{\text{eff}}(\rho\epsilon_k + \tilde{\rho}\mu)}{\rho\epsilon_k(\rho\epsilon_k + 2\tilde{\rho}\mu)}, \tag{4.86}$$

$$\mathcal{A}_k^{aligned} \quad = \quad \frac{-\tilde{T}_{\text{eff}}\tilde{\rho}\mu}{\rho\epsilon_k(\rho\epsilon_k + 2\tilde{\rho}\mu)}, \tag{4.87}$$

which compared to Eqs. (4.34), (4.35), corresponds to a low-energy effective equilibrium statistics with $\tilde{T}_{\text{eff}} = \frac{\mathcal{S}_l(\omega_{\text{BEC}})}{2\sin(\theta)}$ and renormalized couplings $\epsilon_k \to \rho\epsilon_k$, $\mu \to \tilde{\rho}\mu$. This is not surprising since in that case, the generalized Bogoliubov-de Gennes model given by Eq. (4.82) coincides with the low frequency limit Eq. (4.28) of the non-Markovian Langevin equation studied in this paper. We conclude that the alignement configuration of the couplings z and $\tilde{z}$ of Eq. (4.28) corresponds to an effective equilibrium situation, while the general case of non-alignement drives the system out-of-equilibrium, as thoroughly discussed in [176, 177, 2].

Although Eqs. (4.84), (4.85) present deviations from the Rayleigh-Jeans thermal laws $n_k \underset{E_k \to 0}{=} \frac{T_{\text{eff}}(\epsilon_k + \mu)}{E_k^2}$, for a generic choice misalignement of z and $\tilde{z}$ the low-momentum correlations still present a $\frac{1}{k^2}$ equilibrium-like divergence (and we do not expect any particular loss of coherence by driving the system out-of-equilibrium, at least in three dimensions), apart for one specific pathological configuration: if we put ourselves in the specific configuration in which we set the phase θ to 0 and the phase $\tilde{\theta}$ to $\pi/2$, which can be obtained by using Markovian baths, cancelling the photon-photon interactions and adding saturation to the pump (see Sec. 4.5.3.2), we indeed obtain a very different behaviour

$$n_k^{pathological} \quad = \quad \frac{\mathcal{S}_l(\omega_{\text{BEC}})(\epsilon_k^2 + (\tilde{\rho}\mu)^2)}{2\tilde{\rho}\mu\epsilon_k^2}, \tag{4.88}$$

$$\mathcal{A}_k^{pathological} \quad = \quad \frac{i\mathcal{S}_l(\omega_{\text{BEC}})(\epsilon_k + i\tilde{\rho}\mu)\tilde{\rho}\mu}{2\tilde{\rho}\mu\epsilon_k^2}. \tag{4.89}$$

We see that the momentum distribution changes behaviour at long range : $n(k) \simeq \frac{1}{k^4}$, such a features has been already recovered in [35]. Due to these increased low-momenta fluctuations, we might be tempted to conclude that in three dimensions, a non-equilibrium free Bose gas in presence of a pump and saturation, i.e., a 3D VCSEL [85] can not Bose-condense (while the equilibrium free Bose gas is known to condense). However, in this case the Bogoliubov approach is ill-defined and can not be applied in a straightforward manner. Instead, studying the long range properties of this system requires applying the RG theory to this non-equilibrium system keeping all non-linearities (and thus the ones providing from saturation): our understanding is that during the RG flow [176, 177], a small photon-photon interaction should be generated and the true correlations should be thus in $n(k) \simeq \frac{1}{k^2}$, saving thus the convergence. Such effect was verified numerically in [90] by simulating the KPZ equation (however in that case the simulations were done in a 1D configuration).

4.5.2   Momentum-dependent effective temperatures from FDT

It is also interesting to check whether a misalignment of the couplings affects the validity of the FDT. To do so, we will use an exact model providing a quantum Langevin equation valid at all frequencies which leads at low-frequencies and low-momenta to the effective description Eq. (4.82) with non-aligned couplings z and $\tilde{z}$: this model is defined in the next section in Eqs (4.90), (4.93), and we computed the corresponding effective temperatures $\beta_{1,\text{eff}}(\mathbf{k}, \omega)$ and $\beta_{2,\text{eff}}(\mathbf{k}, \omega)$ by mean of the definitions Eqs (4.55). In Fig. 4.6, we show $\beta_{1,\text{eff}}(\mathbf{k}, \omega)$ (resp. $\beta_{2,\text{eff}}(\mathbf{k}, \omega)$) in the left panel (resp. right panel) in function ω in units of Δ_{diss} for various momenta $\mathbf{k}$: we notice that in the region $\omega \ll \Delta_{\text{diss}}$, these effective temperatures do not take anymore identical values, so the low-frequency temperatures are momentum dependent. We conclude that pseudo-thermalization is broken not only at a static level (in the sense that it does not respect perfectly the Rayleigh-Jeans law obtained for a weakly interacting isolated Bose gas) in case of misalignement, but also at a dynamical level, as the FDT is not verified
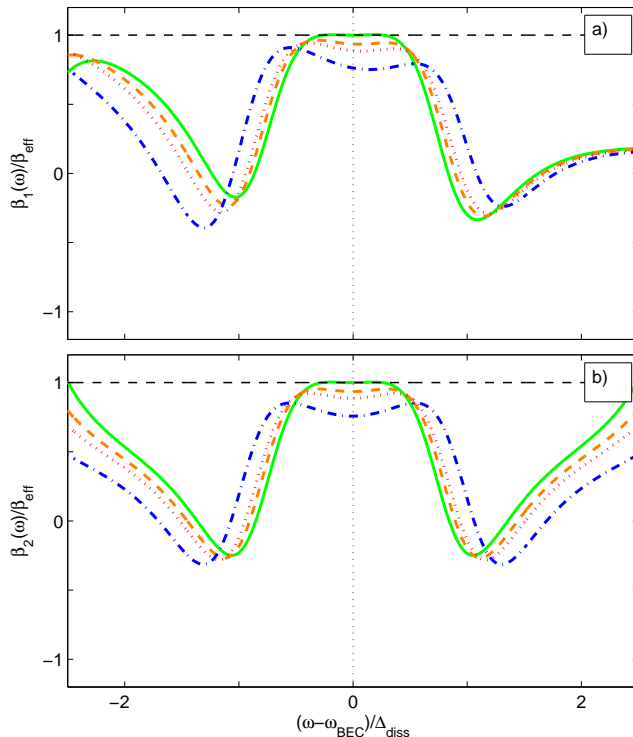
Figure 4.6: Test of the FDT/KMS relation in the presence of dispersion of the emitters. Panel a) (resp. b)): frequency-dependent effective temperature $\beta_{1,\text{eff}}(\mathbf{k},\omega)$ (resp. $\beta_{2,\text{eff}}(\mathbf{k},\omega)$) defined in Eq. (4.5) for a Lorentzian pump, massive emitters and Markovian losses (model defined in Sec.4.5.3.1), in function of the frequency $\omega - \omega_{\text{BEC}}$ in units of Δ_{diss}, and for various momenta $\mathbf{k}$. Parameters: $m = 1$, $M_{\text{at}} = 3$, $\Gamma_l/\Gamma_{\text{em}}^0 = 0.3$, $\Gamma_{\text{em}}/\Delta_{\text{diss}} = 0.01$, $\delta/\Delta_{\text{diss}} = -2$. For each panel, the various curves corresponds to increasing momenta $\mathbf{k}$ (chosen in such a way that the corresponding Bogoliubov spectrum spans all energy above and below the resulting effective temperature $T_{\text{eff}}^{\text{disp}} \equiv 1/\beta_{\text{eff}}^{\text{disp}} = 0.54\Delta_{\text{diss}}$): $k/k_{\text{th}} = 0.18$ for the green solid line, $k/k_{\text{th}} = 3.65$, for the orange dashed line, $k/k_{\text{th}} = 9.1$ for the red dotted line, $k/k_{\text{th}} = 54.7$ for the blue dash-dotted line: $k/k_{\text{th}} = 3 \times 10^{-2}$ for the green solid line, $k/k_{\text{th}} = 1.83$, for the orange dashed line, $k/k_{\text{th}} = 2.43$ for the red dotted line, $k/k_{\text{th}} = 3.66$ for the blue dash-dotted line. Here k_{th} is also defined by $E(\mathbf{k}_{\text{th}}) = T_{\text{eff}}^{\text{disp}}$

at low-frequencies. We remark that at low momenta, the zero-frequency effective inverse temperatures progressively converge toward the value β_{eff} predicted in Secs. 4.3.1.1, 4.3.2.

4.5.3 Examples of modified quantum optics models driving the system out-of-equilibrium

In this section, we discuss various physical ways to obtain the modified Bogogliubov-de Gennes system Eq. (4.82) with misalignement of the complex couplings, by mean of simple modifications with respect to the quantum optics model introduced in Sec. 4.4.

4.5.3.1 Emitters with dispersion

The first model we introduce is very similar to the one presented in Sec. 4.2, except that we add a momentum-dependence to the pump: in the photonic case presented in Sec. 4.4, this can be obtained taking into account the dispersion relation for the emitters which can be two-level massive atoms, and the recoil energy during emission of a photon. We obtain the following Langevin equation:

$$\frac{\partial}{\partial t}\hat{\psi}_{\mathbf{k}}(t) = -i\left[\hat{\psi}_{\mathbf{k}}(t), H_{\text{ph}}(t)\right] + \int_{-\infty}^{\infty} d\tau[\Gamma_{\text{em},\mathbf{k}}(\tau) - \Gamma_{\text{l}}(\tau)]\hat{\psi}_{\mathbf{k}}(t-\tau) + \hat{\xi}_{disp,\mathbf{k}}(t), \quad (4.90)$$

with the non-Markovian momentum-dependent dissipative kernel for pumping

$$\Gamma_{\text{em},\mathbf{k}}(\tau) = \Theta(\tau) \int_{\omega} S_{\text{em},\mathbf{k}}(\omega) e^{-i\omega\tau}, \tag{4.91}$$

and noise correlations in momentum-frequency space

$$\langle \hat{\xi}_{disp,\mathbf{k}}(\omega) \hat{\xi}^{\dagger}_{disp,\mathbf{k}'}(\omega') \rangle = \delta_{\mathbf{k}-\mathbf{k}'} \, \delta_{\omega-\omega'} \mathcal{S}_{\text{l}}(\omega_{\text{BEC}} + \omega), \tag{4.92a}$$

$$\langle \hat{\xi}^{\dagger}_{disp,\mathbf{k}}(\omega) \hat{\xi}_{disp,\mathbf{k}'}(\omega') \rangle = \delta_{\mathbf{k}-\mathbf{k}'} \, \delta_{\omega-\omega'} S_{\text{em},\mathbf{k}}(\omega_{\text{BEC}} + \omega). \tag{4.92b}$$

The pump power spectrum depends now not only on the frequency but also on the momentum. To test the FDT, we use the full non-Markovian theory Eq. (4.90), and apply the Bogoliubov procedure to calculate analytically the correlation functions. We choose the specific form for the momentum-frequency dependent pump power spectrum:

$$S_{\text{em},\mathbf{k}}(\omega) = \Gamma_{\text{em}} \frac{(\Delta_{\text{diss}}/2)^2}{(\omega + \epsilon_{\mathbf{k}}^{\text{em}} - \omega_{\text{em}})^2 + (\Delta_{\text{diss}}/2)^2}. \tag{4.93}$$

This model takes into account the transition frequency of the emitters, shifted by the recoil energy $\epsilon_{\mathbf{k}}^{\text{em}} = \frac{k^2}{2M_{\text{em}}}$ of the emitters. If the mass M_{em} of the emitter is small enough, this effect can be physically relevant at high momenta.

From Eq. (eq:dispersion-quantum-langevin-momentum), applying a Bogoliubov procedure similarly to Sec. 4.2.4, we can derive a low-energy and low-momentum effective theory, as we did in Sec.4.2.6:

$$-i\omega\hat{\Lambda}_{\mathbf{k}}(\omega) = -i\left[z_{disp}\epsilon_{\mathbf{k}}\hat{\Lambda}_{\mathbf{k}}(\omega) + \tilde{z}_{disp}\mu\left(\hat{\Lambda}_{\mathbf{k}}(\omega) + \hat{\Lambda}^{\dagger}_{-\mathbf{k}}(-\omega)\right)\right] + \bar{\xi}_{disp,\mathbf{k}}(\omega). \tag{4.94}$$

The noise correlations are

$$\langle \bar{\xi}_{disp,\mathbf{k}}(\omega) \bar{\xi}^{\dagger}_{disp,\mathbf{k}'}(\omega') \rangle = \delta_{\mathbf{k}-\mathbf{k}'} \, \delta_{\omega-\omega'} \mathcal{S}_{\text{l}}(\omega_{\text{BEC}}), \tag{4.95a}$$

$$\langle \bar{\xi}^{\dagger}_{disp,\mathbf{k}}(\omega) \bar{\xi}_{disp,\mathbf{k}'}(\omega') \rangle = \delta_{\mathbf{k}-\mathbf{k}'} \, \delta_{\omega-\omega'} S_{\text{em},0}(\omega_{\text{BEC}}), \tag{4.95b}$$

where $S_{\text{em},0}(\omega_{\text{BEC}}) = \mathcal{S}_{\text{l}}(\omega_{\text{BEC}})$ and the complex couplings are

$$z_{disp} = (1 + \tilde{\delta} - i\tilde{\Gamma})(1 + 2im \underbrace{\partial_k^2 \Gamma_{\text{em} \, |k=0,\omega=\omega_{\text{BEC}}}}_{<0}), \tag{4.96}$$

$$\tilde{z}_{disp} = (1 + \tilde{\delta} - i\tilde{\Gamma}). \tag{4.97}$$

We obtain some effective complex kinetic energy and chemical potential for the photonic dynamic. However, due to the dispersion of the emitters, an additional multiplicative contribution has been added to the complex kinetic energy inducing thus a misalignement between z_{disp} and $\tilde{z}_{disp}$. In order to test the validity of the fluctuation dissipation theorem we define $\beta_{\text{eff}}^{\text{dis}} \equiv = \frac{\mathrm{d}}{\mathrm{d}\omega} \log\left[\frac{\mathcal{S}_{\text{l}}(\omega)}{S_{\text{em},k}(\omega)}\right]\bigg|_{\omega=\omega_{\text{BEC}},k=0}$.

4.5.3.2 Saturation of the pump/two-body losses

In the second model, we propose to add saturation of the pump or two-body losses. Basing ourselves, on the photonic case presented in Sec. 4.4, some saturation provides from the fact that the emitters are two-level atoms and thus are not perfectly linear systems. In this case, at a qualitative level the Langevin equation for the quantum fluctuations becomes at low frequency:

$$-i\omega\hat{\Lambda}_{\mathbf{k}}(\omega) = -i\left[z_{sat}\epsilon_{k}\hat{\Lambda}_{\mathbf{k}}(\omega) + \tilde{z}_{sat}\mu\left(\hat{\Lambda}_{\mathbf{k}}(\omega) + \hat{\Lambda}^{\dagger}_{-\mathbf{k}}(-\omega)\right)\right] + \bar{\xi}_{sat,\mathbf{k}}(\omega). \tag{4.98}$$

The noise correlations are

$$\langle \bar{\xi}_{sat,\mathbf{k}}(\omega) \bar{\xi}^{\dagger}_{sat,\mathbf{k}'}(\omega') \rangle = \delta_{\mathbf{k}-\mathbf{k}'} \, \delta_{\omega-\omega'} \mathcal{S}_{\text{l}}(\omega_{\text{BEC}}), \tag{4.99a}$$

$$\langle \bar{\xi}^{\dagger}_{sat,\mathbf{k}}(\omega) \bar{\xi}_{sat,\mathbf{k}'}(\omega') \rangle = \delta_{\mathbf{k}-\mathbf{k}'} \, \delta_{\omega-\omega'} S_{l}(\omega_{\text{BEC}}), \tag{4.99b}$$

and the complex couplings are

$$z_{sat} = (1 + \tilde{\delta} - i\tilde{\Gamma}), \tag{4.100}$$

$$\tilde{z}_{sat} = (1 + \tilde{\delta} - i\tilde{\Gamma})(1 - i\gamma_{sat}). \tag{4.101}$$

γ_{sat} is a dimensionless coupling quantifying the saturation effect, i.e, an increase of the dissipation strength with the density $\hat{\Lambda}_{\mathbf{k}}^{\dagger}\hat{\Lambda}_{\mathbf{k}}$, which linearized gives in the Bogoliubov approach a complex contribution proportional to $\hat{\Lambda}_{\mathbf{k}} + \hat{\Lambda}_{-\mathbf{k}}^{\dagger}$. Here again, because of saturation which multiplies the chemical potential by some complex, we also observe a misalignement between z_{sat} and $\tilde{z}_{sat}$. We comment also that in presence of saturation, the noise should present non trivial non-linear autocorrelations depending on the quantum field $\hat{\Lambda}_{\mathbf{k}}$, but for the sake of simplicity we assumed it to be Gaussian as a first level of approximation.

4.6 Conclusion and perspectives

We have explored the effect of pseudo-thermalization, which occurs when the impact of an equilibrated environment is mimicked by several non-thermal and non-Markovian reservoirs, in the specific case of a driven dissipative weakly interacting Bose-Einstein Condensate. Our approach based on a quantum Langevin formalism allowed us to access both static and dynamical properties of the steady-state, and to check for the first time the validity of the Fluctuation Dissipation Theorem in the context of pseudo-thermalization. The relevance of this work for low-temperature exciton-polariton experiments has been highlighted. An alternative possible way of engineer such model in a quantum optics context has been presented, along with a derivation of the Quantum Langevin equation starting from this microscopic model.

We have studied mainly two cases: first, for arbitrary choices of reservoirs, the Kennard-Stepanov relation is verified locally around the lasing frequency but is not verified globally. We have shown in that case that static correlations present a low-energy thermal signature, and demonstrated the validity of the FDT at low-frequencies. Secondly, in the specific case where the Kennard-Stepanov relation is fully mimicked by the environment, we have demonstrated the validity of the FDT at all frequencies, and shown in the specific regime of weak dissipation that the steady-state is in a Gibbs ensemble. In the latter case, the steady state properties are completely undistinguishable from an equilibrium one both at the static and dynamic level. Finally, several approaches allowing to modify the initial model in such a way to break this pseudo-thermalization effect have been discussed, with a particular stress on the role played by the dispersion and the saturation of the emitters.

This work strongly contradicts the well-established belief according to which only open quantum systems in contact with an equilibrated environment can be fully thermalized at all length scales. While this pseudo-thermalization is expected to be very robust and universal in the case where the Kennard-Stepanov relation is fully verified, it is unclear whether low-energy pseudo-thermalization should apply to any physical system, in the case of arbitrary reservoirs where Kennard-Stepanov is only valid locally: future studies will be dedicated in particular to the interplay between pseudo-thermalization and the departure of the Bogoliubov regime, when photon-photon interactions and important noise strongly deplete the condensate, and will assess in a more quantitative way the role played by pseudo-thermalization in exciton-polariton experiments.

Chapter 5

Conclusions and perspectives

A current hot challenge in photonic experiments regards the possibility of stabilizing incompressible quantum phases such as the Mott-Insulator or Fractional Quantum Hall states, which have been observed by now only in isolated systems. From a broader point of view, understanding the emergence of analogous equilibrium properties in driven-dissipative quantum systems often reveals a complex question. Not only overcoming those obstacles would allow to provide some benchmark and give thus an higher level of credibility to quantum optics platforms by putting them forward as possible candidates for quantum simulation tasks, being able to control the degree of non-equilibriumness of an arbitrary open quantum system in a tunable manner could also be the starting point for the exploration of a large panel of new many-body quantum phenomena lying at the frontier between equilibrium and non-equilibrium statistical mechanics. In this Thesis we have addressed some of those open problematics. In particular, our research work provides a direct route toward the generation of strongly correlated many-body phases with light, and might have a significant impact on the development of future experiments.

Recent technological advances in novel photonic platforms strongly indicate the possibility of quantum simulating the dynamics of cornerstone models of many-body physics, and hold the promises of observing strongly correlated quantum phases with light. Still, understanding how to circumvent the effect of losses and other unavoidable dissipative processes so to stabilize a quantum system close to the many-body ground-state of some engineered Hamiltonian still remains in general an unsolved issue, and is currently the object of a important research activity. While former work in the literature focused on the possibility of implementing a simple coherent drive scheme in order to refill the photonic population, it appeared a posteriori that such approach is badly suited for the study of zero temperature physics as it leads to important heating effects and density fluctuations. In Chapter 2 we put forward an alternative method based on the use of an incoherent non-Markovian pump which, in stark contrast with coherent drive schemes, allows for the irreversible (and frequency selective) injection of new photons inside the system. The material presented here was adapted from our initial work which, shortly after a first proposal by other authors regarding the generation of photonic Fractional Quantum Hall fluids, investigated for the first time the potential of such scheme for the quantum simulation of the Mott Insulator physics with light. Both studies focused on the most genuine case of a frequency-dependent emission with a narrow bandpass spectrum, which is obtained when all emitters possess identical transition frequencies. Strikingly, our study confirmed the possibility of stabilizing photonic Fock states in the single cavity configuration, and photonic Mott Insulating states in the lattice configuration under the hypothesis of a weak hopping amplitude, but revealed that the efficiency of this scheme does not extend to the regime in which the photonic bandwidth (induced by the tunneling part of the Hamiltonian) becomes of the order of the emission linewidth: indeed, in this strong hopping regime, a significant depletion of the Mott state associated to the generation of hole excitations was predicted and connected to the presence of a broad continuum of single particle/hole states. The corresponding Mean-Field phase

diagram was then the object of a second study, which highlighted a phase transition from a photonic Mott Insulator toward a Superfluid state, triggered by the non-equilibrium processes related to hole excitation generation that we have mentioned above. This result is of a special interest, as a MI-SF phase transition had never been predicted in the past in any realistic study implementing the effect of photonic losses.

Nevertheless, by elaborating a synthesis of these various studies, we concluded that the full functionality of the first scheme based on a narrow bandbass emission spectrum is somehow model dependent, in the sense that it strongly relies on the existence of flat photonic bands. In particular, the ability of stabilizing the many-body ground-state in some class of topologically protected systems appears to be somehow accidentally related to the existence of iso-energetic Landau levels/quasi-hole excitations, as well as vanishing matrix elements toward higher energy states away from the Laughlin sub-manifold. As a counterpart, in the Bose-Hubbard model the observation of competing quantum effects between localization and delocalization is compromised with such scheme, since its efficiency does not extend to the regime where the hopping is comparable to the interaction strength. In view of broader applications, this restrictive functionality led to us to conceive a more advanced and fully novel model based on tailored non-Markovian reservoirs with broad bandpass spectra (Chapter 3), designed in such a way to mimick the effect of a tunable artificial chemical potential combined with a zero temperature. As a first step, a non-Markovian model featuring a square-shaped spectrum was developed, and the possibility of reproducing the zero temperature equilibrium phenomenology of the Bose-Hubbard model in a wide range of parameters was predicted. In particular, our numerical study confirmed the existence of Mott regions with arbitrary integer densities featuring strong robustness against tunneling and losses processes. The system can then undergo a transition toward a superfluid-like state either by changing the artificial chemical potential or increasing the tunneling. Still, our analysis pointed out exotic behaviours leading to the generation of a weak but non-vanishing entropy in some regions of the phase diagram, and those deviations from the equilibrium physics were related to the existence of non-equilibrium channels allowing for the dynamical creation of doublon excitations. The implementation of additional frequency-dependent losses was finally considered in order to circumvent this effect, and it was then showed that the ground-state was successfully recovered for any choice of parameters. This last scheme, which should be accessible with current technology, is to our knowledge the simplest existing experimental proposal of a reliable and flexible quantum simulator of zero temperature physics in strongly correlated photonic platforms. Since it is only based on generic relaxation mechanisms in the energy landscape, we believe in the universality of our proposal, in the sense that we do not expect neither its efficiency to be limited to the Bose-Hubbard model nor that restrictive constraints on the nature of the aimed many-body system need being imposed.

In addition to the possibility of reproducing zero temperature analogous physics by mean of a specific choice of a tailored environment, we came across an even stranger result in our first work, namely that a quantum system in contact with several non-Markovian and non-equilibrated reservoirs can present a steady-state mapping onto a Gibbs ensemble, with both chemical potential and finite temperature being artificial parameters depending on the reservoir spectral properties. While long-range asymptotic thermal properties had already been predicted to emerge in high enough dimensions by various studies which applied renormalization group methods to non-equilibrium many-body systems, here the observed effective equilibrium stems from the fact that the driven-dissipative dynamics fully mimicks the impact of a single thermal bath, and thus seems to rely on a different physical mechanism. By focusing in a second study on an analytically solvable model we showed (Chapter 4) that this effect, that we called 'pseudo-thermalization', extends at a dynamical level as it is characterized by the validity of the Fluctuation-Dissipation Theorem. One hand, for an arbitrary choice of reservoir spectral dependence, this mechanism appears to be somehow restricted either to near-Markovian baths and high temperatures; in presence of more important non-Markovian effects we have extended this result to the low-energy properties of a restricted class of systems presenting quadratic hamiltonians (such as interacting photons in the Bogoliubov regime). On the other hand, for a fine tuned model where the loss and emission power spectra exactly verify the Kennard-Stepanov relation, pseudo-thermalization then extends to arbitrary energy scales and many-body quantum systems. The latter result

conveys an important conceptual message: a quantum system can present fully thermal properties (both a the static and dynamical level) in some configurations where its environment is not thermal at all (remarkably, the amplifying medium we considered in our work even possesses a negative temperature, as it can only release energy inside the system). In particular, this challenges our understanding of emergent thermal signatures in driven dissipative platforms: before concluding to the presence of a true equilibrium, one should always check the thermal character of correlators between operators involving not only the degrees of freedom of the system of interest, but also the several reservoirs (this should be done both at a static level and by testing the FDT). This might be particularly critical in exciton-polariton experiments, where the structure of the external environment is complex and the microscopical origin of Bose-Einstein distributions observed in some experimental situations is still subject to active debate.

There are many remaining problematics related to this relatively new research direction involving the engineering of non-Markovian reservoirs in the physical context of photonic many-body physics. First, while the scheme we have developed in this work indeed succeeds to stabilize the Hamiltonian ground-state and in particular Mott Insulator states at a static level, the choice of 'square-shaped' emission and loss spectra globally does not verify the Kennard-Stepanov relation. Thus, while up to relatively long time scales the dynamics is expected to be the one of a closed system due to the relatively weak dissipative strength, some very low-frequency deviations from the isolated case might arise as a consequence of losses and pump, and affect in particular the Goldstone mode structure as well as critical properties close to a possible transition point. This leaves some mystery regarding the nature of this exotic strongly interacting open quantum system, which appears to behave as an equilibrium one at a static level but as a non-equilibrium one at a dynamical level. Secondly, our work highlighted an additional surprising effect characterized by a sharp departure from equilibrium and a sudden generation of steady-state entropy in one of the developed schemes. While many arguments support the idea that this feature should survive in the thermodynamic limit, the critical properties of the corresponding transition and the impact on the many-body phase properties are unknown and can not be access directly from our numerical simulations involving finite systems.

Hence, it would be of high interest to develop general tools allowing to tackle the dynamics of strongly interacting non-Markovian open quantum systems. From a broader perspective, the existence of a well-established theoretical framework would be a valuable asset in order to move to the study of different physical systems (such as strongly correlated supersolids, Fractional Quantum Hall states of light or the lower dimensional Tonks Girdardeau gas) and to assist the development of a novel generation of many-body experiments with light. From the analytical point of view, a critical step toward a mean-field calculation of the phase diagram of a strongly interacting quantum system in presence of frequency-dependent dissipation regards the ability of computing multiple-time correlators: indeed, it is a well-known fact that the regression theorem, which allows to access arbitrary Green functions by mean of the Lindblad formalism for Markovian dynamics, does not extend to non-Markovian dynamics. Alternatively, instead of quantum master equation one could imagine to rely on the Keldysh formalism in order to treat dissipation. However such approach has proven to best suited for systems presenting rather weak deviations from the non-interacting regime, and its extension to the strong blockade does not appear to be straightforward. Numerically, the study of non-Markovian quantum dynamics also suffers from a lack of well-established methods. Due to the inherent difficulty of providing systematic analytical predictions, generalizing techniques based on matrix product operators, cluster mean-field analysis, or corner-space renormalization to this new physical context might be an essential step toward the study of thermodynamic limit properties.

Appendix A

Phase diagram of the Bose-Hubbard model in the Mean-field regime

In this Appendix, we present a derivation of the Phase diagram of the Bose-Hubbard in the Mean-field regime, shown in Fig. A.1 and discussed in Sec. 1.2.2. Our discussion, based on the lecture notes [51], will present the initial derivation done in [59] and further developed in [197, 141]. An alternatively decoupling approach leading to identical predictions was discussed in [197]: it is the numerical approach we used in Sec. 2.7 where we study the Gutzwiller mean-field phase diagram of the driven-dissipative photon lattices. At equilibrium, the partition function can be rewritten in terms of a functional integral (i.e., a many-body quantum path integral)

$$Z \equiv \mathrm{Tr}\left[e^{-\beta_{\mathrm{eff}}H^{\mathrm{BH}}}\right] = \int \mathcal{D}[\psi^*, \psi]e^{-\mathcal{S}^{\mathrm{BH}}[\psi^*, \psi]}, \tag{A.1}$$

where

$$H^{\mathrm{BH}} = \sum_i \left[-\mu a_i^\dagger a_i + \frac{U}{2} a_i^\dagger a_i^\dagger a_i a_i\right] - \sum_{i,j} J_{i,j}\left[a_i^\dagger a_j + hc\right] \tag{A.2}$$

is the Bose-Hubbard Hamiltonian, and

$$\mathcal{S}^{\mathrm{BH}}[\psi^*, \psi] = \sum_i \int_0^\beta d\tau \psi_i^* \partial_\tau \psi_i + H^{\mathrm{BH}}[\psi^*, \psi] \tag{A.3}$$

is the associated action. Here $J_{i,j} = [\hat{J}]_{i,j}$ is the hopping amplitude between the two sites i and j, and $\hat{J}$ is the hopping matrix. For the sake of simplicity we focus here on the one-dimensional BH model, as this demonstration will provide identical results in higher dimensions[1], only at the cost of a more complex system of notations. The action $\mathcal{S}^{\mathrm{BH}}[\psi^*, \psi] = \mathcal{S}_{\mathrm{loc}}^{\mathrm{BH}}[\psi^*, \psi] - \sum_{i,j} J_{i,j} [\psi_i^* \psi_j + c.c.]$ can be decomposed in a local part

$$\mathcal{S}_{\mathrm{loc}}^{\mathrm{BH}}[\psi^*, \psi] = \int_0^\beta d\tau \left[\sum_i \psi_i^* \partial_\tau - \mu \psi_i + \frac{U}{2} \psi^* \psi^* \psi \psi\right], \tag{A.4}$$

and a non-local part containing the hopping term. An Hubbard Stratonovich transformation allows to "decouple" the inter-site hopping term in the functional integral of Eq. (A.1)

$$Z = \int \mathcal{D}[\psi^*, \psi, \phi, \phi]e^{-\tilde{\mathcal{S}}^{\mathrm{BH}}[\psi^*, \psi, \phi, \phi]}, \tag{A.5}$$

where the new action

$$\tilde{\mathcal{S}}^{\mathrm{BH}}[\psi^*, \psi, \phi, \phi] = \mathcal{S}_{\mathrm{loc}}^{\mathrm{BH}}[\psi^*, \psi] + \int_0^\beta d\tau \left\{\sum_{i,j} J_{i,j}^{-1} [\phi_i^* \phi_j + c.c.] + \sum_i [\phi_i^* \psi_i + c.c.]\right\} \tag{A.6}$$

---

[1]We stress that we expect the MF theory to be accurate only in high dimensions, not in 1D

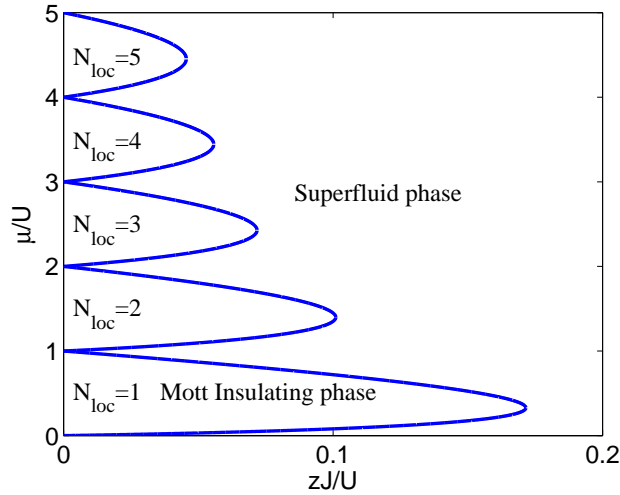## Appendix A. Phase diagram of the Bose-Hubbard model in the Mean-field regime

Figure A.1: Mean-Field phase diagram of the Bose-Hubbard model, in function of the parameters zJ/U and μ/U where z is the lattice number of nearest neighbors ($z = 2$ in 1D).

is local in the physical field ψ, but as a cost features an auxiliary coupled field ϕ with a non-local action. Here $J_{i,j}^{-1} = \left[\hat{J}^{-1}\right]_{i,j}$ is the matrix element of the inverse hopping matrix. Due, to the linear relation between the two-fields, a non-vanishing average $\langle\phi\rangle$ of the auxiliary field ϕ accounts for the presence of a non-vanishing superfluid order parameter $\langle\psi\rangle$.

Finally, the original field ψ can be integrated in the partition function, which can be expressed by mean of a functional integral featuring only the auxiliary field:

$$
\begin{aligned}
Z &= Z_{\text{loc}} \int \mathcal{D}[\phi, \phi] e^{-\int_0^\beta d\tau \sum_{i,j} J_{i,j}^{-1}[\phi_i^* \phi_j + c.c.]} \left\langle e^{\int_0^\beta d\tau \sum_i [\phi_i^* \psi_i + c.c.]} \right\rangle_{\text{loc}} \quad &\text{(A.7)} \\
&= Z_{\text{loc}} \int \mathcal{D}[\phi, \phi] e^{-\mathcal{S}_{\text{eff}}[\phi^*, \phi]}, \quad &\text{(A.8)}
\end{aligned}
$$

where $\langle A[\psi] \rangle_{\text{loc}} \equiv Z_{\text{loc}} \int \mathcal{D}[\psi^* \psi] A[\psi] e^{-\mathcal{S}_{\text{loc}}[\psi^*, \psi]}$ is the average value computed using the local part of the action, and

$$
\mathcal{S}_{\text{eff}} = \int_0^\beta d\tau \sum_{i,j} J_{i,j}^{-1} [\phi_i^* \phi_j + c.c.] - \ln\left[\left\langle e^{\int_0^\beta d\tau \sum_i [\phi_i^* \psi_i + c.c.]} \right\rangle_{\text{loc}}\right]. \quad \text{(A.9)}
$$

Until now, no approximation has been performed, as the functional integral representation of the partition function has just been reexpressed in function of the auxiliary field instead of the physical field. The Mean-Field approximation consists in considering that the order parameter $\propto \phi$ has weak fluctuations: for long range hopping, this can be understood by the fact that the strongly localized gas directly couples to the fully non-local Bose-Einstein Condensate, and no intermediary scales are involved. We can thus perform a saddle point approximation in the complex expectation value of Eq. (A.7) around the value $\langle\phi\rangle$. In the Mott-Phase, $\langle\phi\rangle = 0$ and we keep only the Gaussian contributions in the functional integral representation of ϕ. This leads to the effective quadratic action

$$
\mathcal{S}_{\text{eff}} = \int_0^\beta d\tau \sum_{i,j} J_{i,j}^{-1} [\phi_i^* \phi_j + c.c.] + \int_0^\beta d\tau \int_0^\beta d\tau' \sum_r \phi_i^*(\tau) G_{\text{loc}}(\tau - \tau') \phi_j(\tau'), \quad \text{(A.10)}
$$

where

$$
G_{\text{loc}}(\tau - \tau') = -\langle \psi_r^*(\tau) \psi(\tau') \rangle_{\text{loc}} \quad \text{(A.11)}
$$

is the local Green function computed in absence of hopping term, and whose Fourier trans-

form is

$$G_{\text{loc}}(i\omega) = \int d\omega e^{i\omega\tau} G_{\text{loc}}(\tau - \tau') \tag{A.12}$$

$$= -\frac{N_{\text{loc}} + 1}{i\omega - N_{\text{loc}}U + \mu} + \frac{N_{\text{loc}}}{i\omega + (N_{\text{loc}} - 1)U - \mu}. \tag{A.13}$$

Here, N_{loc} (defined by the inequalities $(N_{\text{loc}} - 1)U \leq \mu \leq N_{\text{loc}}U$) is the integer number particles per site present in the localized Mott phase in absence of hopping at $T = 0$ and chemical potential μ. We deduce thus the propagator for the auxiliary field in the frequency-momentum representation

$$G_{\text{aux}}(k, i\omega) = -\langle \psi^*(k, \omega)\psi(k, \omega)\rangle = \frac{1}{\epsilon_k^{-1} - G_{\text{loc}}(i\omega)}, \tag{A.14}$$

where $\epsilon_k = -\sum_j e^{-ikj} J_{0,j}$ is the kinetic energy of a particle of momentum k in the Bose-Hubbard model ($\epsilon_k = -2J\cos(k)$ for nearest neighbor hopping). The instability of the Mott phase is characterised by the presence of zero energy and zero momentum pole in $G_{\text{aux}}(k, i\omega)$: this leads to the following equation for the phase boundary

$$\epsilon_{k=0}^{-1} - G_{\text{loc}}(0) = 0. \tag{A.15}$$

Eq. (A.15) presents two distinct solutions

$$\mu^{\pm} = U(N_{\text{loc}} - \frac{1}{2}) + \frac{\epsilon_{k=0}}{2} \pm \sqrt{\epsilon_{k=0}^2 - 4\epsilon_{k=0}U\left(N_{\text{loc}} + \frac{1}{2}\right) + U^2} \tag{A.16}$$

forming altogether the N_{loc}-th Mott lobe of the Mean-Field phase diagram, which is shown in Fig. A.1. The tip of the Mott lobe is the point where the two-solution merge and is defined by $\sqrt{\epsilon_{k=0}^2 - 4\epsilon_{k=0}U\left(N_{\text{loc}} + \frac{1}{2}\right) + U^2} = 0$. For nearest neighbor hopping $\epsilon_{k=0} = -2J$ and the tip of the lobe is located at:

$$\begin{cases} \frac{J_c}{U} & = \ N_{\text{loc}} + \frac{1}{2} - \sqrt{N_{\text{loc}}^2 + N_{\text{loc}}} \underset{N_{\text{loc}} \to \infty}{\simeq} \frac{1}{8N_{\text{loc}}} \\ \frac{\mu_c}{U} & = \ U(N_{\text{loc}} - \frac{1}{2}) - J_c \end{cases} \tag{A.17}$$

Appendix B

Derivation of the purely photonic master equation via projective methods

In this Appendix, we give more details on the derivation of the non-Markovian photonic master equation (2.24) involved in Chapters 2 and 3. Starting from the full emitter-cavity master equation (2.5), we show how for a sufficiently small coupling Ω_R the emitter degrees of freedom can be eliminated. The frequency-dependence of the photonic emission is then accounted for as a modified Lindblad term (2.26). Our treatment is based on the discussion in the textbook [21]. We first remind from section 2.2.2 the choice for the projectors

$$\mathcal{P}\rho = \left| e_1^{(1)} e_2^{(1)} e_3^{(1)} ... \right\rangle \left\langle e_1^{(1)} e_2^{(1)} e_3^{(1)} ... \right| \otimes Tr_{\mathrm{at}}(\rho), \tag{B.1}$$

$$\mathcal{Q} = \mathbb{1} - \mathcal{P} \tag{B.2}$$

involved in the application of the projective methods: the projection operation consists in performing a partial trace over the emitters, and then make the tensor product of the density matrix and the emitters density matrix with all emitters in the excited state. The full superoperator determining the {photons+emitters} dynamics

$$\mathcal{L}(\rho) = -i\left[H_{\mathrm{ph}} + H_{\mathrm{at}} + H_{\mathrm{I}}, \rho\right] + \mathcal{L}_{\mathrm{p}} + \mathcal{L}_{\mathrm{l}}, \tag{B.3}$$

was decomposed as $\mathcal{L} = \mathcal{L}_0 + \delta\mathcal{L}$:

$$\mathcal{L}_0(\rho) = -i\left[H_{\mathrm{ph}} + H_{\mathrm{at}}, \rho\right] + \mathcal{L}_{\mathrm{l}}(\rho) - \mathcal{A}(\rho) + \mathcal{P}\mathcal{A}\mathcal{Q}(\rho) \tag{B.4}$$

$$\delta\mathcal{L}(\rho_{\mathrm{tot}}) = -i\left[H_{\mathrm{I}}, \rho_{\mathrm{tot}}\right] + \frac{\Gamma_{\mathrm{p}}}{2}\sum_{i=1}^{L}\sum_{n=1}^{N_{at}} 2\sigma_i^{+(n)}\rho_{\mathrm{tot}}\sigma_i^{-(n)} - \mathcal{P}\mathcal{A}\mathcal{Q}(\rho_{\mathrm{tot}}), \tag{B.5}$$

where

$$\mathcal{A}(\rho) = \frac{\Gamma_{\mathrm{p}}}{2}\sum_{i=1}^{L}\sum_{n=1}^{N_{\mathrm{at}}}\left[\sigma_i^{-(n)}\sigma_i^{+(n)}\rho + \rho\sigma_i^{-(n)}\sigma_i^{+(n)}\right]. \tag{B.6}$$

$\mathcal{L}_0$ and $\delta\mathcal{L}$ were chosen in order to verify the following projection conditions

$$\begin{cases} \mathcal{P}\mathcal{L}_0\mathcal{Q} = \mathcal{Q}\mathcal{L}_0\mathcal{P} = 0 \\ \mathcal{P}\,\delta\mathcal{L}\,\mathcal{P} = 0. \end{cases} \tag{B.7}$$

As we are interested in the regime in which $\Gamma_{\mathrm{p}} \gg \sqrt{N_{\mathrm{at}}}\Omega_R, \Gamma_{\mathrm{l}}$, we will compute the self energy at the lowest non zero order of these two latter parameters. Since Γ_{l} quantifies the photonic loss rate, we will approximate the photonic dynamics as being a Hamiltonian one during the time while the emitter is reinjected in the excited state, ie during the characteristic time $1/\Gamma_{\mathrm{p}}$ of the integration kernel of Eq. (2.13). To this order of precision, the calculation for one cavity containing a single emitter is straightforwardly generalizable to L cavities each containing N_{at} emitters, thus we will restrict for simplicity to the case $L = N_{\mathrm{at}} = 1$.

Appendix B. Derivation of the purely photonic master equation via projective methods

B.1 Self energy calculation

We are going to calculate the self energy to the lowest order in Ω_{R}. We have

$$\delta\mathcal{L} = \mathcal{L}_{\mathrm{p}} - i(H^+ + H^-)_{\mathrm{L}} + i(H^+ + H^-)_{\mathrm{R}} - \mathcal{P}\mathcal{A}\mathcal{Q}, \tag{B.8}$$

with

$$\begin{cases} \mathcal{L}_{\mathrm{p}}(\rho) = \Gamma_{\mathrm{p}}\sigma^+\rho\sigma^- \\ H^+ = \Omega_{\mathrm{R}}\sigma^+ a \\ H^- = \Omega_{\mathrm{R}}\sigma^- a^\dagger \end{cases} \tag{B.9}$$

By $(H^\pm)_{L/R}$ we intend the superoperator multiplying a matrix ρ by the matrix $H^\pm$ on its left/right. First we have $\mathcal{L}_{\mathrm{p}}\mathcal{P} = \mathcal{P}\mathcal{A}\mathcal{Q}\mathcal{P} = H_{\mathrm{L}}^+\mathcal{P} = H_{\mathrm{R}}^-\mathcal{P} = 0$, so starting from a projected state $\mathcal{P}\rho$, we have to start with H_{L}^- or H_{R}^+. In fact to the lowest order in Ω_{R} the non zero contributions to the self energy are :

$$\begin{aligned} A &= -\mathcal{P}H_{\mathrm{L}}^+ H_{\mathrm{L}}^-(t'-t)\mathcal{P} \\ B &= -\mathcal{P}H_{\mathrm{R}}^- H_{\mathrm{R}}^+(t'-t)\mathcal{P} \\ C &= \mathcal{P}H_{\mathrm{R}}^+ H_{\mathrm{L}}^-(t'-t)\mathcal{P} \\ D &= \mathcal{P}H_{\mathrm{L}}^- H_{\mathrm{R}}^+(t'-t)\mathcal{P} \\ E &= \int_{t'}^t d\tilde{t}\,\mathcal{P}\mathcal{L}_{\mathrm{p}}(t)\mathcal{Q}H_{\mathrm{R}}^+(\tilde{t}-t)H_{\mathrm{L}}^-(t'-t)\mathcal{P} \\ F &= \int_{t'}^t d\tilde{t}\,\mathcal{P}\mathcal{L}_{\mathrm{p}}(t)\mathcal{Q}H_{\mathrm{L}}^+(\tilde{t}-t)H_{\mathrm{R}}^-(t'-t)\mathcal{P} \\ G &= -\int_{t'}^t d\tilde{t}\,\mathcal{P}\mathcal{A}\mathcal{Q}H_{\mathrm{R}}^+(\tilde{t}-t)H_{\mathrm{L}}^-(t'-t)\mathcal{P} \\ H &= -\int_{t'}^t d\tilde{t}\,\mathcal{P}\mathcal{A}\mathcal{Q}H_{\mathrm{L}}^-(\tilde{t}-t)H_{\mathrm{R}}^+(t'-t)\mathcal{P}, \end{aligned} \tag{B.10}$$

with

$$\Sigma(0, t'-t) = A + B + C + D + E + F + G + H. \tag{B.11}$$

We then calculate the different processes, applied on some projected matrix $\mathcal{P}\rho$:

$$\begin{aligned} A(\mathcal{P}\rho) &= -\Omega_{\mathrm{R}}^2 e^{(i\omega_{\mathrm{at}}-\Gamma_{\mathrm{p}}/2)(t-t')} a a^\dagger(t'-t)\mathcal{P}\rho \\[4pt] B(\mathcal{P}\rho) &= -\Omega_{\mathrm{R}}^2 e^{-(i\omega_{\mathrm{at}}+\Gamma_{\mathrm{p}}/2)(t-t')} \mathcal{P}\rho a(t'-t)a^\dagger \\[4pt] C(\mathcal{P}\rho) &= \Omega_{\mathrm{R}}^2 e^{(i\omega_{\mathrm{at}}-\Gamma_{\mathrm{p}}/2)(t-t')} a^\dagger(t'-t)\mathcal{P}\rho a \\[4pt] D(\mathcal{P}\rho) &= \Omega_{\mathrm{R}}^2 e^{(-i\omega_{\mathrm{at}}+\Gamma_{\mathrm{p}}/2)(t-t')} a^\dagger \mathcal{P}\rho a(t'-t) \\[4pt] E(\mathcal{P}\rho) &= \Gamma_{\mathrm{p}}\Omega_{\mathrm{R}}^2 \int_{t'}^t d\tilde{t}\, e^{(-i\omega_{\mathrm{at}}-\Gamma_{\mathrm{p}}/2)(t-\tilde{t})} \\ &\qquad e^{(i\omega_{\mathrm{at}}-\Gamma_{\mathrm{p}}/2)(t-t')} a^\dagger(t'-t)\mathcal{P}\rho a(\tilde{t}-t) \\[4pt] F(\mathcal{P}\rho) &= \Gamma_{\mathrm{p}}\Omega_{\mathrm{R}}^2 \int_{t'}^t d\tilde{t}\, e^{(i\omega_{\mathrm{at}}-\Gamma_{\mathrm{p}}/2)(t-\tilde{t})} \\ &\qquad e^{(-i\omega_{\mathrm{at}}-\Gamma_{\mathrm{p}}/2)(t-t')} a^\dagger(\tilde{t}-t)\mathcal{P}\rho a(t'-t) \\[4pt] G(\mathcal{P}\rho) &= -\Gamma_{\mathrm{p}}\Omega_{\mathrm{R}}^2 \int_{t'}^t d\tilde{t}\, e^{(-i\omega_{\mathrm{at}}-\Gamma_{\mathrm{p}}/2)(t-\tilde{t})} \\ &\qquad e^{(i\omega_{\mathrm{at}}-\Gamma_{\mathrm{p}}/2)(t-t')} a^\dagger(t'-t)\mathcal{P}\rho a(\tilde{t}-t) = -E(\mathcal{P}\rho) \\[4pt] H(\mathcal{P}\rho) &= -\Gamma_{\mathrm{p}}\Omega_{\mathrm{R}}^2 \int_{t'}^t d\tilde{t}\, e^{(i\omega_{\mathrm{at}}-\Gamma_{\mathrm{p}}/2)(t-\tilde{t})} \\ &\qquad e^{(-i\omega_{\mathrm{at}}-\Gamma_{\mathrm{p}}/2)(t-t')} a^\dagger(\tilde{t}-t)\mathcal{P}\rho a(t'-t) = -F(\mathcal{P}\rho) \end{aligned} \tag{B.12}$$

where by $a(t'-t)$ we intend the evolution of the photonic annihlation operator in the photonic hamiltonian interaction picture (we remind that we neglected photonic losses during the integration time). We see that the last four contribution cancel each other, and that only the first four contributions remain.

B.2   Master equation

Using the expression for the self-energy $\Sigma(t)$ derived in the last section, as well as general results on the master equation obtained by projective methods in Sec. 2.2.2, we then obtain the (temporally non-local) master equation :

$$
\begin{aligned}
\partial_t \mathcal{P}\rho \;=\; & -i\left[H_{\mathrm{ph}}, \mathcal{P}\rho\right] + \mathcal{L}_\Gamma(\mathcal{P}\rho) \\
& +\Omega_{\mathrm{R}}^2 \int_0^\infty d\tau\, e^{(i\omega_{\mathrm{at}}-\Gamma_{\mathrm{p}}/2)\tau} a^\dagger \left(e^{\mathcal{L}_0(\tau)}\mathcal{P}\rho(t-\tau)\right) a(-\tau) \\
& +\Omega_{\mathrm{R}}^2 \int_0^\infty d\tau\, e^{-(i\omega_{\mathrm{at}}+\Gamma_{\mathrm{p}}/2)\tau} a^\dagger(-\tau) \left(e^{\mathcal{L}_0(\tau)}\mathcal{P}\rho(t-\tau)\right) a \\
& -\Omega_{\mathrm{R}}^2 \int_0^\infty d\tau\, e^{(i\omega_{\mathrm{at}}-\Gamma_{\mathrm{p}}/2)\tau} a a^\dagger(-\tau) \left(e^{\mathcal{L}_0(\tau)}\mathcal{P}\rho(t-\tau)\right) \\
& -\Omega_{\mathrm{R}}^2 \int_0^\infty d\tau\, e^{-(i\omega_{\mathrm{at}}+\Gamma_{\mathrm{p}}/2)\tau} \left(e^{\mathcal{L}_0(\tau)}\mathcal{P}\rho(t-\tau)\right) a(-\tau)a^\dagger.
\end{aligned}
\tag{B.13}
$$

At lowest order in Ω_{R}, we can assume the interaction picture density matrix in the convolution product to be constant, $\hat\rho(t-\tau) \simeq \hat\rho(t)$, i.e. $e^{\mathcal{L}_0 \tau}\rho(t-\tau) \simeq \rho(t)$. Making the trace over the bath we get :

$$
\begin{aligned}
\partial_t \rho \;=\; & -i\left[H_{\mathrm{ph}}, \rho\right] + \mathcal{L}_\Gamma(\rho) \\
& +\Omega_{\mathrm{R}}^2 \int_0^\infty d\tau\, e^{(i\omega_{\mathrm{at}}-\Gamma_{\mathrm{p}}/2)\tau} a^\dagger(-\tau)\rho(t) a \\
& +\Omega_{\mathrm{R}}^2 \int_0^\infty d\tau\, e^{-(i\omega_{\mathrm{at}}+\Gamma_{\mathrm{p}}/2)\tau} a^\dagger \rho(t) a(-\tau) \\
& -\Omega_{\mathrm{R}}^2 \int_0^\infty d\tau\, e^{(i\omega_{\mathrm{at}}-\Gamma_{\mathrm{p}}/2)\tau} a a^\dagger(-\tau)\rho(t) \\
& -\Omega_{\mathrm{R}}^2 \int_0^\infty d\tau\, e^{-(i\omega_{\mathrm{at}}+\Gamma_{\mathrm{p}}/2)\tau} \rho(t) a(-\tau)a^\dagger,
\end{aligned}
\tag{B.14}
$$

then we can perform completely the integral and we get our final form for the non Markovian master equation, which is local in time :

$$
\partial_t \rho = -i\left[H_{\mathrm{ph}}, \rho\right] + \frac{\Gamma_1}{2}\left[2a\rho a^\dagger - a^\dagger a \rho - \rho a^\dagger a\right] + \frac{2\Omega_{\mathrm{R}}^2}{\Gamma_{\mathrm{p}}}\left[\tilde{a}^\dagger \rho a + a^\dagger \rho \tilde{a} - a\tilde{a}^\dagger \rho - \rho \tilde{a} a^\dagger\right], \tag{B.15}
$$

with

$$
\begin{cases}
\tilde{a} = \frac{\Gamma_{\mathrm{p}}}{2} \int_0^\infty d\tau\, e^{(-i\omega_{\mathrm{at}}-\Gamma_{\mathrm{p}}/2)\tau} a(-\tau), \\
\tilde{a}^\dagger = \frac{\Gamma_{\mathrm{p}}}{2} \int_0^\infty d\tau\, e^{(i\omega_{\mathrm{at}}-\Gamma_{\mathrm{p}}/2)\tau} a^\dagger(-\tau) = [\tilde{a}]^\dagger,
\end{cases}
\tag{B.16}
$$

where $a(-\tau)$ means the photonic annihilation operator in the photonic hamiltonian interaction picture. If $|f\rangle$ and $|f\rangle'$ are two eigenstates of the photonic hamiltonian with a photon number difference of one, we see that the matrix elements of the modified annihilation and creation operators $\tilde{a}$ and $\tilde{a}^\dagger$ involved in the emission process are :

$$
\begin{cases}
\langle f| \tilde{a}^\dagger |f'\rangle = \frac{\Gamma_{\mathrm{p}}/2}{-i(\omega_{\mathrm{at}}-\omega_{ff'})+\Gamma_{\mathrm{p}}/2} \langle f| a^\dagger |f'\rangle \\
\langle f'| \tilde{a} |f\rangle = \frac{\Gamma_{\mathrm{p}}/2}{i(\omega_{\mathrm{at}}-\omega_{ff'})+\Gamma_{\mathrm{p}}/2} \langle f'| a |f\rangle.
\end{cases}
\tag{B.17}
$$

The non-Markovianity comes from the energy-dependence of the prefactors in Eq. (B.17).

B.3   Many-cavity and many emitters

For several cavities and N_{at} emitters per cavity, whose distribution of transition frequencies is $\mathcal{D}(\omega)$ ($\mathcal{D}(\omega) = N_{\mathrm{at}}\delta(\omega-\omega_{\mathrm{at}})$ if all transition frequencies are equal, and instead is a smooth function if N_{at} is very large and the frequencies form a continuous spectrum), the reasoning is exactly the same: each emitter brings its own small contribution to the total frequency-dependent emission, and by making the sum of all of these terms we get the multicavity

Appendix B. Derivation of the purely photonic master equation via projective methods

master equation

$$\partial_t \rho = -i\left[H_{\mathrm{ph}}, \rho(t)\right] + \mathcal{L}_{\mathrm{l}}(\rho(t)) + \frac{\Gamma_{\mathrm{em}}^0}{2} \sum_{i=1}^{L} \left[\tilde{a}_i^\dagger \rho a_i + a_i^\dagger \rho \tilde{a}_i - a_i \tilde{a}_i^\dagger \rho - \rho \tilde{a}_i a_i^\dagger\right],$$

where

$$\frac{\Gamma_{\mathrm{em}}^0}{2} \tilde{a}_i = \int_0^\infty d\tau\, \Gamma_{\mathrm{em}}(\tau) a_i(-\tau), \qquad \tilde{a}_i^\dagger = [\tilde{a}_i]^\dagger \tag{B.18}$$

is the modified annihilation operator,

$$\Gamma_{\mathrm{em}}(\tau) = \Gamma_{\mathrm{em}}^{\mathrm{at}} \theta(\tau) \int d\tilde{\omega} \mathcal{D}(\tilde{\omega}) e^{-(i\tilde{\omega}+\Gamma_{\mathrm{p}}/2)\tau} = \theta(\tau) \int \frac{d\omega}{2\pi} \mathcal{S}_{\mathrm{em}}(\omega) e^{-i\omega\tau} \tag{B.19}$$

is the photonic emission kernel, $a_i(-\tau) = e^{-iH_{\mathrm{ph}}\tau} a_i e^{iH_{\mathrm{ph}}\tau}$ is the annihilation operator in the photonic Hamiltonian picture and

$$\mathcal{S}_{\mathrm{em}}(\omega) = \Gamma_{\mathrm{em}}^{\mathrm{at}} \int d\tilde{\omega} \mathcal{D}(\tilde{\omega}) \frac{(\Gamma_{\mathrm{p}}/2)^2}{(\omega - \tilde{\omega})^2 + (\Gamma_{\mathrm{p}}/2)^2} \tag{B.20}$$

is the photonic frequency-dependent emission spectrum. Here $\Gamma_{\mathrm{em}}^0 = \mathrm{Max}\left[\mathcal{S}_{\mathrm{em}}(\omega)\right]$ is the maximum reachable emission rate, and $\Gamma_{\mathrm{em}}^{\mathrm{at}} = \frac{4\Omega_{\mathrm{R}}^2}{\Gamma_{\mathrm{p}}}$ is the maximum emission rate of a single atom, obtained at resonance. $\mathcal{S}_{\mathrm{em}}(\omega)$ is the convolution product of a Lorentzian which represents the Lorentzian broadening of each emitter due to the pumping, and the spectral distribution $\mathcal{D}(\omega)$ of the emitter bare frequencies in absence of pumping. Thus, considering two eigenstates $|f\rangle$ (resp. $|f'\rangle$) of the photonic Hamiltonian with N (resp. $N+1$) photons and energy difference $\omega_{f'f} = \omega_{f'} - \omega_f$, the matrix element of the modified jump operators equals

$$\langle f|\, \tilde{a}_i \,|f'\rangle = \frac{2}{\Gamma_{\mathrm{em}}^0} \Gamma_{\mathrm{em}}(\omega_{f'f}) \langle f|\, a_i \,|f'\rangle : \tag{B.21}$$

the frequency-dependent emission strongly depends on the many-body photonic dynamics. Here

$$\Gamma_{\mathrm{em}}(\omega) = \frac{1}{2}\mathcal{S}_{\mathrm{em}}(\omega) - i\delta_l(\omega) \tag{B.22}$$

is the Fourier transform of the memory kernel $\Gamma_{\mathrm{em}}(\tau)$. While the magnitude of the Lamb-shift $\delta_l(\omega)$ stemming from the imaginary part of $\Gamma_{\mathrm{em}}(\omega)$ is typically small as compared to relevant Hamiltonian scales and thus does not bring important physical effects, the real part $\mathcal{S}_{\mathrm{em}}(\omega)/2$ is physically essential as it provides the frequency-dependent emission rate and while be responsible for transfering in a frequency selective manner the populations between the various eigenstates of H_{ph}. This intuitive representation is highlighted in a very clear way in the App. C, where the photonic master is reformulated in a Lindblad equivalent form in the specific regime of weak dissipation allowing for the application of the secular approximation.

In the case of Chapter. 2, $\mathcal{D}(\omega) = N_{\mathrm{at}}\delta(\omega - \omega_{\mathrm{at}})$ since all transition frequencies are equal and we get for the modified jump operators:

$$\begin{cases} \tilde{a}_i = \frac{\Gamma_{\mathrm{p}}}{2} \int_0^\infty d\tau\, e^{(-i\omega_{\mathrm{at}}-\Gamma_{\mathrm{p}}/2)\tau} a_i(-\tau), \\ \tilde{a}_i^\dagger = \frac{\Gamma_{\mathrm{p}}}{2} \int_0^\infty d\tau\, e^{(i\omega_{\mathrm{at}}-\Gamma_{\mathrm{p}}/2)\tau} a_i^\dagger(-\tau) \end{cases} \tag{B.23}$$

Here again, if $|f\rangle$ and $|f\rangle'$ are two eigenstates of the photonic hamiltonian with a photon number difference of one, and energy difference $\omega_{f'f}$, we have that the matrix element

$$\begin{cases} \langle f|\, \tilde{a}^\dagger \,|f'\rangle = \frac{\Gamma_{\mathrm{p}}/2}{-i(\omega_{\mathrm{at}}-\omega_{ff'})+\Gamma_{\mathrm{p}}/2} \langle f|\, a^\dagger \,|f'\rangle \\ \langle f'|\, \tilde{a} \,|f\rangle = \frac{\Gamma_{\mathrm{p}}/2}{i(\omega_{\mathrm{at}}-\omega_{ff'})+\Gamma_{\mathrm{p}}/2} \langle f'|\, a \,|f\rangle. \end{cases} \tag{B.24}$$

In the case of Chapter 3, the emitters frequencies are uniformly distributed over an interval $[\omega_-, \omega_+]$ and the distribution is square-shaped ($\mathcal{D}^{square}(\omega) = \frac{N_{\mathrm{at}}}{\omega_+ - \omega_-}\theta(\omega - \omega_-)\theta(\omega_+ - \omega)$), so we obtain the form for the emission power spectrum:

$$\mathcal{S}_{\mathrm{em}}^{square}(\omega) = \Gamma_{\mathrm{em}}^{\mathrm{at}} \frac{N_{\mathrm{at}}}{\omega_+ - \omega_-} \int_{\omega_-}^{\omega_+} d\tilde{\omega} \frac{(\Delta_{\mathrm{em}}/2)^2}{(\omega - \tilde{\omega})^2 + (\Delta_{\mathrm{em}}/2)^2}, \tag{B.25}$$

with $\Delta_{\text{em}} = \Gamma_{\text{p}}$. The maximum power spectrum obtained at the middle between the two cutoffs is then

$$
\begin{aligned}
\Gamma_{\text{em}}^0 \quad &= \quad \mathcal{S}_{\text{em}}^{square}\left(\frac{\omega_+ + \omega_-}{2}\right) \\
&= \quad \frac{2\pi N_{\text{at}}\Omega_R^2}{\omega_+ - \omega_-} \qquad \text{for } \Delta_{\text{em}} \ll \omega_+ - \omega_-
\end{aligned}
\tag{B.26}
$$

Appendix C

Reformulation of the photonic master equation in Lindblad form in the secular approximation

In this Appendix, we demonstrate that in the case where the photonic many-body system system has a discrete spectrum (this is true for any system of finite size), it is possible in the so-called secular approximation to write an alternative master implementing non-Markovian effects with a more standard Lindblad form, compatible with Monte Carlo wave-function simulations [43] and giving equivalent driven-dissipative dynamics to the photonic master equation introduced in Chapter. 2 in Chap. 3.

This can be explained by the following argument: in a weak dissipation limit (Γ_{em}^0, Γ_{l} very small with respect to the gaps in the spectrum) terms of the density matrix $\rho_{f,\tilde{f}}$, $\rho_{f',\tilde{f}'}$ which would be rotating at different frequencies $\omega_{f,\tilde{f}}$, $\omega_{f',\tilde{f}'}$ if the system were isolated, are not coupled to each other by dissipation since the coupling Γ_{em}^0, Γ_{l} is negligible with respect to their frequency difference $\Delta\omega = \omega_{f',\tilde{f}'} - \omega_{f,\tilde{f}} = \omega_{f',f} - \omega_{\tilde{f}',\tilde{f}}$. Considering this, all relevant dissipative transitions verify then $\Delta\omega = 0$.

C.1   Lindblad form

Restricting the previous master equation given by Eqs. 2.24,2.26 and 2.31 to these transitions, it is possible to rewrite the dynamics in the following way:

$$\partial_t \rho = -i\left[H_{\mathrm{ph}} + H_{\mathrm{lamb}}, \rho(t)\right] + \mathcal{L}_{\mathrm{l}}(\rho) + \bar{\mathcal{L}}_{\mathrm{em}}(\rho), \tag{C.1}$$

where

$$\bar{\mathcal{L}}_{\mathrm{em}}(\rho) = \frac{\Gamma_{\mathrm{em}}}{2} \sum_{i=1}^{k} \left[2\bar{a}_i^\dagger \rho \bar{a}_i - \bar{a}_i \bar{a}_i^\dagger \rho - \rho \bar{a}_i \bar{a}_i^\dagger\right], \tag{C.2}$$

is a modified emission superoperator in the Lindblad form, which unline it s counterpart in the first form for the photonic master equation Eq. 2.24 involves modified jump operators

$$\langle f'|\, \bar{a}_i^\dagger \,|f\rangle = \sqrt{\frac{\mathcal{S}_{\mathrm{em}}(\omega_{f'f})}{\Gamma_{\mathrm{em}}^0}} \, \langle f'|\, a_i^\dagger \,|f\rangle, \tag{C.3}$$

in a symmetrized manner. The imaginary part of $\Gamma_{\mathrm{em}}(\omega)$ has led to the presence of a Lamb-shift under the form of an Hamiltonian correction

$$\langle f'|\, H_{\mathrm{lamb}} \,|f\rangle = \frac{1}{2} \sum_i \sum_{f''} \langle f'|\, a_i \,|f''\rangle \left[\delta_{\mathrm{l}}(\omega_{f'',f}) + \delta_{\mathrm{l}}(\omega_{f'',f'})\right] \langle f''|\, a_i^\dagger \,|f\rangle, \tag{C.4}$$

where we remind the notation $\delta_{\mathrm{l}}(\omega) = -\mathrm{Im}[\Gamma_{\mathrm{em}}(\omega)]$.

Note that the jump operators $\bar{a}_i^\dagger$ have the same form as the ones considered in [97] and have for effect to modify the transition rate. While the two master equations Eqs. 2.24, C.1 are slightly different, under the considered approximation they are expected to provide equivalent dynamics. The latter form has the advantage of being of Lindblad form, and thus is directly compatible with Monte Carlo wave-functions simulations [43] and might be useful in the future from a numerical point of view (we did not exploit numerically this form in my Ph. D.).

C.2   Derivation

We now move to the derivation of the Lindblad form Eq. C.1. To do this, we calculate the matrix elements $\mathcal{L}_{em,\,f',\tilde{f}',f,\tilde{f}}$ of the emission superoperator coupling the term of the density matrix in the eigenstate basis $\langle f|\,\rho\,|\tilde{f}\rangle$ to $\langle f'|\,\rho\,|\tilde{f}'\rangle$, under the assumption $\Delta\omega = \omega_{f',\tilde{f}'} - \omega_{f,\tilde{f}} = 0$. We first compute the contributions associated to the original terms of the $\tilde{a}_i^\dagger \rho a_i + a_i^\dagger \rho \tilde{a}_i$ featuring both left and right matrix products:

$$\frac{\Gamma_{\text{em}}^0}{2}\,\langle f'|\,\tilde{a}_i^\dagger\,|f\rangle\,\langle f|\,\rho\,|\tilde{f}\rangle\langle \tilde{f}|a_i|\tilde{f}'\rangle + \langle f'|\,a_i^\dagger\,|f\rangle\,\langle f|\,\rho\,|\tilde{f}\rangle\langle \tilde{f}|\tilde{a}_i|\tilde{f}'\rangle =$$
$$\langle f'|\,a_i^\dagger\,|f\rangle\,\langle f|\,\rho\,|\tilde{f}\rangle\langle \tilde{f}|a_i|\tilde{f}'\rangle\left(\Gamma_{\text{em}}^*(\omega_{f'f}) + \Gamma_{\text{em}}(\omega_{\tilde{f}'\tilde{f}})\right). \quad \text{(C.5)}$$

Considering that under the approximation $\Delta\omega \simeq 0$, we have that $\Gamma_{\text{em}}(\omega_{f'f}) \simeq \Gamma_{\text{em}}(\omega_{\tilde{f}'\tilde{f}})$, we obtain thus the following contribution:

$$\frac{\Gamma_{\text{em}}^0}{2}\,\langle f'|\,\tilde{a}_i^\dagger\,|f\rangle\,\langle f|\,\rho\,|\tilde{f}\rangle\langle \tilde{f}|a_i|\tilde{f}'\rangle + \langle f'|\,a_i^\dagger\,|f\rangle\,\langle f|\,\rho\,|\tilde{f}\rangle\langle \tilde{f}|\tilde{a}_i|\tilde{f}'\rangle$$
$$\simeq 2\,\langle f'|\,a_i^\dagger\,|f\rangle\,\sqrt{\frac{\mathcal{S}_{\text{em}}(\omega_{f'f})}{2}}\,\langle f|\,\rho\,|\tilde{f}\rangle\sqrt{\frac{\mathcal{S}_{\text{em}}(\omega_{\tilde{f}'\tilde{f}})}{2}}\,\langle \tilde{f}|a_i|\tilde{f}'\rangle$$
$$= \Gamma_{\text{em}}^0\,\langle f'|\,\bar{a}_i^\dagger\,|f\rangle\,\langle f|\,\rho\,|\tilde{f}\rangle\langle \tilde{f}|\bar{a}_i|\tilde{f}'\rangle, \quad \text{(C.6)}$$

with $\bar{a}_i$ defined in Eq.C.3. We see that the "imaginary" contribution cancels out, and that the "real" contribution has been divided in two multiplicative contributions on the left and the right of the density matrix. We then move to the computation of the terms stemming from the non-Hermitian Hamiltonian-like contributions $a_i\tilde{a}_i^\dagger\rho + \rho\tilde{a}_i a_i^\dagger$. Let us calculate the left product:

$$\frac{\Gamma_{\text{em}}^0}{2}\,\langle f'|\,a_i\,|f''\rangle\,\langle f''|\,\tilde{a}_i^\dagger\,|f\rangle\,\langle f|\,\rho\,|\tilde{f}\rangle \quad = \quad \langle f'|\,a_i\,|f''\rangle\,\Gamma_{\text{em}}^*(\omega_{f''f})\,\langle f''|\,a_i^\dagger\,|f\rangle\,\langle f|\,\rho\,|\tilde{f}\rangle \quad \text{(C.7)}$$
$$= \quad \langle f'|\,a_i\,|f''\rangle\left[\frac{\mathcal{S}_{\text{em}}(\omega_{f''f})}{2} + i\delta_1(\omega_{f''f})\right]\langle f''|\,a_i^\dagger\,|f\rangle\,\langle f|\,\rho\,|\tilde{f}\rangle.$$

Considering that under the approximation $\omega_{f',f} \simeq 0$, we have that $\omega_{f'',f} = \omega_{f'',f'}$, and so:

$$\mathcal{S}_{\text{em}}(\omega_{f''f}) \quad = \quad \sqrt{\mathcal{S}_{\text{em}}(\omega_{f''f})\mathcal{S}_{\text{em}}(\omega_{f''f'})} \quad \text{(C.8)}$$
$$\delta_1(\omega_{f''f}) \quad = \quad \frac{\delta_1(\omega_{f''f}) + \delta_1(\omega_{f''f'})}{2} \quad \text{(C.9)}$$

As a consequence:

$$\frac{\Gamma_{\text{em}}^0}{2}\,\langle f'|\,a_i\,|f''\rangle\,\langle f''|\,\tilde{a}_i^\dagger\,|f\rangle\,\langle f|\,\rho\,|\tilde{f}\rangle \quad \simeq \quad -i\,\langle f'|\,a_i\,|f''\rangle\left(\frac{\delta_1(\omega_{f''f}) + \delta_1(\omega_{f''f'})}{2}\right)\langle f''|\,a_i^\dagger\,|f\rangle\,\langle f|\,\rho\,|\tilde{f}\rangle$$
$$+ \frac{\Gamma_{\text{em}}^0}{2}\,\langle f'|\,\bar{a}_i\,|f''\rangle\,\langle f''|\,\bar{a}_i^\dagger\,|f\rangle\,\langle f|\,\rho\,|\tilde{f}\rangle. \quad \text{(C.10)}$$

Similarly, we get for the right product:

$$\frac{\Gamma_{\text{em}}^0}{2}\,\langle f|\,\rho\,|\tilde{f}\rangle\langle \tilde{f}|a_i|\tilde{f}''\rangle\langle \tilde{f}''|\tilde{a}_i^\dagger|\tilde{f}'\rangle \quad \simeq \quad +i\,\langle f|\,\rho\,|\tilde{f}\rangle\langle \tilde{f}|a_i|\tilde{f}''\rangle\left(\frac{\delta_1(\omega_{\tilde{f}''\tilde{f}}) + \delta_1(\omega_{\tilde{f}''\tilde{f}'})}{2}\right)\langle \tilde{f}''|a_i^\dagger|\tilde{f}\rangle$$
$$+ \frac{\Gamma_{\text{em}}^0}{2}\,\langle f'|\,\bar{a}_i\,|f''\rangle\,\langle f''|\,\bar{a}_i^\dagger\,|f\rangle\,\langle f|\,\rho\,|\tilde{f}\rangle. \quad \text{(C.11)}$$

The sum of all contributions gives the form Eq. (C.1)

Appendix D

Perturbative corrections to the coherences in the weakly non Markovian regime

In this Appendix we show that the lowest-order correction to the coherences between eigenstates (null in the Grand Canonical ensemble of Sec.2.4.2) are quadratic in the inverse pumping rate Γ_{p}^{-1} and not linear as a naive pertubative expansion would suggest. To this purpose, we calculate the first order contributions to the coherences of the operator $\delta\mathcal{M}$ [defined in Eqs. (2.64) and (2.67)] applied to the grand canonical density matrix $\rho_\infty^{\mathrm{eq}} = \frac{1}{\Xi} e^{-\beta_{\mathrm{eff}}(H_{\mathrm{ph}} - \mu\hat{N})}$ and show them to be vanishing at lowest order in $\frac{1}{\Gamma_{\mathrm{p}}}$. Considering the fact that $\rho_\infty^{\mathrm{eq}}$ is diagonal in the photonic eigenbasis, we first reduce the following contributions of $\delta\mathcal{M}$

$$
\sum_i \langle f|\, \delta a_i^\dagger \rho_\infty^{\mathrm{eq}} a_i \,|f'\rangle = \sum_{i,\tilde{f},\tilde{f}'} \langle f|\, \delta a_i^\dagger |\tilde{f}\rangle\langle\tilde{f}|\rho_\infty^{\mathrm{eq}}|\tilde{f}'\rangle\langle\tilde{f}'|a_i\,|f'\rangle \tag{D.1}
$$

$$
= \sum_{i,\tilde{f}} \langle f|\, \delta a_i^\dagger |\tilde{f}\rangle\langle\tilde{f}|\rho_\infty^{\mathrm{eq}}|\tilde{f}\rangle\langle\tilde{f}|a_i\,|f'\rangle \,,
$$

$$
\sum_i \langle f|\, a_i^\dagger \rho_\infty^{\mathrm{eq}} \delta a_i \,|f'\rangle = \sum_{i,\tilde{f},\tilde{f}'} \langle f|\, a_i^\dagger |\tilde{f}\rangle\langle\tilde{f}|\rho_\infty|\tilde{f}'\rangle\langle\tilde{f}'|\delta a_i\,|f'\rangle \tag{D.2}
$$

$$
= \sum_{i,\tilde{f}} \langle f|\, a_i^\dagger |\tilde{f}\rangle\langle\tilde{f}|\rho_\infty|\tilde{f}\rangle\langle\tilde{f}|\delta a_i\,|f'\rangle \,,
$$

where everything has been expressed in the photonic Hamiltonian eigenbasis. Then we know that $\langle f|\, \delta a_i^\dagger |\tilde{f}\rangle = -\frac{i(\omega_{f\tilde{f}} - \omega_{\mathrm{at}})}{\Gamma_{\mathrm{p}}} \langle f|\, a_i^\dagger |\tilde{f}\rangle + \mathcal{O}\left(\frac{1}{\Gamma_{\mathrm{p}}}\right)^2$. Let us choose a reference eigenstate $|f_0\rangle$ of H_{ph} with the same photon number as $|\tilde{f}\rangle$: we have that $\langle\tilde{f}|\rho_\infty^{\mathrm{eq}}|\tilde{f}\rangle = \langle f_0|\, \rho_\infty^{\mathrm{eq}} |f_0\rangle + \mathcal{O}(\Gamma_{\mathrm{p}}^{-1})$. All these additional corrections $\mathcal{O}(\Gamma_{\mathrm{p}}^{-1})$ give second order contributions and we do not keep them in Eqs. (D.1),(D.2). Thus to the lowest order

$$
\sum_i \langle f|\, \delta a_i^\dagger \rho_\infty^{\mathrm{eq}} a_i + a_i^\dagger \rho_\infty^{\mathrm{eq}} \delta a_i \,|f'\rangle = \langle f_0|\, \rho_\infty^{\mathrm{eq}} |f_0\rangle \sum_{i,\tilde{f}} \frac{-i(\omega_{f\tilde{f}} - \omega_{f'\tilde{f}})}{\Gamma_{\mathrm{p}}} \langle f|\, a_i^\dagger |\tilde{f}\rangle\langle\tilde{f}|a_i\,|f'\rangle
$$

$$
= \langle f_0|\, \rho_\infty^{\mathrm{eq}} |f_0\rangle \frac{-i\omega_{ff'}}{\Gamma_{\mathrm{p}}} \sum_{i,\tilde{f}} \langle f|\, a_i^\dagger |\tilde{f}\rangle\langle\tilde{f}|a_i\,|f'\rangle
$$

$$
= \langle f_0|\, \rho_\infty^{\mathrm{eq}} |f_0\rangle \frac{-i\omega_{ff'}}{\Gamma_{\mathrm{p}}} \langle f|\, \sum_i a_i^\dagger a_i \,|f'\rangle
$$

$$
= 0, \tag{D.3}
$$

since the total photon number operator $\hat{N} = \sum_i a_i^\dagger a_i$ is diagonal in any sub-manifold with a fixed total particle number, and since $\omega_{ff'} = 0$ for $|f\rangle = |f'\rangle$. A similar reasoning allows

117

to show that

$$\sum_i \langle f | a_i \delta a_i^\dagger \rho_\infty^{\mathrm{eq}} + \rho_\infty^{\mathrm{eq}} \delta a_i a_i^\dagger | f' \rangle = 0. \tag{D.4}$$

Thus, the superoperator $\delta\mathcal{M}$ does not perturbate the steady-state $\rho_\infty^{\mathrm{eq}}$ of $\mathcal{M}_0$ to the lowest order in the weakly non-Markovian regime $J, U \ll \Gamma_{\mathrm{p}}$, which completes our proof.

Appendix E

Quantum correlations of a driven-dissipative non-Markovian Bose-Einstein Condensation

In this Appendix we compute in the Bogoliubov regime the expressions the normal and anomalous quantum correlations describing the steady-state properties of the non-Markovian quantum Langevin of Chapter 4. After computing the correlations in frequency representation and some useful quantities related to the test of the validity of the FDT theorem, we then move to the computation of static correlations.

E.1 Quantum correlations in frequency and FDT

We first compute the correlation matrix in momentum frequency space $\mathcal{C}_{\mathbf{k}}(\omega)$ defined in Eq. (4.26). Inverting the langevin equation in frequency space Eq. (4.23), we get :

$$
\begin{pmatrix} \hat{\Lambda}_{\mathbf{k}}(\omega) \\ \hat{\Lambda}_{-\mathbf{k}}^{\dagger}(-\omega) \end{pmatrix} = \frac{i}{\omega - \mathcal{L}_{\mathbf{k}}(\omega)} \begin{pmatrix} \tilde{\xi}_{\mathbf{k}}(\omega) \\ -\tilde{\xi}_{-\mathbf{k}}^{\dagger}(-\omega) \end{pmatrix}
\tag{E.1}
$$

After calculation this gives us :

$$
\begin{pmatrix} \hat{\Lambda}_{\mathbf{k}}(\omega) \\ \hat{\Lambda}_{-\mathbf{k}}^{\dagger}(-\omega) \end{pmatrix} = \frac{i}{\left[\omega - \left(\epsilon_k + \mu + i\tilde{\Gamma}(\omega) \right) \right] \times \left[\omega + \epsilon_k + \mu - i\tilde{\Gamma}^*(-\omega) \right] + \mu^2}
$$
$$
\begin{pmatrix} \left(\omega + \epsilon_k + \mu - i\tilde{\Gamma}^*(-\omega) \right) \tilde{\xi}_{\mathbf{k}}(\omega) - \mu \tilde{\xi}_{-\mathbf{k}}^{\dagger}(-\omega) \\ -\mu \tilde{\xi}_{\mathbf{k}}(\omega) + \left(-\omega + \epsilon_k + \mu + i\tilde{\Gamma}(\omega) \right) \tilde{\xi}_{-\mathbf{k}}^{\dagger}(-\omega) \end{pmatrix}, \tag{E.2}
$$

and taking the hermitian conjugate:

$$
\begin{pmatrix} \hat{\Lambda}_{\mathbf{k}}^{\dagger}(\omega) \\ \hat{\Lambda}_{-\mathbf{k}}(-\omega) \end{pmatrix} = \frac{-i}{\left[\omega - \left(\epsilon_k + \mu - i\tilde{\Gamma}^*(\omega) \right) \right] \times \left[\omega + \epsilon_k + \mu + i\tilde{\Gamma}(-\omega) \right] + \mu^2}
$$
$$
\begin{pmatrix} \left(\omega + \epsilon_k + \mu + i\tilde{\Gamma}(-\omega) \right) \tilde{\xi}_{\mathbf{k}}^{\dagger}(\omega) - \mu \tilde{\xi}_{-\mathbf{k}}(-\omega) \\ -\mu \tilde{\xi}_{\mathbf{k}}^{\dagger}(\omega) + \left(-\omega + \epsilon_k + \mu - i\tilde{\Gamma}^*(\omega) \right) \tilde{\xi}_{-\mathbf{k}}(-\omega) \end{pmatrix}. \tag{E.3}
$$

We get after tracing over the various baths the expression for the correlation matrix:

$$
\mathcal{C}_{\mathbf{k}}(\omega) = \frac{1}{N_{\mathbf{k}}(\omega) N_{-\mathbf{k}}(-\omega)} \underbrace{\begin{pmatrix} M_{\mathbf{k}}^{(11)}(\omega) & M_{\mathbf{k}}^{(12)}(\omega) \\ M_{\mathbf{k}}^{(21)}(\omega) & M_{\mathbf{k}}^{(22)}(\omega) \end{pmatrix}}_{\equiv \mathcal{M}(\omega)}, \tag{E.4}
$$

where

$$N_{\mathbf{k}}(\omega) = \left[\omega - \left(\epsilon_k + \mu + i\tilde{\Gamma}(\omega)\right)\right] \times \left[\omega + \epsilon_k + \mu - i\tilde{\Gamma}^*(-\omega)\right] + \mu^2 \tag{E.5a}$$

$$M_{\mathbf{k}}^{(11)}(\omega) = S_{\mathrm{l}}(\omega_{BEC} + \omega) \left|\omega + \epsilon_{\mathbf{k}} + \mu + i\tilde{\Gamma}(-\omega)\right|^2 + S_{\mathrm{em}}(\omega_{BEC} - \omega)\mu^2, \tag{E.5b}$$

$$\begin{aligned} M_{\mathbf{k}}^{(21)}(\omega) = &-S_{\mathrm{l}}(\omega_{BEC} + \omega) \times \left[\omega + \epsilon_{\mathbf{k}} + \mu + i\tilde{\Gamma}(-\omega)\right]\mu \\ &+ S_{\mathrm{em}}(\omega_{BEC} - \omega)\left[\omega - \left(\epsilon_{\mathbf{k}} + \mu + i\tilde{\Gamma}(\omega)\right)\right]\mu, \end{aligned} \tag{E.5c}$$

$$\begin{aligned} M_{\mathbf{k}}^{(12)}(\omega) = &-S_{\mathrm{l}}(\omega_{BEC} + \omega) \times \left[\omega + \epsilon_{\mathbf{k}} + \mu - i\tilde{\Gamma}^*(-\omega)\right]\mu \\ &+ S_{\mathrm{em}}(\omega_{BEC} - \omega)\left[\omega - \left(\epsilon_{\mathbf{k}} + \mu - i\tilde{\Gamma}^*(\omega)\right)\right]\mu, \end{aligned} \tag{E.5d}$$

$$M_{\mathbf{k}}^{(22)}(\omega) = S_{\mathrm{l}}(\omega_{BEC} + \omega)\mu^2 + S_{\mathrm{em}}(\omega_{BEC} - \omega)\left|\omega - \left(\epsilon_{\mathbf{k}} + \mu + i\tilde{\Gamma}(\omega)\right)\right|^2. \tag{E.5e}$$

To test the FDT it is also useful to calculate the ratios $\frac{\langle\hat{\Lambda}_{\mathbf{k}}(\omega)\hat{\Lambda}_{\mathbf{k}}^{\dagger}\rangle}{\langle\hat{\Lambda}_{\mathbf{k}}^{\dagger}(\omega)\hat{\Lambda}_{\mathbf{k}}\rangle}$ and $\frac{\langle\hat{\Lambda}_{\mathbf{k}}(\omega)\hat{\Lambda}_{-\mathbf{k}}\rangle}{\langle\hat{\Lambda}_{\mathbf{k}}(-\omega)\hat{\Lambda}_{-\mathbf{k}}\rangle}$. We obtain the following expressions:

$$\frac{\langle\hat{\Lambda}_{\mathbf{k}}(\omega)\hat{\Lambda}_{\mathbf{k}}^{\dagger}\rangle}{\langle\hat{\Lambda}_{\mathbf{k}}^{\dagger}(\omega)\hat{\Lambda}_{\mathbf{k}}\rangle} = \frac{S_l(\omega_{\mathrm{BEC}} + \omega) + S_{\mathrm{em}}(\omega_{\mathrm{BEC}} - \omega)A_k(\omega)}{S_{\mathrm{em}}(\omega_{\mathrm{BEC}} + \omega) + S_l(\omega_{\mathrm{BEC}} - \omega)A_k(\omega)}, \tag{E.6}$$

$$\frac{\langle\hat{\Lambda}_{\mathbf{k}}(\omega)\hat{\Lambda}_{-\mathbf{k}}\rangle}{\langle\hat{\Lambda}_{\mathbf{k}}(-\omega)\hat{\Lambda}_{-\mathbf{k}}\rangle} = \frac{S_l(\omega_{\mathrm{BEC}} + \omega) + S_{\mathrm{em}}(\omega_{\mathrm{BEC}} - \omega)B_k(\omega)}{S_{\mathrm{em}}(\omega_{\mathrm{BEC}} + \omega) + S_l(\omega_{\mathrm{BEC}} - \omega)B_k(\omega)}, \tag{E.7}$$

with

$$A_k(\omega) = \frac{\mu^2}{\left|\omega + \epsilon_{\mathbf{k}} + \mu + i\tilde{\Gamma}(-\omega)\right|^2}, \tag{E.8}$$

$$B_k(\omega) = \frac{-\omega + \epsilon_{\mathbf{k}} + \mu - i\tilde{\Gamma}^*(\omega)}{\omega + \epsilon_{\mathbf{k}} + \mu - i\tilde{\Gamma}^*(-\omega)}. \tag{E.9}$$

E.2   Static correlations at low energy

We calculate here the static correlations at steady state in the low-energy regime $E_k \ll \Delta_{\mathrm{diss}}$. In this regime, using the definition Eq. (4.29) as well as the fact that $S_{\mathrm{l}}(\omega_{BEC}) = S_{\mathrm{em}}(\omega_{BEC})$, we can approximate the expression Eq. (E.4) of the correlation matrix calculated in the previous section as:

$$\begin{aligned} N_{\mathbf{k}}(\omega) \simeq &= \frac{1}{|z|^2}\left\{\left[\omega - z\left(\epsilon_k + \mu\right)\right]\left[\omega + z^*\left(\epsilon_k + \mu\right)\right] + |z|^2\mu^2\right\} \tag{E.10a} \\ &= \frac{1}{|z|^2}(\omega - \omega_{\mathbf{k}}^+)(\omega - \omega_{\mathbf{k}}^-), \tag{E.10b} \end{aligned}$$

$$M_{\mathbf{k}}^{(11)}(\omega) \simeq \frac{S_{\mathrm{l}}(\omega_{BEC})}{|z|^2}\left[|\omega + z\left(\epsilon_k + \mu\right)|^2 + |z|^2\mu^2\right], \tag{E.10c}$$

$$M_{\mathbf{k}}^{(21)}(\omega) \simeq -2S_{\mathrm{l}}(\omega_{BEC})(\epsilon_k + \mu)\mu, \tag{E.10d}$$

$$M_{\mathbf{k}}^{(12)}(\omega) \simeq -2S_{\mathrm{l}}(\omega_{BEC})(\epsilon_k + \mu)\mu, \tag{E.10e}$$

$$M_{\mathbf{k}}^{(22)}(\omega) \simeq \frac{S_{\mathrm{l}}(\omega_{BEC})}{|z|^2}\left[|\omega - z\left(\epsilon_k + \mu\right)|^2 + |z|^2\mu^2\right], \tag{E.10f}$$

where $\omega_{\mathbf{k}}^{\pm}$ are the complex low energy mode frequencies of the condensate given by Eq. (4.31). From these expressions, we can calculate the dynamic structure factor $\mathcal{S}_{\mathbf{k}}(t)$, which is defined as

$$\mathcal{S}_{\mathbf{k}}(t) = \begin{pmatrix} \langle\hat{\Lambda}_{\mathbf{k}}(t)\hat{\Lambda}_{\mathbf{k}}^{\dagger}(0)\rangle & \langle\hat{\Lambda}_{\mathbf{k}}(t)\hat{\Lambda}_{-\mathbf{k}}(0)\rangle \\ \langle\hat{\Lambda}_{-\mathbf{k}}^{\dagger}(t)\hat{\Lambda}_{\mathbf{k}}^{\dagger}(0)\rangle & \langle\hat{\Lambda}_{-\mathbf{k}}^{\dagger}(t)\hat{\Lambda}_{-\mathbf{k}}(0)\rangle \end{pmatrix}, \tag{E.11}$$

and is related to the correlation matrix $\mathcal{C}_{\mathbf{k}}(\omega)$ as $\int_t \mathcal{S}_{\mathbf{k}}(t)e^{-i\omega t} = \mathcal{C}_{\mathbf{k}}(\omega)$. Using a pole integration in the complex plane we obtain

$$\mathcal{S}_{\mathbf{k}}(t) = \frac{-i|z|^2}{2(\omega_{\mathbf{k}}^+ - \omega_{\mathbf{k}}^-)(\omega_{\mathbf{k}}^+ + \omega_{\mathbf{k}}^-)} \left[\frac{\mathcal{M}(\omega_{\mathbf{k}}^+)\mathrm{e}^{-i\omega_{\mathbf{k}}^+ t}}{2\omega_{\mathbf{k}}^+} - \frac{\mathcal{M}(\omega_{\mathbf{k}}^-)\mathrm{e}^{-i\omega_{\mathbf{k}}^- t}}{\omega_{\mathbf{k}}^-} \right], \qquad \text{(E.12)}$$

where $\mathcal{M}(\omega)$ has been defined in Eq. (E.4). Setting $t = 0$ we find the static correlation matrix :

$$\mathcal{S}_{\mathbf{k}}(0) = \frac{-i|z|^2}{2(\omega_{\mathbf{k}}^+ - \omega_{\mathbf{k}}^-)(\omega_{\mathbf{k}}^+ + \omega_{\mathbf{k}}^-)} \left[\frac{\mathcal{M}(\omega_{\mathbf{k}}^+)}{2\omega_{\mathbf{k}}^+} - \frac{\mathcal{M}(\omega_{\mathbf{k}}^-)}{\omega_{\mathbf{k}}^-} \right]. \qquad \text{(E.13)}$$

It seems a pretty complicated expression, but injecting the expressions given by Eqs. (E.10) as well as the explicit expressions for the condensate frequencies Eq. (4.31), we find:

$$\mathcal{S}_{\mathbf{k}}(0) = \frac{S_\mathrm{l}(\omega_{BEC})|z|^2}{2z_I E_k^2} \begin{pmatrix} \epsilon_k + \mu & -\mu \\ -\mu & \epsilon_k + \mu \end{pmatrix}. \qquad \text{(E.14)}$$

From Eqs. (4.29), (4.5), we have that $\frac{z_I}{|z|^2} = \mathrm{Im}\left(z^{-1}\right) = -\left.\frac{\mathrm{dRe}(\widetilde{\Gamma}(\omega))}{\mathrm{d}\omega}\right|_{\omega=0} = \frac{\beta_\mathrm{eff} S_\mathrm{l}(\omega_{\mathrm{BEC}})}{2}$, from which we deduce the final expression:

$$\mathcal{S}_{\mathbf{k}}(0) = \frac{T_\mathrm{eff}}{E_k^2} \begin{pmatrix} \epsilon_k + \mu & -\mu \\ -\mu & \epsilon_k + \mu \end{pmatrix}. \qquad \text{(E.15)}$$

Bibliography

[1] C. Ciuti A. Verger and I. Carusotto. Polariton quantum blockade in a photonic dot. *Phys. Rev. B*, **73**:193306, 2006. (cited on p. 15)

[2] E. Altman, L. M. Sieberer, L. Chen, S. Diehl, and J. Toner. Two-dimensional super-fluidity of exciton polaritons requires strong anisotropy. *Phys. Rev. X*, **5**:011017, 2015. (cited on pp. 7, 48, 51, 65, 73, 78, and 96)

[3] A. Amo, J. Lefrère, S. Pigeon, C. Adrados, C. Ciuti, I. Carusotto, R. Houdré, E. Giacobino, and A. Bramati. Superfluidity of polaritons in semiconductor microcavities. *Nature Physics*, **5**:805, 2009. (cited on pp. 1 and 7)

[4] D. G. Angelakis, M. F. Santos, and S. Bose. Photon blockade induced mott transitions and xy spin models in coupled cavity arrays. *Phys. Rev. A*, **76**:031805, 2007. (cited on p. 15)

[5] C. Aron, G. Biroli, and L. F. Cugliandolo. Symmetries of generating functionals of langevin processes with colored multiplicative noise. *J. Stat. Mech.*, **2010**:P11018, 2010. (cited on pp. 48 and 73)

[6] A. Baas, J. P. Karr, H. Eleuch, and E. Giacobino. Optical bistability in semiconductor microcavities. *Phys. Rev. A*, **69**:023809, 2004. (cited on pp. 8 and 16)

[7] D. Bajoni, P. Senellart, E. Wertz, I. Sagnes, A. Miard, A. Lemaître, and J. Bloch. Polariton laser using single micropillar gaas-gaalas semiconductor cavities. *Phys. Rev. Lett.*, bf 100:047401, 2008. (cited on pp. 2, 8, 9, and 73)

[8] W. S. Bakr, A. Peng, M. E. Tai, R. Ma, J. Simon, J. I. Gillen, and S. Föö. (cited on p. 15)

[9] R. Balili, V. Hartwell, D. Snoke, L. Pfeiffer, and K. West. Bose-einstein condensation of microcavity polaritons in a trap. *Science*, bf 316:1007, 2007. (cited on pp. 8, 9, 73, 74, and 94)

[10] K. Baumann, C. Guerlin, F. Brennecke, and T. Esslinger. Dicke quantum phase transition with a superfluid gas in an optical cavity. *Nature*, **464**:1301, 2010. (cited on p. 25)

[11] J. J. Baumberg, P. G. Savvidis, R. M. Stevenson, A. I. Tartakovskii, M. S. Skolnick, D. M. Whittaker, and J. S. Roberts. Parametric oscillation in a vertical microcavity: A polariton condensate or micro-optical parametric oscillation. *Phys. Rev. B*, **62**:R16247(R), 2000. (cited on p. 8)

[12] A. Biella, F. Storme, J. Lebreuilly, D. Rossini, I. Carusotto, R. Fazio, and C. Ciuti. Phase diagram of incoherently-driven strongly correlated photonic lattices. *Phys. Rev. A*, **96**:023839, 2017. (cited on pp. 17, 18, 23, 24, 26, 42, 46, 54, 55, 58, and 60)

[13] K. M. Birnbaum, A. Boca, R. Miller, A. D. Boozer, T. E. Northup, and H. J. Kimble. Photon blockade by an optical cavity with one trapped atom. *Nature*, **436**:87, 2005. (cited on pp. 1 and 12)

[14] A. Blais, R.-S. Huang andA. Wallraff, S. M. Girvin, and R. Schoelkopf. Cavity quantum electrodynamics for superconducting electrical circuits: An architecture for quantum computation. *Phys. Rev. A*, **69**:062320, 2004. (cited on pp. 12, 14, and 16)

[15] I. Bloch, J. Dalibard, and W. Zwerger. Many-body physics with ultracold gases. *Rev. Mod. Phys.*, **80**:885, 2008. (cited on p. 16)

[16] A. Le Boité, G. Orso, and C. Ciuti. Steady-state phases and tunneling-induced instabilities in the driven dissipative bose-hubbard model. *Phys. Rev. Lett.*, **110**:233601, 2013. (cited on p. 47)

[17] L. Boltzmann. *Lectures on gas theory*. Berkeley, University of California Press, 1964. (cited on p. 74)

[18] T. Boulier, H. Terças, D. D. Solnyshkov, Q. Glorieux, E. Giacobino, G. Malpuech, and A. Bramati. Vortex chain in a resonantly pumped polariton superfluid. *Sci. Rep.*, **5**:9230, 2015. (cited on p. 8)

[19] R. W. Boyd. *Nonlinear Optics*. Academic Press, 2008. (cited on pp. 1, 16, and 33)

[20] H.-P. Breuer, E.-M.i Laine, and J Piilo. Measure for the degree of non-markovian behavior of quantum processes in open systems. *Phys. Rev. Lett.*, **103**:210401, 2009. (cited on p. 21)

[21] H.-P. Breuer and F. Petruccione. The theory of open quantum systems. Clarendon Press, Oxford, 2006. (cited on pp. 11, 26, 27, 35, 57, 68, and 109)

[22] O. T. Brown and M. J. Hatmann. Localization to delocalization transition in a driven nonlinear cavity array. *arXiv:1709.02165*, 2016. (cited on p. 55)

[23] D. L. Burke, R. C. Field, G. Horton-Smith, J. E. Spencer, D. Walz, S. C. Berridge, W. M. Bugg, K. Shmakov, A. W. Weidemann, C. Bula, K. T. McDonald, E. J. Prebys, C. Bamber, S. J. Boege, T. Koffas, T. Kotseroglou, A. C. Melissinos, D. D. Meyerhofer, D. A. Reis, , and W. Ragg. *Positron Production in Multiphoton Light-by-Light Scattering*. *Phys. Rev. Lett.*, **79**:1626, 1997. (cited on p. 1)

[24] A. Caldeira and A. J. Leggett. Influence of dissipation on quantum tunneling in macroscopic systems. *Phys. Rev. Lett.*, **46**:211, 1981. (cited on p. 73)

[25] A. Canaguier-Durand, C. Genet, A. Lambrecht, T. W. Ebbesen, and S. Reynaud. Non-markovian polariton dynamics in organic strong coupling. *Eur. Phys. J. D*, **69**:24, 2015. (cited on p. 11)

[26] B. Capogrosso-Sansone, N. Prokof'ev, and B. Svistunov. Phase diagram and thermodynamics of the three-dimensional bose-hubbard model. *Phys. Rev. B*, **75**:134302, 2007. (cited on p. 15)

[27] B. Capogrosso-Sansone and S. G. Sö. (cited on p. 15)

[28] I. Carusotto and C. Ciuti. Spontaneous microcavity-polariton coherence across the parametric threshold: Quantum monte carlo studies. *Phys. Rev. B*, **72**:125335, 2005. (cited on p. 8)

[29] I. Carusotto and C. Ciuti. Quantum fluids of light. *Rev. Mod. Phys.*, **85**:299, 2013. (cited on pp. 1, 3, 5, 10, 16, 24, 73, 80, and 82)

[30] I. Carusotto, D. Gerace, H. E. Tureci, S. De Liberato, C. Ciuti, and A. Imamoğlu. Fermionized photons in an array of driven dissipative nonlinear cavities. *Phys. Rev. Lett.*, **103**:033601, 2009. (cited on pp. 16 and 23)

[31] W. Casteels, S. Finazzi, A. L. Boité, F. Storme, and C. Ciuti. Truncated correlation hierarchy schemes for driven-dissipative multimode quantum systems. *New J. Phys.*, **18**:093007, 2016. (cited on p. 6)

[32] C.-K. Chan, T. E. Lee, , and S. Gopalakrishnan. Limit-cycle phase in driven-dissipative spin systems. *Phys. Rev. A*, **91**:051601, 2015. (cited on pp. 49 and 51)

[33] A. Chiocchetta and I. Carusotto. Laser operation and bose-einstein condensation: analogies and differences. *arXiv:1503.02816*. (cited on pp. 73 and 90)

[34] A. Chiocchetta and I. Carusotto. Non-equilibrium quasi-condensates in reduced dimensions. *EPL*, **102**:67007, 2013. (cited on p. 73)

[35] A. Chiocchetta and I. Carusotto. A quantum langevin model for non-equilibrium condensation. *Phys. Rev. A*, **90**:023633, 2014. (cited on pp. 8, 73, 80, 82, and 96)

[36] S. Choi, J. Choi, R. Landig, G. Kucsko, H. Zhou, J. Isoya, F. Jelezko, S. Onoda, H. Sumiya, V. Khemani, C. von Keyserlingk, N. Y. Yao, E. Demler, and D. Lukin M. Observation of discrete time-crystalline order in a disordered dipolar many-body system. *Nature*, **543**:221, 2017. (cited on p. 49)

[37] C. Ciuti, G. Bastard, and I. Carusotto. Quantum vacuum properties of the intersubband cavity polariton field. *Phys. Rev. B*, **72**:115303, 2005. (cited on pp. 13 and 25)

[38] C. Ciuti and I. Carusotto. Input-output theory of cavities in the ultrastrong coupling regime: The case of time-independent cavity parameters. *Phys. Rev. A*, **74**:033811, 2006. (cited on pp. 13 and 25)

[39] C. Ciuti, P. Schwendimann, B. Deveaud, and A. Quattropani. Asymmetric angular emission in semiconductor microcavities. *Phys. Rev. B*, **62**:4825, 2000. (cited on p. 8)

[40] J. Clarke and F. K. Wilhelm. Superconducting quantum bits. *Nature*, **453**:1031, 2008. (cited on p. 12)

[41] M. Combescot, O. Betbeder-Matibet, and F. Dubin. The many-body physics of composite bosons. *Phys. Rep.*, **463**:215, 2008. (cited on p. 3)

[42] L. F. Cugliandolo. The effective temperature. **44**:483001, 2011. (cited on p. 90)

[43] J. Dalibard, Y. Castin, and K. Mölmer. Wave-function approach to dissipative processes in quantum optics. *Phys. Rev. Lett.*, 68:580, 1992. (cited on pp. 115 and 116)

[44] T. Damm, D. Dung, . Vewinger, M. Weitz, and J. Schmitt. First-order spatial coherence measurements in a thermalized two-dimensional photonic quantum gas. *Nat. Commun.*, **8**:158, 2017. (cited on p. 11)

[45] L. S. Dang, D. Heger, R. André, F. Bœuf, and R. Romestain. Stimulation of polariton photoluminescence in semiconductor microcavity. *Phys. Rev. Lett.*, **81**:3920, 1998. (cited on p. 4)

[46] H. Deng, H. Haug, and Y. Yamamoto. Exciton-polariton bose-einstein condensation. *Rev. Mod. Phys.*, **82**:1489, 2010. (cited on pp. 4 and 10)

[47] B. Deveaud. *The Physics of Semiconductor Microcavities*. Wiley-VCH, 2007. (cited on pp. 2 and 3)

[48] M. H. Devoret and R. J. Schoelkopf. Superconducting circuits for quantum information: An outlook. *Science*, **339**:1169, 2013. (cited on pp. 12 and 13)

[49] R. H. Dicke. Coherence in spontaneous radiation processes. *Phys. Rev.*, **93**:99, 1954. (cited on p. 26)

[50] S. Diehl, A. Micheli, A. Kantian, B. Kraus, H. P. Büchler, and P. Zoller. Quantum states and phases in driven open quantum systems with cold atoms. *Nat. Phys.*, **4**:878, 2008. (cited on pp. 16, 20, and 73)

[51] N. Dupuis. *Lecture notes on the Bose-Hubbard model*. (cited on pp. 14 and 105)

[52] S. Ejima, H. Fehske, F. Gebhard, K. z. Münster, M.l Knap, E. Arrigoni, and W. v. d. Linden. Characterization of mott-insulating and superfluid phases in the one-dimensional bose-hubbard model. *Phys. Rev. A*, **85**:053644, 2012. (cited on pp. 14 and 15)

[53] D. V. Else, B. Bauer, and Chetan Nayak. Floquet time crystals. *Phys. Rev. Lett.*, **117**:090402, 2016. (cited on p. 49)

[54] S. J. Van Enk and H. J. Kimble. Single atom in free space as a quantum aperture. *Phys. Rev. A*, **61**:051802, 2000. (cited on p. 12)

[55] A. Faraon, I. Fushman, D. Englund, N. Stoltz, P. Petroff, and J. Vuckovic. Coherent generation of non-classical light on a chip via photon-induced tunnelling and blockade. *Nat. Phys.*, **4**:859, 2008. (cited on pp. 1 and 12)

[56] A.L. Fetter and J.D. Walecka. *Quantum theory of many-particle systems*. Dover Publications, 2003. (cited on p. 45)

[57] R. P. Feynman and F. L. Vernon Jr. The theory of a general quantum system interacting with a linear dissipative system. *Ann. Phys.*, **24**:118, 1963. (cited on p. 73)

[58] S. Finazzi, A. Le Boité, F. Storme, A. Baksic, and C. Ciuti. Corner-space renormalization method for driven-dissipative two-dimensional correlated systems. *Phys. Rev. Lett.*, **115**:080604, 2015. (cited on pp. 42 and 43)

[59] M. P. A. Fisher, P. B. Weichman, G. Grinstei, and D. S. Fisher. Boson localization and the superfluid-insulator transition. *Phys. Rev. B*, **40**:546, 1989. (cited on pp. 1, 13, 14, 16, 18, 40, 43, 60, 61, 62, and 105)

[60] M. Fitzpatrick, N. M. Sundaresan, A. C. Y. Li, J. Koch, and A. A. Houck. Observation of a dissipative phase transition in a one-dimensional circuit qed lattice. *Phys. Rev. X*, **7**:011016, 2017. (cited on pp. 14 and 16)

[61] L. Foini and A. Gambassi L. F. Cugliandolo. Dynamic correlations, fluctuation-dissipation relations, and effective temperatures after a quantum quench of the transverse field ising chain. *J. Stat. Mech.*, page P09011, 2012. (cited on p. 90)

[62] M. Foss-Feig, P. Niroula, J. T. Young, M. Hafezi, A. V. Gorshkov, R. M. Wilson, and M. F. Maghrebi. Emergent equilibrium in many-body optical bistability. *Phys. Rev. A*, **95**:043826, 2017. (cited on p. 16)

[63] C. W. Gardiner and P. Zoller. Quantum Noise. Springer, 2004. (cited on pp. 6, 26, 31, 35, and 57)

[64] T. Giarmarchi. *Quantum physics in one dimension*. Oxford University Press, 2003. (cited on p. 51)

[65] G. Luca Giorgi, F. Galve, and R. Zambrini. Quantum darwinism and non-markovian dissipative dynamics from quantum phases of the spin-1/2 xx model. *Phys. Rev. A*, **92**:022105, 2015. (cited on p. 21)

[66] N. A. Gippius, I. A. Shelykh, D. D. Solnyshkov, S. S. Gavrilov, Yuri G. Ruboand A. V. Kavokin, S. G. Tikhodeev, and G. Malpuech. Polarization multistability of cavity polaritons. *Phys. Rev. Lett.*, **98**:236401, 2007. (cited on pp. 8 and 16)

[67] M. Girardeau. Relationship between systems of impenetrable bosons and fermions in one dimension. *J. Math. Phys.*, **1**:516, 1960. (cited on pp. 1, 16, and 44)

[68] S. M. Girvin. *Lecture notes of les Houches: Circuit QED: Superconducting Qubits Coupled to Microwave Photons*. Oxford University Press, 2014. (cited on pp. 12, 13, and 15)

[69] A D. Greentree, C. Tahan, J. H. Cole, and L. C. L. Hollenberg. Quantum phase transitions of light. *Nat. Phys.*, **2**:856, 2006. (cited on p. 15)

[70] M. Greiner, O. Mandel, T. Esslinger, T. W. Hänsch, and I.l Bloch. Quantum phase transition from a superfluid to a mott insulator in a gas of ultracold atoms. *Nature*, **415**:39, 2002. (cited on p. 15)

[71] G. Grinstein, C. Jayaprakash, and R. Pandit. Conjectures about phase turbulence in the complex ginzburg-landau equation. *Physica D: Nonlinear Phenomena*, **90**:96, 1996. (cited on p. 7)

[72] T. Grujic, S. R. Clark, D. Jaksch, and D. G. Angelakis. Non-equilibrium many-body effects in driven nonlinear resonator arrays. *New. J. Phys.*, **14**:103025, 2012. (cited on p. 15)

[73] G. Grynberg, A. Aspect, and C. Fabre. *Introduction to quantum optics.* Cambridge University press, 2010. (cited on p. 87)

[74] M. Hafezi, P. Adhikari, and J. M. Taylor. Chemical potential for light by parametric coupling. *Phys. Rev. B*, **92**:174305, 2015. (cited on pp. 19 and 20)

[75] S. Haroche and J.-M. Raimond. *Exploring the Quantum: Atoms, Cavities, and Photons.* Oxford Graduate Texts, 2006. (cited on pp. 12 and 50)

[76] M. J. Hartmann. Quantum simulation with interacting photons. *J. Opt.*, **18**:104005, 2016. (cited on pp. 1, 13, 16, 24, 40, and 73)

[77] M. J. Hartmann, Fernando, G. S. L. Brand ao, and M. B. Plenio. Quantum many-body phenomena in coupled cavity arrays. *Las. Phot. Rev.*, **2**:527, 2008. (cited on pp. 12 and 14)

[78] H. Haug, T. D. Doan, and D. B. Tran Thoai. Quantum kinetic derivation of the nonequilibrium gross-pitaevskii equation for nonresonant excitation of microcavity polaritons. *Phys. Rev. B*, **89**:153302, 2014. (cited on p. 8)

[79] H. Haug and A.-P. Jauho. *Quantum Kinetics in Transport and Optics of Semiconductors.* Springer, 2nd edition, 2007. (cited on p. 8)

[80] L. He, L. M. Sieberer, and S. Diehl. Space-time vortex driven crossover and vortex turbulence phase transition in one-dimensional driven open condensates. *Phys. Rev. Lett.*, **118**:085301, 2017. (cited on pp. 7, 48, and 73)

[81] A. J. Hoffman, S. J. Srinivasan, S. Schmidt, L. Spietz, J. Aumentado, H. E. Türeci, and A. A. Houck. Dispersive photon blockade in a superconducting circuit. *Phys. Rev. Lett.*, **107**:053602, 2011. (cited on p. 70)

[82] M. Hohenadler, M. Aichhorn, S. Schmidt, and L. Pollet. Dynamical critical exponent of the jaynes-cummings-hubbard model. *Phys. Rev. A*, **84**:041608, 2011. (cited on p. 15)

[83] J. J. Hopfield. *Theory of the Contribution of Excitons to the Complex Dielectric Constant of Crystals. Phys. Rev.*, **112**:1555, 1958. (cited on p. 1)

[84] A. A. Houck, H. E. Türeci, and J. Koch. On-chip quantum simulation with superconducting circuits. *Nat. Phys.*, 8:292, 2012. (cited on pp. 1, 12, 13, 14, and 24)

[85] K. Iga. Surface-emitting laser-its birth and generation of new optoelectronics field. *IEEE J. Sel. Top. Quantum Electron.*, 6(6):1201, 2000. (cited on pp. 5, 79, and 96)

[86] A. Imamoğlu, H. Schmidt, G. Woods, and M. Deutsch. Strongly interacting photons in a nonlinear cavity. *Phys. Rev. Lett.*, **79**:1467, 1997. (cited on pp. 1 and 12)

[87] D. Rossini J. Jin, M. Leib, M. J. Hartmann, and Rosario Fazio. Steady-state phase diagram of a driven qed-cavity array with cross-kerr nonlinearities. *Phys. Rev. A*, **90**:023827, 2014. (cited on pp. 49 and 65)

[88] C. Gies P. Gartner M.J. Hartmann J. Ruiz-Rivas, E. del Valle. Spontaneous, collective coherence in driven, dissipative cavity arrays. *Phys. Rev. A*, **90**:033808, 2014. (cited on pp. 8 and 17)

[89] Z.-J. Jean. *Quantum field theory and critical phenomena*. Clarendon Press, Oxford, 1996. (cited on p. 47)

[90] K. Ji, Kai, V. N. Gladilin, and M. Wouters. Temporal coherence of one-dimensional nonequilibrium quantum fluids. *Phys. Rev. B*, 91:045301, 2015. (cited on p. 96)

[91] N. Jia, N. Schine, A. Georgakopoulos, A. Ryou, A. Sommer, and J. Simon. Strongly correlated photons on a chip. *arXiv:1705.07475*, 2017. (cited on p. 1)

[92] J. Jin, A. Biella, O. Viyuela, L. Mazza, J. Keeling, R. Fazio, and D. Rossini. Cluster mean-field approach to the steady-state phase diagram of dissipative spin systems. *Phys. Rev. X*, **6**:031011, 2016. (cited on pp. 60 and 65)

[93] J. Jin, D. Rossini, R. Fazio, M. Leib, and M. J. Hartmann. Photon solid phases in driven arrays of nonlinearly coupled cavities. *Phys. Rev. Lett.*, **110**:16605, 2013. (cited on pp. 47 and 65)

[94] W. E. Lamb Jr. Theory of an optical maser. *Phys. Rev.*, **134**:A1429, 1964. (cited on p. 5)

[95] A. Kamenev. *Field Theory of Non-Equilibrium Systems*. Cambridge University Press, 2011. (cited on p. 48)

[96] E. Kapit. Hardware-efficient and fully autonomous quantum error correction in superconducting circuits. *Phys. Rev. Lett.*, **116**:150501, 2016. (cited on pp. 16, 20, 21, and 55)

[97] E. Kapit, M. Hafezi, and S. H. Simon. Induced self-stabilization in fractional quantum hall states of light. *Phys. Rev. X*, **4**:031039, 2014. (cited on pp. 17, 18, 19, 23, 43, 55, and 116)

[98] E. Kapit and E. Mueller. Exact parent hamiltonian for the quantum hall states in a optical lattice. *Phys. Rev. Lett.*, **105**:215303, 2010. (cited on pp. 17, 18, 43, and 55)

[99] J. Kasprzak, M. Richard, S. Kundermann, A. Baas, P. Jeambrun, J. M. J. Keeling, F. M. Marchetti, M. H. Szymańska, R. André, J. L. Staehli, V. Savona, P. B. Littlewood, B. Deveaud, and Le Si Dang. Bose–einstein condensation of exciton polaritons. *Nature*, **443**:409, 2006. (cited on pp. 1, 2, 3, 4, 6, 8, 9, 73, 74, and 94)

[100] J. Kasprzak, D. D. Solnyshkov, R. André, L. S. Dang, and G. Malpuech. Formation of an exciton polariton condensate: Thermodynamic versus kinetic regimes. *Phys. Rev. Lett.*, **101**:146404, 2008. (cited on pp. 8 and 10)

[101] S. Kena-Cohen and S. R. Forrest. Room-temperature polariton lasing in an organic single-crystal microcavity. *Nat. Photon.*, **4**:371, 2010. (cited on pp. 8 and 73)

[102] E. H. Kennard. On the thermodynamics of fluorescence. *Phys. Rev.*, **11**:29, 1918. (cited on pp. 21, 44, and 76)

[103] V. Khemani, A. Lazarides, R. Moessner, and S. L. Sondhi. Phase structure of driven quantum systems. *Phys. Rev. Lett.*, **116**:250401, 2016. (cited on p. 49)

[104] H. J. Kimble. Strong interactions of single atoms and photons in cavity qed. *Phys. Scripta*, **T71**:127, 1998. (cited on p. 12)

[105] P. Kirton and J. Keeling. Nonequilibrium model of photon condensation. *Phys. Rev. Lett.*, **111**:100404, 2013. (cited on pp. 11 and 73)

[106] P. Kirton and J. Keeling. Thermalization and breakdown of thermalization in photon condensates. *Phys. Rev. A*, **91**:033826, 2015. (cited on pp. 11 and 73)

[107] J. Klaers, J. Schmitt, T. Damm, F. Vewinger, and M. Weitz. Statistical physics of bose-einstein-condensed light in a dye microcavity. *Phys. Rev. Lett.*, **108**:160403, 2012. (cited on p. 11)

[108] J. Klaers, J. Schmitt, F. Vewinger, and M. Weitz. Bose–einstein condensation of photons in an optical microcavity. *Nature*, **468**:545, 2010. (cited on pp. 8, 11, and 73)

[109] J. Klaers, F. Vewinger, and M. Weitz. Thermalization of a two-dimensional photonic gas in a 'white wall' photon box. *Nat. Phys.*, **6**:512, 2010. (cited on pp. 8 and 11)

[110] J. Koch and K. Le Hur. Superfluid-mott-insulator transition of light in the jaynes-cummingsb lattice. *Phys. Rev. A*, **80**:023811, 2009. (cited on p. 15)

[111] J. M. Kosterlitz and D. J. J. Thouless. Ordering, metastability and phase transitions in two-dimensional systems. *J. Phys. C: Solid State Phys.*, 6:1180, 1973. (cited on pp. 15, 48, and 51)

[112] R. Kubo. Statistical-mechanical theory of irreversible processes. i. general theory and simple applications to magnetic and conduction problems. *J. Phys. Soc. Jpn.*, **12(6)**:570, 1957. (cited on p. 90)

[113] R. Kubo. The fluctuation-dissipation theorem. *Rep. Prog. Phys.*, **29**:255, 1966. (cited on pp. 37, 74, and 89)

[114] T. D. Kühner, S. R. White, and H. Monien. One-dimensional bose-hubbard model with nearest-neighbor interaction. *Phys. Rev. B*, **61**:12474, 2000. (cited on pp. 15, 61, and 62)

[115] P. P. Orth L. Henriet, Z. Ristivojevic and K. Le Hur. Quantum dynamics of the driven and dissipative rabi model. *Phys. Rev. A*, **90**:023820, 2014. (cited on pp. 16, 23, and 33)

[116] C. Lang, D. Bozyigit, C. Eichler, L. Steffen, J. M. Fink, A. A. Abdumalikov, M. Baur Jr., S. Filipp, M. P. da Silva, A. Blais, and A. Wallraff. Observation of resonant photon blockade at microwave frequencies using correlation function measurements. *Phys. Rev. Lett.*, **106**:243601, 2011. (cited on pp. 1 and 12)

[117] R. B. Laughlin. Anomalous quantum hall effect: An incompressible quantum fluid with fractionally charged excitations. *Phys. Rev. Lett.*, **50**:1395, 1983. (cited on p. 1)

[118] J. Lebreuilly, A. Biella, F. Storme, D. Rossini, I. Carusotto, R. Fazio, and C. Ciuti. Stabilizing strongly correlated photon fluids with non-Markovian reservoirs . *Phys. Rev. A*, **96**:033828, 2017. (cited on pp. 17, 18, and 56)

[119] J. Lebreuilly, I. Carusotto, and M. Wouters. Towards strongly correlated photons in arrays of dissipative nonlinear cavities under a frequency-dependent incoherent pumping. *C. R. Phys.*, **17** (8):836, 2016. (cited on pp. 17, 18, 23, 24, 26, 54, 55, 58, 60, 73, and 74)

[120] J. Lebreuilly, A. Chiocchetta, and I. Carusotto. Pseudo-thermalization in driven-dissipative non-Markovian open quantum systems. *arXiv:1710.09602 (submitted for publication)*. (cited on p. 74)

[121] T. E. Lee, H. Häffner, and M. C. Cross. Antiferromagnetic phase transition in a nonequilibrium lattice of rydberg atoms. *Phys. Rev. A*, **84**:031402, 2011. (cited on p. 49)

[122] E. H. Lieb and W. Liniger. Exact analysis of an interacting bose gas. i. the general solution and the ground state. *Phys. Rev.*, **130**:1605, 1963. (cited on pp. 16 and 44)

[123] B.-H. Liu, L. Li, Y.-F. Huang, C.-F. Li, G.-C. Guo, E.-M. Laine, H.-P. Breuer, and J. Piilo. Experimental control of the transition from markovian to non-markovian dynamics of open quantum systems. *Nat. Phys.*, **7**:931, 2011. (cited on p. 20)

[124] P.-Y. Lo, H.-N. Xiong, and W.-M. Zhang. Breakdown of bose-einstein distribution in photonic crystals. *Sci. Rep.*, **4**:5720, 2014. (cited on p. 21)

[125] H. E. Türeci M. Biondi, G. Blatter and S. Schmidt. Nonequilibrium gas-liquid transition in the driven-dissipative photonic lattice. *arXiv:1611.00697.* (cited on pp. 16, 23, 33, and 47)

[126] R. Ma, C. Owens, A. Houck, D. I. Schuster, and J. Simon. Autonomous stabilizer for incompressible photon fluids and solids. *Phys. Rev. A*, **95**:043811, 2017. (cited on pp. 17, 18, 23, 62, 68, 69, and 71)

[127] H. Mabuchi and A. C. Doherty. Cavity quantum electrodynamics:coherence in context. *Nature*, **298**:1372, 2002. (cited on pp. 12 and 13)

[128] A. Majumdar, M. Bajcsy, and J. Vučković. Probing the ladder of dressed states and nonclassical light generation in quantum-dot–cavity qed. *Phys. Rev. A*, **85**:041801 (R), 2012. (cited on p. 35)

[129] G. Malpuech, A. Kavokin, A. Di Carlo, and J. J. Baumberg. Polariton lasing by exciton-electron scattering in semiconductor microcavities. *Phys. Rev. B*, **65**:153310, 2002. (cited on pp. 8, 11, and 94)

[130] L. Mandel and E. Wolf. *Ordering, metastability and phase transitions in two-dimensional systems. J. of Phys. C*, **6**:1181, 1973. (cited on p. 7)

[131] L. Mandel and E. Wolf. *Optical coherence and quantum optics.* Cambridge University Press, 1995. (cited on pp. 6 and 78)

[132] M. Maragkou, A. J. D. Grundy, T. Ostatnický, and P. G. Lagoudakis. Longitudinal optical phonon assisted polariton laser. *Appl. Phys. Lett.*, **97**:111110, 2010. (cited on pp. 9 and 94)

[133] F. M. Marchetti, M. H. Szymańska, C. Tejedor, and D. M. Whittaker. Spontaneous and triggered vortices in polariton optical-parametric-oscillator superfluids. *Phys. Rev. Lett.*, **62**:063902, 2010. (cited on p. 8)

[134] M. Marthaler, Y. Utsumi, D. S. Golubev., A. Shnirman, and G. Schön. Lasing without inversion in circuit quantum electrodynamics. *Phys. Rev. Lett.*, 107:093901, 2011. (cited on p. 9)

[135] P. C. Martin and J. Schwinger. Theory of many-particle systems. i. *Phys. Rev.*, **115**:1342, 1959. (cited on p. 90)

[136] N. D. Mermin and H. Wagner. Absence of ferromagnetism or antiferromagnetism in one- or two-dimensional isotropic heisenberg models. *Phys. Rev. Lett.*, **17**:1133, 1966. (cited on pp. 48 and 61)

[137] C. Mora and Y. Castin. Extension of bogoliubov theory to quasi-condensates. *Phys. Rev A*, **67**:053615, 2003. (cited on pp. 9, 51, and 78)

[138] N. F. Mott. The basis of the electron theory of metals, with special reference to the transition metals. *Proc. Phys. Soc. Sec. A*, **62**:416, 1949. (cited on p. 15)

[139] V. Mukherjee, V. Giovannetti, R. Fazio, S. F. Huelga, T. Calarco, and S. Montangero. Efficiency of quantum controlled non-markovian thermalization. *New. J. Phys*, **17**:063031, 2015. (cited on p. 21)

[140] C. J. Myatt, B. E. King, Q. A. Turchette, C. A. Sackett, D. Kielpinski, W. M. Itano, C. Monroe, and D. J. Wineland. Decoherence of quantum superpositions through coupling to engineered reservoirs. *Nature*, **403**:269, 2000. (cited on pp. 16 and 20)

[141] K. Sengupta N. and Dupuis. Mott-insulator-to-superfluid transition in the bose-hubbard model: A strong-coupling approach. *Phys. Rev. A*, 71:033629, 2005. (cited on p. 105)

[142] S. Nakajima. On quantum theory of transport phenomena: Steady diffusion. *Prog. Theor. Phys.*, **20**:948, 1958. (cited on p. 26)

[143] P. Nataf and C. Ciuti. No-go theorem for superradiant quantum phase transitions in cavity qed and counter-example in circuit qed. *Phys. Rev. Lett.*, **104**:023601, 2010. (cited on p. 25)

[144] C. Noh and D. G. Angelakis. Quantum simulations and many-body physics with light. *Rep. Prog. Phys.*, **80**:016401, 2017. (cited on pp. 12 and 24)

[145] C. Sánchez Mu noz, E. del Valle, A. González Tudela, K. Müller, S. Lichtmannecker, M. Kaniber, C. Tejedor, J. J. Finley, and F. P. Laussy. Emitters of n-photon bundles. *Nat. Photon.*, **8**:550, 2014. (cited on p. 35)

[146] D. Cotter P. N. Butcher. The Elements of NonlinearOptics. Cambridge University Press, 1991. (cited on pp. 16 and 33)

[147] T. Peyronel, O. Firstenberg, Q.-Y. Liang, S. Hofferberth, A. V. Gorshkov, T. Pohl, M. D. Lukin, and V. Vuletić. Quantum nonlinear optics with single photons enabled by strongly interacting atoms. *Nature*, **488**:57, 2012. (cited on pp. 1 and 12)

[148] F. Piazza and H. Ritsch. Self-ordered limit cycles, chaos, and phase slippage with a superfluid inside an optical resonator. *Phys. Rev. Lett.*, **115**:163601, 2015. (cited on p. 49)

[149] F. Piazza and P. Strack. Umklapp superradiance with a collisionless quantum degenerate fermi gas. *Phys. Rev. Lett.*, **112**:143003, 2014. (cited on p. 25)

[150] D. Pines and P. Nozières. *The Theory of Quantum Liquids, Vol. 2.* Addison-Wesley, 1998. (cited on p. 1)

[151] L. Pitaevskii and S. Stringari. *Bose-Einstein Condensation.* Oxford University Press, 2003. (cited on pp. 1, 6, 7, and 78)

[152] J. D. Plumhof, T. Stöferle, L. Mai, U. Scherf, and R. F. Mahrt. Room-temperature bose–einstein condensation of cavity exciton–polaritons in a polymer. *Nat. Mat.*, **13**:247, 2014. (cited on pp. 8 and 73)

[153] D. Porras, C. Ciuti, J.J. Baumberg, and C. Tejedor. Polariton dynamics and bose-einstein condensation in semiconductor microcavities. *Phys. Rev. B*, **66**:085304, 2002. (cited on pp. 3, 8, 10, 11, 73, and 94)

[154] J. F. Poyatos, J. I. Cirac, , and P. Zoller. Quantum reservoir engineering with laser cooled trapped ions. *Phys. Rev. Lett.*, **77**:4728, 1996. (cited on p. 20)

[155] J. D. Pritchard, D. Maxwell, A. Gauguet, K. J. Weatherill, M. P. A. Jones, and C. S. Adams. Cooperative atom-light interaction in a blockaded rydberg ensemble. *Phys. Rev. Lett.*, **105**:193603, 2010. (cited on p. 12)

[156] M. V. Regemortel, W. Casteels, I. Carusotto, and M. Wouters. Spontaneous beliaev-landau scattering out of equilibrium. *arXiv:1704.01865*, 2017. (cited on p. 6)

[157] A. Reinhard, T. Volz, M. Winger, A. Badolato, K. J. Hennessy, E. L. Hu, and A. Imamoğlu. Strongly correlated photons on a chip. *Nat. Photon.*, **6**:93, 2012. (cited on pp. 1 and 12)

[158] A. Reiserer and G. Rempe. Cavity-based quantum networks with single atoms and optical photons. *Rev. Mod. Phys.*, **87**:1379, 2015. (cited on p. 12)

[159] C. Rigetti, J. M. Gambetta, S. Poletto, B. L. T. Plourde, J. M. Chow, A. D. Córcoles, J. A. Smolin, S. T. Merkel, J. R. Rozen, G. A. Keefe, M. B. Rothwell, M. B. Ketchen, and M. Steffen. Superconducting qubit in a waveguide cavity with a coherence time approaching 0.1 ms. *Phys. Rev. B*, **86**:100506(R), 2012. (cited on pp. 59, 62, and 71)

[160] P. Ring and P. Schuck. *The Nuclear Many-Body Problem.* Springer, 2004. (cited on p. 1)

[161] G. Rochat, C. Ciuti, V. Savona, C. Piermarocchi, A. Quattropani, and P. Schwendimann. Excitonic bloch equations for a two-dimensional system of interacting excitons. *Phys. Rev. B*, **61**:13856, 2000. (cited on p. 3)

[162] F. J. Rodríguez, L. Quiroga, C. Tejedor, M. D. Martín, L. Vi na, and R. André. Control of non-markovian effects in the dynamics of polaritons in semiconductor microcavities. *Phys. Rev. B*, **78**:035312, 2008. (cited on p. 11)

[163] A. Rundquist, M. Bajcsy, A. Majumdar, T. Sarmiento, K. Fischer, K. G. Lagoudakis, S. Buckley, A. Y. Piggott, and J. Vučković. Nonclassical higher-order photon correlations with a quantum dot strongly coupled to a photonic-crystal nanocavity. *Phys. Rev. A*, **90**:023846, 2014. (cited on p. 35)

[164] H. Satz, S. Sarkar, and B. Sinha. *The Physics of the Quark-Gluon Plasma*. Springer, 2010. (cited on p. 1)

[165] P. G. Savvidis, J. J. Baumberg, R. M. Stevenson, M. S. Skolnick, D. M. Whittaker, and J. S. Roberts. Angle-resonant stimulated polariton amplifier. *Phys. Rev. Lett.*, **84**:1547, 2000. (cited on p. 8)

[166] P. G. Savvidis, J. J. Baumberg, R. M. Stevenson, M. S. Skolnick, D. M. Whittaker, and J. S. Roberts. Theory of the angle-resonant polariton amplifier. *Phys. Rev. B*, **62**:R13278, 2000. (cited on p. 8)

[167] A. L. Schawlow and C. H. Townes. Infrared and optical masers. *Phys. Rev.*, **112**:1940, 1958. (cited on p. 7)

[168] N. Schine, A. Ryou, A. Gromov, A. Sommer, and J. Simon. Synthetic landau levels for photons. *Nature*, **534**:671, 2016. (cited on p. 17)

[169] J. Schmitt, T. Damm, D. Dung F. Vewinger, J. Klaers, and Martin Weitz. Thermalization kinetics of light: From laser dynamics to equilibrium condensation of photons. *Phys. Rev. A*, **92**:011602(R), 2015. (cited on pp. 11, 21, and 73)

[170] M. O. Scully and M. S. Zubairy. *Quantum Optics*. Cambridge University Press, 1997. (cited on pp. 5, 17, 31, and 78)

[171] A. Shabani and H. Neven. Artificial quantum thermal bath: Engineering temperature for a many-body quantum system. *Phys. Rev. A*, **94**:052301, 2016. (cited on pp. 38, 74, and 94)

[172] I. A. Shelykh, T. C. H. Liew, and A. V. Kavokin. Spin rings in bi-stable planar semiconductor microcavities. *Phys. Rev. Lett.*, **100**:116401, 2008. (cited on pp. 8 and 16)

[173] F. Shibata and T. Arimitsu. Expansion formulas in nonequilibrium statistical mechanics. *J. Phys. Soc. Jpn.*, **49**:891, 1980. (cited on p. 26)

[174] F. Shibata, Y. Takahashi, and N. Hashitsume. A generalized stochastic liouville equation. non-markovian versus memoryless master equations. *J. Stat. Phys.*, **17**:171, 1977. (cited on p. 26)

[175] L. M. Sieberer, A. Chiocchetta, A. Gambassi, U. C. Täuber, and S. Diehl. Thermodynamic equilibrium as a symmetry of the schwinger-keldysh action. *Phys. Rev. B*, **92**:134307, 2015. (cited on pp. 48 and 73)

[176] L. M. Sieberer, S. D. Huber, E. Altman, and S. Diehl. Dynamical critical phenomena in driven-dissipative systems. *Phys. Rev. Lett.*, **110**:1955301, 2013. (cited on pp. 7, 48, 73, 78, and 96)

[177] L. M. Sieberer, S. D. Huber, E. Altman, and S. Diehl. Nonequilibrium functional renormalization for driven-dissipative bose-einstein condensation. *Phys. Rev. B*, **89**:134310, 2014. (cited on pp. 7, 73, 78, and 96)

[178] D. W. Snoke. The quantum boltzmann equation in semiconductor physics. *Ann. Phys.*, **523**:87, 2011. (cited on p. 6)

[179] I. B. Spielman, W. D. Phillips, and J. V. Porto. Mott-insulator transition in a two-dimensional atomic bose gas. *Phys. Rev. Lett.*, **98**:080404, 2007. (cited on pp. 15 and 16)

[180] B. I. Stepanov. A universal relation between the absorption and luminescence spectra of complex molecules. *Soviet Phys. - Doklady*, **2**:81, 1957. (cited on pp. 21, 44, and 76)

[181] R. M. Stevenson, V. N. Astratov, M. S. Skolnick, D. M. Whittaker, M. Emam-Ismail, A. I. Tartakovskii, P. G. Savvidis, J. J. Baumberg, and J. S. Roberts. Continuous wave observation of massive polariton redistribution by stimulated scattering in semiconductor microcavities. *Phys. Rev. Lett.*, **85**:3680, 2000. (cited on p. 8)

[182] T. Stöferle, H. Moritz, C. Schori, M. Köhl, and T. Esslinger. Transition from a strongly interacting 1d superfluid to a mott insulator. *Phys. Rev. Lett.*, **92**:13, 2004. (cited on p. 15)

[183] M. H. Szymanska, J. Keeling, and P. B. Littlewood. Quantum condensation in an incoherently pumped dissipative system. *Phys.Rev. Lett.*, **96**:230602, 2006. (cited on pp. 80 and 82)

[184] A. I. Tartakovskii, M. Emam-Ismail, R. M. Stevenson, M. S. Skolnick, V. N. Astratov, D. M. Whittaker, J. J. Baumberg, and J. S. Roberts. Relaxation bottleneck and its suppression in semiconductor microcavities. *Phys. Rev. B*, **62**:2283, 2000. (cited on p. 10)

[185] F. Tassone, C. Piermarocchi, V. Savona, A. Quattropani, and P. Schwendimann. Bottleneck effects in the relaxation and photoluminescence of microcavity polaritons. *Phys. Rev. B*, **56**:7554, 1997. (cited on pp. 8 and 10)

[186] F. Tassone and Y. Yamamoto. Exciton-exciton scattering dynamics in a semiconductor microcavity and stimulated scattering into polaritons. *Phys. Rev. B*, **59**:10830, 1999. (cited on pp. 4, 8, and 10)

[187] U. C. Täuber. *A Field Theory Approach to Equilibrium and Non-Equilibrium Scaling Behavior*. Cambridge University Press, 2014. (cited on pp. 47 and 48)

[188] M. Thorwart, J. Eckel, J.H. Reina, P. Nalbach, and S. Weiss. Enhanced quantum entanglement in the non-markovian dynamics of biomolecular excitons. *Chem. Phys. Lett.*, **478**:234, 2009. (cited on p. 21)

[189] M. Tinkham. *Introduction to Superconductivity, 2nd ed.* Dover Publications, 2004. (cited on p. 1)

[190] R. C. Tolman. *The Principles of Statistical Mechanics*. Oxford University Press, 1938. (cited on p. 74)

[191] A. Tomadin, S. Diehl, and P. Zoller. Nonequilibrium phase diagram of a driven and dissipative many-body system. *Phys. Rev. A*, **83**:013611, 2011. (cited on pp. 47 and 51)

[192] A. Tomadin and R. Fazio. Many-body phenomena in qed-cavity arrays. *J. Opt. Soc. Am. B*, **27**:A130, 2010. (cited on pp. 12, 16, 23, and 47)

[193] R. O. Umucalılar and I. Carusotto. Fractional quantum hall states of photons in an array of dissipative coupled cavities. *Phys. Rev. Lett.*, **108**:206809, 2012. (cited on pp. 16 and 23)

[194] R. O. Umucalılar and I. Carusotto. Probing few-particle laughlin states of photons via correlation measurements. *Phys. Rev. A*, **89**:023803, 2014. (cited on pp. 16 and 23)

[195] R. O. Umucalılar and I. Carusotto. Generation and spectroscopic signatures of a fractional quantum hall liquid of photons in an incoherently pumped optical cavity. *arxiv:1708.05441*, 2017. (cited on pp. 17, 18, 19, 23, and 43)

[196] S. Utsunomiya, L. Tian, G. Roumpos, C. W. Lai, N. Kumada, T. Fujisawa, M. Kuwata-Gonokami, A. Löffler, S. Höfling, A. Forchel, and Y. Yamamoto. Observation of bogoliubov excitations in exciton-polariton condensates. *Nat. Phys.*, **4**:700, 2008. (cited on p. 6)

[197] D. van Oosten, P. van der Straten, and H. T. C. Stoof. Quantum phases in an optical lattice. *Phys. Rev. A*, **63**:053601, 2001. (cited on p. 105)

[198] F. Verstraete, J. J. Garcìa-Ripoll, and J. I. Cirac. Matrix product density operators: Simulation of finite-temperature and dissipative systems. *Phys. Rev. Lett.*, **93**:207204, 2004. (cited on p. 42)

[199] G. Wachtel, L. M. Sieberer, E. Altman, and S. Diehl. Electrodynamic duality and vortex unbinding in driven-dissipative condensates. *Phys. Rev. B*, **94**:104520, 2016. (cited on pp. 7, 48, 51, 73, and 78)

[200] Y.-D. Wang and A. A. Clerk. Reservoir-engineered entanglement in optomechanical systems. *Phys. Rev. Lett.*, **110**:253601, 2013. (cited on pp. 16 and 20)

[201] Y. K. Wang and F. T. Hioe. Phase transition in the dicke model of superradiance. *Phys. Rev. A*, **7**:831, 1973. (cited on p. 25)

[202] H. Watanabe and M. Oshikawa. Absence of quantum time crystals. *Phys. Rev. Lett.*, **114**:251603, 2015. (cited on p. 49)

[203] H. Weimer, M. Müller, I. Lesanovsky, P. Zoller, and H. P. Büchler. A rydberg quantum simulator. *Nat. Phys.*, **6**:382, 2010. (cited on pp. 16 and 20)

[204] C. E. Whittaker, B. Dzurnak, O. A. Egorov, G. Buonaiuto, P. M. Walker, E. Cancellieri, D. M. Whittaker, E. Clarke, S. S. Gavrilov, M. S. Skolnick, and D. N. Krizhanovskii. Polariton pattern formation and photon statistics of the associated emission. *Phys. Rev. X*, **7**:031033, 2017. (cited on p. 8)

[205] F. Wilczek. Quantum time crystals. *Phys. Rev. Lett.*, **109**:160401, 2012. (cited on p. 49)

[206] K. G. Wilson. The renormalization group: Critical phenomena and the kondo problem. *Rev. Mod. Phys.*, 47:773, 1975. (cited on p. 47)

[207] M. M. Wolf, J. Eisert, T. S. Cubitt, and J. I. Cirac. Assessing non-markovian quantum dynamics. *Phys. Rev. Lett.*, **101**:150402, 2008. (cited on p. 21)

[208] M. Wouters and I. Carusotto. Excitations in a nonequilibrium bose-einstein condensate of exciton polaritons. *Phys. Rev. Lett.*, **99**:140402, 2007. (cited on pp. 5, 6, 7, 80, and 82)

[209] M. Wouters and I. Carusotto. Superfluidity and critical velocities in nonequilibrium bose-einstein condensates. *Phys. Rev. Lett.*, **105**:020602, 2010. (cited on pp. 6, 7, and 11)

[210] H.-N. Xiong, P.-Y. Lo, , W.-M. Zhang, F. Nori, and D. Hsuan Feng. Non-markovian dynamics impact on the foundations of statistical mechanics. *Sci. Rep.*, **5**:13353, 2015. (cited on p. 21)

[211] F. Galve R. Zambrini and S. Maniscalco. Non-markovianity hinders quantum darwinism. *Sci. Rep.*, **6**:19607, 2016. (cited on p. 21)

[212] J. Zhang, P. W. Hess, A. Kyprianidis, P. Becker, A. Lee, J. Smith, G. Pagano, I.-D. Potirniche, A. C. Potter, A. Vishwanath, N. Y. Yao, and C. Monroe. Observation of a discrete time crystal. *Nature*, **543**:217, 2017. (cited on p. 49)

[213] R. Zwanzig. Ensemble method in the theory of irreversibility. *J. Chem. Phys.*, **33**:1338, 1960. (cited on p. 26)

[214] M. Zwolak and G. Vidal. Mixed-state dynamics in one-dimensional quantum lattice systems: A time-dependent superoperator renormalization algorithm. *Phys. Rev. Lett.*, **93**:207205, 2004. (cited on p. 42)